Scalar Phenomenology in Warped and Composite Models

Peter Jonathan Cox

ORCID ID: 0000-0002-6157-3430

Doctor of Philosophy

June 2016

School of Physics
The University of Melbourne

Submitted in total fulfilment of the requirements of the degree of Doctor of Philosophy

Produced on archival quality paper

Abstract

The hierarchy problem constitutes one of the main theoretical motivations for physics beyond the Standard Model. One well-motivated solution is to assume that the Higgs arises as a bound state of some new strong dynamics, cutting off its sensitivity to physics above the compositeness scale. An alternative possibility is to posit the existence of a warped extra dimension. These two seemingly different scenarios are in fact linked through the AdS/CFT correspondence. In this thesis we explore aspects of such models from both the 4D and 5D viewpoints, with a particular focus on the pseudo-Nambu Goldstone bosons (pNGBs), which are likely the lightest new states.

In Chapter 1 we review the motivation for physics beyond the Standard Model from both experimental observations and theoretical considerations. We then provide a review of models which seek to address the hierarchy problem using warped extra dimensions or a composite, pNGB Higgs boson in Chapter 2. We discuss the generic features of these models and their relationship through the AdS/CFT correspondence, as well as the current bounds provided by experiment.

In Chapter 3 we consider the linear dilaton model, which features a warped metric and a large interbrane distance. We utilise a Goldberger-Wise type mechanism to stabilise the extra dimension and investigate the resulting scalar spectrum. We study the phenomenology of the lightest mode, the radion, in detail and explore the constraints from LHC searches on the parameter space.

We investigate the consequences of radion/dilaton-Higgs mixing in Chapter 4. In the context of the Randall-Sundrum model with a bulk Higgs, we show that both mass and kinetic mixing are generically expected. Furthermore, the radion phenomenology is significantly modified by moving the Higgs into the bulk. We use the 5D formalism to motivate the most general 4D effective Lagrangian describing the Higgs-radion system and investigate the constraints on the parameter space, as well as future search strategies.

Conformal invariance is incompatible with spontaneous breaking, due to the presence of a quartic term in the dilaton potential. However a naturally light dilaton can be obtained via explicit breaking by a marginally relevant operator. In Chapter 5 we construct a gravitational dual of such a model using a soft-wall background. We consider an analytic bulk potential corresponding to a walking coupling in the UV and a fast transition to an order-one β-function in the IR. This provides a

realistic example of a naturally light dilaton where a single operator provides both the explicit breaking and develops a non-zero condensate.

In Chapter 6 we consider the unnatural composite Higgs model, which assumes a large global symmetry breaking scale $f \gtrsim 10\,\text{TeV}$. This leads to a split spectrum, with the pseudo-Nambu Goldstone bosons likely the only new states accessible at colliders. A generic prediction of such models is a colour-triplet partner of the Higgs, which can be metastable. We study the collider phenomenology of this colour-triplet scalar and explore the discovery reach of the LHC and future colliders using prompt, displaced and collider-stable searches.

Declaration of Authorship

This is to certify that:

- the thesis comprises only my original work towards the PhD except where indicated in the Preface,
- due acknowledgement has been made in the text to all other material used,
- the thesis is fewer than 100 000 words in length, exclusive of tables, bibliographies and appendices.

Signed: _____ Date: _____

Peter Jonathan Cox

Preface

This thesis comprises seven main chapters. Chapters 1 & 2 are an original introduction and literature review. Chapter 3 is based on publication [1], Chapter 4 on publications [2] and [6], and Chapters 5 & 6 on publications [3] and [4] respectively. Chapter 7 is the conclusion. The publications were produced in collaboration with James Barnard (publication [4]), Tony Gherghetta (publications [1, 3, 4]), Anibal Medina (publications [2, 6]), Tirtha Sankar Ray (publications [2, 6]) and Andrew Spray (publications [2, 4, 6]).

While much of the original motivation and inspiration for these projects should be attributed to my collaborators, in particular my supervisor Tony Gherghetta, all calculations, results, and analyses presented in this thesis are my own work unless stated otherwise. In Chapter 4, the calculation of the Higgs-radion mixing in the presence of non-zero backreaction presented in Section 4.3.3 was performed by Tirtha Sankar Ray and Andrew Spray, and the discussion of composite Higgs models in Section 4.3.4 is due to Anibal Medina. In Chapter 6, the limits from R-hadron searches in Section 6.3.1 were computed by James Barnard, while the discussion regarding non-minimal models in Section 6.2.3 is due to James Barnard and Andrew Spray.

Finally, the linear dilaton model was also the topic of my MSc thesis. Chapter 3 includes several significant additions and improvements compared to the work presented in that thesis. The two most important additions are: (i) the calculation of the radion profile and mass has been extended to all orders in the boundary mass, which allows the stability of the solution to be addressed; (ii) the constraints on the parameter space from recent LHC searches have been determined.

Acknowledgements

Firstly, I would like to thank my supervisor, Tony Gherghetta, for his guidance and support throughout my PhD and without whom this thesis would not have been possible. Also my collaborators, James Barnard, Jackson Clarke, Anibal Medina, Tirtha Sankar Ray and Andrew Spray for their patience, assistance, and for providing many insightful discussions.

I would also like to thank all the staff, postdocs, and students of CoEPP Melbourne Node for providing a friendly and engaging environment and making my time here a thoroughly enjoyable one. I would like to particularly acknowledge all the students in my office, both for helping me to develop my understanding through many interesting discussions and for their friendship.

To Innes, thank you for your endless, heartfelt encouragement and understanding throughout the writing of this thesis. Finally to my family, thank you so much for your ongoing and unconditional support and for always encouraging me to pursue my intellectual curiosity.

Contents

List of Abbreviations

4D	**4-d**imensional
5D	**5-d**imensional
ADD	**A**rkani-Hamed-**D**imopoulos-**D**vali
AdS	**A**nti-de**S**itter
CCWZ	**C**allan-**C**oleman-**W**ess-**Z**umino
CFT	**C**onformal **F**ield **T**heory
CP	**C**harge, **P**arity
CKM	**C**abbibo-**K**obayashi-**M**askawa
CMB	**C**osmic **M**icrowave **B**ackground
DM	**D**ark **M**atter
EW	**E**lectro**w**eak
EWSB	**E**lectro**w**eak **S**ymmetry **B**reaking
GHU	**G**auge-**H**iggs **U**nification
GIM	**G**lashow-**I**liopoulos-**M**aiani
GUT	**G**rand **U**nified **T**heory
IR	**I**nfra**r**ed
KK	**K**aluza-**K**lein
LEP	**L**arge **E**lectron **P**ositron Collider
LHC	**L**arge **H**adron **C**ollider
MCHM	**M**inimal **C**omposite **H**iggs **M**odel
MSSM	**M**inimal **S**upersymmetric **S**tandard **M**odel
NDA	**N**aive **D**imensional **A**nalysis
NGB	**N**ambu-**G**oldtsone **B**oson
PDF	**P**arton **D**istribution **F**unction
pNGB	**p**seudo **N**ambu-**G**oldtsone **B**oson
QCD	**Q**uantum **C**hromo**d**ynamics
QFT	**Q**uantum **F**ield **T**heory
RGE	**R**enormalisation **G**roup **E**quation
RS	**R**andall-**S**undrum
SM	**S**tandard **M**odel

SUSY	**Su**per**sy**mmetry
UV	**U**ltra**v**iolet
VEV	**V**acuum **E**xpectation **V**alue

List of Figures

Introduction

1.1 The Standard Model

The Standard Model (SM) of particle physics has proven to be one of the great success stories of physics in the past century. Its development has required a dedicated theoretical and experimental effort over many decades, culminating with the discovery of the Higgs boson in 2012 by the ATLAS and CMS collaborations at the Large Hadron Collider (LHC) [1, 2].

The structure of the Standard Model is largely determined by its $\mathrm{SU}(3) \times \mathrm{SU}(2) \times \mathrm{U}(1)_Y$ local gauge symmetry. The associated gauge bosons transform under the adjoint representation of the individual gauge groups, leading to 12 spin-1 degrees of freedom

$$g \sim (\mathbf{8}, \mathbf{1}, \mathbf{0}) \qquad W \sim (\mathbf{1}, \mathbf{3}, \mathbf{0}) \qquad B \sim (\mathbf{1}, \mathbf{1}, \mathbf{0})\,. \tag{1.1}$$

The $\mathrm{SU}(2) \times \mathrm{U}(1)_Y$ electroweak (EW) gauge group is spontaneously broken to its $\mathrm{U}(1)_Q$ subgroup via the Higgs mechanism. This introduces an additional Higgs doublet complex scalar field transforming as

$$H \sim (\mathbf{1}, \mathbf{2}, \frac{\mathbf{1}}{\mathbf{2}})\,, \tag{1.2}$$

which acquires a vacuum expectation value (vev) $\langle H \rangle = 174\,\mathrm{GeV}$. The gauge fields associated with the broken generators then acquire non-zero masses, with the additional longitudinal polarisations provided by the three would-be massless Nambu-Goldstone boson (NGB) degrees of freedom. The unbroken generator is given by $Q = W^3 + B$, such that the mass and gauge eigenstates do not coincide but are related by the transformation

$$A_\mu = \sin\theta_W W^3_\mu + \cos\theta_W B_\mu\,, \tag{1.3}$$

$$Z_\mu = \cos\theta_W W^3_\mu - \sin\theta_W B_\mu\,, \tag{1.4}$$

where θ_W is the Weinberg angle. We are then left with three massive spin-1 degrees of freedom, $W^{\pm}_{\mu}$ and Z_{μ}, while the spin-1 photon, A_{μ}, remains massless. The final degree of freedom contained in the Higgs doublet corresponds to a physical neutral scalar: the Higgs boson.

The fermionic content of the SM is divided into the quarks and leptons, distinguished by their transformation properties under SU(3). The leptons are SU(3) singlets and transform under the electroweak gauge group according to

$$L \equiv \begin{pmatrix} \nu_L \\ e_L \end{pmatrix} \sim (\mathbf{1}, \mathbf{2}, -\frac{\mathbf{1}}{\mathbf{2}}) \,, \qquad e_R \sim (\mathbf{1}, \mathbf{2}, -\mathbf{1}) \,, \tag{1.5}$$

where L (R) denote left- (right-) handed chiral spinors. Their electric charges are determined by their SU(2) isospin and hypercharge according to $Q = \tau_3 + Y$, such that the electron $e_{L,R}$ has charge -1, while the neutrino ν_L is uncharged. The SM contains three copies of this structure, known as generations, with the charged leptons (electron: e, muon: μ, tau: τ) and the corresponding neutrinos (ν_e, ν_μ, ν_τ). The charged leptons acquire masses via Yukawa couplings of the form

$$Y^l_{i,j}\, \bar{L}^i_L H e^j_R + h.c \,, \tag{1.6}$$

where $Y^l_{i,j}$ is a 3×3 complex matrix. The charged-lepton masses obey the hierarchy $m_e < m_\mu < m_\tau$, while the absence of right-handed neutrinos means that the neutrinos remain massless within the Standard Model.

The quarks are charged under SU(3) and transform according to

$$Q_L \equiv \begin{pmatrix} u_L \\ d_L \end{pmatrix} \sim (\mathbf{3}, \mathbf{2}, \frac{\mathbf{1}}{\mathbf{6}}) \,, \qquad \begin{matrix} u_R & \sim (\mathbf{3}, \mathbf{1}, \frac{\mathbf{2}}{\mathbf{3}}) \,, \\ d_R & \sim (\mathbf{3}, \mathbf{1}, -\frac{\mathbf{1}}{\mathbf{3}}) \,. \end{matrix} \tag{1.7}$$

The up- ($u_{L,R}$) and down- ($d_{L,R}$) type quarks then carry electric charges of 2/3 and -1/3 respectively. Similarly to the leptons, the SM contains three generations of quarks, divided into the up-type (up: u, charm: c, top: t) and down-type (down: d, strange: s, bottom: b). They also acquire masses through Yukawa couplings to the Higgs

$$\begin{aligned} &Y^u_{i,j}\, \bar{Q}^i_L \tilde{H} u^j_R + h.c \,, \\ &Y^d_{i,j}\, \bar{Q}^i_L H d^j_R + h.c \,, \end{aligned} \tag{1.8}$$

where $Y^{(u,d)}_{ij}$ are 3×3 complex matrices and $\tilde{H} = \epsilon H^*$ with ϵ the Levi-Cevita symbol. They are often separated into the light quarks which satisfy $m_u < m_d < m_s$ and the heavy quarks, $m_c < m_b < m_t$.

The SU(3) quantum chromodynamics (QCD) gauge group is distinct from the other SM gauge groups in that it exhibits confinement. As a result, isolated quarks are never observed and instead form SU(3) singlet bound states known as hadrons. These include the proton as the lightest baryon (qqq) and the pions as the lightest mesons ($\bar{q}q$). While the SU(3) gauge coupling becomes non-perturbative at low energies leading to confinement, it is asymptotically free at high scales where perturbative techniques can be used as in the electroweak sector.

In addition to its gauge symmetries, the SM Lagrangian contains several accidental global U(1) symmetries. These are baryon number B, under which the quarks have charge $+1/3$ and the three lepton numbers L_e, L_μ and L_τ, under which the charged leptons and neutrinos have charge $+1$.

The SM Lagrangian describes all the known fundamental particles and their interactions in terms of only 19 free parameters, which must be experimentally measured. These can be parametrised by the three gauge couplings, six quark masses, three charged lepton masses, three angles and one phase of the Cabbibo-Kobayashi-Maskawa (CKM) matrix, the Higgs mass, Higgs quartic coupling, and the QCD vacuum angle. The success of the Standard Model lies in the ability to make remarkably precise predictions in terms of only these few parameters; predictions which have time and again been found to be consistent with ever more precise experimental measurements.

1.2 Going Beyond

Despite the overwhelming success of the Standard Model, there are nevertheless many reasons why we should continue to both explore theoretically and search experimentally for what may lie beyond. In fact, we have already observed phenomena in nature which cannot be described within the Standard Model. Furthermore, there are additional theoretical reasons to suggest that the Standard Model is unlikely to provide the complete picture. In this section we will briefly detail the main experimental evidence and theoretical motivation for physics beyond the SM.

1.2.1 Evidence/Motivation for New Physics

1.2.1.1 Dark Matter

It is well known that the matter described by the Standard Model makes up only a very small fraction of the total energy density of our universe. The existence of dark matter is supported by a wealth of astrophysical observations on local to cosmological distance scales, including measurements of galactic rotation curves, weak and strong gravitational lensing, large scale structure and the cosmic microwave background (CMB). The most recent measurements of the CMB by the Planck satellite [3] find that the baryonic matter described by the SM makes up only 5% of the energy density of the universe, while dark matter contributes a further 26%. The remaining 69% is termed dark energy and is consistent with a cosmological constant. Despite the extensive astrophysical evidence for dark matter based on its gravitational interactions, we still know almost nothing about its underlying particle nature; although there are bounds on its interactions with the SM fields from direct and indirect detection, as well as model-dependent constraints on its self-interactions from cluster mergers. There are however numerous beyond the SM dark matter candidates, with weakly interacting massive particles (WIMPs) and axions among the most popular.

1.2.1.2 Neutrino Mass

It is now well established that neutrinos are massive particles, albeit with very small masses, the sum of which are constrained by cosmological measurements to be less than 0.32 eV [3]. The neutrino mass-squared differences and the angles of Pontecorvo–Maki–Nakagawa–Sakata (PMNS) mixing matrix have now been measured by various neutrino oscillation experiments using solar, atmospheric and reactor neutrinos; the CP phases(s) and the mass hierarchy will be probed by future experiments. Nevertheless, neutrinos remain massless within the Standard Model and new physics is required to explain their observed properties. While the straightforward addition of three right-handed neutrinos can account for neutrino masses, this leads to the question of why the corresponding Yukawa couplings should be so small compared to the charged fermions. Alternatively, neutrinos could be Majorana particles, in which case their masses explicitly break the accidental lepton number symmetry of the SM.

1.2.1.3 Matter-Antimatter Asymmetry

The universe we observe today is dominated by matter rather than anti-matter. This is generally quantified in terms of the ratio of the baryon to photon number densities, which is experimentally measured to be $\eta_B/\eta_\gamma = 6.1 \times 10^{-10}$ [3]. Assuming that the universe existed in a symmetric state at early times, this leads to the question of how such an asymmetry could be dynamically generated during its evolution; a process known as baryogenesis. The necessary conditions were determined by Sakharov in 1967 [4]. In principle the Standard Model contains all of the necessary ingredients for baryogenesis, however this possibility is not realised in nature and would require both a larger CKM CP phase and a significantly lighter Higgs mass. This therefore leaves a role for new physics to play in generating the baryon asymmetry of the universe.

1.2.1.4 Strong CP Problem

While CPT (charge, parity, time-reversal) invariance is a necessary ingredient for a Lorentz-invariant quantum field theory, it has been known for a long time that C, P, and their combination CP (and consequently T) are violated in nature. The CP violation which has been observed in meson oscillations and decays is governed by the weak interactions through the CP violating phase in the CKM matrix. However, there is another potential source of CP violation which arises in the strongly interacting sector via the term

$$\mathcal{S} \supset \int d^4x \, \frac{\theta g_s^2}{32\pi^2} \epsilon^{\mu\nu\rho\sigma} F^a_{\mu\nu} F^a_{\rho\sigma} \,, \tag{1.9}$$

where $F^a_{\mu\nu}$ is the QCD field strength tensor and $\epsilon^{\mu\nu\rho\sigma}$ is the fully anti-symmetric Levi-Cevita symbol. This term is a total derivative and does not have any observable consequences if the gauge fields vanish sufficiently fast as $x \to \infty$. However, there are in fact solutions to the classical equations of motion known as instantons [5] for which the above action is both non-zero and finite. Instanton configurations describe non-perturbative effects, but can be important since the QCD coupling constant becomes large at low energies. In particular, the above term gives rise to a non-zero electric dipole moment for the neutron, which is experimentally constrained and leads to the bound $|\theta| \lesssim 10^{-10}$ [6]. The strong CP problem is then the question of why this parameter should be so close to zero in the absence of any symmetry reason. The most common approach to address this problem is via the introduction of an additional Peccei-Quinn $\mathrm{U}(1)_{PQ}$ symmetry [7, 8], which leads to a new light scalar particle known as the axion [9–13].

1.2.1.5 Flavour

The flavour structure of the Standard Model is determined by the Yukawa couplings of the three fermion generations to the Higgs, giving rise to the fermion masses and CKM quark mixing matrix. While the experimental measurements to date are well described by this simple structure, there remain unresolved questions. For example, the large hierarchy of Yukawa couplings in the SM, ranging from $\sim 10^{-6}$ for the electron to ~ 1 for the top quark, is unexplained and there is a priori no reason to expect the existence of exactly three fermion generations. The possibility of naturally generating the fermion mass and mixing hierarchies will be one source of motivation for the beyond the SM scenarios we will consider.

1.2.1.6 Gauge Coupling Unification

The Standard Model couplings can be evolved to high energy scales through the use of the renormalisation group equations (RGEs). Assuming only the SM field content, the three gauge couplings almost intersect at a scale of $\sim 10^{16}\,\text{GeV}$. This provides a tantalising hint that the $\text{SU}(3) \times \text{SU}(2) \times \text{U}(1)_Y$ gauge group of the SM may unify into a single gauge group, for example SU(5) [14] or SO(10) [15, 16], at high energies. These are known as grand unified theories (GUTs). New physics at such high energy scales is of course well beyond the reach of current experiments, however the unification of the gauge couplings is only approximate in the SM and can be improved in certain extensions. This is this case in many supersymmetric models which, if realised in nature, are naturally expected to lead to new states around the TeV scale.

1.2.1.7 Hierarchy Problem

The hierarchy problem [17, 18] arises in quantum field theories which contain both hierarchically separated mass scales and fundamental scalar degrees of freedom. In short, scalar masses are generically sensitive, and receive quantum corrections proportional to the highest scale in the theory. In the Standard Model the only mass scale is the weak scale, which is set by the Higgs vev, $v = 246\,\text{GeV}$. However, if there exist additional states with large masses that cannot be decoupled from the Higgs, they will provide corrections to the Higgs mass parameter and consequently its vev. The masses of the W and Z gauge bosons and the Higgs are then generically expected to take on values of order the high mass scale. This issue was first considered in the context of grand unified theories [19] but is a potential problem

in any extension to the SM involving mass scales significantly larger than the weak scale. A significant concern is that new physics related to quantum gravity, which is expected to arise around the Planck scale, could suggest the Higgs vev should naturally be of order $M_{Pl} = 2.4 \times 10^{18}\,\text{GeV}$. However without a complete quantum theory of gravity we cannot know for certain.

1.2.1.8 Gravity

Gravity is not part of the Standard Model. General relativity has proven time and again to describe gravity remarkably well on large distance scales. Nevertheless, the Einstein-Hilbert action is non-renormalisable and an UV completion is necessary in order to describe physics on distances of order the Planck scale. A new framework is therefore required to describe the quantum properties of gravity and allow it to be treated on the same footing as the other fundamental interactions described by the SM.

1.2.2 Naturalness

The hierarchy problem will provide the primary motivation for the beyond the Standard Model scenarios considered in this thesis. It is therefore worthwhile to explore its origin in more detail. Firstly, it is important to note that the Standard Model, in the absence of gravity and any other sources of new physics, does not suffer from a hierarchy problem. Even at a glance this should be immediately clear since there is only one mass scale in the theory: the Higgs mass parameter[†]. The problem arises once we include new physics beyond the SM that cannot be sufficiently decoupled from the Higgs. This is a generic problem with elementary scalar fields in quantum field theory and can be understood as due to the fact that there is no enhanced symmetry in the limit $m_S \to 0$; in other words this is not a *technically natural* limit as defined by t'Hooft [20]. This is not the case for fermion and gauge field masses, which are protected by chiral symmetry and gauge invariance respectively. The result is that quantum corrections to scalar masses need not be proportional to the mass itself; there can and generically will be additive contributions proportional to every other mass scale in the theory.

In order to see this in practice, let us consider a simple model containing a scalar of mass m_S with a Yukawa coupling λ_f to a fermion with mass m_f. The one-loop

[†]In fact there is another dynamically generated mass scale, Λ_{QCD}, but this plays no role in our discussion. In principle one may also worry about the $\text{U}(1)_Y$ Landau pole at $\sim 10^{40}\,\text{GeV}$, however in practice new physics is expected well below this scale.

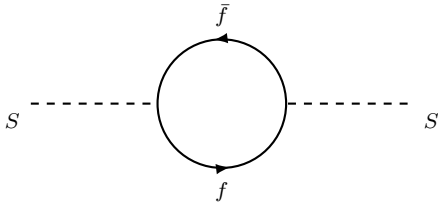

FIGURE 1.1: One-loop correction to the scalar propagator.

fermion contribution to the scalar mass arises from the diagram in Figure 1.1. In the $\overline{\text{MS}}$ renormalisation scheme this leads to the following β-function for the scalar mass

$$\mu \frac{d}{d\mu} m_S^2 = \frac{\lambda_f^2}{4\pi^2} m_S^2 - \frac{6\lambda_f^2}{4\pi^2} m_f^2 \,, \tag{1.10}$$

where μ is the renormalisation scale. As we suspected, the scalar mass receives corrections which are proportional to the other mass scale in the model: the heavy fermion mass m_f. Integrating the above RGE, and neglecting for simplicity the scale dependence of λ_f and m_f, leads to[†]

$$m_S^2(\mu) = m_S^2(\Lambda) \left(1 - \frac{\lambda_f^2}{4\pi^2} \log\left(\frac{\Lambda}{\mu}\right) \right) + \frac{6\lambda_f^2}{4\pi^2} m_f^2 \log\left(\frac{\Lambda}{\mu}\right) , \tag{1.11}$$

where $m_S(\Lambda)$ is the value at some high "input" scale, $\Lambda > m_f$. The problem is now abundantly clear: obtaining a hierarchy such that $m_S^2(m_S)/m_f^2 \ll 1$ requires that $m_S(\Lambda)$ be precisely fine-tuned against the m_f^2 contribution. A small change in the high scale value, $m_S(\Lambda)$, leads to a significant deviation in the mass at low scales due to the steep RG trajectory. In other words, the physics at low-scales is extremely sensitive to the physics at high scales. This runs contrary to our past experience where knowledge of physics on small scales is generally not required in order to describe phenomena on much larger scales. This sensitivity to high scales explicitly violates what is known as the *naturalness principle*. Note that while we have used a simple Yukawa model to elucidate the problem, any field charged under the SM gauge group will introduce a similar correction by three-loop order at the latest.

With this knowledge in hand, there are two different methodologies or approaches that can be taken in order to avoid a naturalness problem as a result of fine tuning in the Higgs mass parameter. The first is to ensure that any new physics added to the SM, for example to address any of the issues discussed in the preceding section, does not introduce a hierarchy problem. This requires that new fields either have masses not too far above the weak scale or can be sufficiently decoupled from the Higgs; note that it is the combination of coupling and mass which appears

[†]Eq. (1.11) is valid for $\mu \geq m_f$. At lower scales f decouples and $m_S^2(\mu < m_f) = m_S^2(m_f)$.

in Eq. (1.10). However, we should clearly state that this approach ignores the unknown but potentially problematic contributions from quantum gravity. The second and perhaps more common approach, which motivates the models discussed in this thesis, is to add new physics not too far above the weak scale which ensures that the Higgs mass becomes completely insensitive to physics at higher energy scales. This provides a strong motivation to search for new physics near the TeV scale and is one of the main reasons for the belief that new physics could be discovered at the LHC.

1.2.3 Strong or Weak?

We are interested in models which seek to address the hierarchy problem by ensuring that the Higgs mass is insensitive to corrections from higher energy scales. There are in particular two very well studied frameworks in which this can be achieved. The first is supersymmetry (SUSY) (for a review see e.g. [21]), which posits the existence of an additional symmetry relating fermions and bosons. The Poincaré algebra is extended to the super-Poincaré algebra by the inclusion of additional fermionic generators. The fact that these additional generators anti-commute allows one to evade the Coleman-Mandula theorem [22], which otherwise prohibits the non-trivial combination of space-time and internal symmetries. Of course supersymmetry is clearly not a symmetry of nature; it would predict, for example, a spin-0 partner of the electron with the same mass, which has not been observed. If realised in the UV it must therefore be broken at low energies. To avoid reintroducing the very problems with the Higgs mass we were seeking to solve, the couplings responsible for this breaking must have positive mass dimension; this is known as *soft* breaking. Supersymmetrising the SM field content and imposing the additional phenomenological requirement of R-parity leads to the so-called Minimal Supersymmetric Standard Model (MSSM). The MSSM and its non-minimal extensions are further motivated by features such as improved gauge coupling unification and a promising dark matter candidate in the form of the lightest supersymmetric particle, which is rendered stable by R-parity. However, this all comes at a price, with the necessity of supersymmetry breaking meaning that the MSSM has 105 additional parameters compared to the SM. Of course in practice many of these additional parameters are assumed to be related, often motivated by a specific supersymmetry breaking mechanism.

The MSSM provides a weakly coupled, perturbative[†] extension to the SM which

[†]Non-minimal extensions to the MSSM with non-perturbative couplings have been considered [23].

addresses the hierarchy problem. The alternative possibility, which shall be the focus of this thesis, addresses the hierarchy problem via the introduction of a new strongly interacting sector. In this case the Higgs boson[†] is assumed to arise as a bound state of a new strongly interacting sector which confines at some scale $\Lambda \gtrsim v$. Above this scale, the Higgs can no longer be considered as an elementary particle and hence its mass cannot be sensitive to physics at higher energies. In order to obtain the weak scale naturally and without resorting to additional fine tuning, the compositeness scale should not be much larger than the weak scale. While we have described models of this type as a strongly coupled solution to the hierarchy problem, it turns out that they have a dual weakly coupled description in terms of extra dimensional models. The existence of a weakly coupled description will prove very useful for calculability, however it also comes with its own limitations and in practice the two descriptions are complementary in exploring these types of scenarios. In the next chapter we will provide a brief review of these models from both the strongly coupled 4-dimensional (4D) and weakly coupled 5-dimensional (5D) perspectives and discuss how they are related, before exploring various aspects of this class of models in the subsequent chapters.

Finally, it is worth mentioning that another mechanism for addressing the hierarchy problem has very recently been proposed [26]. It involves a relaxation mechanism, which causes the Higgs mass to evolve towards its weak scale value during a period of inflation in the very early universe. It remains unclear whether a realistic model, which is consistent with all experimental bounds, can be obtained in this framework but it is nevertheless another intriguing possibility.

1.2.4 New Physics is Hiding

Despite the very strong experimental evidence and theoretical motivation for physics beyond the Standard Model, so far it has yet to be seen. There have been a number of interesting deviations from Standard Model predictions, however as of yet none of them provide unequivocal evidence of new physics and could be due to systematic effects, incorrect theoretical predictions or simply be statistical fluctuations. In recent times, the LHC has been progressively increasing its sensitivity to many well motivated extensions to the SM and is starting to exclude large regions of parameter space. Constraints on new physics scenarios which give rise to new sources of flavour violation are even more stringent, with bounds on the scale of certain effective operators exceeding 10^5 TeV [27]. Nevertheless, while any new

[†]In the past technicolour models [18, 24, 25], which can be thought of as akin to a scaled-up version of QCD, were considered as viable strongly coupled models of EWSB, however these were ruled out by the Higgs discovery.

physics has so far successfully evaded our efforts to find it, the evidence strongly suggests that it is there somewhere waiting to be discovered.

Extra Dimensions and Strong Sectors

In this chapter we provide a brief introduction and review of models which seek to address the hierarchy problem in the context of warped extra dimensions or additional strongly coupled sectors. As we shall discuss, these two seemingly different possibilities are in fact inextricably linked via the AdS/CFT correspondence. The study of theories at strong coupling is notoriously challenging and traditional methods developed for QCD rely on effective field theories based on symmetry considerations or numerical techniques such as lattice simulations. Extra dimensional models provide an additional approach via a (weakly coupled) dual description which can be extremely valuable by enabling us to calculate certain properties of the strongly coupled sector.

We begin by reviewing how these models address the hierarchy problem from the extra-dimensional viewpoint, before providing a brief introduction to the AdS/CFT correspondence. This then leads naturally to a discussion from the dual 4D viewpoint, where we consider a particular class of models in which the Higgs arises as a pseudo-Nambu Goldstone Boson (pNGB).

2.1 Large Extra Dimensions

The earliest attempts to address the hierarchy problem by introducing additional dimensions of spacetime considered the possibility of large, flat, compact extra dimensions [28]. The underlying idea is that the fundamental Planck scale can be significantly lower ($\sim$ TeV) than the observed 4D Planck mass ($M_{Pl} = 2.4 \times 10^{18}$ GeV). In these models gravity necessarily propagates in the full $4 + n$ dimensions, where n is the number of extra dimensions, while the Standard Model fields are localised on a four-dimensional manifold such that they experience an effective 4D Planck mass. Depending on the radius and number of the additional

compact dimensions, the effective Planck mass can be hierarchically larger than the fundamental gravitational scale. More precisely we have

$$M_{Pl}^2 = M^{2+n} R^n \,, \tag{2.1}$$

where M is the fundamental Planck mass in $4+n$ dimensions and R is the radius of the additional compact dimensions.

These models can give potentially striking experimental signatures at the LHC [28–30], in particular the formation and subsequent decay of TeV scale black holes [31, 32] can yield high multiplicity, energetic final states. As a result, both the ATLAS [33, 34] and CMS [35] experiments have been able to disfavour such models and place significant constraints on the parameter space.

2.2 Warped Extra Dimensions

It was subsequently realised that large extra dimensions were not necessary in order to generate a large hierarchy of scales and that this could instead be achieved via a warping of the geometry. This type of scenario was first suggested by Randall and Sundrum [36]. They considered a single extra dimension compactified on a line segment or equivalently a $\mathbb{Z}_2$ orbifold, which can be obtained by compactifying on a circle and then identifying the opposing sides ($S_1/\mathbb{Z}_2$). A four-dimensional brane is then located at each endpoint of the extra dimension. This set-up is shown in Figure 2.1. The inclusion of a non-zero 5D cosmological constant, Λ, then leads to a warping of the fifth dimension. In order to obtain a solution which satisfies 4D Poincaré invariance, this bulk cosmological constant must be tuned against localised values on each of the branes. The subsequent geometry is then five-dimensional Anti-deSitter space (AdS_5) with the warped metric

$$ds^2 = g_{MN} dx^M dx^N = e^{-2ky} \eta_{\mu\nu} dx^\mu dx^\nu + dy^2 \,, \tag{2.2}$$

where y is the extra-dimensional coordinate, the indices $M, N = (\mu, 5)$, and $\eta_{\mu\nu} = \mathrm{diag}(-,+,+,+)$ is the 4D Minkowski metric.

The full 5D action for such a model is written as

$$S = 2 \int_0^{y_c} d^5x \sqrt{-g} \left(\frac{M^3}{2} R + \Lambda \right) - \sum_{i=0,1} \int d^4x \sqrt{-\gamma} \left(2M^3 [K] + \lambda_i \right) \,, \tag{2.3}$$

where the two branes $i = (0, 1)$ are located at $y = (0, y_c)$ and are referred to as the UV and IR branes respectively for reasons which shall become evident. Here

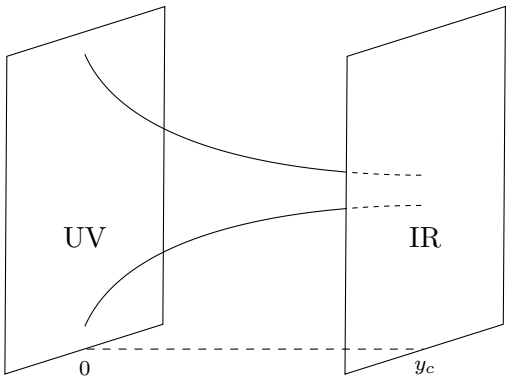

FIGURE 2.1: The Randall-Sundrum set-up.

R is the Ricci scalar, γ is the induced metric on the branes, and λ_i are the brane localised cosmological constants or brane tensions. Finally, $[K]$ denotes the jump in the extrinsic curvature across the brane and corresponds to the Gibbons-Hawking-York boundary term [37, 38] required for a well-posed variational problem in the presence of a spacetime boundary.[†]

The Einstein equations in the bulk and on the boundaries lead to the constraints

$$\Lambda = -6M^3k^2\,, \qquad \lambda_{(0,1)} = \pm 6M^3k\,. \tag{2.4}$$

The first equation simply expresses the AdS curvature scale, k, in terms of the bulk cosmological constant, while the UV boundary condition enforces the tuning of the 4D cosmological constant. The role of the IR boundary condition will be discussed in Section 2.2.2.

Finally, it will sometimes be more convenient to instead consider the conformal coordinate, $z = e^{ky}/k$, such that the metric takes the form

$$ds^2 = \left(\frac{1}{kz}\right)^2 \left(\eta_{\mu\nu}dx^\mu dx^\nu + dz^2\right)\,. \tag{2.5}$$

2.2.1 Solution to the Hierarchy Problem

The effective 4D Planck mass in the Randall-Sundrum (RS) model can be obtained by integrating out the fifth dimension, leading to

$$M_{Pl}^2 = 2M^3\int_0^{y_c} dy\, e^{-2ky} = \frac{M^3}{k}\left(1 - e^{-2ky_c}\right)\,. \tag{2.6}$$

[†]The action can also be expressed as the integral over the full circle, rather than just the line segment, with the location of the branes fixed by Dirac delta functions. There is then no need to explicitly include this term, although the physics is of course unchanged.

The curvature scale is generally taken to be $k \lesssim M$, such that the perturbative expansion is under control and we can neglect higher order terms beyond the Einstein-Hilbert action[†]. We will be interested in the limit $ky_c \gg 1$; the effective 4D Planck mass is then of order the fundamental scale M.

A very different situation arises for mass scales localised on the IR brane. Consider for example a scalar field localised on the IR brane, which we shall denote with some foresight by H. The brane action is given by

$$S_{IR} = -\int d^4x \sqrt{-\gamma} \left(\gamma^{\mu\nu} \partial_\mu H^\dagger \partial_\nu H - m^2 |H|^2 + \lambda |H|^4 \right) . \tag{2.7}$$

Inserting the solution for the metric (2.2) and rescaling the field by $H \to e^{ky_c} H$ such that the kinetic term is canonically normalised we obtain

$$S_{IR} = -\int d^4x \left(\eta^{\mu\nu} \partial_\mu H^\dagger \partial_\nu H - \left(m e^{-ky_c} \right)^2 |H|^2 + \lambda |H|^4 \right) . \tag{2.8}$$

Notice that the mass scale on the IR brane has been "warped-down". This would not be the case for fields localised on the UV brane and thus the physical mass scale depends on the position in the extra dimension. More precisely, the momentum cut-off required to regulate the 5D theory is y-dependent [40]. If we associate this IR brane localised field with the Higgs, we then see that the Higgs mass is exponentially suppressed compared to the curvature scale, $m_H \sim k e^{-ky_c}$. If we wish to address the hierarchy problem and avoid fine tuning of the Higgs mass we require $m_H \sim$ TeV, which for $M \simeq M_{Pl}$ requires $ky_c \simeq 35$.

2.2.2 Stabilisation

The warped geometry of the Randall-Sundrum model allows us to generate a hierarchy of scales, which is determined by the compactification scale or equivalently the interbrane distance, y_c. So far we have assumed that this separation is simply a free parameter of the model, which in order to generate the Planck-electroweak hierarchy is required to be $\mathcal{O}(M_{Pl}^{-1})$. However, after integrating out the extra dimension one finds that y_c develops an effective potential given by

$$V_{eff}(y_c) = \lambda_0 k + \lambda_1 k e^{-4ky_c} + \Lambda \left(1 - e^{-4ky_c} \right) . \tag{2.9}$$

It is now evident that the IR boundary condition in Eq. (2.4) enforces that y_c develop a flat potential. This is simply a consequence of the fact that the AdS

[†]More recently it has been shown that using the NDA estimate for the 5D cutoff, $\Lambda_{cut-off} = 24^{1/3}\pi M$, leads to the bound $k/M_{Pl} < \sqrt{3\pi^3/(5\sqrt{5})}$ [39].

metric is invariant under rescaling of the coordinates $x \to \mu x$, or in other words that the isometry group of AdS_5 is SO(4,2) or the conformal group in four dimensions. However, this flat potential presents a problem, since we now expect a corresponding massless scalar mode or modulus field related to fluctuations in the interbrane distance. Such a massless mode leads to modifications of Newtonian gravity and is excluded [41].

A solution to this problem was suggested by Goldberger and Wise [42, 43] in the form of a stabilisation mechanism for y_c. They proposed the addition of a bulk scalar field, ϕ, with 5D mass m_ϕ and brane localised potentials such that the field develops a non-trivial and y-dependent vacuum expectation value. This leads to the generation of a potential for the modulus field and stabilises the interbrane distance. They considered the brane potentials

$$S_{(0,1)} = -\int d^4x \sqrt{-\gamma}\, \lambda_{(0,1)} \left(\phi^2 - v_{(0,1)}^2\right)^2 , \tag{2.10}$$

where $v_{(0,1)}$ are the vacuum expectation values of ϕ on the UV and IR branes respectively in the $\lambda_{(0,1)} \to \infty$ limit. Taking the limit $\epsilon \equiv m_\phi/(4k) \ll 1$ and $ky_c \gg 1$, the effective potential is given by

$$V_{eff}(y_c) = \epsilon v_0^2 k + 4k e^{-4ky_c} \left(v_1 - v_0 e^{-\epsilon k y_c}\right)^2 . \tag{2.11}$$

This potential has a minimum at

$$ky_c = \frac{4k^2}{m_\phi^2} \ln\left(\frac{v_0}{v_1}\right) . \tag{2.12}$$

The size of the extra dimension has clearly been stabilised and the required value of $ky_c \simeq 35$ can easily be obtained without any fine-tuning of parameters. Furthermore it was shown in Ref [44] that loop effects, while not sufficient to stabilise the extra dimension, do not spoil the classical mechanism described above.

This potential also removes the troublesome massless mode and fluctuations around the above minimum have a mass of order $m_\phi \sim \epsilon k e^{-ky_c}$. However, it is worth noting that this set-up does suffer from an implicit fine-tuning as discussed in Ref. [45]. It is a consequence of considering only a small perturbation on the flat (tuned) y_c potential of the unstabilised solution. Without this tuning a light mode is no longer generically expected in the spectrum; we will discuss how a light mode can still be obtained in Chapter 5.

2.2.3 Back-reaction

We have seen that in order to stabilise the extra dimension, we must include an additional bulk scalar field that develops a non-trivial vacuum expectation value. The full 5D action can then be expressed as

$$S = 2\int_0^{y_c} d^5x\,\sqrt{-g}\left(\frac{M^3}{2}R - \frac{1}{2}g^{MN}\partial_M\phi\partial_N\phi - V(\phi)\right) - \sum_{i=0,1}\int d^4x\sqrt{-\gamma}\left(2M^3[K] + U_i(\phi)\right)\,. \quad (2.13)$$

While neglected in the original Goldberger-Wise model (by taking the $\epsilon \ll 1$ limit), the scalar field will of course induce a back-reaction on the geometry and therefore cause the metric solution to deviate from AdS_5. We are then led to consider the most general ansatz for the metric satisfying 4D Poincaré invariance:

$$ds^2 = A(y)^2\eta_{\mu\nu}dx^\mu dx^\nu + dy^2\,. \quad (2.14)$$

This leads to the following Einstein equations for the metric and scalar field backgrounds

$$\phi'' = -4\frac{A'}{A}\phi' + V'(\phi)\,, \quad (2.15)$$

$$\frac{A''}{A} = \frac{A'^2}{A^2} - \frac{1}{3M^3}\phi'^2\,, \quad (2.16)$$

$$\frac{A'^2}{A^2} = \frac{1}{2}\phi'^2 - \frac{1}{6M^3}V(\phi)\,. \quad (2.17)$$

In addition to the UV/IR boundary conditions

$$\frac{A'}{A} = \mp\frac{1}{6M^3}U_{(0,1)}(\phi)\,, \quad (2.18)$$

$$\phi' = \pm\frac{1}{2}U'_{(0,1)}(\phi)\,. \quad (2.19)$$

It was shown in Ref. [46] that these equations can be reduced to a simpler system of coupled first-order differential equations via the introduction of a superpotential, W.[†] The superpotential is defined in terms of the bulk scalar potential by

$$V(\phi) = \frac{1}{2}W'(\phi)^2 - \frac{2}{3M^3}W(\phi)^2\,. \quad (2.20)$$

[†]While this method originates from supergravity, there is no supersymmetry in this context and the superpotential is simply a theoretical tool used to obtain solutions to the field equations.

This equation is non-linear in W and it is therefore extremely challenging to solve for the superpotential for a given bulk potential. However, if we instead choose to define our model in terms of the superpotential the situation is significantly improved and the corresponding bulk potential can be immediately determined. In terms of this superpotential, the remaining bulk field equations simply reduce to

$$\phi'(y) = W'(\phi)\,, \tag{2.21}$$

$$\frac{A'(y)}{A(y)} = -\frac{1}{3M^3}W(\phi)\,. \tag{2.22}$$

The boundary conditions at the UV/IR branes are also simply given by

$$W(\phi) = \pm\frac{1}{2}U_{(0,1)}(\phi)\,, \tag{2.23}$$

$$W'(\phi) = \pm\frac{1}{2}U'_{(0,1)}(\phi)\,. \tag{2.24}$$

While this method provides a simple way to solve for the background metric and scalar field based on a given superpotential, it turns out that the class of models which arise from analytic superpotentials possess certain undesirable features, which we shall discuss in Chapter 5.

2.2.4 Including the Standard Model

In the original Randall-Sundrum model the entire Standard Model was localised on the IR brane. However this has the unfortunate consequence that higher-dimension operators are only expected to be suppressed by ∼TeV scale [47]. This immediately leads to problems with proton decay, flavour observables, neutrino masses, and electroweak precision measurements. Realistic models therefore assume that the SM fields are allowed to propagate in the bulk [48, 49]. Of course, the Higgs should still be localised towards the IR, although not necessarily on the IR brane [50], so that the hierarchy problem is not reintroduced.

The most immediate consequence of allowing the SM to propagate in the bulk is that for each SM field there will now be a tower of 4D Kaluza-Klein modes, in addition to a zero mode which will be identified with the usual SM particle. While these additional states provide an excellent opportunity to probe these models at the LHC, they still potentially lead to problems with flavour and electroweak precision constraints as we shall discuss shortly. Here we will briefly demonstrate how this tower of KK modes arises for bulk fields and summarise the key results

for scalars [51], fermions [52] and gauge fields [53, 54] living in the bulk. A more detailed review can be found in Ref. [55].

2.2.4.1 Scalar Fields

The action for a bulk complex scalar field is given by

$$S_\phi = -\int d^5x\,\sqrt{-g}\left(g^{MN}\partial_M\phi^\dagger\partial_N\phi + m_\phi^2\phi^\dagger\phi\right)\,, \tag{2.25}$$

which leads to the equation of motion

$$A^2\Box\phi + \partial_5\left(A^4\partial_5\phi\right) - m_\phi^2 A^4\phi = 0\,, \tag{2.26}$$

where $\Box \equiv \eta^{\mu\nu}\partial_\mu\partial_\nu$ is the d'Alembert operator. This equation can be solved by performing a Kaluza-Klein expansion

$$\phi(x^\mu, y) = \sum_{n=0}^{\infty}\phi^{(n)}(x^\mu)f_\phi^{(n)}(y) \tag{2.27}$$

where $\phi^{(n)}(x^\mu)$ satisfy the 4D Klein-Gordon equation $\Box\phi^{(n)} = m_n^2\phi^{(n)}$. Substituting this ansatz into Eq. (2.26) leads to a Sturm-Liouville equation for the eigenfunctions $f_\phi^{(n)}(y)$ which consequently form a complete set and satisfy an orthonormality relation. In the absence of brane localised terms in the action, the $f_\phi^{(n)}(y)$ also satisfy either Neumann or Dirichlet conditions on the branes, which determine the eigenvalues, m_n^2.

It turns out that there are no massless scalar modes for either Neumann or Dirichlet boundary conditions. However, adding a boundary mass term on the UV and IR branes and imposing a tuning relative to the bulk mass parameter[†], $m_\phi^2 \equiv ak^2$, yields a massless zero mode with eigenfunction

$$f_\phi^{(n)}(y) \propto e^{bky}\,. \tag{2.28}$$

Here we have assumed an AdS metric, while b is the boundary mass in units of k and has been tuned[‡] to satisfy $b = 2 \pm \sqrt{4+a}$. The boundary mass thus determines the localisation of the scalar zero mode along the extra dimension. Substituting this solution into the action (2.25) it becomes clear that this mode is localised towards the UV (IR) for $b < 1$ ($b > 1$).

[†]In order to ensure the stability of AdS space $a \geq -4$ [56].
[‡]Such a tuning can be enforced by supersymmetry [49].

In addition to the above zero mode solution, Eq. (2.27) also contains an infinite tower of massive 4D scalar modes. The solutions for the profiles can be expressed in terms of Bessel functions, with a mass spectrum given in the $ky_c \gg 1$ limit by

$$m_n \simeq \left(n + \frac{1}{2}\sqrt{4+a} - \frac{3}{4}\right) \pi k e^{-ky_c} \,. \tag{2.29}$$

2.2.4.2 Gauge Fields

The situation is similar for massless gauge fields in the bulk. For simplicity we shall present the abelian case, however the generalisation to the non-abelian case is straightforward. The action is

$$S_A = -\frac{1}{4g_5^2} \int d^5x \sqrt{-g} \left[F^{MN} F_{MN} + \frac{2}{\xi} \left(g^{\mu\nu} \partial_\mu V_\nu + \xi A^{-2} \partial_5 \left(A V_5 \right) \right)^2 \right] , \tag{2.30}$$

where g_5 is the 5D gauge coupling and ξ a gauge-fixing parameter. With the above choice of gauge fixing term, one obtains decoupled equations of motion for $V_M = (V_\mu, V_5)$

$$\partial_5 \left(A^2 \partial_5 V_\mu \right) = \Box V_\mu - \left(1 - \frac{1}{\xi} \right) \eta^{\nu\rho} \partial_\mu \partial_\nu V_\rho \,, \tag{2.31}$$

$$\xi \, \partial_5^2 \left(A V_5 \right) = \Box V_5 \,. \tag{2.32}$$

Gauge invariance requires that V_μ and V_5 satisfy opposite boundary conditions, such that imposing Dirichlet boundary conditions for V_μ enforces Neumann conditions for V_5 and vice versa. In the case of Neumann boundary conditions for V_μ on the UV and IR branes, the V_5 zero mode then vanishes. Moreover, making the gauge choice $\xi \to \infty$ also removes the massive V_5 modes, which are effectively eaten to give a tower of massive 4D vector modes in addition to a zero mode with eigenfunction

$$f_V^{(0)}(y) = \frac{1}{\sqrt{y_c}} \,. \tag{2.33}$$

Interestingly, this shows that gauge field zero-modes are not localised along the extra dimension. This has important consequences as we will discuss shortly. The tower of spin-1 modes have masses

$$m_n \simeq \left(n \mp \frac{1}{4} \right) \pi k e^{-ky_c} \,, \tag{2.34}$$

where the $\pm$ correspond to the case of Neumann (Dirichlet) boundary conditions and we have taken the limit $ky_c \gg 1$.

It is worth also briefly commenting on the case of gauge fields with 5D mass terms. Such a massive gauge field could arise due to a Higgs mechanism acting in the bulk. The main difference in this case is that the zero mode is lifted and develops a non-zero mass.

2.2.4.3 Fermions

Including fermions in the bulk is somewhat more complicated due to the fact that we are working in a curved spacetime. In five dimensions γ_5 is also part of the Dirac algebra, such that the irreducible spinor representation of the (universal cover of the) Lorentz group is now a Dirac spinor, as opposed to a Weyl spinor in four dimensions. In curved spacetime the Dirac algebra is generalised to

$$\left\{\Gamma^M, \Gamma^N\right\} = 2g^{MN}\,. \tag{2.35}$$

The standard approach to describe spinor fields in curved spacetime is to move to a non-coordinate basis and introduce the vielbein e^M_A, defined by $g^{MN} = e^M_A e^N_B \eta^{AB}$. The gamma matrices γ^A, defined by $\Gamma^M = e^M_A \gamma^A$, then satisfy the usual Dirac algebra. The Dirac action in 5D is, as expected

$$S_\Psi = -\int d^5x\,\sqrt{-g}\left(\frac{i}{2}\left(\bar\Psi\Gamma^M D_M\Psi - D_M\bar\Psi\Gamma^M\Psi\right) + m_\Psi\bar\Psi\Psi\right)\,. \tag{2.36}$$

However the covariant derivative $D_M = \partial_M + \omega_M$ now also includes the spin connection[†], which for our metric ansatz (2.2) is simply $\omega_M = \left(\frac{1}{2}A'(y)\gamma_\mu\gamma^5, 0\right)$.

It is useful to decompose the Dirac spinor into left- and right-handed components defined by $\Psi_\pm = \pm\gamma_5\Psi_\pm$, in terms of which the equations of motion become

$$\gamma^\mu\partial_\mu\Psi_- + A\partial_5\Psi_+ + (c-2)kA\Psi_+ = 0\,, \tag{2.37}$$

$$\gamma^\mu\partial_\mu\Psi_+ - A\partial_5\Psi_- + (c+2)kA\Psi_- = 0\,, \tag{2.38}$$

where $m_\Psi = ck$. Once again we proceed via a KK expansion of the fields $\Psi_\pm$. For a massless zero mode the above equations decouple, yielding the solutions

$$f^{(0)}_\pm(y) \propto e^{(2\mp c)ky}\,. \tag{2.39}$$

However the left- and right-handed components are still connected by the boundary conditions, which in fact enforce that one of the above solutions must vanish. This is a result of compactifying on the orbifold rather than the circle and is essential

[†]The spin connection is given in terms of the Christoffel symbols Γ^R_{MS}, by $\omega^A_{MB} = e^A_R e^S_B \Gamma^R_{MS} - e^R_B \partial_M e^A_S$.

in order to generate the chiral Standard Model from 5D Dirac spinors. It is then immediately obvious that to describe the SM fermions requires two Dirac spinors, Ψ_L and Ψ_R, where the L, R denote the transformation properties of the fields under the SM gauge groups or equivalently the chirality of the zero modes. Note that while one of the zero modes is removed by the boundary conditions, the tower of KK modes remains vector-like with non-zero solutions for both $f_{\pm}^{(n)}$. The mass spectrum is given by

$$m_n \simeq \left(n + \frac{1}{2}|c \pm \frac{1}{2}| - \frac{1}{4}\right) \pi k e^{-ky_c}\,, \tag{2.40}$$

with the upper (lower) sign corresponding to Dirichlet boundary conditions for Ψ_+ (Ψ_-) and a right- (left-) handed zero mode. Finally, substituting Eq. (2.39) into the action (2.36), one finds that the left-handed fermion zero mode is localised towards the UV (IR) brane for $c > 1/2$ ($c < 1/2$); similarly for the right-handed zero mode with the replacement $c \leftrightarrow -c$.

2.2.4.4 Gauge couplings

We have seen that each 5D bulk field gives rise to a KK tower of 4D modes, with a zero mode that we would like to identify with a corresponding Standard Model field. We can construct a 4D effective theory describing the lowest few KK modes by substituting the solutions to the equations of motion into the action and integrating out the extra dimension. This means that the usual SM couplings will be given by the corresponding 5D parameters multiplied by an overlap integral involving the 5D eigenvalue functions.

In the case of the gauge couplings, this leads to the following relation between the 4D and 5D gauge couplings

$$g_4 = g_5 \int dy\, e^{-3ky} f_V^{(0)} f_{\pm}^{(n)} f_{\pm}^{(m)} = \frac{g_5}{\sqrt{y_c}} \delta_{nm}\,. \tag{2.41}$$

This relation could have potentially resulted in a significant problem once we allowed the fermions to be localised differently along the extra dimension: violation of gauge coupling universality. However, the fact that the gauge boson zero mode profile is constant means that the above integral is simply the orthonormality relation for the fermions, leading to the result on the RHS of Eq. (2.41). The delocalisation of the gauge boson zero mode along the extra dimension is therefore essential for the viability of models with fermions in the bulk.

2.2.4.5 Yukawa couplings

The ability to localise fermions differently along the extra dimension, while still preserving gauge-coupling universality, turns out to be extremely useful for generating the 4D Yukawa couplings. In fact, it allows one to generate hierarchically different 4D couplings using only $\mathcal{O}(1)$ 5D parameters and can therefore provide a mechanism to explain the hierarchy of Yukawa couplings in the Standard Model [49, 57]. The underlying mechanism here is known as partial compositeness and shall be discussed from the 4D viewpoint in Section 2.3.2.

For simplicity we take the Higgs to be localised on the IR brane, in which case the overlap integral reduces to evaluating the fermion profiles on the IR brane. In the case of UV localised fermions ($c = c_L = -c_R > 1/2$) the resulting relation between the 4D and 5D Yukawa couplings is [49]

$$\lambda \simeq \lambda_5 k \left(c - \frac{1}{2}\right) e^{(1-2c)ky_c} . \tag{2.42}$$

The 4D Yukawa coupling is then exponentially suppressed due to the small overlap between the UV localised fermions and IR localised Higgs. Taking the fermions to be localised in the IR ($c_L = -c_R < 1/2$) on the other hand leads to

$$\lambda \simeq \lambda_5 k \left(\frac{1}{2} - c\right) . \tag{2.43}$$

In this case the 4D Yukawa couplings can easily be $\mathcal{O}(1)$ and for the top quark we might expect $c \simeq -1/2$.

2.2.4.6 RS GIM mechanism

We mentioned at the beginning of this section that one of the main motivations for moving the Standard Model into the bulk was to suppress dangerous higher-dimension operators which would be suppressed by only the TeV scale in the brane localised case. With the fermions localised in the bulk these higher-dimension operators in the low energy effective theory will still be generated via the exchange of, for example, KK gauge bosons. This leads to very stringent bounds on the KK masses from kaon mixing in models which do not feature a warped geometry [58].

In warped models the bound can be significantly reduced due to the fact that the lowest lying KK modes are localised towards the IR brane, while their profiles are approximately flat in the UV. Therefore, as was the case for the zero mode

gauge fields, they couple universally to UV localised (i.e. first and second generation) fermions. Flavour changing effects (beyond the CKM) are proportional to the difference in the fermion-KK gauge field coupling between generations and can therefore be significantly suppressed [49]. We will discuss the remaining experimental bounds in Section 2.2.6.

2.2.5 Fluctuations of the Metric

We have already seen that allowing the Standard Model fields to propagate in the bulk of the extra dimension leads to a tower of four dimensional KK modes for each 5D field. We should therefore expect a similar situation for the fields associated with the fluctuations of the metric. While the precise bulk field content can vary depending on the model, the following metric degrees of freedom will be unavoidably present and their couplings are largely fixed by general coordinate invariance.

We will also include an additional bulk scalar field in this discussion. The reason being that such a scalar field is required in order to stabilise the extra dimension, as discussed in Section 2.2.2. This scalar will mix with the gravitational degrees of freedom and unless the back-reaction of the scalar can be neglected we must consider the complete, coupled system. The results below have also been generalised to an arbitrary number of additional scalars in Ref. [59].

It is convenient to decompose the fluctuations around the metric (2.2) in terms of fields which transform under irreducible representations of the 4D Lorentz group. Focusing initially on massive 4D fields, the unique decomposition is given by

$$g_{\mu\nu} = A(y)^2 \left[\eta_{\mu\nu}(1+2\Psi) + 2\partial_\mu\partial_\nu E + 2\partial_{(\mu}E^T_{\nu)} + h^{TT}_{\mu\nu}\right] , \tag{2.44a}$$

$$g_{\mu 5} = A(y)\left[\partial_\mu B + B^T_\mu\right] , \tag{2.44b}$$

$$g_{55} = 1 + 2\Phi \, , \tag{2.44c}$$

$$\phi = \phi(y) + \delta\phi(x,y) \, , \tag{2.44d}$$

where $\partial^\mu B^T_\mu = \partial^\mu E^T_\mu = \partial^\mu h^{TT}_{\mu\nu} = h^{TT\mu}_\mu = 0$. With the exception of $h^{TT}_{\mu\nu}$, the fields defined above all transform under 5D diffeomorphisms (see e.g. Ref [60]) and the physical degrees of freedom must of course correspond to gauge invariant combinations.

In the case of massless 4D fluctuations, the above decomposition becomes ambiguous and the tensor and vector modes should instead be decomposed in a light-cone

basis. After gauge fixing, the fluctuations can be expressed as [60]

$$g_{\mu\nu} = A(y)^2 \left[\eta_{\mu\nu}(1+2\Psi) + h^{TT}_{\mu\nu}\right] , \tag{2.45a}$$

$$g_{\mu 5} = A(y) B^T_\mu , \tag{2.45b}$$

$$g_{55} = 1 + 2\Phi , \tag{2.45c}$$

$$\phi = \phi(y) + \delta\phi(x,y) , \tag{2.45d}$$

where B^T_μ and $h^{TT}_{\mu\nu}$ are also spatially transverse, $\partial^i B^T_i = \partial^i h^{TT}_{i\nu} = 0$.

With the above decompositions for the massive and massless modes, the Einstein equations reduce to the following equations of motion for the various fields.

2.2.5.1 Tensor

The tensor equation of motion in both the massive and massless case is given by

$$A^2 h^{TT\prime\prime}_{\mu\nu} + 4\frac{A'}{A} h^{TT\prime}_{\mu\nu} + \Box h^{TT}_{\mu\nu} = 0 . \tag{2.46}$$

The boundary condition is $h^{TT\prime}_{\mu\nu} = 0$. Hence there is a massless zero mode, to be identified with the usual graviton, in addition to a KK tower of spin-2 states. For an AdS metric and in the limit $ky_c \gg 1$, these have masses given by

$$m_n \simeq \left(n + \frac{1}{4}\right) \pi k e^{-ky_c} , \tag{2.47}$$

As one would expect for a graviton, these modes couple to other fields through the energy-momentum tensor, but with couplings suppressed by only ∼TeV [61]. The graviton zero mode on the other hand is UV localised and couples with gravitational strength.

2.2.5.2 Vector

In the massive case, only the gauge invariant combination $B^T_\mu - A E^{T\prime}_\mu$ enters into the vector equations of motion

$$\Box \left(B^T_\mu - A E^{T\prime}_\mu\right) = 0 , \tag{2.48}$$

$$\left(A^3 \left(B^T_\mu - A E^{T\prime}_\mu\right)\right)' = 0 . \tag{2.49}$$

The first equation clearly implies that there are no massive vector modes. For a massless vector the equation of motion becomes simply $(A^3 B^T_\mu)' = 0$; however this mode vanishes due to the boundary conditions at the branes.

2.2.5.3 Scalar

For the massive scalar degrees of freedom the equation of motion is given by

$$\frac{1}{A^4\beta^2}\frac{d}{dy}\left(A^4\beta^2\zeta_n'\right) + \frac{m_n^2}{A^2}\zeta_n = 0\,, \tag{2.50}$$

where we have defined the convenient variable $\beta = \phi' A/A'$ and the gauge invariant combination $\zeta = \Psi - \delta\phi/\beta$. There is also an additional constraint equation

$$\Psi' - \frac{A'}{A}\Phi + \frac{1}{3M^3}\phi'\,\delta\phi = 0\,. \tag{2.51}$$

The boundary conditions are given by

$$\delta\phi' - \phi'\Phi = \pm\frac{1}{2}U''_{(0,1)}(\phi)\,\delta\phi\,, \tag{2.52}$$

while the normalisation condition is obtained after diagonalising the action and can be found in Ref. [62].

In the case of massless scalars, Eq. (2.50) is replaced by the system

$$\begin{aligned}\zeta' &= 0\,,\\ \zeta &= -\frac{1}{2A^2}\frac{d}{dy}\left(\frac{A^2}{\phi'}\delta\phi\right)\,,\end{aligned} \tag{2.53}$$

and we have used the additional constraint equation $\Phi = -2\Psi$. Notice that in the massless case there are two dynamical degrees of freedom before imposing the boundary conditions.

2.2.6 Experimental Constraints

So far we have discussed how warped extra dimensional models can address the hierarchy problem, while successfully reproducing the Standard Model and providing a mechanism for generating the fermion mass hierarchy. These models also predict many new states, in particular the KK excitations of the SM fields, as well as additional spin-0 and spin-2 modes. This plethora of new states leads to a rich phenomenology and a wide range of possibilities for probing these models experimentally. However, experiments have yet to see any clear signatures of physics beyond the SM and instead there are a variety measurements which constrain the parameter space of these models. These experimental constraints can be broadly divided into three categories which we shall discuss in turn: electroweak precision measurements, flavour observables, and direct resonance searches.

2.2.6.1 Electroweak Precision Constraints

There is a wealth of precision experimental data on the electroweak sector of the Standard Model, which provides non-trivial constraints on many new physics scenarios. These include measurements at LEP 1 and SLAC on the Z-pole, W boson mass measurements, scattering measurements at LEP 2, and low energy observables from, for example, deep inelastic scattering and atomic parity violating experiments. It turns out that in many models the effects of new physics on the precision electroweak measurements occur only via corrections to the electroweak gauge boson propagators, known as *oblique corrections*. More precisely, this is the case in *universal* models where new physics couples to the SM fermions only through the SM gauge currents. In warped models this assumption is generally a good approximation, but is broken by the fermion localisation; this can lead to non-oblique corrections, such as to the $Z\bar{b}_L b_L$ coupling. The oblique corrections can be conveniently described in terms of only four parameters [63, 64] S, T, W and Y, which are defined in terms of the gauge boson self-energies. Their effects are equivalently related to the presence of the following higher-dimension operators in the low-energy effective Lagrangian

$$\mathcal{O}_S = H^\dagger \sigma_i H W^i_{\mu\nu} B^{\mu\nu} \,, \tag{2.54a}$$

$$\mathcal{O}_T = |H^\dagger D_\mu H|^2 \,, \tag{2.54b}$$

$$\mathcal{O}_W = \left(D_\rho W^i_{\mu\nu}\right)^2 \,, \tag{2.54c}$$

$$\mathcal{O}_Y = \left(\partial_\rho B_{\mu\nu}\right)^2 \,, \tag{2.54d}$$

where σ_i are the Pauli matrices. In practice it is often sufficient to consider only the S and T parameters, as is the case in warped models where the corrections to W and Y are suppressed by ky_c. The relevant bounds obtained from the electroweak precision data are then given by $S = 0.00 \pm 0.08$ and $T = 0.05 \pm 0.07$ [65].

In warped models, there is a tree-level contribution to the oblique parameters which arises from the exchange of electroweak KK gauge bosons. The dominant constraint comes from corrections to the T parameter (see Figure 2.2) and leads to a lower bound on the KK masses of $m_{KK} \gtrsim 13\,(7)\,\text{TeV}$ in the case of a brane (bulk) Higgs [66]. Additionally, there are one-loop contributions with KK top-quarks propagating in the loop, which are calculable in the case of a bulk Higgs but expected to be subdominant. There have been several approaches developed to alleviate these otherwise very stringent bounds on the KK spectrum. One possibility is to introduce an extended custodial $\mathrm{SU}(2)_L \times \mathrm{SU}(2)_R \times \mathrm{U}(1)_{B-L}$ gauge symmetry in the bulk, which is explicitly broken to the SM electroweak subgoup on

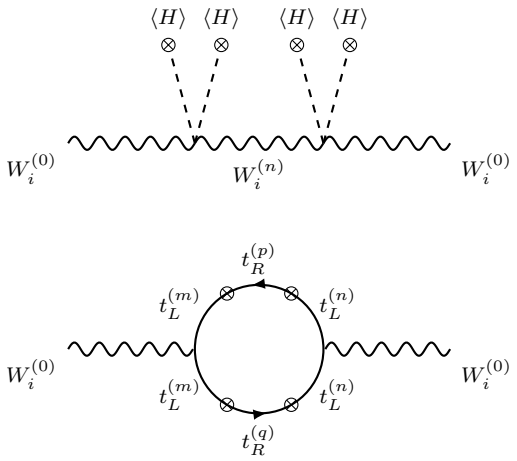

FIGURE 2.2: Tree-level and one-loop contributions to the T parameter from KK gauge bosons and KK top quarks respectively.

the UV brane [67]. This leads to the improved bound $m_{KK} \gtrsim 3\,\text{TeV}$ [66]. Imposing an additional $L \leftrightarrow R$ parity can also provide protection against corrections to the $Z\bar{b}_L b_L$ coupling [68]. Another approach is to modify the geometry such that it deviates from AdS in the IR. This is the case in *soft-wall* models [69–71] where the bound on the KK masses can be as low as 0.8 TeV [66]. Finally, the bounds can also be reduced by including brane-localised kinetic terms for the gauge bosons [72, 73]. Such terms are necessarily generated by loop effects in the bulk [74], however significantly reducing the above bounds requires much larger coefficients than those generated radiatively.

2.2.6.2 Flavour Constraints

Flavour measurements in both the quark and lepton sectors provide some of the most stringent constraints on models of warped extra dimensions (for a review see e.g. [75]) and new physics models in general. In the quark sector the strongest constraints come from CP violating, $\Delta F = 2$ processes and in particular neutral Kaon mixing via corrections to the ϵ_K parameter. The dominant new physics contribution is due to the tree-level exchange of KK gluons and while somewhat ameliorated by the RS GIM mechanism discussed in Section 2.2.4.6, still leads to strong lower limits on their mass. However, as is the case for many flavour observables, the precise bounds are quite model dependent. In this case they depend on the localisation of the Higgs and the values of the 5D Yukawa couplings. Assuming anarchic 5D Yukawa couplings, scans over the parameter space suggest that a KK gluon mass of 3 TeV requires a fine-tuning at the few percent level [76, 77]. These bounds can be alleviated by imposing flavour symmetries that restrict the 5D Yukawa couplings [78–81], metric deviations in the IR [77, 82], or introducing

pseudo-axial gluons [83]. Additionally there are strong bounds from the charm sector, in particular CP violation in $D - \bar{D}$ mixing [76, 84], while weaker bounds arise from B mesons, and CP conserving and $\Delta F = 1$ observables. Finally, there are constraints from contributions to the electric dipole moment of the neutron [85] that give a similar bound on the KK gluon mass of $m_{KK} \gtrsim 3\,\text{TeV}$, although this can be evaded by considering spontaneous CP violation [86].

There are also strong constraints arising from the lepton sector, which provide bounds on the masses of the electroweak KK gauge bosons and KK leptons. The lepton flavour violating decay $\mu \to e\gamma$ leads to the strongest bound $m_{KK} \gtrsim 13\,\text{TeV}$ [75, 87, 88], although the precise value is again sensitive to the Higgs localisation and also the mechanism for neutrino mass generation. Once again the bounds can be reduced by imposing additional symmetries [89–92] or modifying the geometry [93]. Other rare decays and $\mu \to e$ conversion in nuclei also provide somewhat weaker bounds.

2.2.6.3 Direct Searches

The most obvious constraint on new physics models comes from direct searches for the production and decay of new heavy resonances. Currently the most stringent limits are in most cases from searches by the ATLAS and CMS experiments at the LHC. At a proton-proton collider, such as the LHC, the production cross sections for coloured particles are significantly larger than for other particles; the strongest limits on new resonance masses are therefore generally for coloured states.

In warped models, an obvious candidate to search for at the LHC is therefore the heavy KK partners of the gluon. Searches at ATLAS [94] and CMS [95] for KK gluons decaying into top quark pairs constrain the KK gluon mass to be $m_{g_{KK}} > 2.5\,\text{TeV}$. It turns out that there are even stronger limits on the spin-2 KK modes of the graviton. While uncoloured, these states have an effective coupling to gluons and hence a relatively large production cross section. Additionally, they can decay into the experimentally clean dilepton and diphoton final states. Here the results from ATLAS [96, 97] and CMS [98, 99] place constraints on the graviton mass of $m_{G_{KK}} \gtrsim 3.1\,\text{TeV}$ for $k/M_{Pl} = 0.1$. Finally, the radion or spin-0 mode associated with modulus stabilisation provides another promising search strategy. This is especially the case in certain models where it is expected to be the lightest new state. We will provide a detailed discussion of the experimental bounds on the radion in Chapter 4.

2.3 AdS/CFT

So far we have focused our discussion on 5D models in AdS space. Somewhat surprisingly, these models also have a dual description in terms of a 4D conformal field theory (CFT). This AdS/CFT correspondence was originally discussed by Maldacena [100] in the context of string theory. He conjectured that type IIB string theory on $AdS_5 \times S_5$ is dual to $\mathcal{N} = 4$ supersymmetric SU(N) Yang Mills gauge theory in four dimensions.

As a first check, it is clear that the symmetries are the same on both sides of the correspondence. The isometry of AdS_5 is SO(4,2), or the conformal group in four dimensions (see Appendix A), while the isometry of S_5 is $SO(6) \cong SU(4)$, which is the R-symmetry group of the supersymmetric gauge theory. One also finds that the parameters on either side of the correspondence are related according to

$$\frac{R_{AdS}^4}{l_s^4} = 4\pi g_{YM}^2 N \,, \tag{2.55}$$

where $R_{AdS} = 1/k$ is the AdS radius, l_s is the string length and g_{YM} is the SU(N) gauge coupling. It is particularly insightful to consider the limit in which quantum gravitational effects can be neglected and we can calculate quantities on both sides of the correspondence. We are therefore interested in the limit $1/k \ll l_s$, which using Eq (2.55) corresponds to $g_{YM}^2 N \gg 1$ or strong coupling in the 4D gauge theory. Additionally we require that $k/M \sim 1/N < 1$ [101] and so we are considering the gauge theory in the large N limit. Loop effects in the gravitational theory therefore correspond to subleading effects in the $1/N$ expansion in the gauge theory. While the conjecture is that the duality holds in the full (non-perturbative) string theory, we will restrict ourselves to the weaker form of the correspondence defined in this limit and also in the absence of supersymmetry. We then end up with a strong-weak coupling duality between the 4D CFT and the 5D gravity description in AdS. The 5D gravity description therefore provides us with a very useful tool for calculating quantities in the gauge theory at strong coupling!

The precise relationship between observables on both sides of the correspondence was established in Refs. [102, 103]. For each bulk field, ϕ, in AdS there is an associated operator, $\mathcal{O}$, in the CFT. The value of the bulk field on the AdS boundary at $y = -\infty$ ($z = 0$) then acts as a source of the operator in the CFT. In other words, the generating functional of the CFT is given in terms of the gravitational action according to

$$Z[\phi_0] = \int \mathcal{D}\phi_{CFT}\, e^{-S_{CFT}[\phi_{CFT}] - \int d^4x\, \phi_0 \mathcal{O}} = \int_{\phi_0} \mathcal{D}\phi\, e^{-S_{bulk}[\phi]} \,. \tag{2.56}$$

where S_{CFT}, S_{bulk} are the actions in the CFT and the bulk of AdS respectively and ϕ_0 is the boundary value of the bulk field ϕ. In the limit we are considering, one can integrate over the on-shell gravitational action in the bulk, subject to appropriate boundary conditions, to obtain an effective action $S_{eff}[\phi_0]$. We then have a straightforward prescription for computing connected correlation functions in the CFT

$$\langle \mathcal{O} \cdots \mathcal{O} \rangle = \frac{\delta^n S_{eff}}{\delta\phi_0 \cdots \delta\phi_0} \,. \tag{2.57}$$

There is also a relation between the mass of the bulk field and the scaling dimension of the operator in the CFT. This can be verified by computing 2-point correlation functions, which leads to

$$\Delta = 2 + \sqrt{4 + m_\phi^2/k^2} \,, \tag{2.58}$$

where m_ϕ is the bulk mass of the field ϕ. Bulk fields with $m_\phi > 0$ ($-4 \leq m_\phi < 0$) then clearly describe irrelevant (relevant) operators in the CFT. A similar prescription between mass and operator dimensions holds for fields of higher spin and is given in Section 2.3.3.

Finally, it is worth mentioning that the above prescription for the AdS/CFT correspondence is often referred to as *standard quantisation*. It is also possible to consider the so-called *alternative quantisation* whereby the derivative of the bulk field on the boundary is identified with the source in the CFT[†] [104]. In this case the gravitational action is identified with the effective action, or generating functional of 1PI correlation functions, in the CFT. The relation between the operator dimension and bulk mass is then given by $\Delta = 2 - \sqrt{4 + m_\phi^2/k^2}$. This prescription therefore describes operators of dimension $1 \leq [\mathcal{O}] \leq 2$.

2.3.1 Slice of AdS/Breaking the CFT

We have so far limited our discussion to general aspects of the AdS/CFT correspondence. In particular, our discussion has involved the full AdS space ($-\infty < y < \infty$). In this section we will focus on the application of the correspondence to Randall-Sundrum type models and on the role of the UV/IR branes and their interpretation in the context of the dual CFT. The discussion summarised below was developed in Refs. [105–107].

The presence of the UV and IR branes cuts off part of AdS space and breaks the corresponding shift symmetry. They are therefore clearly expected to be related

[†]This corresponds to Neumann boundary conditions for the bulk field as opposed to Dirichlet boundary conditions in the standard case.

to the breaking of conformal invariance in the CFT. The remaining questions are then whether this breaking is explicit or spontaneous and whether the operator responsible for the breaking relevant or irrelevant.

Let us firstly discuss the role of the UV brane, which corresponds to imposing a cut-off on the CFT at some scale $\Lambda_{UV} \lesssim M_{Pl}$, and hence to an explicit breaking of conformal invariance. The inclusion of the UV brane results in the graviton zero mode becoming normalisable and in the dual description we have a CFT coupled to 4D gravity. Another important consequence of adding the UV brane is that source fields on the boundary of AdS become dynamical. Fields living on the UV brane therefore describe an elementary sector coupled to the CFT via Planck suppressed operators. Finally, the presence of the UV brane does not modify the bulk geometry and the CFT clearly remains conformal below the cut-off. The UV brane therefore corresponds to explicit breaking via an irrelevant operator.

The IR brane, on the other hand, corresponds to a spontaneous breaking of the CFT. This can be clearly understood by the presence of a massless mode, the radion, related to fluctuations in the position of the IR brane. This mode is localised towards the IR and remains in the spectrum even in the absence of the UV brane. It is identified with the Nambu-Goldstone boson (NGB) of spontaneously broken scale invariance, known as the dilaton, in the dual CFT. This interpretation of the IR brane can also be established by computing correlation functions on both sides of the correspondence. The two-point function of an operator with dimension, d, in a spontaneously broken CFT is given by

$$\langle \mathcal{O}(p)\mathcal{O}(-p)\rangle = \frac{b_0}{p^{4-2\Delta}} + \sum_i b_i \frac{\langle \mathcal{O}_i\rangle}{p^{4-2\Delta+\Delta_i}}\,, \tag{2.59}$$

where b_i are constants, and $\langle \mathcal{O}_i\rangle$ and Δ_i are respectively the vevs and scaling dimensions of the CFT operators which spontaneously break the conformal invariance. The result obtained via the AdS description [105] shows an exponential suppression in the deviation from conformal invariance (as opposed to the power law behaviour above), demonstrating that the presence of the IR brane corresponds to spontaneous breaking of the CFT by an infinite dimensional operator.

Finally, we discussed in Section 2.2.4 that, once the IR brane is introduced, bulk fields give rise to an infinite KK tower of massive 4D modes. This is completely consistent with the interpretation of the dual CFT as a confining SU(N) gauge theory in the large N limit, where the two-point function is known to be [108–110]

$$\langle \mathcal{O}(p)\mathcal{O}(-p)\rangle = \sum_{n=1}^{\infty} \frac{f_n^2}{p^2 + m_n^2}\,, \tag{2.60}$$

and $f_n = \langle 0|\mathcal{O}|\phi_n\rangle \propto \sqrt{N}/(4\pi)$.

2.3.2 Partial Compositeness

The AdS/CFT correspondence provides us with a dual description of 5D warped models in terms of a strongly-coupled, spontaneously broken 4D CFT that is weakly coupled to an additional elementary sector. As a result, we expect that the physical mass eigenstates will correspond to some admixture of the elementary fields and bound states of the CFT. This is known as *partial compositeness* [111] and in fact has a QCD analogue in the form of photon-ρ meson mixing.

Whether this mixing plays an important role at low-energies will depend on the dimension of the composite operator to which the elementary field is coupled. Consider the following Lagrangian describing an elementary fermion, ψ_L, coupled to a fermionic operator, $\mathcal{O}_R$, in the CFT [112]

$$\mathcal{L} = \mathcal{L}_{CFT} + iZ_\Psi \bar{\psi}_L \gamma^\mu \partial_\mu \psi_L + \left(\frac{\omega}{\Lambda_{UV}^{\Delta_R - 5/2}} \bar{\psi}_L \mathcal{O}_\mathcal{R} + \text{h.c.} \right) . \tag{2.61}$$

For operator dimension $\Delta_R > 5/2$, the coupling responsible for the mixing is irrelevant and can be neglected at low energies. The above Lagrangian then describes an elementary massless fermion external to the CFT. On the other hand if $3/2 < \Delta_R < 5/2$, the mixing arises from a relevant coupling and consequently the massless mode will be a non-trivial admixture of the elementary fermion and CFT bound states.

In order to see this more clearly we can define the dimensionless running coupling $\xi(\mu) = (\mu/\Lambda_{UV})^{\Delta_R - 5/2}\, \omega(\mu)/\sqrt{Z_\Psi(\mu)}$, which satisfies the RG equation

$$\mu \frac{d\xi}{d\mu} = \left(\Delta_R - \frac{5}{2} \right) \xi + a \frac{N}{16\pi^2} \xi^3 + \dots . \tag{2.62}$$

The second term in this expression arises due to wavefunction renormalisation of ψ_L by the CFT, where a is a constant. Solving this equation gives

$$\xi(\mu) = \left(\frac{\mu}{\Lambda_{UV}} \right)^{\Delta_R - \frac{5}{2}} \left[\frac{1}{\xi(\Lambda_{UV})^2} + \frac{aN}{16\pi^2} \frac{1}{\Delta_R - 5/2} \left(1 - \left(\frac{\mu}{\Lambda_{UV}} \right)^{2\Delta_R - 5} \right) \right]^{-\frac{1}{2}} . \tag{2.63}$$

It is then immediately clear that ξ increases (decreases) towards the IR, $\mu \ll \Lambda_{UV}$, for $\Delta_R < 5/2$ ($\Delta_R > 5/2$).

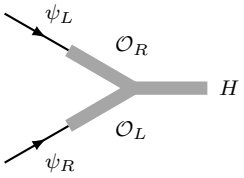

FIGURE 2.3: The Yukawa coupling generated via elementary-composite mixing for light, mostly elementary fermions.

We are now in a position to understand the generation of hierarchical Yukawa couplings in warped models (see Section 2.2.4.5) from the 4D viewpoint. In the case of light, UV localised fermions ($c > 1/2$), the Yukawa coupling to the Higgs is generated via the elementary-composite mixing shown in Figure 2.3. Hence it should take the form[†]

$$\lambda \sim \frac{\sqrt{N}}{4\pi}\xi_L(\Lambda_{IR})\xi_R(\Lambda_{IR})\,. \tag{2.64}$$

where $\Lambda_{IR} \sim$ TeV. As was the case for a bulk scalar, the operator dimension in the CFT is related to the 5D bulk fermion mass according to $d_{L,R} = 3/2 + |c_{L,R} \pm 1/2|$. For $c_L = -c_R > 1/2$, $\xi_{L,R}$ is rapidly decreasing towards the IR and consequently the Yukawa coupling will be suppressed. Substituting the RS expressions for the UV and IR scales we then arrive (up to order one factors) at the 5D expression for the Yukawa coupling in Eq. (2.42). This leads to a relation between the 5D Yukawa couplings and the number of colours in the dual CFT[‡]

$$\lambda_5 k \sim \frac{4\pi}{\sqrt{N}}\,. \tag{2.65}$$

Finally, the elementary-composite mixing can also be seen from the 5D KK viewpoint by making use of the holographic basis [113, 114]. By relating this basis to the usual KK expansion, one finds that UV localised zero modes correspond to mostly elementary states, while IR localised zero modes correspond to massless bound states of the CFT. An exception to this rule is the delocalised gauge field zero modes. Here the mixing arises from a marginal coupling and the gauge zero modes are mostly elementary states.

2.3.3 AdS/CFT Dictionary

To complete our discussion of the AdS/CFT correspondence we provide a useful dictionary which can be used to relate objects on both sides of the correspondence.

[†]The large N scaling can be understood from the fact that the three-point vertex scales as $(4\pi)/\sqrt{N}$ [110].

[‡]The 5D gauge couplings also satisfy a similar relation, $g_5\sqrt{k} \sim (4\pi)/\sqrt{N}$.

Slice of AdS_5	4D CFT + elementary sector
Bulk field, $\phi(x^\mu, y)$	Operator, $\mathcal{O}$
5D bulk mass	Operator dimension, $\Delta_\mathcal{O}$
Scalar	$2 + \sqrt{4 + m_\phi/k}$
Fermion[†]	$\frac{3}{2} + \lvert m_\Psi/k \pm \frac{1}{2}\rvert$
Gauge field	3
Graviton	4
UV localised zero mode	Elementary state
IR localised zero mode	Massless CFT bound state
KK modes ($m_n \neq 0$)	CFT bound states
Gauge symmetry $\mathcal{G}$, broken to $\mathcal{H}_1$ on the IR brane, broken to $\mathcal{H}_2$ on UV brane	Global symmetry $\mathcal{G}$, spontaneously broken to subgroup $\mathcal{H}_1$, with weakly gauged subgroup $\mathcal{H}_2$

2.4 Composite Higgs

So far we have reviewed how models with a warped extra dimension can address the hierarchy problem via an IR localised Higgs field. This can be understood, via the AdS/CFT correspondence, as the statement that the Higgs arises as a bound state of a new strongly interacting sector and is therefore protected from mass scales above the confinement scale. However, the absence of a plethora of new resonances at the LHC suggests that if this scenario is realised in nature, the Higgs should be significantly lighter than the other strong sector resonances. This immediately brings to mind the example of the pions in QCD, which have masses much smaller than Λ_{QCD}. The pions are the Nambu-Goldstone bosons of spontaneously broken chiral symmetry ($\mathrm{SU}(2)_L \times \mathrm{SU}(2)_R \to \mathrm{SU}(2)_V$) and would be massless if not for the small explicit breaking of the symmetry by the quark masses. It therefore seems reasonable that the Higgs could arise as a pseudo-Nambu Goldstone boson of a new strongly interacting sector, where its pNGB nature will protect it from corrections to its mass of order the confinement scale. This idea was originally proposed by Georgi and Kaplan [115] and developed in Refs. [116–120]. In this section we will briefly review some general aspects of composite Higgs models (see e.g. [121, 122] for a more detailed review).

[†]The upper (lower) signs correspond to the case of a left- (right-) handed zero mode.

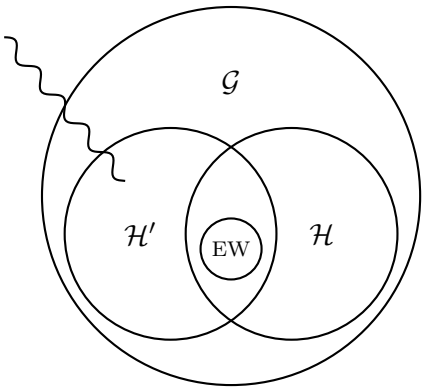

FIGURE 2.4: General symmetry structure for models in which the Higgs arises as a pNGB.

2.4.1 Higgs as a pNGB

We begin by describing the general symmetry breaking structure and conditions necessary to realise a composite Higgs model. Consider a strongly interacting sector with a global symmetry group $\mathcal{G}$, which is spontaneously broken to a subgroup $\mathcal{H}$ at some scale f. The spontaneous breaking will of course result in a set of $n_{NG} = \dim(\mathcal{G}) - \dim(\mathcal{H})$ Nambu-Goldstone bosons living on the coset space $\mathcal{G}/\mathcal{H}$. Now, suppose we gauge a subgroup $\mathcal{H}'$ of the original global symmetry by coupling the strong sector to a set of external gauge bosons. This results in $n_0 = \dim(\mathcal{H}') - \dim(\mathcal{H} \cap \mathcal{H}')$ of the NGBs being "eaten" to give mass to the gauge fields, with $n_{NG} - n_0$ massless modes remaining in the spectrum. This situation is shown in Figure 2.4 and describes the general symmetry breaking pattern of a strongly interacting sector that is weakly gauged by a set of external gauge fields.

Recall that the aim is to be able to identify a subset of the NGBs with a composite Higgs. This leads to two further conditions on the general structure described above. Firstly, we require that the coset space $\mathcal{G}/\mathcal{H}$ should contain an $SU(2)$ doublet which can be identified with the Higgs doublet. Secondly, we assume that the SM electroweak gauge group can be embedded within the unbroken global symmetry, $\mathrm{SU}(2) \times \mathrm{U}(1)_Y \subset \mathcal{H}$. Notice that this means that electroweak symmetry remains unbroken by the $\mathcal{G} \to \mathcal{H}$ symmetry breaking. This is already distinct from the case of QCD (and technicolour) where the vacuum in fact breaks electroweak symmetry and one can consider the pions as being eaten and giving (a very small) mass to the W and Z. This distinction is a key feature of composite Higgs models and allows the electroweak scale, v, to be separated from the $\mathcal{G} \to \mathcal{H}$ symmetry breaking scale, f, via a mechanism known as *vacuum misalignment* [115, 123].

The strong sector symmetry breaking we have just described gives rise to a set of electroweak preserving, equivalent vacuua related by $\mathcal{H}$ transformations. Once

we include the effect of SM gauge interactions, and potentially other couplings to external fields, the symmetry $\mathcal{G}$ is explicitly broken, generating a potential for the NGBs and breaking the vacuum degeneracy. This explicit breaking is characterised by the misalignment angle, θ, which describes the misalignment of the vacuum with respect to the electroweak preserving direction. It is often expressed in terms of the parameter ξ, defined by

$$\xi \equiv \frac{v^2}{f^2} = \sin^2\langle\theta\rangle \,. \tag{2.66}$$

The limit $\xi \to 0$ ($f \to \infty$) then corresponds to the Standard Model, where the Higgs remains light but the strong sector decouples. On the other hand, $\xi \to 1$ is the technicolour limit where there is no separation between the electroweak and compositeness scales. The interesting case for composite Higgs models is $\xi \ll 1$. However, as we shall discuss in Section 2.4.4, one generically expects $\xi \sim 1$ and this leads to a source of fine tuning in these models.

2.4.2 CCWZ Formalism

The general theory of Nambu-Goldstone bosons arising from non-linearly realised or spontaneously broken symmetries was developed by Callan, Coleman, Wess and Zumino (CCWZ) in Refs. [124, 125]. This CCWZ prescription provides a systematic way to construct effective field theories describing the NGBs, including their interactions with non-NGB fields. Here we will briefly give some key results; a more detailed review can be found in Refs. [122, 126].

Consider a compact, connected, semi-simple Lie Group $\mathcal{G}$, with subgroup $\mathcal{H}$. Every group element g, in some neighbourhood of the identity[†], can then be decomposed as

$$g = e^{iu_\alpha X^\alpha} e^{i\xi_i T^i} \,, \tag{2.67}$$

where ξ_i, u_α are real parameters. This separation of generators into those (T^i) which generate the subgroup $\mathcal{H}$ and those which do not (X^α) is known as the Cartan decomposition. The generators then satisfy the commutation relations

$$\left[T^i, T^j\right] = if^{ij}{}_k T^k \equiv T^k \left(t^i_{\mathbf{Ad}}\right)_k{}^j \,, \tag{2.68a}$$

$$\left[T^i, X^\alpha\right] = if^{i\alpha}{}_\beta X^\beta \equiv X^\beta \left(t^i_{\mathbf{r}}\right)_\beta{}^\alpha \,, \tag{2.68b}$$

$$\left[X^\alpha, X^\beta\right] = if^{\alpha\beta}{}_k T^k + if^{\alpha\beta}{}_\gamma X^\gamma \,, \tag{2.68c}$$

[†]For perturbatively describing the NGBs we will only be concerned with local fluctuations and not the global group structure.

for some structure constants, $f^{ij}{}_{k}$. The result in the second line is obtained using the Jacobi identity, where $t^i_{\mathbf{r}}$ is the representation $\mathbf{r}_{\mathcal{H}}$ of $\mathcal{H}$ given by $\mathbf{Ad}_{\mathcal{G}} = \mathbf{Ad}_{\mathcal{H}} \oplus \mathbf{r}_{\mathcal{H}}$.

Now consider a field $\Phi(x)$, which transforms linearly under the group $\mathcal{G}$ and is related to a representative vacuum configuration, $\overrightarrow{F}$, by a local $\mathcal{G}$ transformation

$$\overrightarrow{\Phi}(x) \equiv g(x)\overrightarrow{F}\,. \tag{2.69}$$

Using the fact that any element of $\mathcal{G}$ can be decomposed according to Eq. (2.67), combined with the fact that the vacuum is by definition invariant under $\mathcal{H}$ transformations this expression can be reduced to

$$\overrightarrow{\Phi}(x) = U[\pi]\overrightarrow{F}\,, \tag{2.70}$$

where we have defined the Goldstone matrix

$$U[\pi] \equiv e^{i\frac{\sqrt{2}}{f}\pi_\alpha(x)X^\alpha}\,. \tag{2.71}$$

We see that the Goldstone matrix contains only the fields $\pi_\alpha(x)$ associated with the broken generators. This is consistent with the expectation from Goldstone's theorem which says there should be a massless degree of freedom for each broken generator. Furthermore, it is clear that the NGBs span the coset space $\mathcal{G}/\mathcal{H}$, which identifies elements of $\mathcal{G}$ modulo $\mathcal{H}$.

We are interested in how $U[\pi]$ transforms under $\mathcal{G}$. This will clearly be non-trivial, since a general element of $\mathcal{G}$ cannot be expressed only in terms of the broken generators. However, using Eq.(2.67) it can be defined implicitly by

$$g \cdot U[\pi] = U[\pi'] \cdot h[g,\pi]\,, \tag{2.72}$$

where $h[g,\pi] = \exp(iu' \cdot T)$, and π' and u' are in general non-linear functions of g and π. This then leads to the transformation

$$U[\pi] \to U[\pi'] = g \cdot U[\pi] \cdot h^{-1}[g,\pi]\,. \tag{2.73}$$

It is now clear that $U[\pi]$ transforms *non-linearly* under $\mathcal{G}$, or alternatively that $\mathcal{G}$ is non-linearly realised. If we consider instead a transformation under the subgroup $\mathcal{H}$ such that

$$U[\pi] \to h \cdot U[\pi] \cdot h^{-1}\,, \tag{2.74}$$

one can show using the commutation relations (2.68) and the Baker-Campbell-Hausdorff relation that the NGBs transform according to

$$\pi_\alpha \to \pi_\alpha^{(\mathcal{H})} = \left(e^{iu_i t^i_{\mathbf{r}}}\right)_\alpha^{\ \beta} \pi_\beta \,. \tag{2.75}$$

Hence the NGB fields transform *linearly* under the unbroken subgroup $\mathcal{H}$ in the representation $\mathbf{r}_\mathcal{H}$. On the other hand, the transformation of the NGBs along the broken generators is non-trivial, but for an infinitesimal transformation can be expanded as

$$\pi_\alpha \to \pi_\alpha^{(\mathcal{G}/\mathcal{H})} = \pi_\alpha + \frac{f}{\sqrt{2}}\xi_\alpha + \mathcal{O}\left(\xi\,\pi^2\right) \,. \tag{2.76}$$

This demonstrates the well-known shift symmetry acting on the NGBs.

Finally, we shall briefly discuss how one can construct $\mathcal{G}$ invariant effective Lagrangians involving the NGB fields. A consequence of the above shift symmetry is that any non-trivial invariants must contain derivatives. It turns out that all the invariant terms[†] can be obtained using only two objects, d_μ and e_μ, defined by decomposing the Maurer-Cartan form[‡] in terms of the broken and unbroken generators

$$iU[\pi]^{-1}\partial_\mu U[\pi] = d_{\mu,\alpha}[\pi]X^\alpha + e_{\mu,i}[\pi]T^i \equiv d_\mu + e_\mu \,. \tag{2.77}$$

Unsurprisingly, these objects transform non-linearly under $\mathcal{G}$ through representations of $\mathcal{H}$ in a similar way to $U[\pi]$:

$$d_\mu \to h \cdot d_\mu \cdot h^{-1} \,, \tag{2.78}$$

$$e_\mu \to h \cdot (e_\mu - i\partial_\mu) \cdot h^{-1} \,, \tag{2.79}$$

where $h = h[g, \pi]$. It should then be clear that constructing $\mathcal{G}$ invariant terms is equivalent to constructing terms that are *locally* $\mathcal{H}$ invariant. Under $\mathcal{H}$ transformations, d_μ transforms linearly in the $\mathbf{r}_\mathcal{H}$ representation, while e_μ transforms as a gauge field in the adjoint representation. The latter can therefore be used to construct a field strength and covariant derivative, which is essential in order to include non-NGB fields.

The lowest order (two-derivative) effective Lagrangian then contains (at least) the invariant term

$$\mathcal{L} = \frac{f^2}{4}\mathrm{Tr}\left[d^\mu d_\mu\right] = \frac{1}{2}\partial^\mu\pi^\alpha\partial_\mu\pi_\alpha + \ldots \,. \tag{2.80}$$

In the case of symmetric cosets, this is equivalent to the term $\frac{f^2}{4}\mathrm{Tr}\left[\partial^\mu U^\dagger \partial_\mu U\right]$.

[†]If $\mathcal{G}$ is anomalous there is also the Wess-Zumino-Witten term [127–129].

[‡]The formalism can be straightforwardly extended to include gauge fields in the case that $\mathcal{G}$ is gauged by considering $U^{-1}(A_\mu + i\partial_\mu)U$.

2.4.3 Minimal Models

We will not review any specific composite Higgs models in detail here, and instead refer the interested reader to the extensive literature, where models based on many different cosets have been proposed [130–147]. However, we will briefly mention a few of the minimal models and highlight some additional features which are phenomenologically desirable. In Chapter 6 we shall motivate and investigate the phenomenology of a particular model based on the $\mathrm{SU}(7)/\mathrm{SU}(6)\times\mathrm{U}(1)$ coset [148].

As discussed previously, the minimal requirements on the strong sector are that the unbroken symmetry, $\mathcal{H}$, contains $\mathrm{SU}(2)\times\mathrm{U}(1)_Y$ as a subgroup and the coset space contains an $\mathbf{2_{1/2}}$ multiplet corresponding to the Higgs. However, it is generally assumed that the unbroken symmetry group is enlarged to contain the custodial group $\mathrm{SO}(4)\cong\mathrm{SU}(2)_L\times\mathrm{SU}(2)_R$, with the Higgs transforming as a **4**-plet of SO(4) or equivalently an $\mathrm{SU}(2)_L\times\mathrm{SU}(2)_R$ bidoublet. This custodial symmetry is explicitly broken by the gauging of $\mathrm{U}(1)_Y$ embedded in $\mathrm{SU}(2)_R$ and by the Yukawa couplings. On the other hand, when the Higgs acquires a vev the symmetry is only broken to the custodial group $SO(3)$ or $\mathrm{SU}(2)_V$, under which the three $\mathrm{SU}(2)_L$ gauge bosons transform as a triplet. This is then sufficient to protect the W/Z mass ratio or ρ parameter, which has been precisely measured at LEP. Equivalently, from the point of view of the effective Lagrangian, the SO(4) custodial symmetry forbids the dimension-6 operator in Eq. (2.54b) which would otherwise provide large corrections to the T parameter. The requirement of custodial symmetry strongly disfavours, for example, the minimal $\mathrm{SU}(3)\to\mathrm{SU}(2)\times\mathrm{U}(1)_Y$ coset.

The minimal coset that includes this custodial symmetry is SO(5)/SO(4), which gives rise to four Nambu-Goldstone bosons transforming as a **4**-plet of SO(4). The family of so-called Minimal Composite Higgs Models (MCHMs) [137] are based on this symmetry breaking pattern. Freedom in the choice of fermion representations under SO(5) means that the symmetry breaking pattern alone does not specify a unique model. In the partial compositeness paradigm, the elementary fermions with SM quantum numbers couple linearly to strong sector operators, which must necessarily come in representations of SO(5). It turns out for the MCHM coset that the global symmetry group must be extended by an additional $\mathrm{U}(1)_X$ in order for these operator multiplets to have the correct quantum numbers when decomposed under the electroweak gauge group. This additional $\mathrm{U}(1)_\mathrm{X}$ remains unbroken and therefore does not affect the symmetry breaking or give rise to any additional NGBs. The most commonly considered fermion representations for the SM quarks are the **5** and **10** of SO(5) giving rise to what are known as the MCHM_5

and MCHM_{10} respectively [149]†. A useful table listing non-minimal cosets that have been considered in the literature is provided in Ref. [150].

Our discussion of composite Higgs models has so far focused on their global symmetry structure, which is sufficient in order to write down an effective Lagrangian describing the NGBs. However, these low-energy effective Lagrangians must ultimately be replaced by some UV completion. An important additional consideration is then whether the desired symmetry breaking pattern can be achieved in a realistic UV completion, in particular without the need for the reintroduction of additional elementary scalars. Such considerations may favour certain symmetry breaking patterns [151–153].

2.4.4 Higgs Potential

By construction, the symmetry breaking in the strong sector leaves the electroweak gauge group unbroken and therefore an external, explicit breaking of the symmetry $\mathcal{G}$ is required in order to trigger electroweak symmetry breaking (EWSB). An immediate source of explicit breaking is provided by the gauging of the $\text{SU}(2) \times \text{U}(1)_Y$ subgroup by the external gauge bosons. This will generate a potential for the NGBs, and in particular the Higgs, at loop-level via diagrams of the type shown in Figure 2.5. Resumming these 1-loop diagrams leads to the usual Coleman-Weinberg form for the potential [154], which can be expressed schematically as

$$V(h) \sim \int \frac{d^4q}{(2\pi)^4} \log\left(1 + \frac{1}{4}\frac{\Pi_1(q^2)}{\Pi_0(q^2)}\sin^2(h/f)\right) . \tag{2.81}$$

Notice that unlike the textbook case involving elementary fields, here we have the appearance of momentum-dependent strong sector form factors $\Pi_{0,1}(q^2)$, in this case related to the gauge field propagator and the vertex respectively. These form factors depend on the details of the strong sector and cannot be calculated in perturbation theory. The large q^2 dependence of these form factors also determines the convergence of the above integral. While the form factors cannot be calculated, use of the operator production expansion, in addition to the assumptions of large N and vector meson dominance, lead to the Weinberg sum-rules [155], which can be used to evaluate the potential. Applying this method to, for example, QCD allows one to calculate the difference between the charged and neutral pion masses in terms of m_ρ and m_{a_1}.

†The spinorial **4** representation of SO(5) has also been considered [137], but leads to unacceptably large corrections to the $Z\bar{b}_L b_L$ coupling.

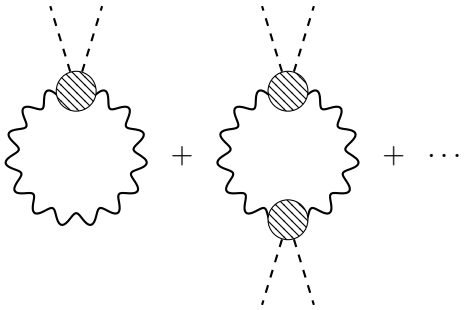

FIGURE 2.5: One-loop contributions of the SM gauge fields to the Higgs potential.

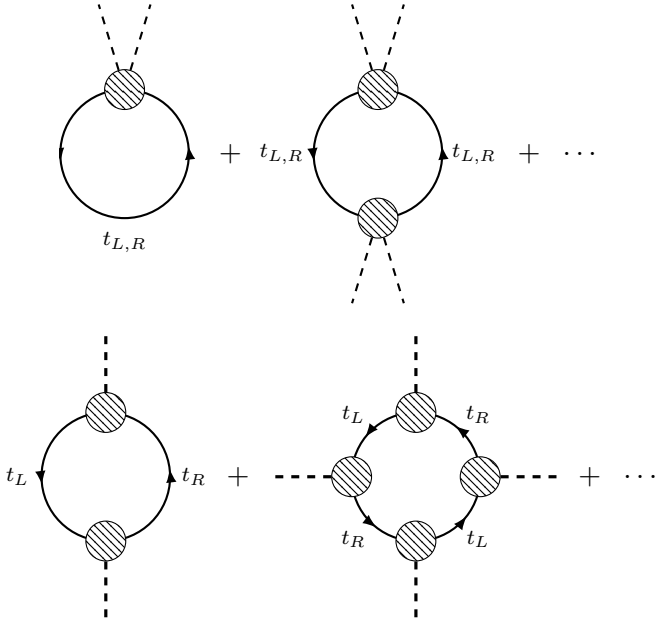

FIGURE 2.6: One-loop contributions from the top quark to the Higgs potential.

However, it was shown by Witten in Ref. [156] that for a general vector-like, confining gauge theory, the radiative potential generated by the gauge fields always aligns the vacuum such that the gauge symmetry is preserved. An additional source of explicit breaking is then necessary to induce EWSB. In the original Georgi and Kaplan paper [115], this was provided by an additional elementary scalar which mixed with the Higgs. Another possibility is to enlarge the external gauge group by an additional U(1) such that the entire gauge group cannot be embedded in $\mathcal{H}$ [117]. It is now well known that the SM top quark can also provide an additional source of explicit breaking proportional to the top Yukawa, which gives another contribution to the pNGB potential (see Figure 2.6) that can trigger EWSB [137]. This is the mechanism employed in most modern constructions.

For the purposes of this discussion we wish to remain model-independent, while still discussing the qualitative features of the Higgs potential. It is useful to expand the Higgs potential in powers of h/f, which we expect to be a good approximation

due to the constraint $v/f \ll 1$ from precision measurements. Combining this with the fact that the potential is radiatively generated leads to the form

$$V(h) = \frac{g_{SM}^2 m_*^2}{16\pi^2}\left(-a|h|^2 + \frac{b}{2f^2}|h|^4\right) + \dots . \tag{2.82}$$

Here we have assumed that some SM couplings g_{SM} are responsible for generating the potential, m_* is the mass of the lightest non-NGB resonance of the strong-sector and acts as a cut-off scale, and a, b are unknown $\mathcal{O}(1)$ coefficients. The various factors in this expression arise from using naive dimensional analysis (NDA)[†] [159, 160] and can be simply understood as follows: $1/(16\pi^2)$ is the one loop factor, each strongly interacting field comes with a factor $1/f$, and there is an overall factor of m_*^4/g_*^2.

The ratio of the two scales appearing in Eq. (2.82), $g_* \equiv m_*/f$, can be interpreted as the generic coupling between states in the strong sector and as a result should satisfy $g_* \lesssim 4\pi$ [159]. If the underlying strong dynamics is described by a large N gauge theory, it can also be related to the number of colours as $g_* \sim (4\pi)/\sqrt{N}$, consistent with the fact that in the $N \to \infty$ limit there is a tower of non-interacting mesons. Interestingly, the discovery of the Higgs boson and in particular the measurement of its mass at $m_h = 125\,\text{GeV}$ suggests that this coupling should be $g_* \ll 4\pi$, contrary to the expectation in early composite Higgs or technicolour-like models and distinct from the case of QCD. In other words, while arising from some strongly coupled sector, the resonances themselves are in fact expected to be *weakly coupled*! This can be seen by expressing v and m_h in terms of the parameters defined in Eq. (2.82) as

$$v^2 = \frac{a}{b}f^2\,, \qquad m_h^2 = 4bv^2\frac{g_{SM}^2 g_*^2}{16\pi^2}\,, \tag{2.83}$$

where taking $g_{SM}^2 = N_c\, y_t^2$ then requires $g_* \simeq 2$ for $b \sim \mathcal{O}(1)$.

From the above equation we can also identify the main source of fine-tuning in composite Higgs models that arises from the requirement that $v/f \ll 1$. Notice that to obtain $v/f \ll 1$ one could imagine taking b to be large; this is precisely what happens in Little Higgs models [130, 131], where collective symmetry breaking [161] suppresses the $|h|^2$ term, while the quartic is generated at tree-level. However, it's clear from Eq. (2.83) that this would also have the unwanted effect of raising the Higgs mass. Naively this could be compensated for by further reducing g_*; however

[†]More generally NDA requires that the effective Lagrangian take the form $\mathcal{L} = \frac{m_*^4}{g_*^2}\left[\frac{\partial}{m_*}, \frac{g_*\pi}{m_*}, \frac{g_*\sigma}{m_*}, \frac{g_*\Psi}{m_*^{3/2}}, \frac{g\cdot A_\mu}{m_*}, \frac{\lambda\psi}{m_*^{3\cdot 2}}\right]$ for NGBs (π), scalar/vector and fermionic composite resonances (σ, Ψ) and external gauge fields and fermions (A_μ, ψ) [157, 158].

in practice it's generally not possible to have $g_* < g_{SM}$, consistent with treating the explicit breaking due to the SM fields as a perturbation on the strong sector. The remaining option is then to require that $a \ll 1$, which can generally only be achieved by fine-tuning between the various contributions to the potential. Current experimental bounds lead to a fine tuning of order $\Delta \sim 1/\xi \lesssim 5 - 10\%$ [150, 162].

So far we have assumed that the strong sector satisfies what is known as *one-scale-one-coupling*, which is the idea that the strong sector resonances can be described using only f and g_*. This is commonly generalised to allow the vector and fermion resonances to be described by separate couplings, g_ρ and g_ψ. The reason for this is straightforward. Firstly, the vector resonances are constrained to be heavy in order to avoid large corrections to the S parameter. To satisfy this constraint without introducing additional fine tuning we would like to increase g_ρ rather than raising f. On the other hand, in many models the dominant contribution to the Higgs quartic actually arises from the light fermionic resonances which mix with the top quark [149, 163], the so-called *top partners*. In order to obtain the correct Higgs mass, without additional fine tuning in b, we would therefore like g_ψ to be small (i.e. $m_\psi \ll m_\rho$). This gives rise to the statement that the light Higgs mass means we should expect the presence of light, coloured, fermionic top-partners at the LHC [162, 163].

Finally, an interesting alternative which we will not discuss here are *twin Higgs* models [138], where a discrete $\mathbb{Z}_2$ symmetry allows the top partners to be colour singlets under the Standard Model SU(3). The twin Higgs mechanism has recently been combined with the composite Higgs framework [164–166]. These models are a subset of a more general class of so-called *neutral naturalness* models.

2.4.5 Gauge-Higgs Unification

We have already seen that 5D warped models have a dual description, via the AdS/CFT correspondence, in terms of a strongly-coupled 4D CFT in the large N limit. It is therefore perhaps unsurprising that the composite Higgs models we have been describing can also be realised in the context of a warped model. These models go under the name of Gauge-Higgs unification (GHU) [135, 137], where the Higgs is identified as the fifth component of a bulk gauge field [167, 168]. They are particularly useful due to the fact that both the meson spectrum and, perhaps more importantly, the Higgs potential are calculable.

In our discussion of gauge fields in warped extra dimensions in Section 2.2.4.2, we found that a 5D gauge field gives rise to a tower of massive 4D vector modes,

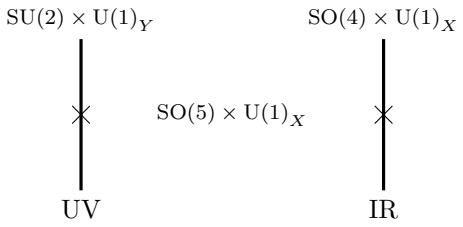

FIGURE 2.7: Symmetry structure for a Gauge-Higgs unification model based on the SO(5)/SO(4) coset.

possibly in addition to a massless vector or scalar mode depending on the boundary conditions. Previously we considered the case of Neumann boundary conditions for A_μ on the two branes, which results in a massless 4D vector mode to be identified with a SM gauge field. Alternatively, taking Neumann boundary conditions for A_5 yields a massless 4D scalar mode, which is crucially localised towards the IR brane. An interesting possibility is that such a scalar zero mode could in fact play the role of the Higgs boson.

This motivates considering an enlarged bulk gauge group $\mathcal{G}$, which is broken by the boundary conditions to the subgroups $\mathcal{H}'$ and $\mathcal{H}$ on the UV and IR branes respectively. There is then a set of massless 4D vector modes, $A_\mu^{a(0)}$, transforming under $\mathcal{H}' \cap \mathcal{H}$ and massless 4D scalars, $A_5^{\hat{a}(0)}$, living on $\mathcal{G}/\mathcal{H}' \cap \mathcal{G}/\mathcal{H}$. Moreover, in terms of the dual CFT description, the IR breaking corresponds to a *spontaneous* breaking of the CFT's global symmetry, while the UV breaking corresponds to *gauging* a subgroup of the global symmetry. The 5D situation described above is then completely analogous to the general framework of composite Higgs models described in Section 2.4.1, where here the $A_5^{\hat{a}(0)}$ are identified as the NGBs of the spontaneously broken symmetry.

It is straightforward to apply this framework to specific composite Higgs models, such as the MCHM as shown in Figure 2.7. In this case the SO(5) × U(1)$_X$ bulk gauge is symmetry broken down to SU(2) × U(1)$_Y$ and SO(4) × U(1)$_X$ by the boundary conditions on the UV and IR branes respectively.

We still need to consider how to generate a potential for the NGBs from the 5D perspective, since a tree-level potential for the $A_5^{\hat{a}}$ modes is forbidden by 5D gauge invariance. However, a potential can be generated by non-local operators [169, 170], which can be constructed from the gauge invariant Wilson line

$$\begin{aligned} &\mathrm{Tr}\,\mathcal{P}\,\exp\left[-i\int_0^{y_c} dy\, e^{ky} A_5^{\hat{a}}(x^\mu, y) t^{\hat{a}}\right] \\ =&\mathrm{Tr}\,\mathcal{P}\,\exp\left[-i\,\frac{g_5\sqrt{k}}{\sqrt{2}\,k e^{-ky_c}} A_5^{\hat{a}(0)}(x^\mu) t^{\hat{a}}\right], \end{aligned} \tag{2.84}$$

where $A_5(x^\mu, y) = g_5\sqrt{2k}\, e^{k(y-y_c)} A_5^{(0)}(x^\mu)$. The related variable with endpoints located in the bulk can be made to vanish via a gauge transformation and so the potential corresponds to a finite-volume effect, generated by bulk loops which connect the two branes. This should not be surprising given that the spontaneous and explicit breakings occur on separate branes. Furthermore, the potential is necessarily finite since any divergences could not be absorbed by a local counterterm in 5D. It will clearly be a periodic function of $A_5^{(0)}$ as expected for a pNGB, where we can also identify $f \sim \sqrt{2}\, k e^{-ky_c}/(g_5\sqrt{k})$. There will be contributions to the potential from loops of both bulk gauge fields and bulk fermions, however in practice it is often simpler to compute the one-loop potential by using the standard Coleman-Weinberg formula and explicitly summing over the KK modes [171].

Finally, another related possibility is to employ dimensional deconstruction [172, 173], effectively discretising the extra dimension and replacing it with a 4D model containing a number of connected sites. Such *multi-site* models [174, 175] provide an effective description of the lowest (few) KK modes, in addition to the pNGBs. The effective potential can be rendered finite by collective symmetry breaking [161].

2.4.6 Experimental Constraints

Finally, we come to the constraints on composite Higgs models from precision experiments and direct searches. Some of these have already been discussed in the preceding sections, however we will reiterate them here for completeness. Furthermore, many of the constraints are similar to those discussed in the context of warped models, which is not particularly surprising given that they are linked through AdS/CFT. That being said, the additional global symmetry structure necessary in composite Higgs models does lead to qualitatively different phenomenology and hence additional experimental constraints. The precise constraints will of course depend on both the global symmetry structure and the fermion representations. Since our goal is to provide a model-independent overview, we will restrict ourselves to a qualitative discussion. A review of quantitative bounds for several MCHMs can be found in Ref. [122].

2.4.6.1 Electroweak Precision Constraints

As was the case in warped models, the heavy vector and fermion resonances in composite Higgs models give corrections to the oblique parameters at tree and one-loop level respectively. This leads to stringent lower bounds on the masses of these resonances from electroweak precision measurements. In almost all realistic

models, these bounds are reduced by imposing custodial symmetry, which forbids tree-level contributions to the T parameter. However, in MCHMs the constraint from corrections to the S parameter still leads to a bound of $m_\rho \gtrsim 2\,\text{TeV}$ on the mass of the vector resonances [122]. An additional correction to the oblique parameters arises from modification of the Higgs couplings to the electroweak gauge bosons due to the non-linear dynamics [176]. Note that we did not consider such corrections in the context of warped models, where modifications of the Higgs couplings are generally taken to be small. The leading contributions are entirely determined by the symmetry breaking pattern and for SO(5)/SO(4) the correction to the T parameter provides the dominant constraint, leading to the bound $f \gtrsim 1.1\,\text{TeV}$. This is then clearly a significant cause of fine-tuning in composite Higgs models. However, including the contributions from the vector and fermion resonances can lead to cancellations in the corrections to S and T, potentially reducing the bound.

There are also important constraints from non-oblique/non-universal effects due to the partial compositeness of the fermions. Such effects are negligible for the first two generations, but can be large for the third generation where a high degree of compositeness is required to generate the large top mass. The most stringent constraint is due to corrections to the $Z\bar{b}_L b_L$ coupling; this leads to strong bounds on the masses of the fermionic resonances, in particular the bottom partners [177] which give a tree-level contribution. As was the case in warped models, the bounds can be evaded by expanding the custodial symmetry from $\text{SO}(4) \simeq \text{SU}(2)_L \times \text{SU}(2)_R$ to O(4) via the inclusion of a left-right parity, P_{LR} [68]. Finally, one also generally expects deviations in the coupling of the Z to top quarks, which may provide competitive constraints in the future with more precise measurements of V_{tb} [178].

2.4.6.2 Flavour Constraints

Flavour bounds provide potentially some of the most stringent constraints on composite Higgs models and the situation is again similar to generic warped models. Within the partial compositeness framework, the most commonly considered possibility is for the couplings generating the elementary-composite mixing to be of the same order in the UV, such that the mass and CKM hierarchies are generated by the different operator dimensions; this is the so-called *anarchic* scenario. The dominant bounds in the quark sector then arise from CP violating processes, in particular neutral Kaon mixing. In the case of a pNGB Higgs the bound is stronger than in generic warped models [179] and requires $f \gtrsim 10\,\text{TeV}$. The bounds can be

reduced by moving away from the anarchic scenario and requiring that the composite sector satisfy additional flavour symmetries [180–183] in order to realise minimal flavour violation[†]. However, these models generally come at the expense of a natural explanation for the quark mass and mixing hierarchy.

If the anarchic scenario is also implemented in the leptonic sector, there are even more stringent constraints arising from bounds on the electron electric dipole moment and the decay $\mu \to e\gamma$, which require $f \gtrsim 11,25\,\text{TeV}$ respectively [87, 122, 184]. Once again, these bounds can be reduced by imposing discrete [185–187] or continuous [188] flavour symmetries.

2.4.6.3 Direct Searches

Composite Higgs models lead to a potentially rich collider phenomenology and both heavy vector and fermionic resonances, as well as any additional pNGBs, could potentially be discovered at the LHC. We have previously seen that naturalness arguments, when combined with the observed Higgs mass, generally suggest that we should expect the presence of light fermionic partners of the top quark. These therefore provide an extremely promising way to probe natural composite Higgs models at the LHC. Depending on the global symmetry group and the fermion embedding, the top partners can have a variety of quantum numbers under the SM gauge group. In the case of the MCHM$_5$, one expects two $\text{SU}(2)_L$ doublets with hypercharges 1/6 and 7/6, as well as a state with the same quantum numbers as the right-handed top. The second doublet leads to an exotic charge 5/3 state and more generally other such exotic states are possible. As a result, both ATLAS [189–194] and CMS [195–199] have a variety of searches for vector-like quarks, with dedicated searches for both heavy vector-like top and bottom resonances as well as charge 5/3 states. These lead to lower bounds on the fermionic resonance masses in the range 700–900 GeV.

Electroweak precision and flavour constraints suggest that we should expect the vector resonances to be significantly heavier than their fermionic counterparts. Nevertheless, we can obtain lower bounds on their masses from LHC searches in a variety of final states. In addition to heavy (or KK) gluons, discussed in the context of warped models, there are potentially a variety of other resonances depending on the unbroken symmetry in the strong sector. In MCHMs one expects triplets and singlets under $\text{SU}(2)_L \times \text{SU}(2)_R$, with bounds in the range 1–3 TeV [200, 201]. Finally, the vector resonances' decay chain could involve intermediate heavy

[†]Minimal flavour violation (MFV) requires that the $\text{U}(3)_{q_L} \times \text{U}(3)_{u_R} \times \text{U}(3)_{d_R}$ flavour symmetry is broken only by the Yukawa matrices.

fermions given the expected mass separation. In this case the bounds from the existing searches can be significantly weaker, motivating the need for dedicated searches [202, 203].

Linear Dilaton

3.1 Introduction

In the preceding chapter we reviewed how extra dimensional models provide one possibility for addressing the hierarchy problem. Firstly we discussed the case of large extra dimensions, where the fundamental scale of gravity can be near the TeV scale, while the 4D effective Planck mass arises as a consequence of the large extra-dimensional volume. We then presented a detailed discussion of warped models, where the warping of the metric causes the cut-off to depend on the location along the extra dimension. The Higgs is localised towards the IR brane where the cut-off is exponentially suppressed. In this chapter we shall consider an interesting model which draws upon features of both of these scenarios. It contains both a relatively large extra dimension ($\sim$nm) as in ADD models, but has a warped metric with branes located at the endpoints of the extra dimension as in RS models.

The model we will consider was originally motivated by considering stacks of NS-5 branes in string theory. In the limit of zero string coupling, where gravity decouples, the NS-5 branes give rise to Little String Theory; a strongly-coupled nonlocal theory in six dimensions with no (apparent) Lagrangian description [204, 205]. Through the use of holographic arguments [100, 206] (of which the AdS/CFT correspondence discussed in Section 2.3 is an example), a seven dimensional dual gravitational description can be obtained and used to study the phenomenology of TeV Little String Theory [207]. Compactifying two of the extra dimensions leads to an effective 5D description known as the linear dilaton model [208]. In this chapter we investigate some phenomenological aspects of this 5D effective model, which is known to exhibit a distinctive graviton Kaluza-Klein spectrum, consisting of a $\sim$ TeV mass gap followed by a near continuum of KK resonances separated by only $\sim$ 30 GeV [208, 209].

Just like in previous solutions to the hierarchy problem involving extra dimensions, the issue of stabilising the extra dimension is important. The purpose of

this work is to investigate the stabilisation of the 5D linear dilaton model and study the resulting radion phenomenology. An interesting feature of this model is that it already comes equipped with a bulk scalar field, the dilaton[†], that can be used to stabilise the extra dimension. By adding boundary potentials, as in the Goldberger-Wise mechanism, a stabilising potential can be obtained. The usual simplifying assumption, following from Ref. [42], is to consider infinite boundary mass terms. However in our analysis we will relax this condition and wherever possible consider finite, or else finite but large boundary mass terms, similar to the general analysis considered in Ref [59, 62]. Apart from the usual radion couplings to the trace of the energy-momentum tensor, this leads to new radion couplings to SM fields that are confined to the brane. We present the Feynman rules and use them to study the radion phenomenology in this setup.

We find that, similar to the graviton KK spectrum, the radion mass spectrum consists of a near continuum of resonances spaced by ~ 30 GeV together with a massive radion zero mode. The radion zero-mode and lowest KK mode masses can be parametrically lighter than the $\sim$ TeV mass gap by suitably choosing the boundary mass parameters. The radion couples to the trace of the energy-momentum tensor in the usual way, but in addition there is a new direct coupling between the dilaton and the SM fields. The typical strength of these couplings is of order $(10\ \text{TeV})^{-1}$, with the dilaton coupling being further suppressed by a factor inversely proportional to the boundary mass term. The SM fields have larger couplings to the radion compared to the near-continuum, and therefore the zero mode will be the first observable mode.

Furthermore, as is well known, the radion can kinetically mix with the Higgs boson via a Higgs-curvature interaction, but since the typical coupling strength is of order $(10\ \text{TeV})^{-1}$ the effects on Higgs phenomenology are negligible. On the other hand, the production and decay of the radion does lead to observable signals at the LHC. In particular, due to the additional coupling between the radion and gauge boson kinetic terms, the branching fraction to $\gamma\gamma$ can be significantly enhanced and we show that searches in this channel provide the strongest constraints on the parameter space of the model.

The outline of this chapter is as follows. In Section 3.2 we briefly review the 5D linear dilaton model of Ref. [208]. In Section 3.3 we identify the radion and solve for the KK mass spectrum in the limit of large but finite boundary mass terms. The radion couplings to SM fields are computed in Section 3.4 where the effects of

[†]Throughout this chapter we use the term *dilaton* to refer to the 5D bulk field in order to remain consistent with the original literature [208]. In subsequent chapters we will use *dilaton* to refer to the 4D field associated with the spontaneous breaking of scale invariance.

mixing from a Higgs-curvature interaction are also included. The phenomenology of the radion is presented in Section 3.5 where the radion decay widths, branching fractions and production at the LHC are studied. Recent LHC results are then used to constrain the parameter space of the model. Finally in Section 6 we summarise our results. Further details of the computations are included in Appendix B, including the Feynman rules for the radion couplings.

3.2 Linear Dilaton Model

The set-up of the linear dilaton model is similar to the Randall-Sundrum scenario, with a finite extra dimension, z, compactified on a $\mathbb{Z}_2$ orbifold, except that we take the TeV scale to be the fundamental scale and the 4D Planck mass as the derived scale. There are two branes, which we refer to as the visible and hidden branes, located at $z = 0$ and $z = r_c$ respectively. The Standard Model fields are confined to the $z = 0$ brane[†]. We also introduce a 5D bulk scalar field known as the dilaton. In the Einstein frame we have the following action [208]

$$S_{bulk} = \int d^5x\sqrt{-g}\left[M^3\left(\mathcal{R} - \frac{1}{3}(\partial\phi)^2\right) - e^{\frac{2}{3}\phi}\Lambda\right] - \int d^4x\sqrt{-\hat{g}}\, e^{\frac{1}{3}\phi}\left(\mathcal{L}_{vis(hid)} - U_{vis(hid)}\right) , \quad (3.1)$$

where ϕ is the dilaton field and M is the fundamental scale, which is of order the TeV scale. For later convenience we have also chosen a non-standard normalisation for ϕ, which differs from the general scalar-gravity action given in Eq. (2.13). In the conformal coordinate, z, the background solutions to the field equations are given by

$$\phi(z) = \alpha|z| , \quad (3.2)$$

$$ds^2 = e^{-\frac{2}{3}\alpha|z|}\left(\eta_{\mu\nu}dx^\mu dx^\nu + dz^2\right) , \quad (3.3)$$

where $\phi(z)$ denotes the background value of the dilaton field, ϕ, and $|\alpha| < \frac{3M}{2\sqrt{7}}$ is required to ensure the 5D curvature is smaller than the fundamental scale. There are also the following constraints

$$\Lambda = -M^3\alpha^2, \quad U_{vis} = -U_{hid} = 4\alpha M^3 , \quad (3.4)$$

[†]Allowing the SM gauge fields to propagate in the bulk results in an effective 4D gauge coupling that is too suppressed [208].

which include the usual tuning of the 4D cosmological constant and radion effective potential.

Taking the curvature term in the action (3.1) and integrating over the fifth dimension yields the effective 4D Planck mass,

$$M_{Pl}^2 = 2\int_0^{r_c} dz\, e^{-\alpha|z|} M^3 = -2\frac{M^3}{\alpha}\left(e^{-\alpha r_c} - 1\right) . \tag{3.5}$$

We then clearly require that $\alpha < 0$ and $|\alpha r_c| \sim 70$ in order to obtain the required value for M_{Pl}.

In order to allow a straightforward comparison with the RS model, we can perform the following coordinate transformation $dy = e^{-\frac{1}{3}\alpha z} dz$. In the new coordinate the metric becomes

$$ds^2 = \left(1 + \frac{|\alpha y|}{3}\right)^2 \eta_{\mu\nu} dx^\mu dx^\nu + dy^2 . \tag{3.6}$$

We can now see that this model exhibits a power-law warping as opposed to the exponential warping of the RS model. The size of the extra dimension must therefore be substantially larger in this case in order to obtain the necessary hierarchy. Taking $|\alpha| \sim$ TeV and enforcing the correct value for M_{Pl} allows us to determine the proper length of the extra dimension, giving $y_c \sim 10$ nm. This compares with a proper length of ~ 0.1 mm in the ADD model (for two extra dimensions) and $\sim 10^{-31}$ cm in the RS model.

The linear dilaton model has an interesting spectrum of graviton KK modes. There is a single massless mode, which has a flat profile in the extra dimension and is identified with the usual 4D graviton. In addition, there is a KK tower of excited states, with a mass spectrum given by

$$m_n^2 = \frac{\alpha^2}{4} + \left(\frac{n\pi}{r_c}\right)^2 , \tag{3.7}$$

where $n = 1, 2, 3, \ldots$. Of particular interest is the large mass gap between the massless graviton and the first of the KK modes, which are then closely spaced. The mass gap is determined by the curvature scale, α, and for a TeV mass gap we find that $r_c \sim (30 \text{ GeV})^{-1}$ and the KK modes essentially form a continuum of states. The graviton KK modes are localised near the SM ($z = 0$) brane, and their couplings to the Standard Model fields are given in Ref. [208]. They are found to couple to SM fields with a strength of order $(80 \text{ TeV})^{-1}$ for the lowest mode.

3.2.1 Stabilisation

In order to truly solve the hierarchy problem the interbrane distance must be stabilised. In the linear dilaton solution of Ref. [208] this can be done by using a variation of the Goldberger-Wise mechanism. Unlike the Randall-Sundrum scenario, the linear dilaton model naturally includes a bulk scalar field, the dilaton, that can in fact play the role of the stabilising field once it acquires a vacuum expectation value on the branes.

We begin by taking boundary potentials of the form

$$U_{vis(hid)}(\phi) = \pm\lambda_{vis(hid)} + \mu_{vis(hid)}M^3(\phi - \phi_{vis(hid)})^2\,, \tag{3.8}$$

where $\lambda_{vis(hid)}$, $\mu_{vis(hid)}$ and $\phi_{vis(hid)}$ are constants. At this point it is useful to formulate the model in terms of the solution generating method of [46], by considering the superpotential $W(\phi) = W_0 e^{\frac{\phi}{3}}$, where W_0 is a constant. The background field equations include two junction conditions at the boundaries, which can now be expressed as

$$W(\phi) = \pm\frac{1}{2}e^{\frac{\phi}{3}}U_{vis(hid)}(\phi)\,, \tag{3.9}$$

$$\frac{\partial W(\phi)}{\partial\phi} = \pm\frac{1}{2}\frac{\partial}{\partial\phi}\left(e^{\frac{\phi}{3}}U_{vis(hid)}(\phi)\right)\,. \tag{3.10}$$

Using Eq. (3.8), these equations can only be simultaneously satisfied if $\phi = \phi_{vis(hid)}$ on the boundaries. Thus we see that ϕ has developed a non-zero vacuum expectation value on the branes as a result of imposing the boundary potentials (3.8) (setting $\mu_{vis(hid)} = 0$ also satisfies the conditions, however this simply reproduces the unstabilised case). It is worth noting that an additional linear term can be added to the boundary potential, however this simply shifts the value of the VEV and the potential can always be rewritten in the form (3.8). The requirement that $\phi = \phi_{vis(hid)}$ on the boundaries then gives

$$\lambda_{vis(hid)} = W_0 = 2\sqrt{-\Lambda M^3}\,, \tag{3.11}$$

where we have used the definition of the bulk potential from the action (3.1). The condition (3.11) includes the usual tuning of the 4D cosmological constant in (3.4) necessary to obtain a flat brane solution.

The background solution for the bulk scalar is once again given by

$$\phi(z) = \alpha|z| + \bar{\phi}\,, \tag{3.12}$$

where here we have included the integration constant, $\bar{\phi}$, which was previously taken to be zero. Imposing the boundary conditions $\phi = \phi_{vis}$ and $\phi = \phi_{hid}$ on the $z = 0$ and $z = r_c$ branes respectively, we then find that

$$\bar{\phi} = \phi_{vis}\,, \tag{3.13}$$

$$\alpha r_c = \phi_{hid} - \phi_{vis}\,. \tag{3.14}$$

The second expression clearly shows that we have indeed stabilised the brane separation, r_c. In order to achieve the correct hierarchy, we previously required that $|\alpha r_c| \sim 70$. This can be achieved without the need for any extreme fine-tuning of the parameters. In the proper coordinates (3.6) this corresponds to stabilising the interbrane distance at $y_c \sim 10^{10}|\alpha|^{-1}$, much larger than in RS models. Finally, it is important to note that since ϕ_{vis} appears in the exponential dilaton factor in the boundary action (3.1), we require that $\phi_{vis} = 0$ in order to successfully reproduce the Standard Model. This is the case we shall consider from now on.

3.3 Identification of the Radion

In this section we identify the physical radion and KK modes and calculate the mass spectrum. It will be convenient to work in the gauge $E = B = 0$ such that the scalar perturbations in Eqs. (2.44) reduce to

$$ds^2 = e^{-\frac{2}{3}\alpha|z|}\left[(1+2\Psi)\eta_{\mu\nu}dx^\mu dx^\nu + (1+2\Phi)dz^2\right]\,, \tag{3.15}$$

$$\phi(x,z) = \phi(z) + \delta\phi(x,z)\,. \tag{3.16}$$

We then obtain the linearised Einstein equations for the perturbations, which include the following constraint equations

$$\Phi + \frac{3}{\alpha}\dot{\Psi} + \frac{1}{3}\delta\phi = 0\,, \tag{3.17}$$

$$\Phi = -2\Psi\,. \tag{3.18}$$

where dots denote differentiation with respect to the conformal coordinate z. The presence of these non-dynamical equations reflects the fact that the gravitational and dilaton scalar perturbations are coupled and the action must be diagonalised in order to identify the physical degree of freedom of the system. Using these constraint equations the dynamical equation can be expressed as

$$\left[\Box + \frac{d^2}{dz^2} - \frac{\alpha^2}{4}\right]\left(e^{-\frac{1}{2}\alpha z}\Phi\right) = 0\,. \tag{3.19}$$

There are also two junction conditions at the boundaries. The first is obtained by simply evaluating (3.17) at the boundaries, while the second contains additional physical information and is given by

$$\delta\phi = \pm \frac{4M^3 e^{\frac{1}{3}\alpha z}}{\frac{\partial^2}{\partial\phi^2}\left(3e^{\frac{\phi}{3}}U_{vis(hid)}(\phi)\right)}\left(\delta\dot{\phi} - \alpha\Phi\right) , \tag{3.20}$$

One of the nice features of this model is that the equations of motion for the perturbations can be solved analytically. While the boundary conditions are non-trivial, they become considerably simpler in the limit $\frac{\partial^2}{\partial\phi^2}(e^{\frac{\phi}{3}}U) \to \infty$, which forces $\delta\phi \to 0$ on the branes. This is the limit most often considered in the literature, including the original Goldberger-Wise case. However, this will be insufficient for our purposes since many of the interesting phenomenological features of this model arise due to the non-zero coupling of the dilaton field to the SM Lagrangian on the brane, as shall be seen in Sections 3.4 and 3.5.

We begin by performing a KK decomposition

$$\Phi(x^\mu, z) = \sum_{n=0}^{\infty} \Phi_n(z) Q_n(x^\mu) , \tag{3.21}$$

where $Q_n(x^\mu)$ are the 4D Kaluza-Klein modes which satisfy the Klein-Gordon equation, and Φ_n are the profiles in the fifth dimension. The equation of motion is then simply given by

$$\left[\frac{d^2}{dz^2} + m_n^2 - \frac{\alpha^2}{4}\right]\left(e^{-\frac{1}{2}\alpha z}\Phi_n\right) = 0 , \tag{3.22}$$

with the boundary condition

$$\frac{3}{2\alpha}\dot{\Phi}_n - \Phi_n = \frac{2}{2\alpha \pm 9\mu_{vis(hid)}}\left(\frac{9}{2\alpha}\ddot{\Phi}_n - 3\dot{\Phi}_n - \alpha\Phi_n\right) . \tag{3.23}$$

We obtain the following solution for Φ_n,

$$\Phi_n(z) = N_n e^{\frac{1}{2}\alpha z}\left[\sin(\beta_n z) - \frac{6\beta_n\mu_{vis}}{4\beta_n^2 + \alpha(\alpha - \mu_{vis})}\cos(\beta_n z)\right] , \tag{3.24}$$

where we have defined $\beta_n^2 \equiv m_n^2 - \frac{\alpha^2}{4}$, N_n is an overall normalisation factor, and we have used the boundary condition at $z = 0$ to fix one of the constants. The mass spectrum is then obtained by evaluating the boundary condition at the $z = r_c$ boundary. The complete mass spectrum can be determined analytically by taking $\mu_{vis(hid)}$ to be large and solving as an expansion in $|\alpha|/\mu_{vis(hid)}$. However, an exact expression can also be obtained for the radion and lowest KK mode in the limit

$|\alpha r_c| \gg 1$. We then find that

$$m_{rad}^2 = \frac{\alpha^2}{4} - \frac{\alpha^2}{16\epsilon_{vis}^2}\left(3 - \sqrt{9 + 4\epsilon_{vis} + 4\epsilon_{vis}^2}\right)^2 , \qquad 0 < \epsilon_{vis} < \infty , \tag{3.25}$$

where $\epsilon_{vis(hid)} \equiv |\alpha|/\mu_{vis(hid)}$ and $\mu_{vis(hid)} > 0$ is required to ensure there are no tachyonic modes. Note that dependence on ϵ_{hid} in (3.25) is suppressed in the $|\alpha r_c| \gg 1$ limit. We also solve the boundary condition as an expansion in $\epsilon_{vis(hid)}$ to obtain the complete KK spectrum at first order

$$m_{rad}^2 = \frac{2}{9}\alpha^2\left(1 - \frac{2\epsilon_{vis}}{9}\right) , \tag{3.26}$$

$$m_n^2 = \frac{\alpha^2}{4} + \frac{n^2\pi^2}{r_c^2}\left[1 - \frac{4(4n^2\pi^2 + 3|\alpha r_c|^2)}{12n^2\pi^2|\alpha r_c| + |\alpha r_c|^3}\left(\epsilon_{vis} + \epsilon_{hid}\right)\right] , \tag{3.27}$$

where $n = 1, 2, 3, \ldots$. Note that in the limit $\epsilon_{vis(hid)} \to 0$, corresponding to $\mu_{vis(hid)} \to \infty$, we obtain the result given in Ref. [62].

We see that this model also gives rise to a rather interesting mass spectrum for the scalar fluctuations. Both the radion and lowest KK mode have masses of order the curvature scale, but can be parametrically lighter depending on the values of $\epsilon_{vis(hid)}$. The spacing of the KK modes is then determined by the size of the extra dimension as we would expect. Once again we have $r_c \sim (30\ \text{GeV})^{-1}$ and the KK spectrum forms a near continuum of modes above a mass of approximately half the curvature scale.

The mass spectrum is plotted as a function of ϵ in Figure 3.1, where the KK modes have been determined numerically and we have taken $\epsilon_{vis} = \epsilon_{hid}$. Note however that as seen in Eq. (3.25), the lowest mode is dependent only on ϵ_{vis}, while the second lowest mode depends only on ϵ_{hid} for $\epsilon_{hid} \gtrsim 1$. We find that the exact and approximate solutions are well matched when ϵ is small, justifying our expansion. Interestingly, we observe that both the radion and lowest KK mode are highly sensitive to the boundary mass terms and as ϵ is increased there are two distinct modes below the near continuum of KK states. In the $\epsilon \to \infty$ limit, corresponding to the unstabilised case with $\mu_{vis(hid)} = 0$, the KK spectrum is identical to the graviton spectrum (3.7) with a $\sim$ TeV mass gap. Note that the constraint equation (3.17) becomes dynamical when considering massless scalar perturbations and hence we expect two massless modes in this limit, where the additional mode arises due to the extra bulk scalar field (the dilaton).

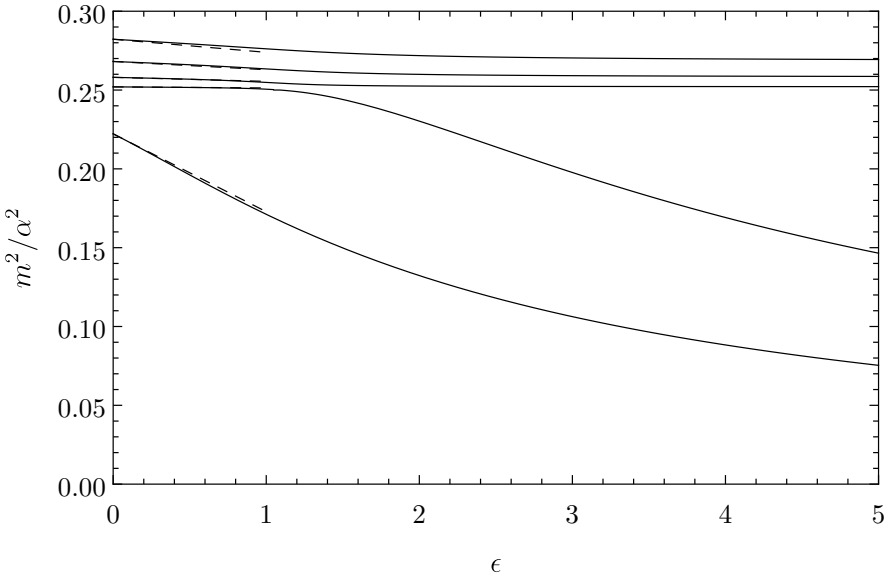

FIGURE 3.1: The radion and KK mass spectrum as a function of ϵ, where we have taken $\epsilon_{vis} = \epsilon_{hid}$. The lowest five modes are shown and the dashed lines denote the approximate solutions.

3.4 Coupling to the Standard Model

In this section we calculate the couplings of the radion and KK modes to the Standard Model fields. The relevant term in the boundary action is

$$S = \int d^4x \sqrt{-\hat{g}}\, e^{\frac{\delta\phi}{3}} \mathcal{L}_{SM}\,, \tag{3.28}$$

where $\mathcal{L}_{SM}$ is the SM Lagrangian and $\hat{g}$ is the induced metric on the $z = 0$ brane. We clearly see that the radion couples to the SM fields through the induced metric on the brane and also via the exponential dilaton factor. This dilaton factor is not present in the usual RS models and gives rise to an additional coupling between the radion and SM fields. Expanding the above action to first order in the perturbations, we obtain the following interaction action between the radion KK modes, Q_n, and the SM fields

$$S_{int} = \frac{1}{2}\sum_n \Phi_n(0) \int d^4x \sqrt{-\hat{g}_0}\, Q_n\, \hat{g}_0^{\mu\nu} T_{\mu\nu} + \frac{1}{3}\sum_n \delta\phi_n(0) \int d^4x \sqrt{-\hat{g}_0}\, Q_n\, \mathcal{L}_{SM}\big|_{\hat{g}=\hat{g}_0}\,, \tag{3.29}$$

where $\hat{g}_0$ is the induced background metric on the brane and $T_{\mu\nu}$ is the SM energy-momentum tensor. The first term in Eq. (3.29) is the usual coupling of the radion to the trace of the energy momentum tensor, while the second term arises due to the presence of the dilaton and produces a direct coupling between the radion

and SM Lagrangian. This additional coupling can have a significant effect on the radion phenomenology, as we shall see in Section 3.5.

For convenience we define the following coupling constants

$$\frac{\kappa_{\Phi,n}}{M} \equiv \frac{\Phi_n(0)}{2}\,, \qquad \frac{\kappa_{\phi,n}}{M} \equiv \frac{\delta\phi_n(0)}{3}\,. \tag{3.30}$$

The couplings can now be determined by correctly normalising the solutions for the perturbations obtained in Section 3.3. The couplings for the radion can be determined analytically in the $|\alpha r_c| \gg 1$ limit, while the KK couplings can only be obtained as an expansion in $\epsilon_{vis(hid)}$. The exact expression for the radion coupling is non-trivial and does not provide additional insight, so here we give only the approximate solutions. The couplings to the energy-momentum tensor are given by

$$|\kappa_{\Phi,rad}| = \frac{1}{6\sqrt{2}}\sqrt{\frac{|\alpha|}{M}}\left(1+\frac{4}{9}\epsilon_{vis}\right)\,, \tag{3.31}$$

$$|\kappa_{\Phi,n}| = \frac{4n\pi}{\sqrt{6}|\alpha r_c|^{3/2}}\sqrt{\frac{|\alpha|}{M}}\left(1-\epsilon_{vis}\right)\,, \tag{3.32}$$

where we have also taken $|\alpha r_c| \gg 1$, since the expressions simplify significantly in this limit. We see that the coupling strength is largely determined by the fundamental scale, M, and also the ratio α/M. Additionally, the couplings for the KK modes are suppressed by a factor of $|\alpha r_c|^{3/2}$ relative to the radion mode. Hence, we always expect the single radion mode to be observed first by experiments, even when the radion mass is close to that of the KK near continuum or when there are two light modes. It is also interesting to note that the couplings for the KK modes increase with n, however this remains true only for small n since Eq. (3.31) is no longer valid when $n^2 \sim |\alpha r_c|$.

Using the constraint equation for the perturbations (3.17) evaluated at the $z = 0$ brane we can also determine the couplings to the SM Lagrangian, which are given by

$$|\kappa_{\phi,rad}| = \frac{\sqrt{2}}{27}\sqrt{\frac{|\alpha|}{M}}\epsilon_{vis}\,, \tag{3.33}$$

$$|\kappa_{\phi,n}| = \frac{2n\pi}{\sqrt{6}|\alpha r_c|^{3/2}}\sqrt{\frac{|\alpha|}{M}}\epsilon_{vis}\,. \tag{3.34}$$

We see that unlike κ_Φ above, these couplings do not include a zeroth order term, consistent with the fact that $\delta\phi \to 0$ in the $\mu_{vis} \to \infty$ limit. The couplings to the SM Lagrangian are therefore suppressed by an additional factor of $|\alpha|/\mu_{vis}$, which

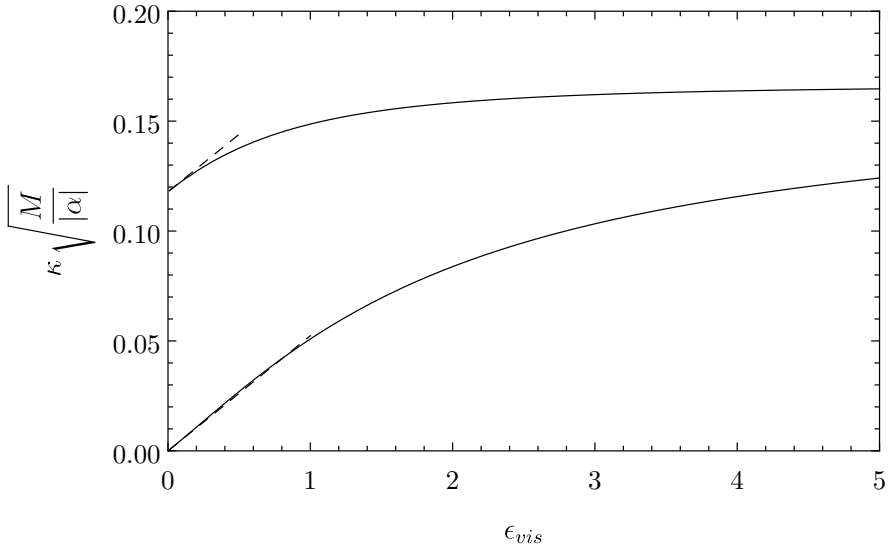

FIGURE 3.2: The radion couplings as a function of ϵ_{vis}. The upper and lower curves correspond to κ_Φ and κ_ϕ respectively. The dashed lines denote the approximate solutions.

must be small in order to justify our expansion. Once again, the couplings of the KK modes are further suppressed relative to the radion mode.

Figure 3.2 shows the radion couplings as a function of ϵ_{vis}, where the upper and lower curves correspond to κ_Φ and κ_ϕ respectively. Once again we see that the approximate and exact solutions are in good agreement when ϵ_{vis} is small. We also find that $\kappa_\Phi > \kappa_\phi$, even for larger values of ϵ_{vis} where our approximate solution is no longer valid. Taking $M \sim$ TeV, $|\alpha|/M \sim 0.5$ and $\epsilon_{vis} = 3$, we find that $\kappa_{\Phi,rad} \sim 0.11$ and $\kappa_{\Phi,rad}/M$ will be of order $\sim (9 \text{ TeV})^{-1}$. Similarly, $\kappa_{\phi,rad} \sim 0.07$ and $\kappa_{\phi,rad}/M$ will be of order $\sim (14 \text{ TeV})^{-1}$. Note also that while the overall sign of the couplings is undetermined by the normalisation condition, the relative sign is fixed giving $\kappa_\Phi/\kappa_\phi > 0$.

3.4.1 Higgs-curvature interaction

An interesting situation arises for scalar fields, since they can couple non-minimally to gravity. This allows us to introduce the following additional Higgs-curvature interaction term to the 4D effective action

$$S_\xi = \int d^4x \sqrt{-\hat{g}}\, e^{\frac{\delta\phi}{3}} \xi\, \mathcal{R}(\hat{g}) H^\dagger H \,, \tag{3.35}$$

where $\mathcal{R}(\hat{g})$ is the Ricci scalar obtained from the 4D induced metric on the brane. For an arbitrary scalar field ψ, we could also in principle include the linear coupling $\mathcal{R}(\hat{g})\psi$, however in the case of the Higgs this is forbidden by the gauge symmetry.

As we shall see, this additional interaction term results in a mixing between the Higgs and the radion. The analysis given below follows that performed for the RS model in [210, 211], however here we include the additional effects of the dilaton field.

After substituting the expression for the 4D Ricci scalar, Eq (3.35) leads to the following Lagrangian for the interaction

$$\mathcal{L}_\xi = -6\xi e^{\frac{\delta\phi}{3}}(1-\Phi)^{1/2}\eta^{\mu\nu}\partial_\mu\partial_\nu(1-\Phi)^{1/2}H^\dagger H\,, \tag{3.36}$$

where from here onwards we use η to refer to the 4D Minkowski metric with signature $(+,-,-,-)$. Then expanding the Higgs field around its vacuum expectation value, $H = (h+v)/\sqrt{2}$, where $v \simeq 246$ GeV, we have to quadratic order in the fields

$$\mathcal{L}_\xi = -3\xi\left(\frac{1}{4}v^2\Phi\Box\Phi - \frac{1}{6}v^2\delta\phi\Box\Phi - vh\Box\Phi\right)\,, \tag{3.37}$$

where $\Box \equiv \eta^{\mu\nu}\partial_\mu\partial_\nu$ is the d'Alembert operator. Finally, inserting the KK expansion for the fields and considering only the radion mode, r, we obtain the following complete Higgs-radion Lagrangian

$$\mathcal{L} = -\frac{1}{2}h\Box h - \frac{1}{2}m_h^2h^2 - \frac{1}{2}\left[1+\frac{6\xi\kappa_\Phi v^2}{M^2}(\kappa_\Phi-\kappa_\phi)\right]r\Box r - \frac{1}{2}m_r^2r^2 + \frac{6\xi\kappa_\Phi v}{M}h\Box r\,, \tag{3.38}$$

where m_h, m_r are the Higgs and radion masses respectively in the $\xi = 0$ limit. The ξ term then clearly introduces a kinetic mixing between the Higgs and radion fields. The Lagrangian must therefore be diagonalised to identify the physical mass eigenstates of the system. We begin by diagonalising the kinetic terms via the following transformation

$$h = h' + \frac{6\xi\kappa_\Phi v}{\Omega M}r'\,, \qquad r = \frac{r'}{\Omega}\,, \tag{3.39}$$

where

$$\Omega^2 = 1 + \frac{6\xi\kappa_\Phi v^2}{M^2}\left((1-6\xi)\kappa_\Phi - \kappa_\phi\right)\,. \tag{3.40}$$

This in fact also enables us to place a constraint on the parameter ξ, since Ω^2 must be positive in order to ensure that the radion mass term retains the correct sign and we avoid encountering a ghost radion field. We therefore require that ξ lies in the range

$$\frac{1}{12\kappa_\Phi}\left(\rho - \sqrt{\rho^2+\frac{4M^2}{v^2}}\right) \leq \xi \leq \frac{1}{12\kappa_\Phi}\left(\rho + \sqrt{\rho^2+\frac{4M^2}{v^2}}\right)\,, \tag{3.41}$$

where $\rho \equiv \kappa_\Phi - \kappa_\phi$. Taking $\kappa_\Phi = 0.11$, $\kappa_\phi = 0.07$ and $M = 1$ TeV, we find that this places a limit of $-6.1 < \xi < 6.2$.

So far, we have successfully diagonalised the kinetic terms in the Lagrangian, however this now introduces a mixing in the mass matrix, which must be diagonalised via the rotation

$$\begin{aligned} h' &= \cos\theta\, h_m + \sin\theta\, r_m\,, \\ r' &= -\sin\theta\, h_m + \cos\theta\, r_m\,, \end{aligned} \tag{3.42}$$

where h_m, r_m are the physical mass eigenstates and the mixing angle is given by

$$\tan 2\theta = \frac{12\xi\kappa_\Phi v\Omega}{M}\frac{m_h^2}{m_r^2 - m_h^2\left(\Omega^2 - \frac{36\xi^2\kappa_\Phi^2 v^2}{M^2}\right)}\,. \tag{3.43}$$

We can now express the gauge eigenstates in terms of the mass eigenstates as

$$\begin{aligned} h &= \left(\cos\theta - \frac{6\xi\kappa_\Phi v}{\Omega M}\sin\theta\right) h_m + \left(\sin\theta + \frac{6\xi\kappa_\Phi v}{\Omega M}\cos\theta\right) r_m\,, \\ r &= -\frac{\sin\theta}{\Omega} h_m + \frac{\cos\theta}{\Omega} r_m\,. \end{aligned} \tag{3.44}$$

We can also calculate the corresponding mass eigenvalues, which are given by

$$\begin{aligned} m^2_{r_m,h_m} = \frac{1}{2\Omega^2}\Bigg[& m_r^2 + m_h^2\left(1 + \frac{6\xi\kappa_\Phi^2 v^2}{M^2}\right) \\ & \pm\left(\left(m_r^2 - m_h^2\left(1 + \frac{6\xi\kappa_\Phi^2 v^2}{M^2}\right)\right)^2 + \frac{144\xi^2\kappa_\Phi^2 v^2 m_r^2 m_h^2}{M^2}\right)^{1/2}\Bigg]\,. \end{aligned} \tag{3.45}$$

In the following section we shall only be considering the radion interactions described in Eq. (3.29) and will not be concerned with higher-dimension operators, which are suppressed by higher powers of M. It therefore makes sense to expand the above results to leading order in $1/M$. The mixing angle then becomes

$$\tan 2\theta \approx \frac{12\xi\kappa_\Phi v}{M}\frac{m_h^2}{m_r^2 - m_h^2}\,. \tag{3.46}$$

Now, provided that $m_r \not\approx m_h$, the mixing angle is small and our results simplify to

$$\begin{aligned} h &= h_m + \frac{6\xi\kappa_\Phi v}{M}\frac{m_r^2}{m_r^2 - m_h^2}\, r_m\,, \\ r &= -\frac{6\xi\kappa_\Phi v}{M}\frac{m_h^2}{m_r^2 - m_h^2}\, h_m + r_m\,. \end{aligned} \tag{3.47}$$

This mixing can in principle have an interesting effect on the Higgs phenomenology, since a strong mixing would lead to a reduced cross section for the Higgs. However, Eq. (3.47) shows that the extent of the mixing is largely determined by the factor $\kappa_\Phi v/M$ and is therefore small, except in the case when m_r is very near to m_h, or if we take ξ to be large. While the mixing may not have any significant effect on the Higgs, it still plays an important role in determining the radion phenomenology, since the same suppression scale determines both the mixing and the radion couplings.

When $m_r \approx m_h$, Eq. (3.47) is no longer valid and we must include higher order terms in the expression for the mixing angle (3.46) or else consider the full expressions in Eq. (3.44). In this case we find that the mixing becomes large and the two mass eigenstates are now essentially part Higgs and part radion. The result is two states with closely spaced masses, both of which interact in a similar way to the SM Higgs but with a reduced cross section.

We also note that at leading order in $1/M$ our result does not depend on κ_ϕ and the dilaton does not contribute significantly to the Higgs-radion mixing. Our results are then equivalent to those for the RS case given in [210, 211]. In this limit, the mass eigenvalues also simply reduce to m_r, m_h. The above analysis can also be performed with the inclusion of the radion KK modes and is given in Appendix B.2. The mixing effect is sub-dominant compared to the radion only case.

3.4.2 SM-Radion Interactions

As we have shown, the radion couples to the trace of the Standard Model energy-momentum tensor as well as directly to the SM Lagrangian. We now derive in detail the radion interactions with the SM fields and present the corresponding Feynman rules for the interaction terms in Appendix B.3.

Following on from our discussion of the previous section, we consider the case where there is a mixing between the radion and Higgs fields and express the interactions in terms of the physical mass eigenstates. In order to simplify the expressions, we shall use the following general formulae relating the gauge and mass eigenstates, where the values of the coefficients can be read off from Eq. (3.44):

$$\begin{aligned} h &= a_0 h_m + a_1 r_m \,, \\ r &= b_0 h_m + b_1 r_m \,. \end{aligned} \tag{3.48}$$

We shall also restrict ourselves to interactions up to quadratic order in the SM fields, since these will provide the dominant contributions when considering the

radion decay modes in the following section. The SM energy-momentum tensor is then given in the unitary gauge by

$$T^{\mu}_{\mu} = -2m_W^2 W^+_\mu W^{-\mu} - m_Z^2 Z_\mu Z^\mu + 2m_h^2 h^2 - \partial_\mu h \partial^\mu h + \sum_f \frac{3i}{2}\left(\left(D_\mu \bar{\Psi}\right)\gamma^\mu \Psi - \bar{\Psi}\gamma^\mu D_\mu \Psi\right) + 4m_\Psi \bar{\Psi}\Psi \,. \quad (3.49)$$

We begin by considering the interactions of the radion with the massive gauge bosons, which are given by

$$\mathcal{L}_{int} = -\frac{b_1 \kappa_\phi}{4M} r_m \left(2W^\dagger_{\mu\nu} W^{\mu\nu} + Z_{\mu\nu} Z^{\mu\nu}\right) + \left(\frac{b_1}{M}\left(\frac{\kappa_\phi}{2} - \kappa_\Phi\right) + \frac{a_1}{v}\right) r_m \left(2m_W^2 W^\dagger_\mu W^\mu + m_Z^2 Z_\mu Z^\mu\right) \,. \quad (3.50)$$

We see that as a result of the dilaton coupling to the SM Lagrangian, there is now a coupling between the radion and the gauge boson kinetic terms, which will become important at large momenta. As we shall see, this additional coupling is particularly significant for the massless gauge fields.

We now consider the interactions with the SM fermions which are given by

$$\mathcal{L}_{int} = \frac{ib_1}{2M}\left(\kappa_\phi - 3\kappa_\Phi\right) r_m \left(\bar{\Psi}\gamma^\mu D_\mu \Psi - \left(D_\mu \bar{\Psi}\right)\gamma^\mu \Psi\right) + m_\Psi \left(\frac{b_1}{M}\left(4\kappa_\Phi - \kappa_\phi\right) - \frac{a_1}{v}\right) r_m \bar{\Psi}\Psi \,. \quad (3.51)$$

In the case of on-shell fermions, the above Lagrangian can be significantly simplified by using the Dirac equation. Furthermore, it was shown in Ref. [212] that the additional contributions for off-shell fermions cancel in physical processes and the complete radion-fermion couplings can simply be expressed as

$$\mathcal{L}_{int} = m_\Psi \left(\frac{b_1 \kappa_\Phi}{M} - \frac{a_1}{v}\right) r_m \bar{\Psi}\Psi \,. \quad (3.52)$$

Of course, the Dirac Lagrangian vanishes after using the equations of motion and hence our interaction term is independent of κ_ϕ.

There are additional considerations when looking at the radion interactions with the Higgs boson. As a result of the mixing between the radion and the Higgs, the interactions will now be dependent on the radion potential as well as the Higgs self-interaction terms. In addition to this, there are interaction terms which arise from the Higgs-curvature term (3.35). Following the analysis in Section 3.4.1, but here considering terms which are cubic in the fields, gives the following interaction

term to leading order in $1/M$

$$\mathcal{L}^{\xi}_{int} = \frac{6\xi\kappa_\Phi a_0^2 b_1}{M}\left(\partial_\mu h_m \partial^\mu h_m + h_m \Box h_m\right) r_m \,. \tag{3.53}$$

Now putting this together with the other interaction terms we obtain

$$\mathcal{L}_{int} = \frac{a_0^2 b_1}{M}\left((6\xi-1)\kappa_\Phi + \frac{\kappa_\phi}{2}\right) r_m \partial_\mu h_m \partial^\mu h_m + \frac{6\xi\kappa_\Phi a_0^2 b_1}{M} r_m h_m \Box h_m \\ + a_0^2 m_h^2 \left(\frac{b_1}{M}(2\kappa_\Phi - \frac{\kappa_\phi}{2}) - \frac{3a_1}{2v}\right) r_m h_m^2 \,, \tag{3.54}$$

where the final term arises from the cubic Higgs self-interaction term in the SM Lagrangian. We have excluded the effects of the radion potential terms, which we shall assume to be small.

Finally, we consider the interactions with the massless gauge bosons. Here we must also include the contributions to T^μ_μ from the trace anomaly, which is reviewed in Ref. [213]. The interaction with the gluons is given by

$$\mathcal{L}_{int} = -\frac{b_1}{M}\left(\frac{\kappa_\phi}{4} + \kappa_\Phi\, b_{QCD}\frac{\alpha_s}{8\pi}\right) r_m \mathcal{F}^a_{\mu\nu}\mathcal{F}_a^{\mu\nu} \,, \tag{3.55}$$

where $b_{QCD} = 11 - 2n_f/3$ with $n_f = 6$. For the gluons it turns out that the direct coupling of the dilaton and the additional coupling due to the trace anomaly are of comparable strength, due to the relatively large value of α_s and the suppression of κ_ϕ relative to κ_Φ.

The interaction with the photon is similarly

$$\mathcal{L}_{int} = -\frac{b_1}{M}\left(\frac{\kappa_\phi}{4} + \kappa_\Phi(b_2 + b_Y)\frac{\alpha_{EM}}{8\pi}\right) r_m F_{\mu\nu}F^{\mu\nu} \,, \tag{3.56}$$

where $b_2 = 19/6$ and $b_Y = -41/6$. However in this case the anomalous contributions to T^μ_μ are insignificant due to the much smaller value of α_{EM}. We similarly ignored the effects of the trace anomaly when considering the W and Z gauge bosons above.

3.5 Radion Phenomenology and Constraints

3.5.1 Decay Widths

From the interaction terms given above and the Feynman rules given in Appendix B.3 we calculate the partial decay widths of the radion into WW, ZZ,

hh, $\bar{f}f$, $\gamma\gamma$, and gg. We have taken our results to leading order in $1/M$ and used the expression (3.47) for the Higgs-radion mixing. The decay widths are given by

$$\Gamma(r\to W^+W^-) = \frac{m_r^3}{16\pi M^2}\sqrt{1-x_W}\left[\frac{3\kappa_\phi^2}{4}\right. \\ +\kappa_\Phi^2\left(1-x_W+\frac{3}{4}x_W^2\right)\left(1-\frac{6\xi m_r^2}{m_r^2-m_h^2}\right)^2 \\ \left.-\kappa_\phi\kappa_\Phi\left(1+\frac{1}{2}x_W\right)\left(1-\frac{6\xi m_r^2}{m_r^2-m_h^2}\right)\right], \quad (3.57)$$

$$\Gamma(r\to ZZ) = \frac{1}{2}\Gamma(r\to W^+W^-), \quad (3.58)$$

$$\Gamma(r\to hh) = \frac{m_r^3}{32\pi M^2}\sqrt{1-x_h}\left[\frac{\kappa_\phi^2}{4}+\kappa_\Phi^2\left(1+x_h+\frac{1}{4}x_h^2-12\xi-6\xi x_h+36\xi^2\right.\right. \\ -\frac{36\xi m_h^2}{m_r^2-m_h^2}-\frac{72\xi m_h^4}{m_r^2(m_r^2-m_h^2)}+\frac{216\xi^2 m_h^2}{m_r^2-m_h^2}+\frac{324\xi^2 m_h^4}{(m_r^2-m_h^2)^2}\Big) \\ \left.-\kappa_\phi\kappa_\Phi\left(1+\frac{1}{2}x_h-6\xi-\frac{18\xi m_h^2}{m_r^2-m_h^2}\right)\right], \quad (3.59)$$

$$\Gamma(r\to \bar{f}f) = \frac{N_c\kappa_\Phi^2 m_f^2 m_r}{8\pi M^2}\left(1-x_f\right)^{3/2}\left(1-\frac{6\xi m_r^2}{m_r^2-m_h^2}\right)^2, \quad (3.60)$$

$$\Gamma(r\to \gamma\gamma) = \frac{m_r^3}{64\pi M^2}\left|\kappa_\phi+\frac{\alpha_{EM}\kappa_\Phi}{2\pi}\left[b_2+b_Y\right.\right. \\ -\left(1-\frac{6\xi m_r^2}{m_r^2-m_h^2}\right)\left(2+3x_W+3x_W(2-x_W)f(x_W)\right) \\ \left.\left.+\frac{8}{3}\left(1-\frac{6\xi m_r^2}{m_r^2-m_h^2}\right)x_t\left(1+(1-x_t)f(x_t)\right)\right]\right|^2, \quad (3.61)$$

$$\Gamma(r\to gg) = \frac{m_r^3}{8\pi M^2}\left|\kappa_\phi+\frac{\alpha_s\kappa_\Phi}{2\pi}\left[b_{QCD}\right.\right. \\ \left.\left.+\left(1-\frac{6\xi m_r^2}{m_r^2-m_h^2}\right)x_t\left(1+(1-x_t)f(x_t)\right)\right]\right|^2, \quad (3.62)$$

where

$$f(x) = \begin{cases} \left[\sin^{-1}\left(\frac{1}{\sqrt{x}}\right)\right]^2, & x \geq 1\,, \\ -\frac{1}{4}\left[\ln\frac{1+\sqrt{1-x}}{1-\sqrt{1-x}} - i\pi\right]^2, & x < 1\,, \end{cases} \tag{3.63}$$

and we have defined $x_i = 4m_i^2/m_r^2$, $(i = W, Z, h, f)$ and $N_c = 3(1)$ for quarks (leptons). When calculating the partial decay widths to gg and $\gamma\gamma$, we have also included the one-loop contributions of the top quark and the W boson, which become important when the mixing is strong. We have neglected one-loop corrections proportional to κ_ϕ. Finally, in the limit $\xi = 0$ and $\kappa_\phi \to 0$ our results reduce to those for the RS case given in [214, 215].

3.5.2 Branching Fractions

In this section we use our previous results to look at the branching fractions of the various radion decay modes. We begin by considering the case where there is no mixing between the radion and the Higgs ($\xi = 0$). Figure 3.3 shows the radion branching fractions as a function of its mass where we have taken $\epsilon_{vis} = 3$ and $M = 4$ TeV.

We see that in the low mass range the branching fractions are dominated by the gg and $\gamma\gamma$ channels, while in the high mass range gg and WW are the dominant decay modes, but with significant contributions from several other channels. The large branching fraction to $\gamma\gamma$ is of particular interest and is a direct result of the dilaton coupling to the gauge boson kinetic terms. It also remains significant even at high radion masses.

If we compare the branching fractions for the linear dilaton model shown here with those of the RS model [214], we note that the most important difference comes in the branching fraction to $\gamma\gamma$. This is significantly enhanced in the linear dilaton model, since the dilaton coupling is much stronger than the trace anomaly and one-loop contributions, which are proportional to α_{EM}. We conclude that the large branching fraction to photons seen in Figure 3.3 is therefore an important distinguishing feature of this model.

Next we look at the case where there is a mixing between the radion and Higgs. We shall take $\xi = 1/6$, which corresponds to the conformal limit when we also take m_h=0. The radion branching fractions are then shown in Figure 3.4. We observe that at high mass, the situation is similar to the zero mixing case in Figure 3.3, except that the hh decay mode is now suppressed as a result of the mixing. In

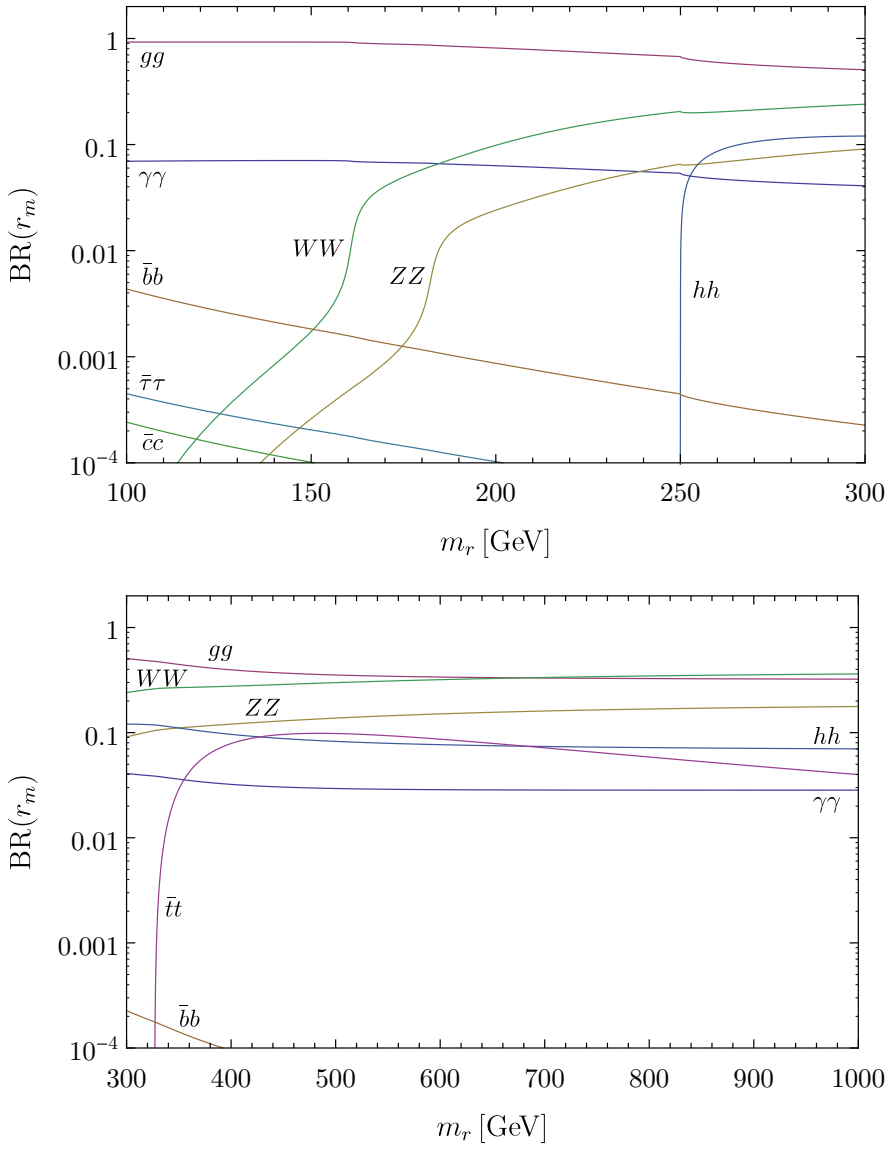

FIGURE 3.3: Branching fractions of r_m as a function of its mass with $\epsilon_{vis} = 3$, $M = 4$ TeV and $\xi = 0$. The top and bottom panels are the same but cover a different range in mass.

the low mass region we observe an interesting drop in the branching fractions to gg and $\gamma\gamma$ when the radion mass is near to that of the Higgs. This is the result of a cancellation in the partial widths (3.61), (3.62) due to the strong mixing in this region.

3.5.3 Production

In this section we briefly discuss the production of the radion at colliders. At hadron colliders, such as the LHC, radion production will be dominated by gluon-gluon fusion. The production cross section for this process at a hadron collider

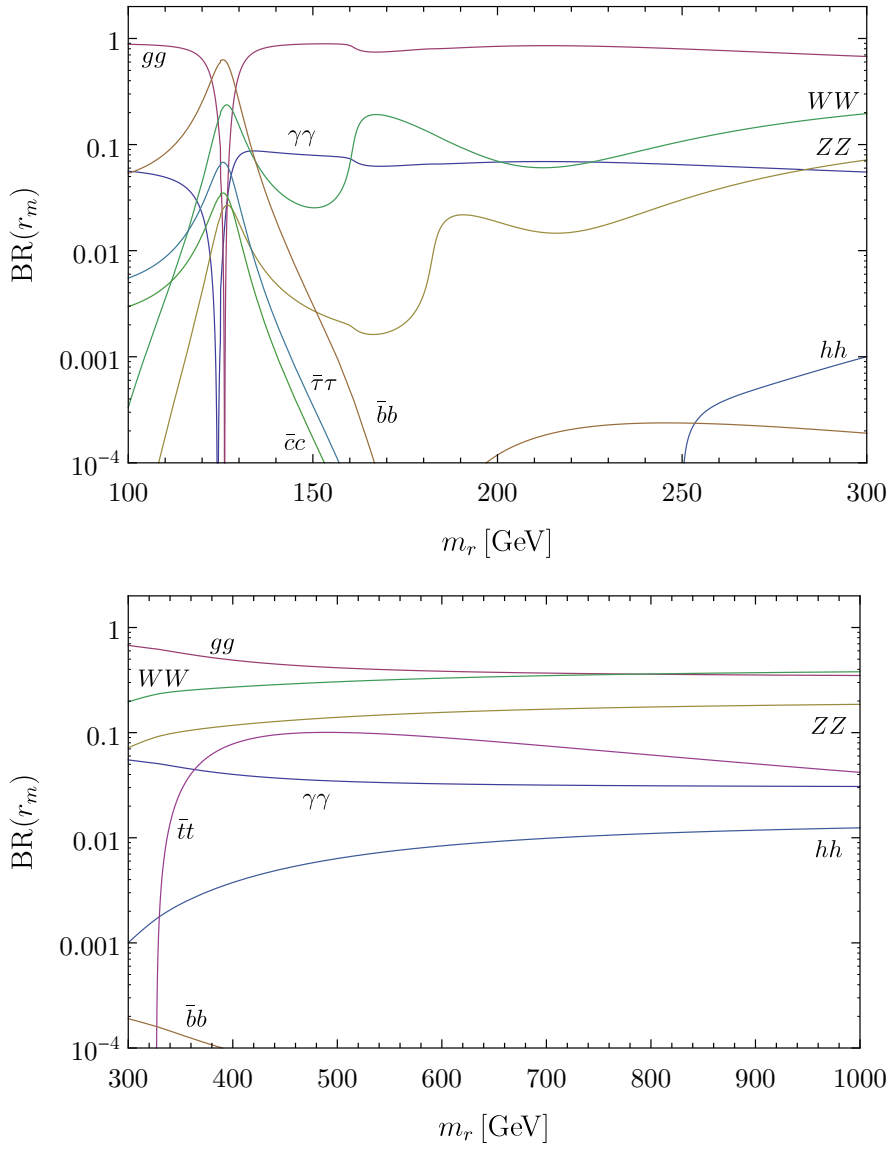

FIGURE 3.4: Branching fractions of r_m as a function of its mass with $\epsilon_{vis} = 3$, $M = 4$ TeV and $\xi = 1/6$. The top and bottom panels are the same but cover a different range in mass.

with centre of mass energy $\sqrt{s}$ is given by

$$\sigma(pp\to r) = \int_{m_r^2/s}^{1} \frac{dx}{x} g(x, m_r) g\left(\frac{m_r^2}{sx}, m_r\right) \frac{m_r^2}{s} \hat{\sigma}(gg\to r)\,, \tag{3.64}$$

where $g(x, Q)$ is the gluon parton distribution function (PDF) at momentum fraction x and renormalisation scale Q, and $\hat{\sigma}(gg\to r)$ is the gluon-gluon fusion subprocess cross section

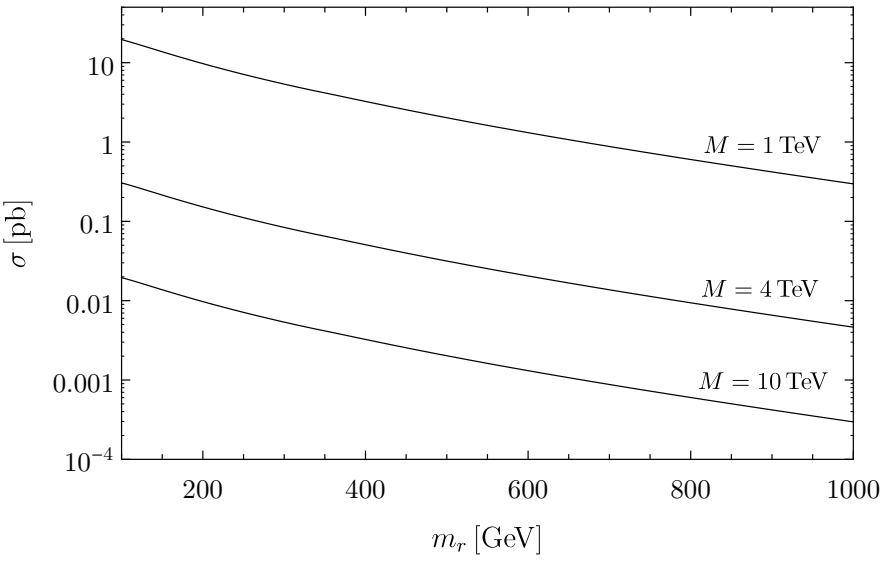

FIGURE 3.5: Gluon-gluon fusion production cross section for the radion at the LHC with a centre of mass energy of 8 TeV. We have taken $\epsilon_{vis} = 3$ and $\xi = 0$.

$$\hat{\sigma}(gg\to r) = \frac{\pi}{64M^2}\left|\kappa_\phi + \frac{\alpha_s}{2\pi}\kappa_\Phi\,(b_{QCD} + \left(1 - \frac{6\xi m_r^2}{m_r^2 - m_h^2}\right) x_t\,(1 + (1 - x_t)f(x_t))\right)\right|^2 . \quad (3.65)$$

The gluon-gluon fusion production cross section at the LHC for a centre of mass energy of 8 TeV is shown in Figure 3.5 in the case of zero mixing ($\xi = 0$) for several values of the fundamental sale, M. We have used the CTEQ5L [216] parton distribution functions. It is clear that even for relatively large values of M the radion production cross section remains significant. This suggests good prospects for searches at the LHC, as we shall see in the following section.

3.5.4 Constraints on Parameter Space

The ATLAS and CMS experiments at the LHC have now performed a number of searches for new scalar resonances in a variety of final states, which can be used to obtain constraints on the radion in this model. Before imposing these limits on the model parameter space, it is first insightful to compare the expected radion cross sections to those for the well-studied case of the SM Higgs. In the narrow width approximation the ratio is simply given by

$$\frac{\sigma(pp\to r\to X)}{\sigma_{SM}(pp\to h\to X)} = \frac{\Gamma(r\to gg)}{\Gamma(h\to gg)}\frac{Br(r\to X)}{Br(h\to X)}\,, \quad (3.66)$$

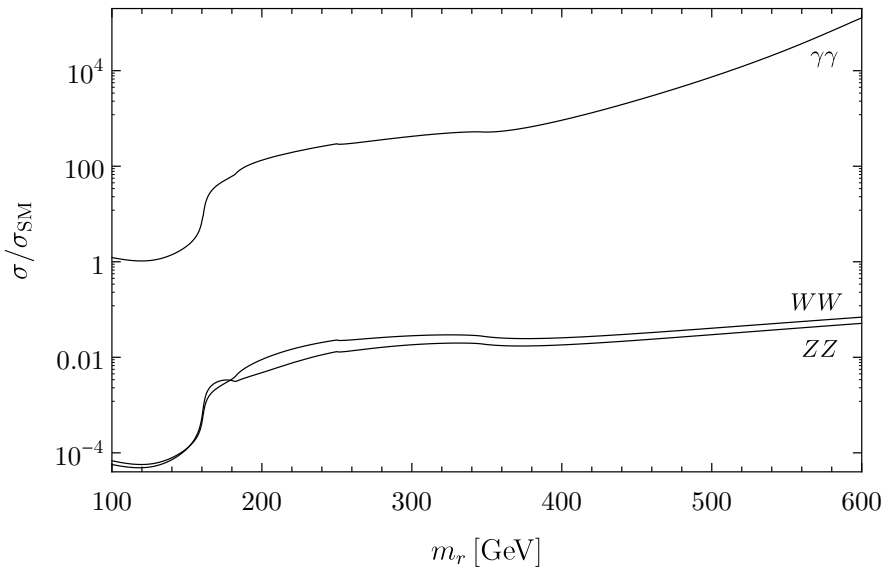

FIGURE 3.6: σ/σ_{SM} as a function of the radion mass. We have taken $\epsilon_{vis} = 3$, $M = 4$ TeV and $\xi = 0$.

and is plotted as a function of the radion mass for the WW, ZZ and $\gamma\gamma$ decay channels in Figure 3.6. Notice that for the $\gamma\gamma$ final state this ratio is greater than one for almost all radion masses, due to its large branching ratio to this decay mode. The $\gamma\gamma$ channel was famously one of the discovery channels for the Higgs and we expect it to provide the strongest constraints on the radion.

We use the recent ATLAS and CMS results from Run-I of the LHC at $\sqrt{s} = 8\,\text{TeV}$, which place bounds on the cross section×branching ratio for a new scalar resonance decaying into $\gamma\gamma$ [217], WW [218, 219], ZZ [220], hh [221] and $\bar{t}t$ [95] final states. The results are shown in Figure 3.7 where we have presented the constraints in terms of the parameters of the model, namely the fundamental scale, M, and the curvature scale, α. We have assumed zero mixing with the Higgs and taken $\epsilon_{vis} = 3$. As expected the strongest constraints arise in the diphoton final state, which constrain $M \gtrsim 3.5\,\text{TeV}$ in the range $0.5 \lesssim |\alpha| \lesssim 2.6\,\text{TeV}$. The remaining resonance searches are only able to probe regions of parameter space where the curvature is greater than M and the 5D theory is not under perturbative control. The dashed line in Figure 3.7 also shows the bound from the KK graviton resonances using ADD total cross section searches at the LHC with $\sim 2\,\text{fb}^{-1}$ of integrated luminosity at $\sqrt{s} = 7\,\text{TeV}$, as derived in Ref. [209]. These searches are expected to provide a significantly stronger bound using the latest data at $\sqrt{s} = 13\,\text{TeV}$.

In deriving the constraints we have focused on the case of zero Higgs-radion mixing ($\xi = 0$). Comparing Figures 3.3 & 3.4 we see that the branching ratio to photons is relatively unaffected by the mixing, except in the case where $m_r \sim m_h$. We therefore expect similar bounds on the radion in the case of non-zero mixing.

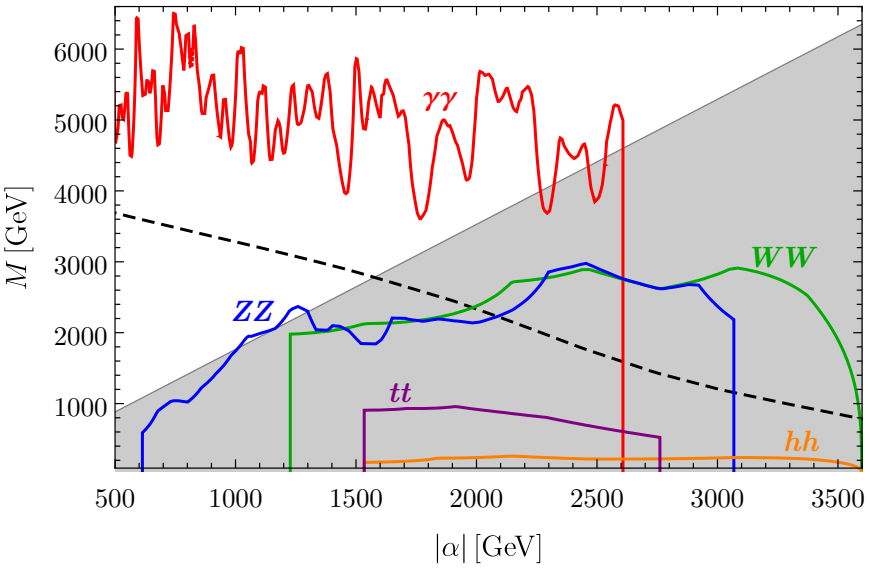

FIGURE 3.7: Constraints on the model parameters, α and M, from recent LHC resonance searches. The shaded region is where $M^2 < \frac{28}{9}\alpha^2$ and the gravitational description can no longer be trusted. The dashed line shows the constraints from ADD total cross section searches at the LHC taken from Ref. [209]. We have taken $\epsilon_{vis} = 3$ and $\xi = 0$.

Additionally, Higgs measurements can in principle constrain the mixing parameter through modification of the Higgs couplings. However, the bound will be weak since the mixing is suppressed by $M/\kappa_\Phi \gtrsim 10\,\text{TeV}$.

3.6 Summary

Motivated by Little String Theory, the 5D linear dilaton model provides a distinctive solution to the hierarchy problem. It is characterised by a graviton KK mass spectrum which consists of a $\sim$ TeV scale mass gap, followed by a near continuum of resonances spaced $\sim$ 30 GeV apart. The scalar sector of the model plays a crucial role, since it contains a scalar field, the dilaton, which can be used to stabilise the extra dimension. Just like in the Goldberger-Wise mechanism, the dilaton acquires a non-zero vacuum expectation value on the branes after imposing appropriate boundary potentials. A large volume is then stabilised with an interbrane proper distance of $y_c \sim 10^{10}|\alpha|^{-1}$. The correct hierarchy is achieved without the need for any extreme fine tuning.

The coupled scalar fluctuations about the metric and dilaton fields were then considered. We solved the equations of motion for the system and obtained the wavefunctions and masses of the modes. It was found that the radion and lowest

KK mode both obtain masses of order the curvature scale, but can be parametrically lighter depending on the boundary mass parameters. The KK modes were then closely spaced and essentially formed a near continuum of modes of order the curvature scale and above.

This model introduces a direct coupling in the boundary action between the dilaton and the Standard Model fields. It was shown that this results in a coupling between the radion and SM Lagrangian, in addition to the standard coupling to the trace of the energy-momentum tensor. The strength of these couplings was calculated, with a typical strength of order $(10\text{ TeV})^{-1}$, and a suppression in the coupling to the SM Lagrangian by a factor inversely proportional to the boundary mass term. Additionally, the couplings of the KK modes were suppressed relative to the radion, so that we would initially expect to observe only a single mode in experiments, despite the closely spaced mass spectrum.

We also considered the situation where the Higgs couples non-minimally to gravity and included an additional Higgs-curvature interaction term, resulting in a kinetic mixing between the radion and the Higgs. However, we found that at leading order the dilaton did not contribute to the mixing and our results reduced to those for the RS case. The mixing then had virtually no effect on the Higgs phenomenology, except in the case when the difference between the radion and Higgs masses was small. The contribution of the KK modes to the mixing was also investigated. However, we found that despite their close mass spacings, the cumulative effect of the KK modes was still too small to significantly effect the Higgs phenomenology.

The decay widths and branching fractions of the radion were calculated in Section 3.5 and found to be substantially different to the RS radion. This was largely due to the additional coupling between the radion and the gauge boson kinetic terms. In particular this led to a significantly increased branching fraction to $\gamma\gamma$, which provides an interesting distinguishing feature of this model and a promising search channel at the LHC.

The production of the radion via gluon-gluon fusion at the LHC was also discussed and found to be significant even for relatively large values of M. Finally, we determined the bounds on the parameter space from recent resonance searches at the LHC. Currently the only relevant constraint is from searches in the $\gamma\gamma$ final state, which gives a bound of $M \gtrsim 3.5 - 6.5\,\text{TeV}$ for values of $|\alpha|$ in the range 0.5-2.6 TeV when $\mu_{vis} = \frac{1}{3}|\alpha|$.

Higgs-Radion Mixing

4.1 Introduction

We previously explored the possibility of Higgs-radion mixing via the presence of a brane-localised $\xi R_4 H^\dagger H$ term in the context of the linear dilaton model, where it was found to have a relatively minor effect on the Higgs and radion phenomenology. However, more generally this mixing can play a very important role, which we now investigate in detail by returning our focus to the Randall-Sundrum model with the Standard Model in the bulk. We know that in order to avoid reintroducing large corrections to the Higgs mass, which from the dual perspective corresponds to ensuring that the Higgs mass operator remains irrelevant, the Higgs must be localised towards the IR brane. As a result, the simplest and most commonly considered possibility is to localise the Higgs on the IR brane. In this case, the Higgs-radion mixing which arises from a boundary localised coupling to the 4D Ricci scalar has been well studied [210, 222–224]. We shall explore the alternative possibility where the Higgs is allowed to propagate in the bulk and show that it leads to qualitatively distinct phenomenology, which has important experimental consequences.

The Higgs-radion system is of particular interest, since these may be the two lightest states arising from a new strongly-interacting sector or its dual warped description. Of course the Higgs is now known to be relatively light and its mass has been precisely determined by the LHC experiments: $m_h = 125.09 \pm 0.24$ [225]. On the other hand, if the conformal symmetry is broken by a marginally relevant operator it's possible for the radion to be parametrically lighter than the generic KK resonances due to its origin as the pNGB of spontaneously broken scale invariance [226–229].

In this chapter we consider a Higgs localised in the bulk of the extra dimension and study the effect of the coupling to the 5D Ricci scalar, $\xi R_5 H^\dagger H$. As in the brane-localised case, such a term leads to kinetic mixing between the radion

and the Higgs. Additionally the mechanism necessary for stabilising the extra dimension and giving mass to the radion will cause the background metric to deviate from AdS_5. We show that this leads to an additional source of mass mixing between the radion and the Higgs. We find that the radion couplings are also substantially modified in the case of a bulk Higgs, which can have a significant effect on the radion phenomenology. Most importantly, the bulk geometry (or equivalently conformal symmetry) enforces that the radion coupling to 4D scalar kinetic terms vanishes, which strongly suppresses the coupling to massive gauge bosons.

It is well known that generic warped models now require significant tuning ($\sim 1\%$) as ever stronger experimental bounds on new resonances increase the required little hierarchy between the electroweak and KK scales. However, a possibility that still remains relatively natural is that the Higgs itself arises as a pNGB of global symmetry breaking in the new strong sector. Its mass is then protected by a shift symmetry and it can be naturally lighter than the generic resonances. As we discussed in Section 2.4.5, explicit realisations of this scenario can be constructed using a warped framework, known as gauge-Higgs unification. We consider both possibilities with the aim of remaining relatively model independent. The 5D warped framework is used as a tool to motivate and calculate the various sources of Higgs-radion mixing and the couplings between the radion and Standard Model fields. We then use these results to construct the most general effective 4D Lagrangian describing the Higgs-radion system, which we use to study the LHC phenomenology.

Using this effective 4D Lagrangian, we then perform a numerical scan over the relevant parameters and impose the recent constraints from LHC measurements of the Higgs properties and exotic resonance searches. Matching the lighter mixed state's mass and signal strengths to the measured Higgs properties, we are able to constrain the production cross section and branching ratios of the heavier mixed state and identify the most promising search channels. Interestingly we find that in some regions of parameter space, the production of two light mixed states via the decay of the heavier mixed state can contribute as much as 30% to the total Higgs production cross section. Furthermore, in the case of negligible mixing, a light scalar state with a sizeable cross section into diphotons is still permitted by the LHC constraints used in our analysis, which provides a very interesting motivation to search in the diphoton channel at larger invariant masses. Since the completion of this analysis, such a search has been performed by the LHC collaborations and we discuss how this further constrains the relevant region of parameter space.

Finally, the ATLAS and CMS experiments have observed an intriguing excess of diphoton events at an invariant mass of 750 GeV in early Run-II data [97, 99, 230, 231]. We discuss the possibility that this excess could be due to a radion in the bulk Higgs scenario. We show that for a compositeness scale $\Lambda_r \gtrsim 2$ TeV and an extra dimension of size $kL \lesssim 20$ the excess can be explained while simultaneously satisfying the bounds from $\sqrt{s} = 8\,\text{TeV}$ resonance searches.

This chapter is organised as follows. In Sections 4.2 and 4.3 we introduce the radion and a simplified model of a bulk Higgs in warped 5D space and compute the different mixing terms that arise in the presence of the bulk $\xi R_5 H^\dagger H$ term. In Sections 4.4 and 4.5 we write the 4D effective Lagrangian describing the mixing between the radion/dilaton and the Higgs and provide the relevant couplings and branching fractions. Sections 4.6 and 4.7 discuss the LHC constraints and the phenomenology of the heavier mixed state, including future search strategies. Finally, we discuss the possibility that the radion could be responsible for the observed excess in diphoton events in Section 4.8. We summarise our results in Section 4.9.

4.2 The Radion

In this chapter we shall take the following convenient parametrisation of the 5D metric

$$ds^2 = e^{-2\tilde{A}(y)}\eta_{\mu\nu}dx^\mu dx^\nu - dy^2\,, \tag{4.1}$$

where $\eta_{\mu\nu} = \text{diag}(+,-,-,-)$ and $e^{-\tilde{A}(y)}$ is a convex function of y, with $\tilde{A}(y) = ky$ corresponding to the Randall-Sundrum solution. As discussed previously, an appropriate gauge choice allows one to decouple the spin-0 (radion) from the spin-2 (graviton) fluctuations of the metric such that the spin-0 fluctuations are given by,

$$ds^2 = e^{-2\tilde{A}(y)}\left(1-\Phi\right)\eta_{\mu\nu}dx^\mu dx^\nu - (1+2\Phi)dy^2\,. \tag{4.2}$$

In the absence of a stabilising mechanism, the radion is massless and it is simple to check that it consists of a single state with a profile in the extra-dimension given by

$$\Phi(x,y) = e^{2\tilde{A}(y)}\frac{2e^{-kL}}{\sqrt{3}M_{Pl}}r(x) \equiv e^{2(\tilde{A}(y)-kL)}\frac{2}{\Lambda_r}r(x)\,, \tag{4.3}$$

where we have used that $M_{Pl}^2 \approx M_5^3/k$.

The inclusion of an additional bulk scalar field to stabilise the extra dimension leads to a mixing of the gravity and scalar sectors and generates a mass for the physical state associated with the radion. This will produce deviations from the pure AdS_5

solution for the geometry; however, provided the back-reaction is not too large, the deviations tend to be small and the approximate form for the radion profile $\Phi(y) \sim e^{2ky}$ holds [46]. We will comment in Section 4.3.3 on the consequences of the back-reaction on the radion-Higgs mixing, which are important once the Higgs is moved to the bulk of the extra dimension.

4.3 Radion-Higgs Mixing

Light radion/dilaton phenomenology and mixing with an IR-brane localised Higgs has been studied extensively in the literature [210, 222, 232–234]. It has been found that recent LHC measurements, in particular of the Higgs mass and signal strengths, already put significant constraints on the parameter space of these models [235–237]. In this paper we study the consequences of moving the Higgs into the bulk of the extra dimension and mixing it with the gravity sector via a bulk term $\xi R_5 H^\dagger H$. Such a bulk mixing term was also considered in [50] but in the context of higher curvature Gauss-Bonnet terms. We motivate an effective 4D low energy action that describes all the possible mixing terms that one may encounter between the two light states in the model, the radion and the Higgs. We also derive the parametric size of these mixing terms. In this context let us briefly survey the possible localisation of the Higgs, what this implies for the radion-Higgs mixing in the theory, and the possibility of the Higgs as a pNGB.

4.3.1 The Brane Higgs Scenario

In this case one can simply write the Higgs part of the Lagrangian as follows:

$$S_{brane} = \int d^4x \sqrt{|\gamma(r(x))|} \left[|\mathcal{D}H|^2 - V(H) + \xi R_4 H^\dagger H \right] , \tag{4.4}$$

where γ is the induced metric on the boundary. After the Higgs gets a vev, v, one can perform a Taylor expansion of the potential,

$$V(H) = \sum \frac{\delta^n V(H)}{\delta H^n}\bigg|_{H\to v} h^n \, . \tag{4.5}$$

The mass mixing term that can arise from the $n = 1$ term in the above equation vanishes exactly due to the minimisation condition. No mixing of any type arises from the kinetic term, as $\partial_\mu v = 0$. This is the reason for the absence of any mass mixing in brane Higgs models. Only kinetic mixing via the usual term $\xi R_4 H^\dagger H$ is expected.

4.3.2 The Bulk Higgs Scenario

Let us now consider a scenario where the Higgs and the SM fields can access the 5D bulk. We use this model as a tool to motivate our effective action in Section 4.4 and therefore we briefly describe the process of EWSB and Higgs mass generation. Technical details of the calculation that are similar to those of [238] are deferred to Appendix C. In this case the full Higgs-radion action may be written as

$$S_{bulk} = \int_0^L d^5x\,\sqrt{g}\left[\left(\frac{M^3}{2}+\xi H^\dagger H\right)R_5 + |D_M H|^2 - V(H)\right] - \sum_{\alpha=0,1}\int d^4x\,\sqrt{\gamma}\left[\left(M^3+2\xi H^\dagger H\right)[K]+\lambda_\alpha(H)\right], \quad (4.6)$$

where $V(H) = -6k^2M^3 + c^2k^2|H|^2$ is the 5D bulk potential (c a dimensionless localisation parameter), $\lambda_\alpha(H)$ are the 4D brane potentials, γ is the induced metric, and $[K]$ denotes the jump in the extrinsic curvature across the brane. Note that in adding the direct coupling between the Higgs and the scalar curvature in the bulk, we must also modify the Gibbons-Hawking-York term to ensure the correct cancellation of boundary terms and a well-posed variational problem. EWSB is induced on the IR brane by taking

$$\lambda_1(H) = \frac{1}{2}\frac{\tilde{\lambda}}{k^2}\left(|H|^2 - \frac{\tilde{v}_{IR}^2 k^3}{2}\right)^2, \quad (4.7)$$

where $\tilde{\lambda}$ and $\tilde{v}_{IR}$ are dimensionless quantities. On the UV brane, we simply add a mass term

$$\lambda_0(H) = m_{UV}|H|^2\,. \quad (4.8)$$

To simplify our analysis, we assume that the Higgs back-reaction on the metric is negligible. This requires that the Higgs vev satisfy

$$|\xi|v^2 \ll M^3, \qquad |v'^2 - c^2k^2v^2 + 16\xi\tilde{A}'v\,v'| \ll 12\tilde{A}'^2M^3\,. \quad (4.9)$$

The explicit mixing terms of Eq. (4.6) contribute to the effective bulk and brane masses for the Higgs. It is straightforward to solve for the Higgs vev $v(y)$. Expressing it in terms of the physical observable v_{ew}, we find

$$v(y) = \sqrt{2(1+\beta)k}\,e^{ky}e^{(1+\beta)k(y-L)}v_{ew}\,, \quad (4.10)$$

where $\beta^2 = 4 + c^2 + 20\xi$. The explicit relation between v_{ew} and the 5D parameters is

$$v_{ew}^2 \approx \frac{\tilde{\lambda}\tilde{v}_{IR}^2 + 16\xi - 2(2+\beta)}{2(1+\beta)\tilde{\lambda}}\,\tilde{k}^2\,, \tag{4.11}$$

where $\tilde{k} \equiv ke^{-kL}$ and we have neglected terms suppressed by additional powers of e^{-kL}. Inserting our expression for $v(y)$ into Eq.(4.9), we find that the back-reaction is negligible for $O(1)$ values of ξ, β, and c, provided that both $k/M < 1$ and $v_{ew}/\tilde{k} < 1$.

The Higgs fluctuation $h(x,y) = \mathcal{H}(y)h(x)$, with mass m_h, has a more complex form. In the limit that the Higgs mass is small compared to the RS scale $\tilde{k}$, we find that the profile is approximately proportional to the vev:

$$\mathcal{H}(y) = \sqrt{2(1+\beta)k}\,e^{ky}e^{(1+\beta)k(y-L)} + \mathcal{O}(m_h^2/\tilde{k}^2)\,. \tag{4.12}$$

Using the IR b.c. one also can determine the mass m_h. The resultant equation is complicated in the general case. However, in our limiting case $m_h \ll \tilde{k}$, one can obtain an approximate analytical expression for the lightest mode given by

$$m_h^2 \approx 4(1+\beta)^2\tilde{\lambda}v_{ew}^2\,. \tag{4.13}$$

To investigate the mass mixing induced by the bulk Lagrangian Eq. (4.6), we expand the scalar curvature using the AdS_5 metric and the replacement $\Phi(x,y) = \Phi(y)r(x)$:

$$\begin{aligned} R_5 = &\Big(20\tilde{A}'(y) - 8\tilde{A}''(y)\Big) - e^{2\tilde{A}}\Phi(y)\,\partial^2 r(x) + \Big(-40\Phi(y)\tilde{A}'(y)^2 \\ &+ 28\tilde{A}'(y)\Phi'(y) + 16\Phi(y)\tilde{A}''(y) - 4\Phi''(y)\Big)\,r(x) + \mathcal{O}\big(r(x)\big)^2\,, \\ [K] = &\,4\tilde{A}'(y) + \mathcal{O}\big(r(x)\big)^2\,. \end{aligned} \tag{4.14}$$

Now using Eq. (4.3) and $\tilde{A}(y) \sim ky$ we find that the expressions reduce to

$$R_5 = 20k^2 - e^{2\tilde{A}}\Phi(y)\,\partial^2 r(x) \quad \text{and} \quad [K] = 4k\,. \tag{4.15}$$

The non-derivative terms linear in the radion vanish. There could be a residual mass mixing that arises from the product of the constant terms in Eq. (4.15) with the linear fluctuation in the volume element. However, as discussed below Eq. (4.9), these constant terms are effective bulk and brane masses for the Higgs, and are more naturally associated with the mixing from the potentials. Indeed, one can explicitly redefine the Lagrangian mass parameters to absorb these constant

terms:

$$c^2 \to c^2 - 20\xi\,, \qquad \tilde{v}_{IR}^2 \to \tilde{v}_{IR}^2 - \frac{16\xi}{\tilde{\lambda}}\,, \qquad m_{UV} \to m_{UV} + 8\xi k\,. \tag{4.16}$$

This will naturally lead to modifications to the definition of β, and the relation between v_{ew} and the Lagrangian parameters. Finally we compute the mass mixing that might arise from the potential terms in the bulk (a) and on the IR brane (b) and the kinetic term in the bulk (c),

$$-\int d^5x\sqrt{g}\,c^2k^2|H|^2 \;\to\; 2(\beta^2-4)\frac{v_{ew}}{\Lambda_r}\tilde{k}^2\,h(x)r(x)\,, \tag{4.17a}$$

$$-\int d^4x\sqrt{\gamma}\,\lambda_1(H) \;\to\; -8(1+\beta)(2+\beta)\frac{v_{ew}}{\Lambda_r}\tilde{k}^2\,h(x)r(x)\,, \tag{4.17b}$$

$$\int d^5x\sqrt{g}\,g^{55}D_5H^\dagger D_5H \;\to\; 6(2+\beta)^2\frac{v_{ew}}{\Lambda_r}\tilde{k}^2\,h(x)r(x)\,. \tag{4.17c}$$

We have neglected the UV potential as the Higgs is localised near the IR brane.[†] We find that these contributions cancel exactly and leave us with no mass mixing between the Higgs and the radion.

The derivative terms in Eq. (4.15) lead to a kinetic mixing, as in the brane Higgs case. A quantitative difference from the brane scenario is that the size of the induced mixing is β-dependent. Specifically,

$$\int d^5x\,\sqrt{g}\,\xi\,R_5H^\dagger H \to 2\xi\frac{1+\beta}{2+\beta}\,\frac{v_{ew}}{\Lambda_r}\,(\partial^\mu h(x))(\partial_\mu r(x))\,. \tag{4.18}$$

The mixing term also gives contributions to the radion kinetic term. One contribution arises when the linear derivative term combines with the linear term in $\sqrt{g}$. Another contribution of the same order comes from the terms in R_5 quadratic in the radion. The net result is

$$\int d^5x\,\sqrt{g}\,\xi\,R_5H^\dagger H \to 3\xi\frac{1+\beta}{3+\beta}\,\frac{v_{ew}^2}{\Lambda_r^2}\,(\partial^\mu r(x))(\partial_\mu r(x))\,. \tag{4.19}$$

4.3.3 Bulk Higgs with Back-reaction

In the above discussion we did not consider the back-reaction of the Higgs and the radion on the metric. This will modify the bulk profiles of the Higgs, the Higgs vev and the radion. The Higgs back-reaction can be assumed to be small as already argued; even if we include its effect, it can at most induce a mass mixing proportional to the Higgs mass $\sim m_h^2 v_{ew}/\Lambda_r$. A mass mixing of this order can also

[†]One can show that the contribution from the UV potential cancels with additional exponentially suppressed terms that have been omitted in Eq. (4.17).

arise if we include the differences between the Higgs and Higgs vev bulk profiles $v(y) \neq \mathcal{H}(y)$; that is, if we expand the Bessel functions in Eq. (C.17) to include sub-leading terms in ϵ_h.

A larger contribution to the mass mixing may arise due to the back-reaction of the radion. Let us assume that the stabilising mechanism results in a small perturbation in the bulk profile of the fields. We can write the following ansatz for the perturbed radion profile and the metric

$$\begin{aligned} \Phi(y) &\sim N_r e^{2ky}(1 + l^2 f(y)) \,, \\ \tilde{A}(y) &\sim ky + \frac{l^2}{6} e^{-2uy} \,, \end{aligned} \tag{4.20}$$

where $uL = \phi_T/\phi_P$; $\phi_{T(P)}$ is the radion vev on the TeV (Planck) brane introduced to stabilise the bulk; and $l^2 = \phi_P/\sqrt{2M^3}$. The equation of motion for the radion field can be solved using the above ansatz as an expansion in $u/k = \epsilon \sim 1/37$ [222]. Expanding up to ϵ^2 we obtain

$$f(y) = \frac{1}{3}\left((1-\epsilon)e^{-2uy} + \epsilon^2\left(e^{-2ky} - e^{2k(y-L)}\right)\right) . \tag{4.21}$$

One can then solve for the normalisation factor at this order in the expansion

$$N_r = \frac{2}{\Lambda_r}\left(1 + e^{-2uL}\frac{l^2}{6}(-1 + \epsilon + 2\epsilon^2)\right) . \tag{4.22}$$

Solving for the Higgs vev in the same approximation yields

$$v(y) = Be^{(2+\beta)ky}\left(1 + \frac{l^2}{3}\,\frac{2+\beta}{\beta}\left(1 + \frac{\epsilon}{\beta} + \frac{\epsilon^2}{\beta^2}\right)e^{-2\epsilon ky}\right) , \tag{4.23}$$

where B is given by

$$\begin{aligned} B^2 = 2kv_{ew}^2(1+\beta)e^{-2(1+\beta)kL}\Bigg(1 + \frac{l^2}{3\beta^3}\Big(&-(4+\beta)\beta^2 \\ &+\frac{(\beta(\beta+8)+4)\beta}{\beta+1}\epsilon - \frac{\beta(5\beta^3+18\beta+14)+4}{(\beta+1)^2}\epsilon^2\Big)\Bigg) . \end{aligned} \tag{4.24}$$

Finally we will assume that

$$h(x,y) = h(x)\left(\frac{v(y)}{v_{ew}} + \mathcal{O}(m_h^2)\right) . \tag{4.25}$$

Thus including the radion back-reaction, the Higgs-radion mixing action at leading order can now be written as

$$S_{h-r} = \int d^4x \left[-\xi \frac{2(1+\beta)}{2+\beta} \frac{v_{ew}}{\Lambda_r} h(x) \partial_\mu \partial^\mu r(x) + \left(\xi \frac{2(7+4\beta)}{2+\beta} - \frac{2(1+\beta)}{\beta} \right) \frac{v_{ew}}{\Lambda_r} m_r^2 h(x) r(x) \right] , \quad (4.26)$$

where m_r is the radion mass given by [222]

$$m_r^2 = \frac{8}{3} l^2 (k\epsilon)^2 e^{-2kL} . \quad (4.27)$$

As expected we find that the mass mixing terms arising from the radion back-reaction are proportional to the radion mass.

4.3.4 Composite Higgs Models

As discussed in Section 2.4.5, the 5D analogue of the pNGB composite Higgs is the GHU scenario where the Higgs is identified as the fifth component of a 5D gauge boson $A_M = (A_\mu, A_5)$ belonging to the coset group $\mathcal{G}/\mathcal{H}$. The higher-dimensional gauge symmetry translates to a 4D shift symmetry of the Higgs. In a slice of AdS_5, the A_5 sector of the gauge boson kinetic term in the bulk Lagrangian is

$$\begin{aligned} & -\frac{1}{2} \int d^4x\, dy\; e^{-2ky} \left[(\partial A_5)^2 - 2\eta^{\mu\nu} \partial_\mu A_5 \partial_5 A_\nu \right] + \dots \\ & \xrightarrow{\text{gauge-fixing}} \quad -\frac{1}{2} \int d^4x\, dy\; e^{+2ky} (\partial_\mu A_5^{(0)}(x))^2 + \dots . \end{aligned} \quad (4.28)$$

Notice that the higher-dimensional gauge symmetry prevents a tree-level mass for A_5 both in the bulk and on the brane. Also, the antisymmetric nature of the field strength tensor prevents a term like $|\partial_y A_5(y,x)|^2$. This immediately implies that a composite Higgs cannot have mass mixing with the radion even when the back-reaction is considered. The only possible mixing can be introduced on the brane after the shift symmetry is explicitly broken by the Yukawa and SM gauge interactions to develop a potential. The relevant brane term reads,

$$S_{CH}|_{h-r} = \int d^4x\, \xi_4 R_4 H^\dagger H . \quad (4.29)$$

One can estimate the size of ξ_4 by recalling that pNGB potentials are generated at loop level primarily through the top Yukawa which is also responsible for the

Higgs developing a potential. Naive dimensional analysis suggests that

$$\xi_4 \sim \frac{m_h^2}{f^2}\,\Gamma(v_{ew}/f)\,, \tag{4.30}$$

where f is the compositeness scale given by ke^{-kL} and $\Gamma(v_{ew}/f)$ is a generic function of v_{ew}/f. Thus, we expect the kinetic mixing induced by this term to be very small.

4.4 Effective Action

So far we have worked with a 5D warped scenario, considering two particular examples of EWSB, in both of which the Higgs resides in the bulk of the extra dimension. In this way we have been able to determine the possible induced mixing terms between the radion and the Higgs. Though we have determined these mixing terms for a particular scenario we expect their dependence on physical quantities to be general. In fact, from the 4D point of view through the AdS/CFT correspondence, we are describing a scenario of a conformal sector that is spontaneously broken leading to a light pseudo-Nambu-Goldstone boson known as the dilaton. This light state can mix with the other light state in the theory, the Higgs, via the conformally covariant generalisation of the gauge covariant derivative [239, 240]:

$$\left|\left(D_\mu - \Delta\frac{\partial_\mu r(x)}{r(x)}\right)H\right|^2 + (1-6\xi)H^\dagger D_\mu H\frac{\partial^\mu r(x)}{r(x)}\,, \tag{4.31}$$

where Δ is the Higgs conformal weight, D_μ is the gauge covariant derivative and we have included an additional term as suggested in Ref. [240] in order to account for the breaking of the special conformal symmetries, which in the 5D picture corresponds to the case $\xi \neq 1/6$. This interaction leads to kinetic mixing as found in the previous section and is always expected to be present. It is also the only mixing allowed when the CFT is broken spontaneously, as we also saw in our simplified 5D calculation. An explicit breaking of the conformal symmetry is signalled by the presence of a non-vanishing dilaton mass and consequently the possibility of a mass mixing term between the dilaton and the Higgs field. This is represented in the 5D picture by the deformation of AdS_5 space due to back-reaction effects responsible for the stabilisation of the extra dimension and thus, for the generation of the radion mass. As we saw, this explicit breaking of the conformal symmetry leads to mass mixing between the radion and the Higgs in the 5D picture as described in Eq. (4.26).

It is then clear that from a purely 4D perspective, we can represent the most general effective phenomenological Lagrangian describing the light degrees of freedom of a spontaneously broken conformal sector by,

$$\mathcal{L}_{eff} = \frac{1}{2}\partial_\mu h(x)\partial^\mu h(x) - \frac{1}{2}m_h^2 h(x)^2 + \frac{1}{2}\left(1 + c_2\frac{v_{ew}^2}{\Lambda_r^2}\right)\partial_\mu r(x)\partial^\mu r(x) - \frac{1}{2}m_r^2 r(x)^2 - c_1\frac{v_{ew}}{\Lambda_r}\partial_\mu h(x)\partial^\mu r(x) - c_3\frac{v_{ew}}{\Lambda_r}m_r^2 h(x)r(x)\,, \tag{4.32}$$

where c_1, c_2 and c_3 are $\mathcal{O}(1)$ numerical coefficients, and we use the terms radion/dilaton interchangeably. From this point onwards we focus on this phenomenological Lagrangian to describe the possible mixing scenarios that may arise:

1. The no mass mixing scenario, $c_3 = 0$. From the 5D point of view, this case corresponds to a pure AdS_5 slice where the back-reaction on the geometry from the radion potential that stabilises the extra dimension can be neglected. Strictly speaking, it is not compatible to have a massive radion and no mass mixing unless a tuning of the parameters is involved such that $c_3 = 0$. From the 4D point of view, this corresponds to no explicit conformal breaking parameter in the dilaton self interactions and thus to a CFT that is not badly broken.

2. The generic scenario where $c_1, c_3 \neq 0$ corresponds from the 5D point of view to including the leading back-reaction contributions of the radion potential and from the 4D point of view to explicit conformal breaking terms in the dilaton potential.

3. The 5D GHU or 4D pNGB composite Higgs scenarios correspond to $c_1 \ll 1$ and $c_3 = 0$ when explicit sources of conformal breaking are neglected.

Despite the fact that a brane or a bulk Higgs may fall into the same mixing category, the phenomenology can be very different due to the way in which they perceive the conformal breaking, as we will see in the next section. For the purposes of studying the radion-Higgs mixing and its effect on both the Higgs and radion phenomenology at colliders, we shall consider c_1, c_2 and c_3 as free parameters. We will see in the next section that the GHU/pNGB composite Higgs scenario reduces phenomenologically to the case of a brane Higgs with $c_1 \ll 1$, and has therefore been covered by previous radion studies [237]. Hence we focus our parameter scans on covering all possible values of c_1, c_2 and c_3 for a bulk scalar Higgs, which provides phenomenologically distinct signatures with respect to the brane Higgs case.

One can diagonalise the kinetic term in Eq. (4.32) by going to a new basis

$$\begin{aligned} h &= h' + c_1(v_{ew}/\Lambda_r)r'/Z\,, \\ r &= r'/Z\,, \end{aligned} \tag{4.33}$$

where $Z^2 = 1 + (c_2 + c_1^2)\frac{v_{ew}^2}{\Lambda_r^2}$. This transformation decouples the kinetic mixing but introduces additional mass mixing terms. The mass matrix in the basis (r', h') then takes the form

$$\begin{aligned} M &= \begin{pmatrix} \frac{m_r^2}{Z^2} + \frac{1}{Z^2}\frac{v_{ew}^2}{\Lambda_r^2}(c_1^2 m_h^2 + 2c_1 c_3 m_r^2) & \frac{1}{Z}\frac{v_{ew}}{\Lambda_r}(c_1 m_h^2 + c_3 m_r^2) \\ \frac{1}{Z}\frac{v_{ew}}{\Lambda_r}(c_1 m_h^2 + c_3 m_r^2) & m_h^2 \end{pmatrix} \\ &\equiv \begin{pmatrix} M_{11} & M_{12} \\ M_{12} & M_{22} \end{pmatrix}. \end{aligned} \tag{4.34}$$

The mass eigenbasis is obtained by the orthogonal transformation

$$\begin{pmatrix} r' \\ h' \end{pmatrix} = \begin{pmatrix} U_{r,-} & U_{r,+} \\ U_{h,-} & U_{h,+} \end{pmatrix} \begin{pmatrix} \phi_- \\ \phi_+ \end{pmatrix}, \tag{4.35}$$

where $\Delta = \sqrt{(M_{11} - M_{22})^2 + 4M_{12}^2}$ and

$$\begin{aligned} U_{r,-} &= \frac{M_{11} - M_{22} - \Delta}{\sqrt{(M_{11} - M_{22} - \Delta)^2 + 4M_{12}^2}}\,, & U_{r,+} &= \frac{M_{11} - M_{22} + \Delta}{\sqrt{(M_{11} - M_{22} + \Delta)^2 + 4M_{12}^2}}\,, \\ U_{h,-} &= \frac{2M_{12}}{\sqrt{(M_{11} - M_{22} - \Delta)^2 + 4M_{12}^2}}\,, & U_{h,+} &= \frac{2M_{12}}{\sqrt{(M_{11} - M_{22} + \Delta)^2 + 4M_{12}^2}}\,. \end{aligned} \tag{4.36}$$

There are correspondingly two eigenstates; a lighter one $\phi_- = U_{r,-}r' + U_{h,-}h'$ and a heavier one $\phi_+ = U_{r,+}r' + U_{h,+}h'$, with masses

$$m_{\phi_\pm}^2 = \frac{1}{2}(M_{11} + M_{22} \pm \Delta)\,. \tag{4.37}$$

The gauge basis is related to the mass basis according to

$$\begin{aligned} r &= r_+\phi_+ + r_-\phi_-\,, \\ h &= h_+\phi_+ + h_-\phi_-\,, \end{aligned} \tag{4.38}$$

where we have defined

$$\begin{aligned} r_\pm &= \frac{U_{r,\pm}}{Z}\,, \\ h_\pm &= U_{h,\pm} + \frac{c_1}{Z}\frac{v_{ew}}{\Lambda_r}U_{r,\pm}\,. \end{aligned} \tag{4.39}$$

Note that because of the non-unitary transformation, $c_+^2 + c_-^2 \neq 1$ for $c = h, r$. However, this definition is useful to determine the couplings in the mass basis. In fact, notice that h_+ and r_- provide respectively the SM Higgs-like and radion-like couplings of the heavier and lighter mass eigenstates $\phi_+(x)$ and $\phi_-(x)$, and moreover due to the non-unitary transformation between the different bases, $h_+ = 0$ does not imply that $r_- = 0$ and vice versa.

4.5 Higgs and Radion Couplings, Mixing and Branching Ratios

4.5.1 Higgs and Radion Couplings

Though we motivated our effective theory by studying a particular 5D scenario, we ultimately decided to focus on an effective 4D picture wherein we consider two types of Higgs sector: i) the Higgs is identified with a light scalar doublet charged under the gauge group $SU(2)_L \times U(1)_Y$; or ii) the Higgs field is identified with a composite pNGB of an enlarged broken global symmetry group that contains $SU(2)_L \times U(1)_Y$ as a subgroup. In both cases there is an associated conformal sector that is spontaneously broken at an energy scale f and that in our effective theory translates into the existence of a possible light state; the dilaton. One may be worried about possible contributions to the Higgs couplings arising from mixing or loop-effects involving resonances of the conformal sector. However, notice that in case i) the only symmetry additional to those already found in the SM is the spontaneously broken conformal symmetry. We expect any possible additional composite resonances besides the dilaton to have masses of the order $m_\rho \sim g_\rho f$, with $g_\rho \gg 1$ the strong coupling in the conformal sector, making their effects on the Higgs couplings strongly suppressed. In case ii) due to the enlarged global group in which SM particles are embedded and due to the shift symmetry protection of the Higgs, there is a relationship between the Higgs mass and light top fermionic resonances of the form $m_h^2 \propto m_t^2 m_Q^2 / f^2$. Therefore in order to reproduce a light Higgs mass, one usually finds the existence of light fermionic resonances that couple strongly to the Higgs, with masses $m_Q \sim g_\psi f \ll g_\rho f$. This can have significant effects, in particular for Higgs couplings to gluons or photons. It has been shown nonetheless that due to the pseudo-Nambu-Goldstone nature of the Higgs, the resonant fermionic loop contributions cancel against the modified top quark Yukawa coupling, and lead to modifications in the coupling to gluons that

are suppressed by the ratio $v^2/f^2 \lesssim 0.01$ [241]. Therefore, in the two Higgs scenarios considered, we do not expect sizeable deviations of the Higgs couplings from their SM values, and thus for simplicity we restrict the couplings to SM values.[†]

Allowing for the possibility of a bulk Higgs implies that some of the known radion couplings to SM fields are modified, in particular those involving radion couplings to the Higgs field itself, as well as to massive gauge bosons. We use the 5D language as a tool to calculate the couplings and assume a given warp factor, kL, that solves the hierarchy problem; however our results are general with the replacement $\Lambda_r = f$. As was shown in Ref. [243], the bulk radion couples at linear order to SM fields through the bulk stress energy tensor as

$$S_{radion} = \int d^4x dz \sqrt{g}\, \frac{\Phi(x,z)}{2} \left[\Theta^M_M - 3 g_{zz}\Theta^{zz}\right] , \tag{4.40}$$

where the conformal coordinate z is related to the extra-dimensional coordinate y as $dy = e^{-\tilde{A}} dz$, and Θ^{MN} is the bulk stress energy tensor which can be written as

$$\Theta^{MN} = -\frac{2}{\sqrt{g}} \frac{\delta(\mathcal{L}_{bulk}\sqrt{g})}{\delta g_{MN}} = -2\frac{\delta(\mathcal{L}_{bulk})}{\delta g_{MN}} + g^{MN}\mathcal{L}_{bulk}\,. \tag{4.41}$$

Focusing on the coupling to SM gauge bosons (massive or massless), one can easily show using Eq. (4.40) that there will always be a non-vanishing coupling arising from the bulk kinetic terms for the gauge fields

$$S_{radion} = -\frac{1}{4}\int d^4x dy\, \Phi(x,y) F_{\mu\nu}F^{\mu\nu} = -\int d^4x\, \frac{r(x)}{4\Lambda_r}\frac{1}{kL} F_{\mu\nu}F^{\mu\nu}\,, \tag{4.42}$$

where we used $\Theta^{MN} = -F^{MP}F^N_P + \frac{1}{4} g^{MN} F_{PQ}F^{PQ}$. As was argued in [243], the fact that this tree level coupling is non-vanishing implies that loop effects merely renormalise this tree-level operator. Therefore, loop effects are prominent on the branes where no tree-level coupling is allowed, and are stronger on the IR brane where the radion is usually closely localised. This provides the main mechanism of radion production through gluon fusion as is usual in radion scenarios. We refer the reader to Ref. [243] for the appropriate expressions for the radion-digluon and

[†]In the case of generic warped extra dimensional scenarios the mass scale of the lowest lying KK fermions $m_{KK} \lesssim \Lambda_r$. A naive estimate of the shift in the Higgs coupling to gluons due to the KK towers of the SM fermions is as follows,

$$\frac{\delta\Gamma^{KK}_{gg}}{\Gamma^{SM}_{gg}} \sim 4C_2(\nabla_{NP}) N_f \sum_n \frac{v}{m^{(n)}_{KK}} \frac{\partial m^{(n)}_{KK}}{\partial v} \sim \mathcal{O}(1)\left(\frac{v}{ke^{-\pi kL}}\right)^2 ,$$

where $C_2(\nabla_{NP})$ is the quadratic Casimir of the KK states and $N_f = 6$. This translates into a lower limit on the mass of the lightest KK state that may be as large as 3.2 TeV for a 20% shift in the decay width, which is the resolution of current experimental data. A detailed calculation of this is rather model dependent [242].

radion-diphoton couplings, including the contributions from fermion loops as well as the QCD and QED trace anomalies respectively.

In addition, via electroweak symmetry breaking, there is in principle a possibly large additional coupling of the radion to a pair of massive gauge bosons, which dominates in the case of a brane-localised Higgs. As is well-known, the gauge bosons acquire their mass through the kinetic term of the Higgs field, which in the case of a bulk Higgs scalar leads to mass terms for the gauge bosons of the form

$$\mathcal{L}_{bulk} = D^M H^\dagger D_M H \to m_W^2 W_\mu^+ W^{\mu,-} + \frac{1}{2} m_Z^2 Z_\mu Z^\mu \,. \tag{4.43}$$

It follows that the contribution to the stress energy tensor is

$$\Theta^{MN} = -2D^M H D^N H^\dagger + g^{MN} D^P H^\dagger D_P H \,, \tag{4.44}$$

which implies that $\Theta^M_M = 3D^M H D_M H^\dagger = 3e^{2\tilde{A}} D^\mu H D_\mu H^\dagger$, where the last index is contracted using the 5D Minkowski metric. Now, $-3g_{zz}\Theta^{zz} = -3e^{2\tilde{A}} D^\mu H D_\mu H^\dagger$, which exactly compensates the contribution from Θ^M_M. Thus the linear radion coupling to the electroweak gauge boson mass terms vanishes in the case of a bulk Higgs. This result can also be checked by simply expanding the metric in its spin-0 fluctuations in the action

$$\begin{aligned}
\mathcal{S}_{bulk} &= \int d^4x dy \sqrt{g}\, D^M H^\dagger D_M H \\
&\to \int d^4x dy\, e^{-4\tilde{A}(y)} \sqrt{(1-\Phi)^4(1+2\Phi)}\, e^{2\tilde{A}(y)} (1-\Phi)^{-1} D^\mu H^\dagger D_\mu H \\
&= \int d^4x dy\, (1+\mathcal{O}(\Phi^2))\, e^{-2\tilde{A}(y)} D^\mu H^\dagger D_\mu H \,,
\end{aligned} \tag{4.45}$$

where the Greek indices are contracted using the 4D Minkowski metric. Therefore we also see in this way that the coupling vanishes. Notice that this result is completely general and holds for the kinetic term of any scalar. We can understand this result from the 4D point of view as follows. As we just noticed, the vanishing of this particular coupling is geometrical from the 5D point of view. As a matter of fact we can take both the UV and IR branes to infinity, and the results would still hold in pure AdS_5-space. In that particular case, it is clear that the conformal symmetry is exact. If we look at the 4D picture this implies that the 4D-analogue of the radion, the dilaton field, can only couple derivatively to conformally invariant operators, in particular to $D_\mu \Phi D^\mu \Phi$, where Φ is a 4D-scalar field. Therefore from Lorentz invariance we see that no linear coupling can be written that derivatively couples the radion to $D_\mu \Phi D^\mu \Phi$. This has important consequences for the radion phenomenology when the Higgs is a scalar in the bulk, since then its coupling

to pairs of massive SM gauge bosons only comes from Eq. (4.40) and is highly suppressed.

In the case of gauge-Higgs unification scenarios, the Higgs field is identified with the fifth component $A_5(x,y)$ of a gauge field belonging to the coset $\mathcal{G}/\mathcal{H}$ of an enlarged gauge group $\mathcal{G}$ that is broken down to the subgroup $\mathcal{H}$ via boundary conditions. In that case the equivalent of the scalar kinetic term is given by

$$\mathcal{S}_{bulk} = \int d^4x dy \sqrt{g}\, g^{\mu\nu} g^{55} \mathrm{Tr}[F_{\mu 5} F_{\nu 5}]\,, \tag{4.46}$$

Due to the additional metric factor in the kinetic term, there is a non-vanishing radion coupling proportional to the EWSB induced masses

$$\begin{aligned} &\int d^4x dy\, e^{-4\tilde{A}(y)} \sqrt{(1-\Phi)^4(1+2\Phi)}\, e^{2\tilde{A}(y)} (1-\Phi)^{-1}(1+2\Phi)^{-1}\, \mathrm{Tr}[F_{\mu 5} F^{\mu 5}] \\ &= \int d^4x dy\, e^{-2\tilde{A}(y)} (1 - 2\Phi + \mathcal{O}(\Phi^2))\, \mathrm{Tr}[F_{\mu 5} F^{\mu 5}]\,, \end{aligned} \tag{4.47}$$

where the indices are contracted using the Minkowski metric. Thus, in these kinds of scenarios the radion coupling to massive SM gauge bosons is similar to that encountered for a Higgs localised on the IR brane.

Another potential difference with respect to the brane Higgs scenario is in the Yukawa induced SM fermion-radion interactions arising from the term

$$\Delta\mathcal{L}_Y = -\int d^4x dy \sqrt{g}\, Y_5 \left[H \bar{f} f + h.c. \right]\,, \tag{4.48}$$

where Y_5 is the 5D Yukawa coupling. We shall make use of the following normalised left-handed and right-handed profiles for the fermion zero modes

$$f_L(y) = \frac{e^{(\frac{1}{2} - c_L)ky}}{N_L}\,, \qquad f_R(y) = \frac{e^{(\frac{1}{2} + c_R)ky}}{N_R}\,, \tag{4.49}$$

where $f_L(y)$ and $f_R(y)$ satisfy

$$\int_0^L dy f_{L,R}^2(y) = 1 \qquad \longrightarrow \qquad N_{L,R} = \sqrt{\frac{e^{(1 \mp 2c_{L,R})kL} - 1}{(1 \mp 2c_{L,R})k}}\,. \tag{4.50}$$

The upper and lower signs correspond to N_L and N_R respectively, while $c_{L,R}$ are the fermion bulk mass parameters defined by $M_{L,R} = c_{L,R} k$. Using Eq. (4.10) for the Higgs vev, we can obtain an expression for the SM fermion masses by integrating the zero-mode profiles for the fermions and the Higgs vev along the

extra dimension

$$m_f = \int_0^L dy\, e^{-\tilde{A}(y)}\, f_L(y) f_R(y) v(y) Y_5$$
$$= \frac{1}{N_R}\frac{1}{N_L}\sqrt{2(1+\beta)k}\, v_{ew} e^{-(1+\beta)kL}\frac{(e^{(2-c_L+c_R+\beta)kL}-1)}{(2-c_L+c_R+\beta)k} Y_5\,. \qquad (4.51)$$

The interaction in Eq. (4.48), once expanded in the spin-0 fluctuation of the metric, takes the form

$$-\int d^4x dy\, e^{-\tilde{A}(y)}\,(-\Phi(y))\, Y_5\, f_L(y)\, f_R(y)\, v(y)\,(r(x)\bar{f}^0(x) f^0(x) + h.c.)$$
$$\simeq \frac{2m_f}{\Lambda_r}\frac{(2-c_L+c_R+\beta)}{(4-c_L+c_R+\beta)}\int d^4x\,(r(x)\bar{f}^0(x) f^0(x) + h.c.)\,, \qquad (4.52)$$

where in the last line we assume that the fermion and Higgs profiles are IR localised and satisfy $1-c_L+c_R+\beta > 0$. So contrary to the gauge-boson case, we notice that the coupling of the radion to, in particular, the top quark can be non-negligible. In order to remain model-independent we will henceforth approximate the radion-fermion coupling by m_f/Λ_r, which is equivalent to the case of a brane localised Higgs.

Finally we look at the coupling of the radion to two Higgs. For this coupling there is a kinetic mixing contribution coming from $\sqrt{g}R_5 H^\dagger H$ as well as contributions from the Higgs kinetic term, bulk Higgs mass $\sqrt{g}c^2k^2H^\dagger H$ and important boundary contributions from the IR-brane potential $\sqrt{g_4}\lambda_{IR}(H)$. The Higgs kinetic and bulk mass contributions cancel against some of the IR-brane contributions and after replacing $\tilde{\lambda}$ in terms of m_h^2 and v_{ew}^2 using Eq. (4.13), one can write the radion-diHiggs coupling in the form

$$\int d^4x \frac{1}{\Lambda_r}\left(2m_h^2 - \frac{c_1}{2}m_r^2\right) r(x) h(x)^2\,. \qquad (4.53)$$

We have also used the radion equation of motion $\Box r(x) = -m_r^2 r(x)$. Given Eq. (4.53), we do not expect large differences arising in comparison with the brane localised Higgs counterpart.

To summarise, after studying the radion couplings to SM particles, we expect the largest modifications in the phenomenology of the bulk scalar Higgs scenario to arise due to the vanishing of the radion-massive diboson coupling proportional to the gauge boson mass. We list for completeness in Table 4.1 the most relevant couplings of the unmixed Higgs and radion states, where $\tau_{i,(h,r)} = 4m_i^2/m_{(h,r)}^2$, $F_{1/2}$ and F_1 are the usual integrals over fermion and gauge boson states running in the loop and $b_{QED} = -11/3$ and $b_{QCD} = 7$ are the β-function coefficients.

	$h(x)$	$r(x)$
$f\bar{f}$	$-\frac{m_f}{v}$	$\frac{m_f}{\Lambda_r}$
$W^\mu W_\mu$	$\frac{2m_W^2}{v}$	–
$Z^\mu Z_\mu$	$\frac{m_Z^2}{v}$	–
$W^{\mu\nu} W_{\mu\nu}$	–	$\frac{-1}{2\Lambda_r}\frac{1}{kL}$
$Z^{\mu\nu} Z_{\mu\nu}$	–	$\frac{-1}{4\Lambda_r}\frac{1}{kL}$
hh	–	$\frac{1}{\Lambda_r}\left(2m_h^2 - \frac{c_1}{2}m_r^2\right)$
$\gamma\gamma$	$\frac{-1}{4v}\left(F_1(\tau_{W,h}) + \frac{4}{3}F_{1/2}(\tau_{t,r})\right)\frac{\alpha_{EM}}{2\pi}$	$\frac{-1}{4\Lambda_r}\left(\frac{1}{kL} + \left[b_{QED} - \frac{4}{3}F_{1/2}(\tau_{t,h})\right]\frac{\alpha_{EM}}{2\pi}\right)$
gg	$\frac{-1}{4v}\frac{\alpha_3}{4\pi}F_{1/2}(\tau_{t,h})$	$\frac{-1}{4\Lambda_r}\left(\frac{1}{kL} + \left[b_{QCD} - \frac{1}{2}F_{1/2}(\tau_{t,r})\right]\frac{\alpha_3}{2\pi}\right)$

TABLE 4.1: Phenomenologically relevant couplings of the gauge states $h(x)$ and $r(x)$ to SM particles.

4.5.2 Mixing and Branching Ratios

Most of the interactions between the radion and SM particles, except those with massive gauge bosons and to the Higgs itself, have the same structure as those of the SM Higgs to fermions and gauge bosons. So one can easily obtain most of the decay rates of the mixed states by inspecting the well-known expressions for the Higgs decay rates (see for example [244]) and using the replacements: $m_h \to m_{\phi_\pm}$ and $g_h \to g_\pm$, where from Eq. (4.38),

$$g_\pm = \left(U_{h,\pm} + \frac{c_1}{Z}\frac{v_{ew}}{\Lambda_r}U_{r,\pm}\right) g_h + \frac{1}{Z}U_{r,\pm}\, g_r \,, \tag{4.54}$$

with g_h and g_r the Higgs and radion couplings to SM particles respectively.

The interactions that have a structure different than those of the Higgs to SM particles are those of the mixed states to massive gauge bosons and among the mixed states themselves. In this case, the decay rate of the mixed states into massive gauge bosons can be written as

$$\Gamma_{\phi_\pm WW} = \frac{m_{\phi_\pm}}{32\pi}\sqrt{1-4\frac{m_W^2}{m_{\phi_\pm}^2}} \times \left[\frac{U_{r,\pm}^2}{Z^2}\frac{g_{rWW}^2}{4}m_{\phi_\pm}^2\left(1-4\frac{m_W^2}{m_{\phi_\pm}^2}+6\frac{m_W^4}{m_{\phi_\pm}^4}\right)\right.$$
$$+\frac{U_{r,\pm}}{Z}\left(U_{h,\pm}+\frac{c_1}{Z}\frac{v_{ew}}{\Lambda_r}U_{r,\pm}\right)\frac{3}{2}g_{rWW}g_{hWW}\left(1-2\frac{m_W^2}{m_{\phi_\pm}^2}\right)$$
$$\left.+2\left(U_{h,\pm}+\frac{c_1}{Z}\frac{v_{ew}}{\Lambda_r}U_{r,\pm}\right)^2\frac{g_{hWW}^2}{4m_W^4}m_{\phi_\pm}^2\left(1-4\frac{m_W^2}{m_{\phi_\pm}^2}+12\frac{m_W^4}{m_{\phi_\pm}^4}\right)\right], \quad (4.55)$$

where g_{rWW} and g_{hWW} are among the couplings listed in Table 4.1, and for decays into Z pairs one needs to divide Eq. (4.55) by 2, replace $m_W \to m_Z$, $g_{rWW} \to 2g_{rZZ}$ and $g_{hWW} \to 2g_{hZZ}$.

Using Eq. (4.53) and assuming that the ϕ_+ state is mostly radion while ϕ_- is mostly Higgs, as experimental constraints seem to suggest, we can calculate the decay rate of ϕ_+ to a pair of ϕ_- states,

$$\Gamma_{\phi_+\phi_-\phi_-} = \frac{m_{\phi_+}^3}{8\pi\Lambda_r^2}\sqrt{1-4\frac{m_{\phi_-}^2}{m_{\phi_+}^2}} \times \left[\frac{U_{r,+}}{Z}\left(U_{h,-}+\frac{c_1}{Z}\frac{v_{ew}}{\Lambda_r}U_{r,-}\right)^2\left(2\frac{m_h^2}{m_{\phi_+}^2}-\frac{c_1}{2}\right)\right.$$
$$\left.+\left(U_{h,+}+\frac{c_1}{Z}\frac{v_{ew}}{\Lambda_r}U_{r,+}\right)\left(U_{h,-}+\frac{c_1}{Z}\frac{v_{ew}}{\Lambda_r}U_{r,-}\right)^2\left(-\frac{m_h^2}{2v_{ew}}\right)\frac{\Lambda_r}{m_{\phi_+}^2}\right]^2. \quad (4.56)$$

Now that we have all the relevant decay rates, we display in Figures 4.1 and 4.2 the branching fractions of ϕ_+ as a function of m_{ϕ_+} for different values of $c_1 = c_2 = c_3$. In the case of no-mixing ($c_1 = c_2 = c_3 = 0$), where $\phi_+ = r$, $\phi_- = h$ and the results are independent of Λ_r, the dominant decay channels are $t\bar{t}$, gg and hh. As already mentioned, decays to massive dibosons only go through their kinetic terms as in the $\gamma\gamma$ channel and tend to be suppressed[†]. Thus the relevant final states for searches are multijets, pairs of b-jets and possibly leptons plus missing energy. Depending on the mass difference between m_r and m_h, we could also have fat-jets if the subsequent $h \to b\bar{b}$ decay is highly boosted. For radion masses slightly larger than 125 GeV ($m_r \gtrsim m_h$), gg dominates with $b\bar{b}$ the second most important decay mode. Here we expect mostly final states involving jets, which will be difficult to differentiate from the SM QCD background. It is interesting to note that the diphoton channel can have a branching fraction comparable to the SM Higgs for this range of masses and furthermore remains relevant out to higher masses, making it an appealing discovery channel in the small mixing scenario.

[†]In contrast to the gg channel where the QCD trace anomaly dominates, in the $\gamma\gamma$ channel the anomaly contribution is sub-dominant with respect to the conformal $1/kL$ contribution.

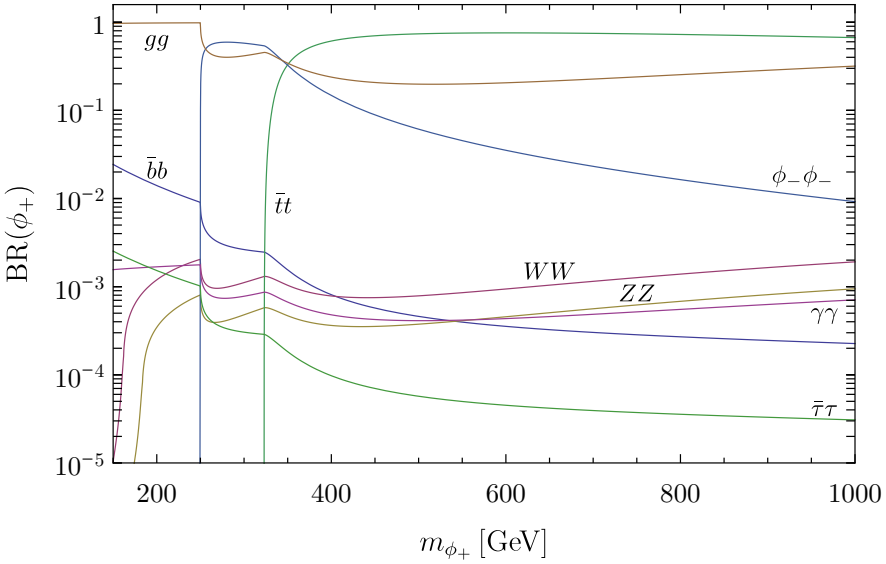

FIGURE 4.1: Branching ratios for ϕ_+ as a function of mass with $c_1 = c_2 = c_3 = 0$, independent of Λ_r.

As shown in Figure 4.2, once the mixing increases the branching fractions to WW and ZZ rapidly become more relevant and at $c_1 = c_2 = c_3 = 1$ they dominate above threshold, relegating the other decay branching fractions to be below 10%. For smaller mixing, $c_1 = c_2 = c_3 = 0.1$, decays into gg, $b\bar{b}$ and $\phi_-\phi_-$ are still important in the low, intermediate and high m_{ϕ_+} regions respectively. In this case we also observe a sharp drop in the branching fraction to $\phi_-\phi_-$ near $m_{\phi_+} \sim 750\,\text{GeV}$ due to a cancellation between the various contributions to the partial width. As the mixing is increased, this cancellation occurs at smaller values of m_{ϕ_+} and eventually moves below the $\phi_-\phi_-$ threshold and is not observed at $c_1 = c_2 = c_3 = 1$.

4.6 Constraints from LHC Searches

Starting with the effective Lagrangian Eq. (4.32), we are now in a position to investigate the constraints on the allowed parameter space. We consider the case where the lightest eigenstate, ϕ_-, is identified with the 125 GeV Higgs. Measurements of the Higgs signal strengths as well as direct searches for the heavier eigenstate, ϕ_+, can then be used to constrain the allowed parameter space for models which can be described by Eq. (4.32).

The effective Lagrangian we are considering contains six parameters; the mass scales m_h, m_r, Λ_r, and the $\mathcal{O}(1)$ dimensionless parameters c_1, c_2 and c_3. One can immediately eliminate m_h by requiring the mass of the lightest eigenstate to be 125 GeV. In addition, we expect c_2 to have a very small effect on the phenomenology since the relevant term in the Lagrangian is suppressed by an additional factor

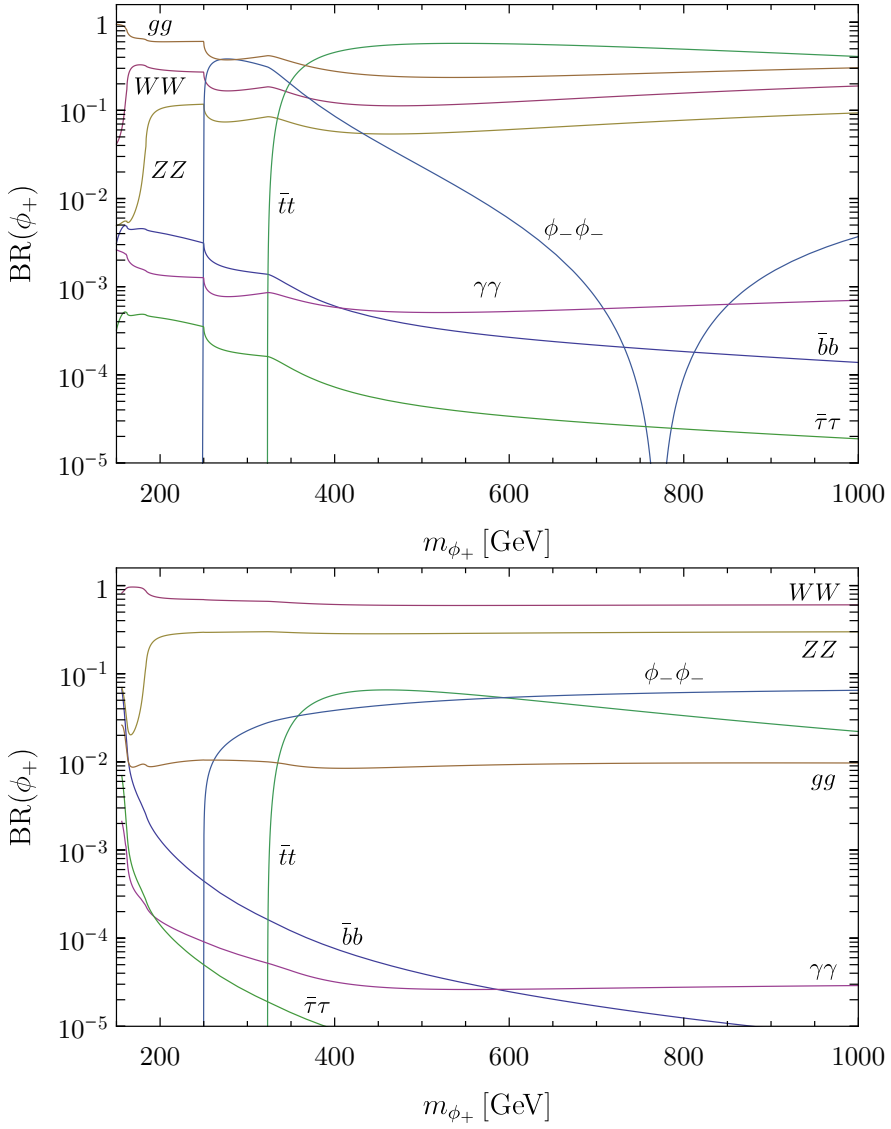

FIGURE 4.2: Branching ratios for ϕ_+ as a function of mass for $\Lambda_r = 3\,\text{TeV}$. The top and bottom panels are for $c_1 = c_2 = c_3 = 0.1$ and $c_1 = c_2 = c_3 = 1$ respectively.

of v_{ew}/Λ_r. Therefore we choose to fix $c_2 = 1$ before scanning over the remaining 4-dimensional parameter space. We perform a random scan with flat priors over the mass of the radion gauge state, m_r, from 160 to 1500 GeV and the kinetic and mass mixing coefficients, c_1 and c_3, from -3 to 3, while considering fixed values of 1, 3 and 5 TeV for the scale of the radion couplings, Λ_r. We also note that there is a theoretical bound on c_1 in order to ensure that we do not encounter a ghost-like kinetic term for ϕ_+. For example when $c_3 = 0$ and $\Lambda_r = 1\,\text{TeV}$ this gives a bound of $|c_1| \lesssim 4$.

Since we have chosen to identify the lightest eigenstate, ϕ_-, with the 125 GeV Higgs, we impose the constraints from the measured Higgs signal strengths in the $\gamma\gamma$, $ZZ^{(*)} \to 4l$, $WW^{(*)} \to l\nu l\nu$, $b\bar{b}$ and $\tau\bar{\tau}$ decay channels. We focus on the

Channel	μ_X
$\gamma\gamma$	0.98 ± 0.28
VV	0.91 ± 0.16
$b\bar{b}$	0.97 ± 0.38
$\tau\bar{\tau}$	1.07 ± 0.71

TABLE 4.2: Best fit values for the Higgs signal strengths in various decay channels at 125 GeV [245].

dominant gluon-gluon fusion (ggF) production mode in all channels, with the exception of $b\bar{b}$ where the best measurements are obtained by considering production in association with a W or Z boson (VH). In the case of gluon fusion, the signal strength is defined in the narrow width approximation by

$$\mu_X^{ggF} = \frac{\Gamma(\phi_- \to gg)}{\Gamma(h_{SM} \to gg)} \frac{Br(\phi_- \to X)}{Br(h_{SM} \to X)} \,. \tag{4.57}$$

We use the combined ATLAS, CMS and Tevatron best fit values for the signal strengths given in Ref. [245], which are shown in Table 4.2, and require that the signal strength for the ϕ_- state satisfy these bounds at the 1-sigma level.

However, for masses $125 < m_{\phi_+} < 160\,\text{GeV}$, one must carefully consider the contribution of both states to the measured signal strength in the $WW^{(*)}$ channel, since unlike $\gamma\gamma$ and $ZZ^{(*)}$ the final state is not fully reconstructable. Additionally, interference effects must be taken into account if the two states have a very small mass separation. We therefore restrict $m_r > 160\,\text{GeV}$, allowing us to consider the two states separately in the WW channel.

We must also consider the possibility that, when kinematically allowed, the 125 GeV state may be produced via the decay $\phi_+ \to \phi_-\phi_-$, which will result in an enhancement in the signal strengths for ϕ_-. In the case of the $WW^{(*)}$ analysis, such events will not contribute significantly due to vetoes on additional leptons and jets. On the other hand, the $\gamma\gamma$ and $ZZ^{(*)}$ analyses are quite inclusive and this additional contribution to the production cross section can be important. In fact, in certain regions of parameter space this process can become the dominant production mechanism for ϕ_-. In this case we define the signal strength as

$$\mu_X^{ggF} = \left(\frac{\Gamma(\phi_- \to gg)}{\Gamma(h_{SM} \to gg)} + \frac{2\sigma_{ggF}(pp \to \phi_+ \to \phi_-\phi_-)}{\sigma_{ggF}(pp \to h_{SM})} \right) \frac{Br(\phi_- \to X)}{Br(h_{SM} \to X)} \,. \tag{4.58}$$

In addition to the constraints on the 125 GeV eigenstate, the ATLAS and CMS Higgs searches can also be used to constrain the heavier eigenstate. We therefore require that the ϕ_+ state satisfies the exclusion limits from the CMS $H \to WW \to 2l2\nu$ [246] and $H \to ZZ \to 4l$ [247] searches and the ATLAS high mass $H \to$

$WW \to e\nu\mu\nu$ search [248]. The Higgs searches in the remaining channels ($\gamma\gamma$, $b\bar{b}$ and $\tau\bar{\tau}$) currently only provide constraints for masses below $\sim 150\,\text{GeV}$. Finally, we also impose the additional constraints provided by the CMS semi-leptonic $t\bar{t}$ resonance search [95] in the 500 GeV to 1 TeV mass range.

There are in principle other searches performed at the LHC which could be adapted to our particular model, for example the searches for resonant ZZ production in the dilepton plus dijet channel [249] and resonant WW production in the lepton plus dijet channel [250]. These searches focus on dibosons produced by KK graviton decay and thus cannot be directly translated to our model without determining the signal acceptance via a Monte Carlo simulation of our signal with appropriate selection cuts. We leave these particular collider studies for subsequent work. While we do not expect these searches to currently constrain our model, they will become important at the 14 TeV LHC. The high mass diphoton [251] and dijet [252] searches may also be able to provide constraints in the future.

4.7 Radion-Higgs Phenomenology for LHC14

We performed a scan of 200,000 points for each value of Λ_r, imposing the above experimental constraints on the ϕ_- and ϕ_+ states. We find that the current experimental constraints already rule out a significant fraction of the parameter space, in particular at low values of Λ_r and small masses, m_+. Figures 4.3, 4.4 & 4.5 show the ϕ_+ mass eigenstate component of the Higgs gauge eigenstate, h_+, as a function of the mass for $\Lambda_r = 1, 3, 5\,\text{TeV}$ respectively. This is a useful variable for characterising the extent of the mixing between the two states; note that non-zero h_+ leads to Higgs-like couplings for the heavier eigenstate and that h_+ can be greater than one due to the non-unitary transformation resulting from the kinetic mixing. The red points in Figures 4.3, 4.4 & 4.5 are excluded by measurements of the 125 GeV Higgs signal strengths, while the black points satisfy these constraints but are ruled out by direct searches for the heavier state. The green points pass all of the current experimental bounds.

We see that for $\Lambda_r = 1\,\text{TeV}$ virtually all of the points are ruled out, with the exception of a few points with very small mixing. In the 250 to 350 GeV range, this is due to enhanced production of the 125 GeV state via $\phi_+ \to \phi_-\phi_-$, as discussed previously. The remaining points which satisfy the Higgs signal strength bounds are excluded by searches for ϕ_+ in the WW and ZZ channels, as well as the $t\bar{t}$ channel above 500 GeV. In the $\Lambda_r = 3\,\text{TeV}$ case we find that, as expected, a significantly larger fraction of the points survive the experimental constraints.

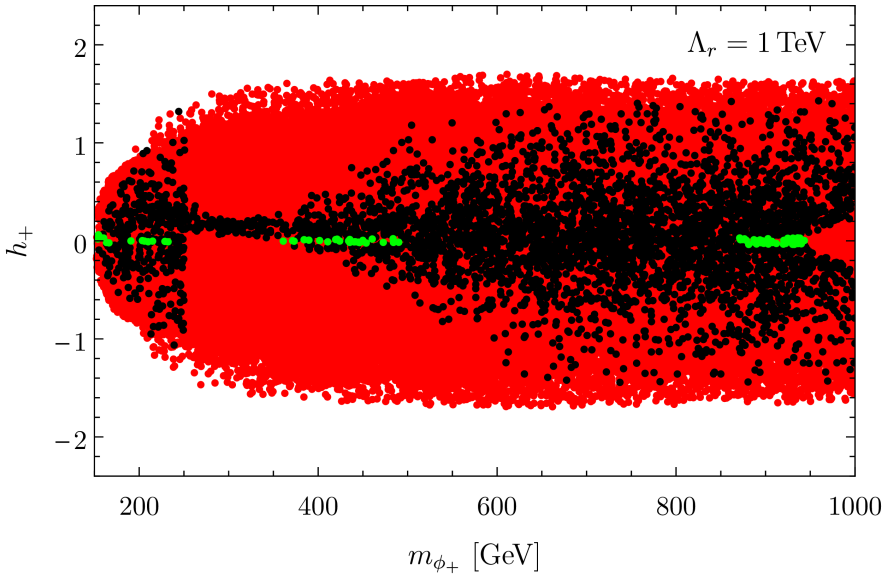

FIGURE 4.3: The ϕ_+ component of the Higgs gauge eigenstate as a function of the mass. The red points are excluded by measurements of the 125 GeV Higgs signal strengths, while the black points satisfy these constraints but are ruled out by direct searches for ϕ_+. The green points pass all of the current experimental bounds. We have set $\Lambda_r = 1\,\text{TeV}$.

Below 500 GeV the bounds from WW and ZZ searches still rule out most of the points with large mixing, while between 450 and 900 GeV we find that they also disfavour negative values of h_+. This is the result of constructive interference between the Higgs and radion couplings to the top quark, which enhances the ϕ_+ gluon fusion cross section for negative h_+. For masses above 1 TeV there are no constraints on ϕ_+ from current searches. Furthermore, notice that only the red points extend to larger values of h_+, which indicates that for large mixing one is unable to satisfy the Higgs signal strength constraints independently of the ϕ_+ mass. Finally, for $\Lambda_r = 5\,\text{TeV}$ there are once again significantly more allowed points for masses below 1 TeV, although negative values of h_+ are disfavoured by WW and ZZ searches between 250 and 600 GeV.

Using these results we can also derive bounds on the parameters of our effective Lagrangian, in particular c_1 and c_3. For $\Lambda_r = 1\,\text{TeV}$ we find that $-0.2 < c_3 < 0.04$, while the constraints are somewhat weaker for $\Lambda_r = 3\,\text{TeV}$, giving $-2.1 < c_3 < 0.6$. These bounds are of course also dependent on the value of m_r and can be significantly stronger, particularly for lower masses. Considering c_1 on the other hand, for $\Lambda_r = 1\,\text{TeV}$ we find $-0.2 < c_1 < 0.3$, while for $\Lambda_r = 3\,\text{TeV}$ c_1 is unconstrained for values of $m_r > 1\,\text{TeV}$ but for masses below 450 GeV we obtain a bound of $-0.7 < c_1 < 2.7$.

Finally, we investigate the phenomenology of the regions of parameter space which are allowed by current measurements and discuss the prospects for future searches

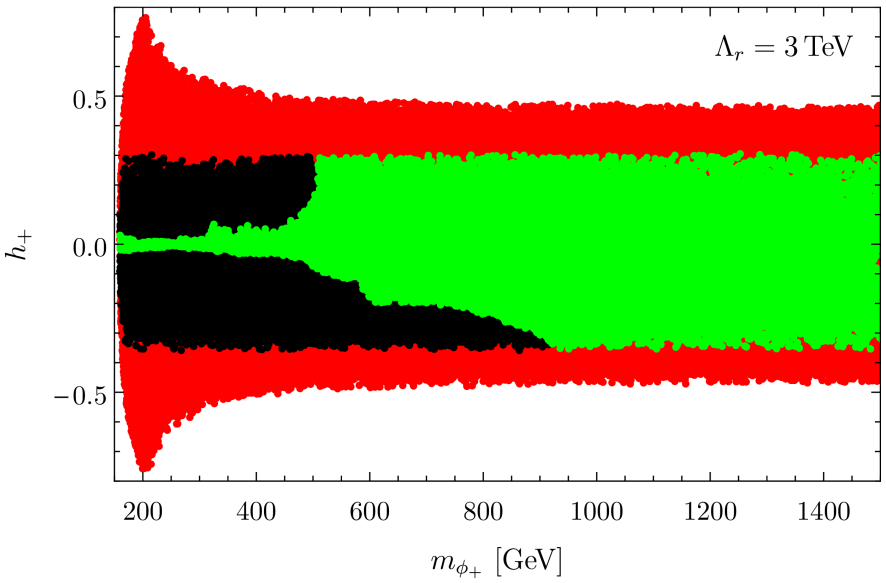

FIGURE 4.4: As in Figure 4.3 but with $\Lambda_r = 3\,\text{TeV}$.

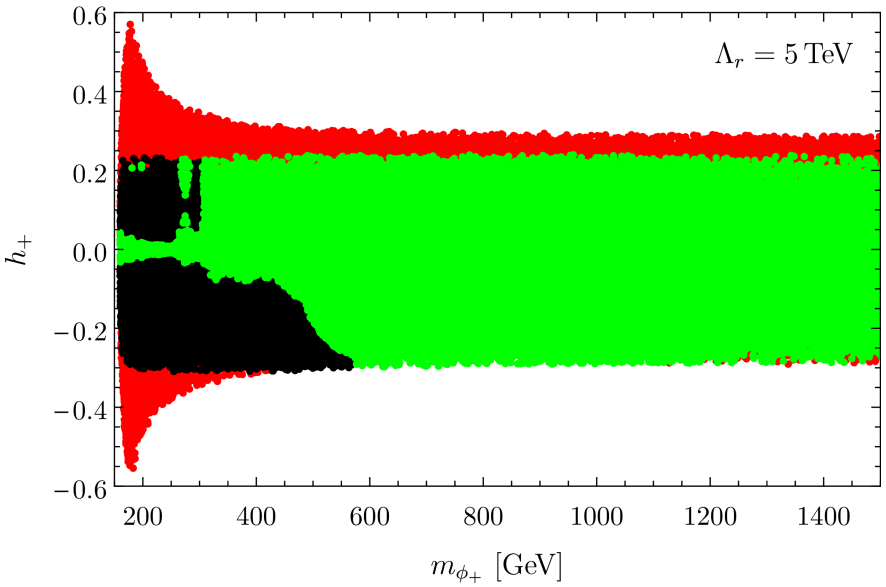

FIGURE 4.5: As in Figure 4.3 but with $\Lambda_r = 5\,\text{TeV}$.

during the next run of the LHC. We plot in Figure 4.6 the diphoton cross section due to a ϕ_+ produced via gluon fusion at a centre-of-mass energy of 14 TeV, as a function of m_{ϕ_+}. In this and subsequent plots all points satisfy the experimental constraints discussed in Section 4.6. The black, blue and cyan points correspond to $\Lambda_r = 1$, 3 and 5 TeV respectively. First of all, notice that the cross section tends to decrease for larger m_{ϕ_+}, as expected due to the mass suppression in the gluon fusion ϕ_+ production. We concentrate first on the analysis of the $\Lambda_r = 1\,\text{TeV}$ (black) points. As mentioned above, the lack of points in the 250–350 GeV mass range can be attributed to the contribution of ϕ_+ decays to ϕ_- pair-production. This constraint becomes suppressed for larger values of Λ_r, and for larger m_{ϕ_+}

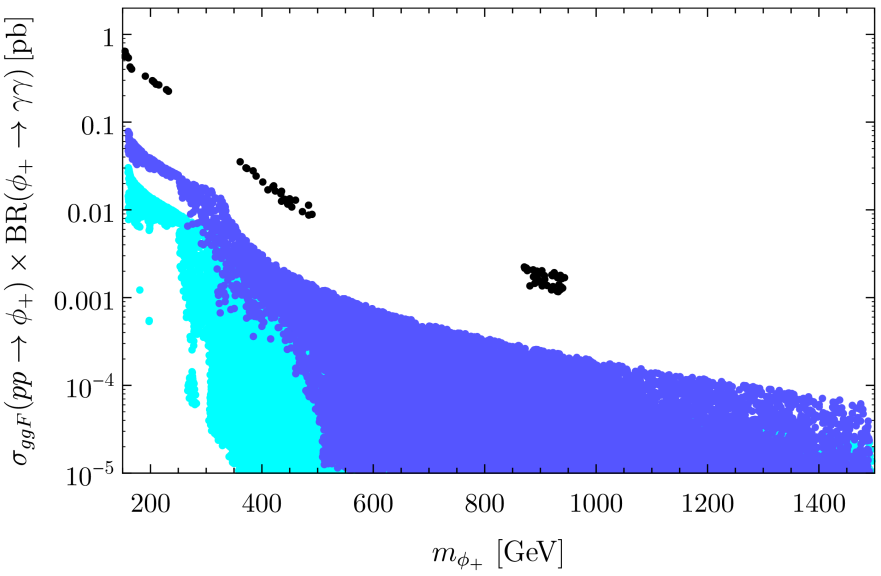

FIGURE 4.6: Gluon fusion cross section times branching ratio for $\phi_+ \to \gamma\gamma$ at $\sqrt{s} = 14\,\mathrm{TeV}$. The black, blue and cyan points are for $\Lambda_r = 1$, 3 and 5 TeV respectively.

due to the reduction in the ϕ_+ production cross section. Similarly, the second empty region is related to the $t\bar{t}$ constraints that kick in at an invariant mass $m_{t\bar{t}} \approx 500\,\mathrm{GeV}$ and which can again be evaded by increasing Λ_r.

Another feature that stands out is the relatively large diphoton cross sections attained for $m_{\phi_+} \in [160, 250]\,\mathrm{GeV}$. Recall that the points in this region correspond to the case of small mixing and therefore the branching ratios of ϕ_+ are dominated by gg and $b\bar{b}$. However, any signal in these channels will be buried under the large QCD background found at the LHC. On the other hand, the clean diphoton signal remains competitive, even overtaking the well-known SM Higgs diphoton cross section for the same mass range. This can be clearly understood from the fact that ϕ_+ has an enhanced coupling to gluons via the trace anomaly, increasing the production cross section. The diphoton channel is therefore the most promising search channel in this mass range and even extending up to the $t\bar{t}$ threshold since, unlike the SM Higgs, the branching fraction to photons does not drop off at higher masses due to the conformal contribution to the coupling. This strongly motivates extending the diphoton searches to invariant masses above $m_{\gamma\gamma} = 150\,\mathrm{GeV}$. Since the completion of our study, both ATLAS and CMS have extended their diphoton searches to larger invariant masses [217, 253]. These updated searches impose additional constraints for $m_{\phi_+} \lesssim 270\,\mathrm{GeV}$, which exclude all of the $\Lambda_r = 1\,\mathrm{TeV}$ points in this mass range and also start to probe larger values of Λ_r.

Figure 4.7 shows a similar plot of the cross section for a ϕ_+ produced via gluon fusion and then decaying to $t\bar{t}$. While this search channel currently only provides

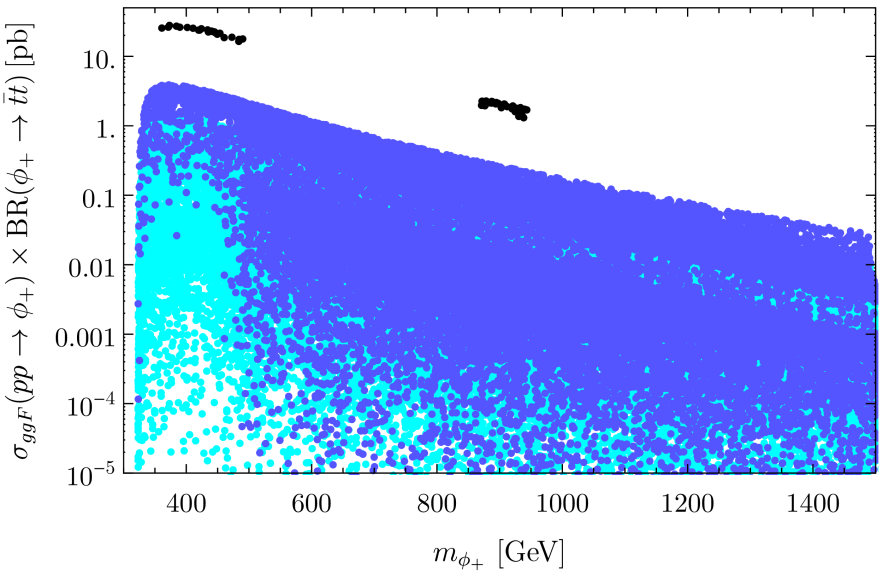

FIGURE 4.7: Gluon fusion cross section times branching ratio for $\phi_+ \to t\bar{t}$ at $\sqrt{s} = 14\,\mathrm{TeV}$. The black, blue and cyan points are for $\Lambda_r = 1$, 3 and 5 TeV respectively.

constraints for $\Lambda_r = 1\,\mathrm{TeV}$, we expect it to become an important channel for masses $m_{\phi_+} > 500\,\mathrm{GeV}$ with additional integrated luminosity. It provides sensitivity to scenarios with small mixing, where the branching fraction to $t\bar{t}$ dominates. It is particularly sensitive to cases where the mixing parameters in our effective Lagrangian are negative, since this results in an enhanced coupling to $t\bar{t}$ due to the Higgs and radion couplings to the top quark combining constructively. Searches in the $t\bar{t}$ channel will also be important in the high mass region, $m_{t\bar{t}} \gtrsim 1\,\mathrm{TeV}$, where the decay products are highly boosted and may be collimated into a single jet. Such boosted topologies are already considered by current searches at high invariant mass [95], although do not currently provide constraints on our model.

Finally, in Figure 4.8 we show the cross section times branching ratio for ϕ_+ decaying to ZZ. Again one can clearly see the regions below 1 TeV, and in particular below 500 GeV, where searches in this channel are already restricting the allowed parameter space, even for larger values of $\Lambda_r = 5\,\mathrm{TeV}$. We also note that there are a significant number of points with relatively large cross sections, ~ 0.1 pb, for $m_{\phi_+} \gtrsim 1\,\mathrm{TeV}$. These points correspond to cases where there is a large mixing, since as discussed in Section 4.5, the radion coupling to massive gauge bosons is suppressed when the Higgs is placed in the bulk. On the other hand there are a large number of points with smaller mixing where the cross section is highly suppressed. This ability to suppress the signal in the ZZ (and WW) channels provides a distinct difference from the commonly considered brane Higgs scenarios. Hence, while the ZZ channel has sensitivity across the entire mass range

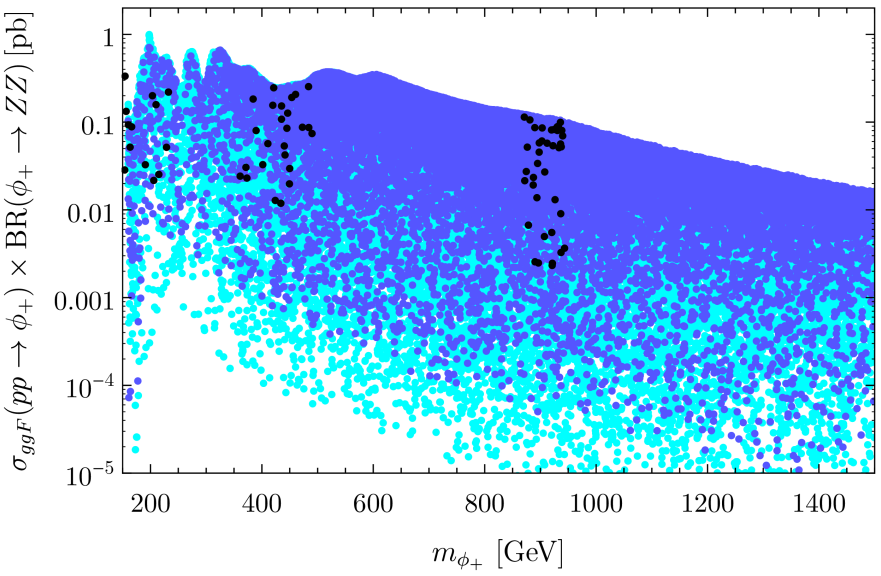

FIGURE 4.8: Gluon fusion cross section times branching ratio for $\phi_+ \to ZZ$ at $\sqrt{s} = 14\,\text{TeV}$. The black, blue and cyan points are for $\Lambda_r = 1$, 3 and 5 TeV respectively.

considered, other channels will be essential to probe the full parameter space. In conclusion we note that the various searches are in fact complementary, with the ZZ/WW channels providing the best sensitivity in cases with large mixing, while the $\gamma\gamma$ and $t\bar{t}$ channels are important to probe cases where the mixing is small.

4.8 An Excess at 750 GeV?

Recently, the ATLAS and CMS collaborations have reported a mild excess in the diphoton channel around an invariant mass of 750 GeV, with a few fb^{-1} of data from collisions at $\sqrt{s} = 13$ TeV [97, 99, 230, 231]. While the observed excess may turn out to be simply a statistical fluctuation, it is nevertheless interesting to consider the possibility that new physics could be responsible. Assuming the excess is due to a hypothetical new particle with a mass of 750 GeV, it currently remains unclear whether the data favours a large or narrow width resonance; the ATLAS data prefers a broad resonance with $\Gamma \approx 45$ GeV, while CMS obtains a better fit with a narrower width. Furthermore, the excess events do not appear to contain additional energetic particles in the final state, and the absence of a significant signal in the previous run of the LHC at $\sqrt{s} = 8$ TeV may favour certain production modes. This observation has already inspired an enormous number of theoretical investigations, including in the context of warped models [254–268]. Here we discuss the possibility that the radion could be responsible for the observed excess and show that the bulk Higgs scenario is particularly advantageous

Final State	Observed Bound	
$t\bar{t}$	< 300 fb	[95]
WW	< 38 fb	[218, 219]
ZZ	< 12 fb	[220]
$Z\gamma$	< 4.0 fb	[270, 271]
$\gamma\gamma$	< 1.4 fb	[217, 253]
hh	< 36 fb	[221]
jj	< 2.5 pb	[272, 273]

TABLE 4.3: Constraints on the radion from 8 TeV resonance searches.

by allowing otherwise stringent bounds from Run-I to be evaded. It will however prove necessary to slightly generalise our previous framework, by taking the size of the extra dimension kL to be a free parameter. In the dual 4D picture, this will correspond to lowering the UV cut-off above which the physics is no longer conformal, and is consistent with treating the RS framework as a tool to analyse a 4D CFT. The possibility that the radion is responsible for the diphoton excess has also subsequently been considered in Refs. [254, 257, 258].

We take the best-fit cross sections for the diphoton excess from the CMS combined 8+13 TeV analysis [231] and extracted from the ATLAS analysis [230] in Ref. [269]:

$$\mu^{\text{ATLAS}}_{13\text{ TeV}} = \sigma(pp \to S)_{13\text{ TeV}} \times \mathcal{B}(S \to \gamma\gamma) = 10^{+4}_{-3}\text{ fb}\,, \tag{4.59}$$

$$\mu^{\text{CMS}}_{13\text{ TeV}} = \sigma(pp \to S)_{13\text{ TeV}} \times \mathcal{B}(S \to \gamma\gamma) = 3.7^{+1.5}_{-1.3}\text{ fb}\,. \tag{4.60}$$

We also summarise in Table 4.3 the most important constraints from 8 TeV resonance searches. The radion couplings to light fermions are suppressed by the fermion mass and so set no meaningful constraints.

From Table 4.3, we see that the constraints on a putative 750 GeV resonance decaying to gauge bosons are an order of magnitude stronger than on decays to $t\bar{t}$. In contrast, a scalar of that mass with Higgs-like couplings will dominantly decay to WW and ZZ. This has important consequences for our model since the radion and the Higgs generically have both mass and kinetic mixing, as shown in Eq. (4.32). In order to sufficiently suppress the heavier state decay to gauge bosons, it must be radion-like with any Higgs-like couplings strongly suppressed. Large mixing between the two states would also modify the properties of the 125 GeV scalar resonance discovered at the LHC. Decays of the heavier state to hh could also affect the Higgs measurements, however this contribution will turn out to be negligible in the viable regions of parameter space.

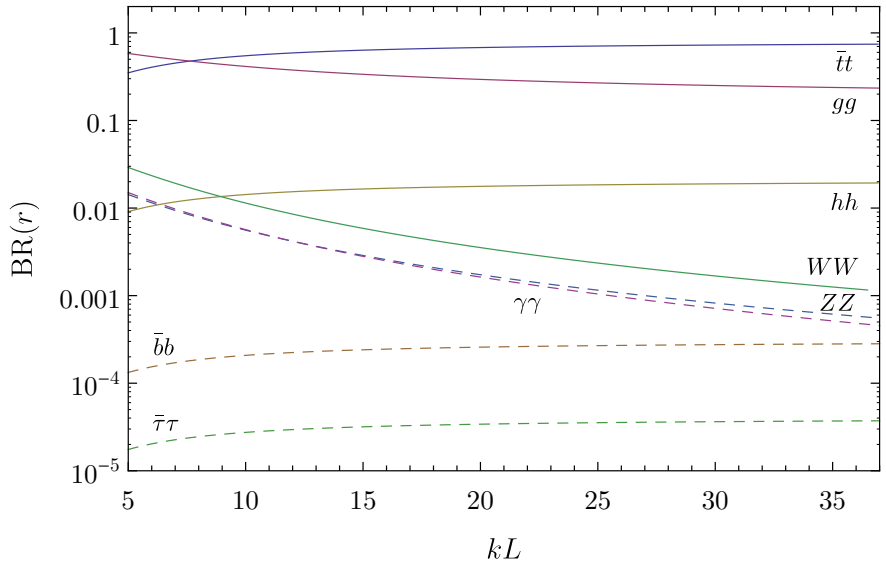

FIGURE 4.9: Branching ratios for a 750 GeV radion to various SM final states in the limit of zero mixing with the SM Higgs.

With the radion couplings to massive gauge bosons suppressed, inspecting Table 4.1 reveals that the other potentially large couplings are to gluons, top-quark pairs, and the lighter Higgs-like state. The decay $r \to t\bar{t}$ is enhanced over $r \to hh$ by colour and spin degrees of freedom, enough that the former typically sets the dominant limits despite the stronger constraints on hh final states listed in Table 4.3. Note from Table 4.1 that all radion couplings scale with Λ_r in the same way. Therefore in the zero-mixing limit the branching ratios depend only on the size of the extra dimension kL. We plot those in Figure 4.9, and see that $\mathcal{B}(r \to t\bar{t}) \approx 40\,\mathcal{B}(r \to hh)$.

Our model contains only four free parameters: Λ_r, kL, c_1 and c_3. The observed masses for the Higgs and the diphoton excess fix m_r, m_h in terms of these parameters, while c_2 has a negligible effect as discussed previously. In order to identify the regions of parameter space which both satisfy the current experimental bounds and are consistent with the observed diphoton excess we once again perform a scan over these parameters. We take flat priors in the range $-2 \leq c_1, c_3 \leq 2$, $5 \leq kL \leq 35$ and $1 \leq \Lambda_r \leq 5\,\text{TeV}$, and require that the 750 GeV state satisfy the constraints from the resonance searches in Table 4.3, while the 125 GeV state must be consistent with the updated measurements of the Higgs signal strengths [274, 275] at the 2-sigma level. The radion production cross sections are obtained by scaling the Higgs 8 TeV cross section [276] by the radion effective coupling to gluons and, for $\sqrt{s} = 13$ TeV, by the parton luminosity ratio:

$$\frac{\sigma(pp \to r)_{13\text{ TeV}}}{\sigma(pp \to r)_{8\text{ TeV}}} \approx 4.7\,. \tag{4.61}$$

The results of the scan are shown in Figure 4.10, where all points satisfy the current experimental constraints and the green points are also consistent with the observed diphoton excess. In the top panel we have plotted the 750 GeV component of the Higgs gauge state, h_+, as a function of kL, clearly showing that the current data already enforces small Higgs-radion mixing. Recall that h_+ gives a measure of the Higgs-like couplings possessed the heavier eigenstate, and that for $h_+ \approx 0$ the heavier eigenstate has vanishing Higgs-like couplings. Large mixing is immediately excluded by measurements of the 125 GeV state; however it turns out that for much of the parameter space resonance searches in the ZZ and WW final states provide the stronger constraint. The bound on the mixing is therefore weaker at large kL and large Λ_r, where the radion production cross section is reduced. Furthermore, the points consistent with the diphoton excess (green points) are concentrated at small kL where the radion branching ratio to photons is enhanced.

In the $v_{ew}/\Lambda_r \ll 1$ limit, h_+ is given in terms of the Lagrangian parameters by

$$h_+ = (c_1 + c_3)\,\frac{m_r^2}{m_r^2 - m_h^2}\,\frac{v_{ew}}{\Lambda_r} + \mathcal{O}\left((v_{ew}/\Lambda_r)^3\right), \tag{4.62}$$

and hence the heavier state is strongly radion-like along the line[†] $c_1 = -c_3$, which we refer to as the alignment case. This is evident in the bottom panel of Figure 4.10 where the allowed points are all located along the diagonal. Notice that there are no allowed points with $c_1 \approx -c_3$ at large values of c_1. This region of parameter space is excluded by hh resonance searches due to the enhanced radion coupling to hh (see Table 4.1). Enhancing the coupling to hh also results in a decreased branching ratio to photons, hence the points satisfying the diphoton excess are concentrated around small values of c_1. These points are also aligned along the diagonal; the off-diagonal points corresponding to increased mixing generally have larger values of kL, again suppressing the branching ratio to photons.

It is clear that current experimental constraints impose small Higgs-radion mixing. Providing an explanation for the diphoton excess additionally restricts us to the region where $|c_1| \lesssim 0.5$ and requires that we be quite close to the alignment case. Hence we now restrict ourselves to the case $c_1 = -c_3$ in order to explore the (kL, Λ_r) parameter space in detail. In Figures 4.11 and 4.12 we show the regions in the kL–Λ_r plane consistent with the observed diphoton excess, as well as the constraints from other LHC searches. We have taken two benchmark points corresponding to $c_1 = 0$ and $c_1 = 0.5$.

[†]The lighter state is not necessarily strongly Higgs-like for $c_1 = -c_3$ due to the non-unitary transformation. That is instead determined by $|r_-| = \frac{c_1 m_h^2 + c_3 m_r^2}{m_h^2 - m_r^2}\,\frac{v_{ew}}{\Lambda_r} + \mathcal{O}((v_{ew}/\Lambda_r)^3)$, where $r_- = 0$ corresponds to a purely Higgs-like state.

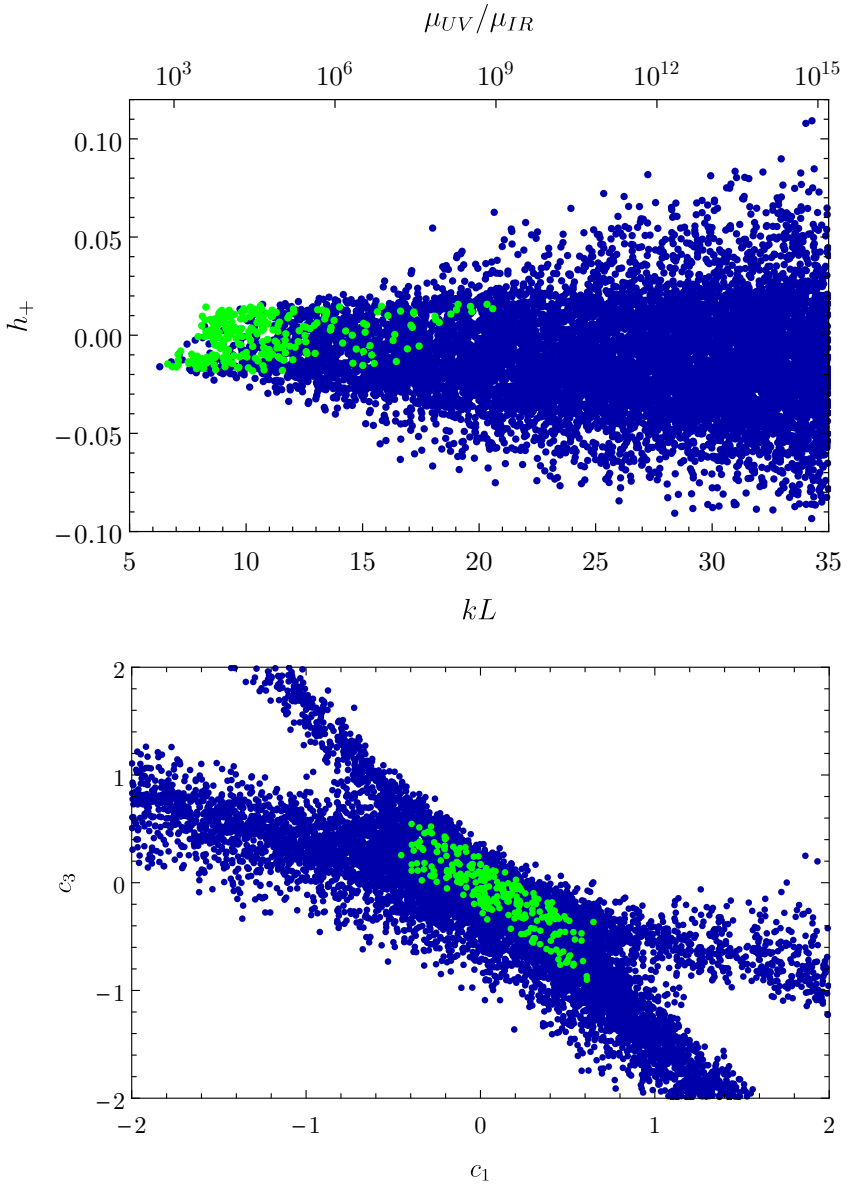

FIGURE 4.10: Results of the Λ_r, kL, c_1, c_3 parameter scan. All points shown satisfy the constraints from resonance searches and Higgs measurements, while the green points are additionally consistent with the diphoton excess. We have taken the cross section for the diphoton excess to be the weighted average of Eqs. (4.59) and (4.60), giving $4.9 \pm 1.3\,\text{fb}$.

Focusing on Figure 4.11 ($c_1 = 0$), we see that $t\bar{t}$ searches give the approximate bound $\Lambda_r \gtrsim 2$ TeV, while obtaining a sufficiently large diphoton signal requires taking smaller values of $kL \lesssim 20$ than those used to obtain the Planck-electroweak hierarchy in RS-models ($kL \sim 35$). This can be understood by noting that to simultaneously have a 6 fb diphoton signal at 13 TeV while avoiding the constraints from ditop searches, we must have

$$\frac{\mathcal{B}(r \to t\bar{t})}{\mathcal{B}(r \to \gamma\gamma)} < \frac{300}{6} \times \frac{\sigma(pp \to r)_{13\text{ TeV}}}{\sigma(pp \to r)_{8\text{ TeV}}} \approx 235\,. \tag{4.63}$$

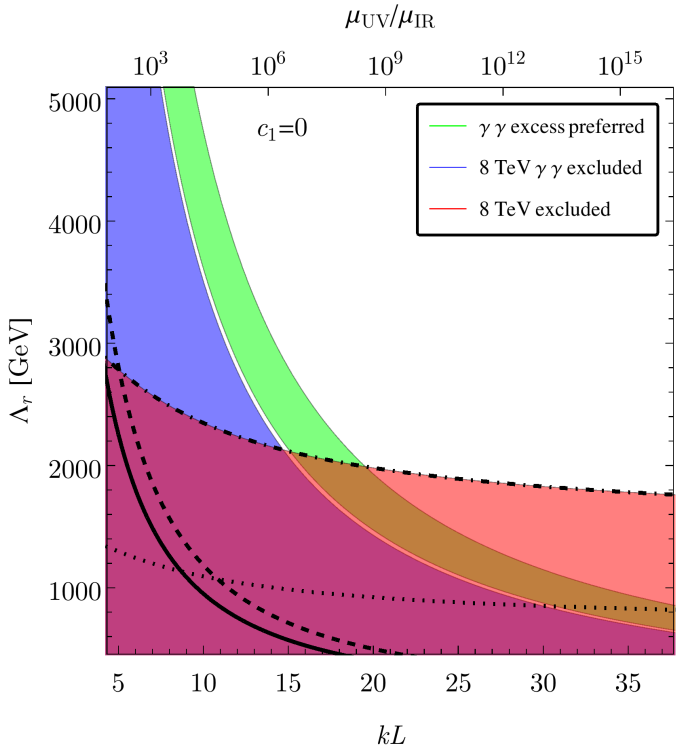

FIGURE 4.11: The region of parameter space consistent with the observed diphoton excess is shaded in green, while the blue and red regions are excluded by the 8 TeV diphoton and other resonance searches respectively, and the grey region is excluded by Higgs measurements. Regions below and to the left of the solid, dashed, dotted and dot-dashed lines are individually excluded by the WW, ZZ, hh and tt searches listed in Table 4.3. We have taken $c_1 = c_3 = 0$.

As can be seen from Figure 4.9, this is not satisfied at $kL = 35$. Decreasing the size of the extra dimension increases the coupling to $\gamma\gamma$ (and gg, increasing the production cross section) allowing us to satisfy this constraint. In contrast, attempting to tune the mass and kinetic mixings between the radion and the Higgs to suppress the decay $r \to t\bar{t}$ while maintaining a sufficiently large production cross section reintroduces constraints from either the decays to WW or hh, as can be inferred from Figure 4.10.

Moving away from $c_1 = 0$ leads to an increased branching ratio to hh and this channel provides the strongest constraint for $c_1 \gtrsim 0.35$, as can be seen in Figure 4.12. Satisfying this constraint in addition to the diphoton excess then requires even smaller values of kL. Also note that while the heavier state is radion-like when $c_1 = -c_3$, the lighter state is not necessarily Higgs-like due to the non-unitary transformation arising from the kinetic mixing. This leads to bounds from measurements of the Higgs couplings, which exclude the region $\Lambda_r \lesssim 2\,\text{TeV}$.

Let us briefly comment on the theoretical implications of a reduced value for kL. Models with smaller warping factors have previously been considered in the "Little

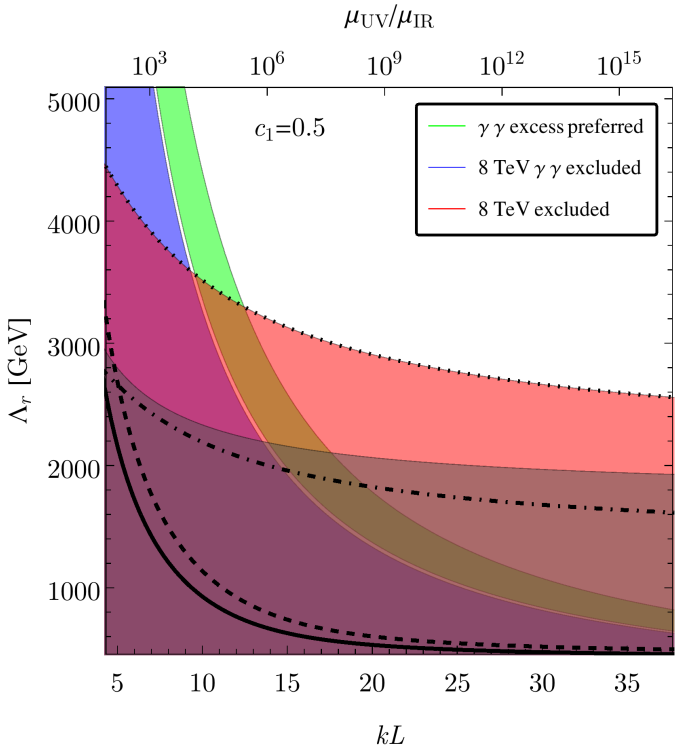

FIGURE 4.12: Same as Figure 4.11 but with $c_1 = -c_3 = 0.5$.

Randall-Sundrum" paradigm for flavour [277]. They are most naturally interpreted in the 4D context, where the UV scale $\mu_{UV} = \mu_{IR}\, e^{kL} \sim \Lambda_r\, e^{kL}$ is the UV cut-off above which the physics is no longer conformal. Flavour constraints typically require $\mu_{UV} > 10^3$ TeV, which is satisfied for all points we show in Figures 4.11 and 4.12. However, from the 5D viewpoint one may be concerned that such models lead to graviton couplings which are too strong. This can be resolved by simply projecting out the graviton zero mode with Dirichlet boundary conditions as in Refs. [277, 278]. Alternatively, one can construct models which still include a 4D theory of gravity by introducing a scalar curvature term on the UV brane [279]. In either case the radion phenomenology is largely unchanged due to its IR localisation and our analysis is therefore insensitive to the details.

Finally, we address future prospects for testing this model. From Figure 4.9, we see that the dominant decay modes of the radion are $t\bar{t}$ and gg. While it might be difficult to observe the dijet final state, the possibility to explore this scenario with the ditop final state is certainly within the reach of the LHC Run-II. In the case of non-zero mixing, it is clear that searches involving massive gauge boson final states will be the main tool in constraining/discovering these kinds of models. However, in the particular alignment case $c_1 \approx -c_3$ where the heavier eigenstate is strongly radion-like, an interesting situation may arise in which, due to the linear c_1 dependence of the radion-diHiggs coupling, searches in the diHiggs final state

become the best way to probe the model for $c_1 \gtrsim 0.35$. Notice that both the diboson and the diHiggs searches are more model dependent, whereas the ditop signature is relatively insensitive to assumptions about the mixing and thus a particularly promising channel. Additionally, we note that the width of the radion is quite small, $\Gamma \lesssim 1$ GeV. If the excess is ultimately due to a broad resonance, as suggested by the ATLAS data, that would disfavour this model as a possible explanation. Lastly, we have worked in the 4D effective theory of Eq. (4.32), but in the full theory we expect additional resonances at masses of a few TeV. If these are not too heavy, they might also be discoverable.

4.9 Summary

In this chapter we have explored in detail the Higgs-radion system in the Randall-Sundrum model with the Higgs located in the bulk of the extra dimension. We considered the effect of a bulk $\xi R_5 H^\dagger H$ term, which leads to kinetic mixing between the Higgs and the radion. The extra dimension must be stabilised, breaking the conformal symmetry and generating a mass for the radion. Including the back-reaction of the stabilising field on the metric then leads to an additional mass mixing between the radion and the Higgs, which is distinct from the more commonly considered case of a brane localised Higgs.

Allowing the Higgs to propagate in the bulk of the extra dimension also has a significant effect on the radion phenomenology. In the case of a brane localised Higgs or in gauge-Higgs unification models, the radion phenomenology is dominated by its coupling to the electroweak gauge boson mass terms. We have shown that this coupling vanishes for the case of a bulk Higgs, which can be understood as a consequence of the conformal symmetry in the bulk. This coupling is then only reintroduced via the Higgs-radion mixing and is associated with an explicit breaking of the conformal symmetry. Provided that the mixing is small this allows the radion to evade many of the bounds from existing experimental searches.

We used the 5D picture to motivate the most general 4D effective Lagrangian describing the Higgs-radion/dilaton system and performed an extensive scan over the relevant parameter space. Identifying the lighter, Higgs-like state with the observed 125 GeV Higgs, we uncovered the regions of parameter space consistent with all existing experimental constraints. We find that radion masses at least as light as 160 GeV are allowed and may have remained hidden in the existing searches. Beyond $\Lambda_r = 1$ TeV, increased mixing between the radion and the Higgs can also be tolerated by the present data. Furthermore, when kinematically

accessible, decays of the heavier state into the lighter Higgs-like state can contribute significantly to its production.

The heaviest mostly radion-like state can be divided into several categories depending on its mass and the extent of the mixing. Below 250 GeV the surviving region corresponds to an almost pure radion-like state with suppressed couplings to massive gauge bosons. The $\gamma\gamma$ channel may be the most sensitive in this region and potentially remain viable at higher masses. Above 500 GeV, both the $t\bar{t}$ and diboson channels will be important at Run-II of the LHC, in cases of small and large mixing respectively. We find that the diphoton, diboson and $t\bar{t}$ channels are complementary and together can be used to explore large regions of the parameter space.

Finally, we have shown that the recently observed excess in diphoton events at an invariant mass of 750 GeV in early Run-II data could be explained by the radion in a bulk Higgs scenario. The suppressed coupling of the radion to electroweak gauge bosons is crucial in evading the otherwise stringent constraints from Run-I searches. We find that we can satisfy the observed excess while avoiding all 8 TeV searches for a compositeness scale $\Lambda_r \gtrsim 2$ TeV and an extra dimension of size $kL \lesssim 20$. This relatively small kL is necessary to enhance the radion coupling to photons. Mixing between the radion and the Higgs is already strongly constrained by WW/ZZ resonance searches, which require being near the alignment limit $c_1 = -c_3$. The dominant decay mode of the radion is then $t\bar{t}$, which provides both the most stringent bounds and the best prospects for probing these kinds of scenarios in a model-independent way in the immediate future. Lastly, the radion branching ratio to hh can be enhanced in certain regions of parameter space, potentially providing an additional channel to probe this scenario.

Soft Wall Dilaton

5.1 Introduction

In the previous two chapters we have explored the phenomenology of the radion in two different warped models. As reviewed in Chapter 2, such models also have a dual description in terms of a 4D conformal field theory via the AdS/CFT correspondence. In this picture, the radion is dual to the Nambu-Goldstone boson of the spontaneously broken scale invariance[‡]; the dilaton.

Under the scale transformation $x^\mu \to x'^\mu = e^{-\omega} x^\mu$, the dilaton undergoes a shift according to $\sigma(x) \to \sigma(x') + \omega f$, where ω is a constant parameter and f is the spontaneous breaking scale. For the purpose of writing the low-energy effective Lagrangian, it is more convenient to consider the field

$$\chi(x) = f e^{\sigma(x)/f} \,, \tag{5.1}$$

which transforms linearly under scale transformations according to $\chi(x) \to e^{\omega} \chi(x')$. Meanwhile a general operator, $\mathcal{O}$, transforms according to its scaling dimension, Δ, as $\mathcal{O}(x) \to e^{\omega\Delta} \mathcal{O}(x')$. The effective Lagrangian can then be straightforwardly constructed by using the dilaton as a conformal compensator to obtain invariant terms of the form $(\chi/f)^{4-\Delta}\mathcal{O}$.

As one would expect for a NGB, the dilaton is protected by its shift symmetry, which ensures that it remains massless. However, unlike the spontaneous breaking of an internal (non-spacetime) symmetry, the transformation of χ clearly allows for the presence of a non-derivative, quartic self-interaction of the dilaton in the action. This quartic potential leads to a preferred value for $\langle\chi\rangle$ and is incompatible with the spontaneous symmetry breaking unless the quartic coupling vanishes. This can occur either by a fine-tuning or due to an additional symmetry, such as

[‡]The spontaneous breaking of the special conformal transformations does not lead to any additional NGBs [280, 281] and we use scale and full conformal invariance interchangeably for the purposes of our discussion.

supersymmetry. This implies that generically conformal invariance is not spontaneously broken and there is no massless dilaton.

A way to avoid requiring special conditions is to introduce a small amount of explicit breaking of conformal symmetry. In this case the dilaton obtains a mass but can remain naturally light. The conditions under which this is possible were considered by Contino, Pomarol and Rattazzi [282]. By assuming that conformal invariance is explicitly broken by a Lagrangian deformation $\lambda\mathcal{O}$, a naturally light dilaton occurs for a near-marginal operator so that the running coupling $\lambda(\mu)$ remains close to marginality throughout the renormalisation-group evolution. Similar effects were also studied in the four-dimensional effective theory in Ref [233]. Explicit holographic realisations were subsequently given in [226, 283] where the near-marginal deformation of the CFT corresponds to introducing a nearly massless bulk scalar field. The approximately constant bulk scalar potential preserves an approximate shift symmetry which leads to a renormalisation-group flow with a small β-function. However to obtain a dilaton in the low-energy spectrum, these explicit realisations also assumed the presence of an IR brane (or hard wall) which corresponds to spontaneously breaking the conformal symmetry by another operator which has an arbitrarily large dimension. Thus by introducing two scalar operators there is a simple, although idealised way to obtain a light dilaton.

A more realistic framework to study the properties of the dilaton is to consider a soft-wall background. This corresponds to introducing a single bulk scalar field with a non-trivial bulk scalar potential. The solutions of the coupled Einstein-scalar equations of motion can then lead to a scalar profile that grows in the IR, causing a back-reaction on the metric that deviates from AdS. Thus the "soft wall" produced by the single scalar field causes the spontaneous breaking of conformal symmetry with a mass gap in the spectrum. Equivalently, in the holographic description, there is a single operator $\mathcal{O}$ that is responsible for explicitly breaking the conformal symmetry and generating a condensate $\langle\mathcal{O}\rangle$. The fluctuations about the condensate $\langle\mathcal{O}\rangle$ are then identified with the dilaton.

Nearly-marginal deformations in a soft-wall background can still lead to a naturally light dilaton and were first considered in Ref. [228]. As long as the holographic β-function remains small at the condensation scale and then transitions sufficiently quickly to an order-one constant in the IR, an approximate shift symmetry can be retained. This translates into requiring a bulk scalar potential that must transform from an approximately constant potential near the UV brane to an exponential potential in the IR. If the transition region is sufficiently small then an approximate shift symmetry can be preserved with a corresponding light dilaton. In Ref. [228]

an approximate piecewise solution was constructed that exhibited these features in a soft-wall background and an approximate mass formula for the dilaton was derived.

In this chapter we present soft-wall solutions that provide a simple description of the dilaton from the UV to the IR scale. Using the superpotential method we first derive an analytic solution of the coupled Einstein-scalar equations of motion with an asymptotically AdS metric and non-trivial scalar profile that grows in the IR. This solution parametrises the explicit and spontaneous breaking of conformal symmetry by operators with dimensions in the range $1 < [\mathcal{O}] < 4$. A light dilaton is obtained when there is spontaneous breaking of the conformal symmetry and a hierarchy between the UV and IR scales. This is similar to the result obtained in Ref. [59] where a general analysis of scalar fluctuations in a soft-wall background was given. In addition, we show that a light dilaton is obtained in the case of explicit breaking by an operator of dimension $[\mathcal{O}] \simeq 2$. However, in both cases this corresponds to a tuning in the quartic coupling of the dilaton effective potential. This is a consequence of using an analytic superpotential and presumably the tuning could be understood from an underlying supersymmetry.

The scalar potential derived from the superpotential is then generalised to allow for non-analytic terms in the β-function. This allows for a deformed CFT with a nonzero condensate $\langle\mathcal{O}\rangle$. We find that a naturally light dilaton only occurs for nearly-marginal operators. In this case the β-function is approximately constant in the UV and then transitions rapidly to an approximately order-one constant in the IR with the corresponding scalar potential respecting an approximate shift symmetry. This agrees with the results derived in Ref. [228]. Furthermore with our solution we quantify how fast the rise to confinement must be in order to obtain a naturally light dilaton. We also find that in our case the β-function has a steep slope in the transition region precisely when the operator is close to marginality.

The outline for this chapter is as follows. In Section 5.2 we review the soft-wall background and the holographic interpretation. An analytic superpotential solution is presented in Section 5.3 where we give the conditions for a discrete spectrum and calculate the dilaton mass. A light dilaton occurs when conformal invariance is spontaneously broken and there is a hierarchy between the UV and IR scales. Alternatively in the case when there is an explicit UV breaking a light dilaton occurs when the operator dimension is near two. Both cases correspond to tuned scenarios. In Section 5.4 we consider a generalised analytic bulk scalar potential. In this case we show that a naturally light dilaton does occur but only for nearly-marginal operators. We summarise our results in Section 5.5.

5.2 The Soft-Wall Solution

We begin by considering the general 5D action given in Eq. (2.13) and included again below for convenience

$$S = 2\int_{y_0}^{y_c} d^5x\,\sqrt{-g}\left(\frac{M^3}{2}R - \frac{1}{2}(\partial\phi)^2 - V(\phi)\right) - \int_{UV} d^4x\,\sqrt{-\gamma}\left(2M^3[K] + U(\phi)\right)\,, \quad (5.2)$$

where $V(\phi)$ is the bulk scalar potential and $U(\phi)$ the UV boundary potential. Throughout this chapter we will be considering the case where a single 4D brane located at y_0 provides a UV cut-off, while y_c represents a curvature singularity. The scalar profile $\phi = \phi(y)$ will in general be a non-trivial function of the 5th coordinate and the functions $A(y)$ and $\phi(y)$ therefore characterise the soft-wall background.

As usual, it is convenient to express the Einstein equations as a simple first-order system in terms of a superpotential, W, defined by [46]

$$V(\phi) = \frac{1}{2}\,W'^2(\phi) - \frac{2}{3M^3}\,W^2(\phi)\,. \quad (5.3)$$

The bulk equations of motion and the boundary condition on the UV brane are then given by Eqs. (2.21, 2.23).

5.2.1 Holographic β-function

In order to investigate the behaviour of a given soft-wall solution and its interpretation in terms of a 4D CFT we shall make use of the holographic β-function [284–286]. As usual, the AdS/CFT correspondence allows us to relate the warp factor to the energy scale, μ, in the 4D theory according to

$$\mu = kA(y) \simeq k\,e^{-ky}\,. \quad (5.4)$$

It is well known in the case of RS models with a Goldberger-Wise field that the UV value of the bulk scalar can be identified with the UV value of a coupling responsible for deforming the CFT [106]. The definition of the holographic β-function, $\beta(\phi)$, then immediately follows:

$$\beta(\phi) \equiv A\partial_A\phi = -3M^3\frac{W'(\phi)}{W(\phi)}\,, \quad (5.5)$$

where we have used the bulk equations (2.21). The above equation can be solved to obtain the superpotential in terms of β and so a given model can be equivalently defined in terms of either the β-function or superpotential. The most common situation is to consider β-functions possessing a UV fixed point, corresponding to a bulk potential with an AdS extremum. However, it is still possible to obtain a wide variety of RG flows and spectra depending on the behaviour of the β-function in the IR. This has been discussed in detail in [287] in terms of the superpotential and also recently in [228].

We shall be interested in cases which result in a confining geometry with a discrete spectrum; this translates into a limit on the asymptotic value of the β-function as $\phi \to \infty$,

$$\sqrt{3M^3} < -\beta_\infty < 2\sqrt{3M^3}\,. \tag{5.6}$$

The lower bound arises from the requirement that the theory is confining in the IR[†]. The upper bound is obtained after imposing boundary conditions in the IR. The simplest condition is to require that the solution satisfies the Einstein equations at the dynamically generated boundary [287]. Alternatively AdS/CFT can be used to restrict to physical singularities with a finite temperature field theory dual [288]; in either case the same restriction on the β-function is obtained. For a given bulk potential, imposing these IR boundary conditions fixes the integration constant in the solution for the superpotential (or β-function) in Eq. (5.3).

5.2.2 UV Behaviour

In order to characterise the type of RG flow described by a given β-function it is useful to consider the behaviour of the solutions near the UV fixed point. Taking a bulk potential with an AdS extremum, which we assume to be at $\phi = 0$ without loss of generality, and expanding around this point we have

$$V(\phi) = -6k^2M^3 + \frac{1}{2}m_\phi^2\phi^2 + O(\phi^3)\,, \tag{5.7}$$

where k is the AdS curvature scale and m_ϕ is the scalar bulk mass. Solving Eq. (5.3) the superpotential then takes the form[‡]

$$W(\phi) = 3kM^3 + \frac{1}{2}k\Delta_\pm\phi^2 + \dots\,, \tag{5.8}$$

[†]The case -$\beta_\infty = \sqrt{3}$ is marginal and depends on the detailed behaviour of the β-function as $\phi \to \infty$ [287].

[‡]In the case $\Delta_+ = \Delta_- = 2$, the Δ_--type superpotential is $W(\phi) \simeq 3kM^3 + k\,\phi^2\left(1 + \frac{1}{\log\phi}\right)$ and $\phi(A) \simeq \lambda\, A^{-2}\log(A) + \langle\mathcal{O}\rangle\, A^{-2}$.

where the $\Delta_\pm$ are given in terms of the bulk mass by $\Delta_\pm = 2 \pm \sqrt{4 + m_\phi^2/k^2}$. For a given bulk potential there are therefore two possible asymptotic forms for the superpotential, which shall be referred to as Δ_+ and Δ_--type. It was shown in Ref. [289] that Δ_--type solutions also admit a leading non-perturbative term of the form ϕ^{4/Δ_-}, resulting in a family of Δ_--type solutions parametrised by the integration constant in Eq. (5.3). Such a term is forbidden for Δ_+-type solutions, which are either isolated or located at an infinite distance in parameter space from any Δ_--type solution.

From Eq. (2.21) and using the fact that the metric is asymptotically AdS the solution for the bulk scalar in terms of the warp factor is

$$\phi(A) = \lambda\, A^{-\Delta_-} + \frac{\langle \mathcal{O} \rangle}{2\Delta_+ - 4}\, A^{-\Delta_+} + \dots \,. \tag{5.9}$$

Assuming Dirichlet UV boundary conditions for the bulk scalar, the two leading terms can then be related to the running coupling and the condensate of the deforming operator in the CFT [104]. The $\Delta_\pm$ are related to the dimension of the operator according to $[\mathcal{O}] = \Delta_+ = 4 - \Delta_-$, leading to the standard AdS/CFT relation between the operator dimension and bulk mass. Provided that $1 \leq \Delta_- \leq 2$, one can also consider Neumann or mixed boundary conditions in which case we have an alternative CFT description where the leading term is now identified with the condensate and the operator dimension is given by Δ_-.

Considering more carefully the two types of superpotential solutions, it is clear that in the case of Δ_+-type solutions the leading term in Eq. (5.9) will be absent and therefore these solutions correspond to a CFT with purely spontaneous breaking of the conformal symmetry (assuming Dirichlet boundary conditions). On the other hand, Δ_--type solutions correspond to a deformed CFT and one finds that the coefficients of the two terms are in fact related according to

$$\langle \mathcal{O} \rangle = \frac{4\xi}{\Delta_-}\, \lambda^{\frac{\Delta_+}{\Delta_-}} \,, \tag{5.10}$$

where the coefficient of the ϕ^{4/Δ_-} term in the superpotential is proportional to ξ.

Finally, the above discussion can also be framed in terms of the β-function [228] leading to $\Delta_\pm$-type solutions of the form

$$\beta(\phi) = -\Delta_\pm \phi + \dots \,, \tag{5.11}$$

where once again the Δ_--type solutions admit a leading non-perturbative term of the form $\phi^{4/\Delta_- - 1}$.

5.3 An Analytic Superpotential Model

After this brief introduction we next present simple examples that exhibit the possible properties of the dilaton. We shall initially consider the following simple model described by the superpotential

$$W(\phi) = 3kM^3 \cosh\left(\sqrt{\frac{\alpha}{3M^3}}\,\phi\right), \tag{5.12}$$

where α is a constant parameter. This superpotential is analytic in ϕ^2 and will allow us to straightforwardly solve for the metric and scalar backgrounds. As we shall see, the above choice of superpotential leads to the 5D gravity dual of a strongly coupled conformal sector where conformal invariance is spontaneously broken via the condensation of a finite dimensional operator. Also note that by defining our model in terms of the superpotential we have implicitly fixed the integration constant in Eq. (5.3).

The bulk potential corresponding to our superpotential is

$$V(\phi) = \frac{3}{2}k^2M^3\left[(\alpha-4)\cosh^2\left(\sqrt{\frac{\alpha}{3M^3}}\,\phi\right) - \alpha\right]. \tag{5.13}$$

Notice that this reduces to the familiar constant potential $V = -6k^2M^3$ if we take $\alpha = 4$[†]. Solving the equation of motion (2.21) we obtain the background solution

$$\begin{aligned} A(y) &= e^{-ky_c}\left[2\sinh(k\alpha(y_c-y))\right]^{\frac{1}{\alpha}}, \\ \phi(y) &= -\sqrt{\frac{3M^3}{\alpha}}\log\left[\tanh\left(\frac{1}{2}k\alpha(y_c-y)\right)\right]. \end{aligned} \tag{5.14}$$

This solution has an AdS vacuum as $y_0 \to -\infty$, which we have chosen to be at $\phi = 0$ without loss of generality. Notice that the scalar profile is singular in the IR and there is a naked curvature singularity at $y = y_c$. We therefore have a dynamically generated boundary or "soft-wall" with spacetime ending at $y = y_c$. The solutions are plotted in Figure 5.1.

For completeness we also take the following UV boundary potential

$$U(\phi) = \Lambda_{UV} + m_{UV}k(\phi-\phi_0)^2, \tag{5.15}$$

[†]This case corresponds to the model considered in [226]. As we shall discuss, values of $\alpha \geq 4$ require the introduction a hard cut-off in the IR. By considering the more general form for the superpotential (5.12) we are able to construct a true soft-wall model of spontaneous conformal symmetry breaking.

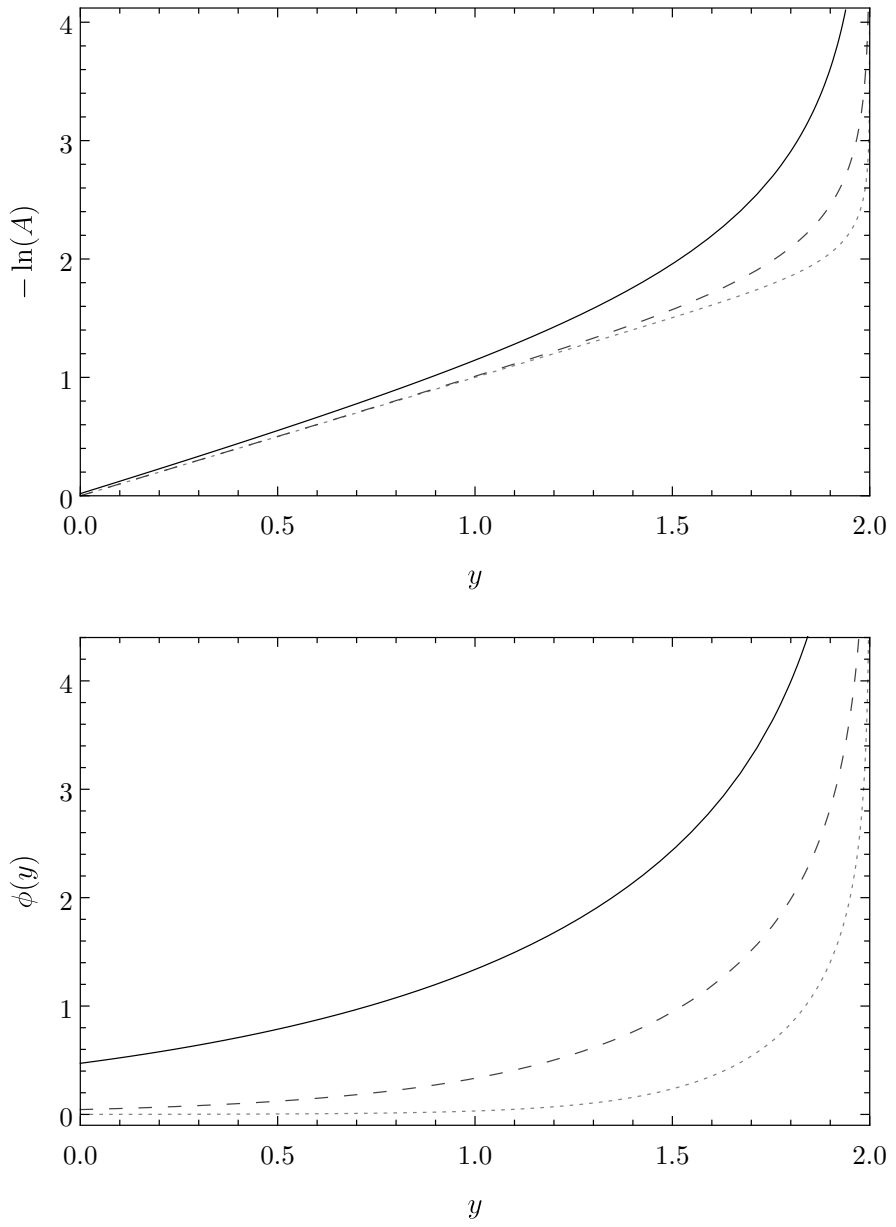

FIGURE 5.1: Background solutions for the warp factor (top) and scalar profile (bottom) as a function of y. We have set $M = 1$, $k = 1$, and $y_c = 2$. The solid, dashed and dotted curves correspond to $\alpha = 1, 2$ and 4 respectively.

where Λ_{UV} is the UV brane tension and m_{UV} is the UV boundary mass. However in most cases we will take the infinite boundary mass limit, which forces $\phi = \phi_0$ on the brane; the exact form of the potential is then unimportant. Imposing the boundary conditions (2.23) enforces the usual tuning of the 4D cosmological constant in addition to fixing the IR scale according to

$$k(y_c - y_0) = \frac{2}{\alpha} \operatorname{arctanh}\left(e^{-\sqrt{\frac{\alpha}{3M^3}}\phi_0}\right) , \tag{5.16}$$

where we have taken the limit $m_{UV} \to \infty$. It is clear that generating a large

hierarchy then requires a hierarchically small value of ϕ_0. In the case of purely spontaneous breaking of the conformal symmetry this small boundary value for ϕ will be directly related to the ratio of the condensate and UV cut-off scales.

It is straightforward to evaluate the β-function corresponding to our superpotential to obtain

$$\beta(\phi) = -\sqrt{3M^3\alpha}\,\tanh\left(\sqrt{\frac{\alpha}{3M^3}}\,\phi\right)\,, \tag{5.17}$$

or expressed in terms of the background solutions

$$\beta(\phi(y)) = \frac{A(y)\phi'(y)}{A'(y)} = -\sqrt{3M^3\alpha}\,\mathrm{sech}(k\alpha(y_c - y))\,. \tag{5.18}$$

The limit on the asymptotic value of the β-function in Eq. (5.6) then leads to the requirement that

$$1 < \alpha < 4\,. \tag{5.19}$$

For $\alpha \leq 1$ a continuous spectrum is obtained, while for $\alpha \geq 4$ it becomes necessary to introduce a hard cut-off/IR brane in order to satisfy the boundary condition. In other words, our choice of superpotential no longer satisfies the IR boundary condition for $\alpha \geq 4$. In the dual 4D description, the introduction of an IR brane corresponds to the spontaneous breaking of the conformal symmetry by an infinite dimensional operator.

We now want to look at the behaviour near the UV fixed point in order to interpret the soft-wall solution in terms of the dual CFT. Firstly, expanding the bulk potential (5.13) around $\phi = 0$ gives

$$V(\phi) = -6k^2M^3 + \frac{1}{2}k^2\alpha(\alpha-4)\phi^2 + O(\phi^4)\,. \tag{5.20}$$

This allows us to evaluate $\Delta_\pm$ for our solution according to

$$\Delta_\pm = 2 \pm \sqrt{4 + m_\phi^2/k^2} = 2 \pm |\alpha - 2|\,. \tag{5.21}$$

We can also expand (5.17) around $\phi = 0$ to obtain

$$\beta(\phi) = -\alpha\,\phi + \ldots \quad = \begin{cases} -\Delta_-\phi + \ldots & , \quad \alpha < 2 \\ -\Delta_+\phi + \ldots & , \quad \alpha \geq 2 \end{cases}\,. \tag{5.22}$$

We therefore have a Δ_+-type β-function for $\alpha \geq 2$, which (for Dirichlet boundary conditions) corresponds to a CFT with purely spontaneous conformal symmetry breaking via the condensation of an operator $\mathcal{O}$ (i.e. $\lambda = 0$). On the other hand, for $\alpha < 2$ our solution is of the Δ_--type and we have a deformed CFT where conformal

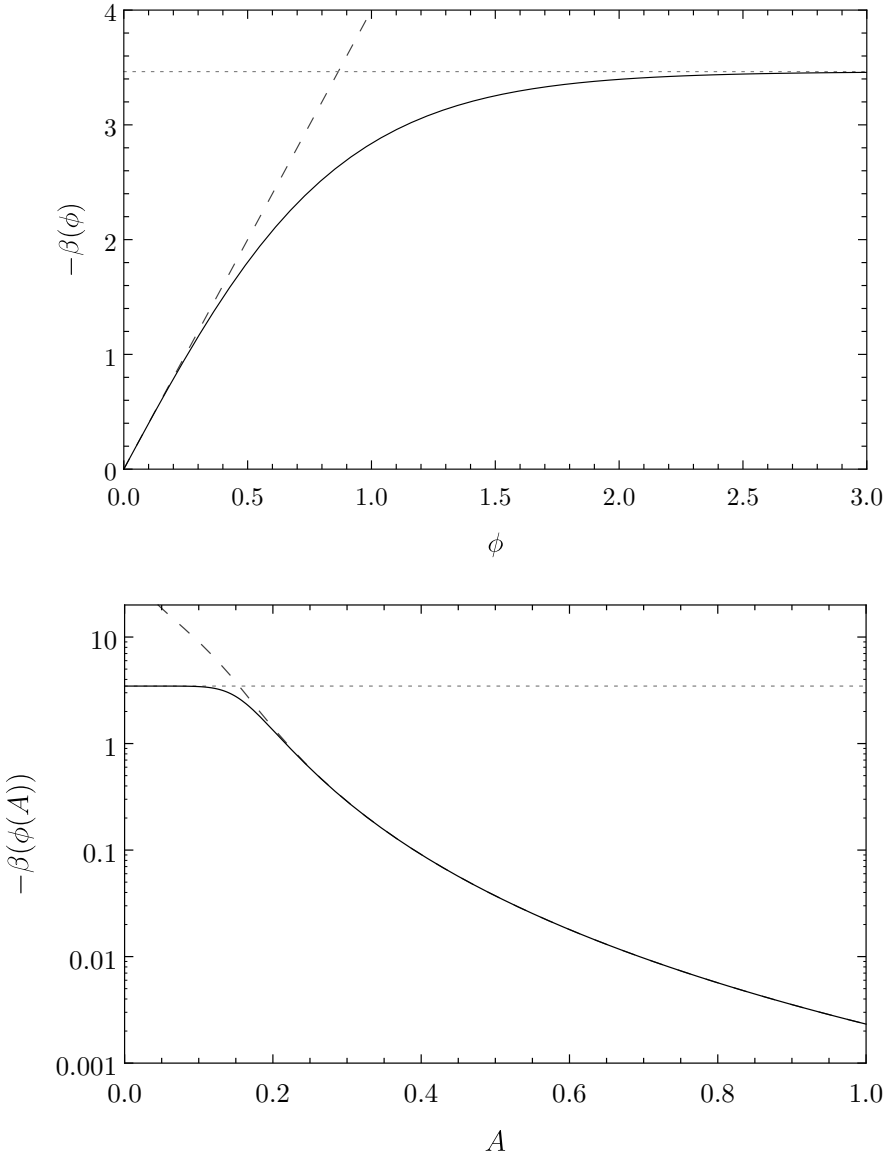

FIGURE 5.2: Holographic β-function as a function of ϕ and A in the top and bottom panels respectively. The solid line corresponds to the full β-function (5.17), while the dashed line shows the leading-order term when expanded around $\phi = 0$. The dotted line denotes the asymptotic value in the IR. We have set $M = 1$, $k = 1$, $\alpha = 2$ and $y_c = 2$.

invariance is explicitly broken by the coupling λ. Note that due to the fact that our superpotential is analytic in ϕ^2 there can be no non-perturbative piece in the β-function ($\xi = 0$) and therefore there is no condensate in this case. Depending on the value of α, our solution therefore describes a CFT either spontaneously broken or deformed by an operator of dimension $2 \leq [\mathcal{O}] < 4$. If we instead consider the alternative CFT description and assume Neumann boundary conditions for the scalar then the situation is reversed and we have spontaneous breaking for $1 < \alpha < 2$ and a deformed CFT with no condensate for $2 \leq \alpha \leq 3$, corresponding to operator dimensions $1 \leq [\mathcal{O}] \leq 2$. The beta function is shown in Figure 5.2.

5.3.1 Fine-tuning and Spontaneous Breaking

It is well known that a purely spontaneously broken CFT is expected to be tuned. The issue arises from the fact that unlike non-linearly realised internal symmetries, a non-derivative quartic coupling for the dilaton is permitted by scale invariance. Naive dimensional analysis suggests that generically this coupling should be large ($\sim 16\pi^2$), however a massless dilaton arising from spontaneous breaking can only be obtained in the special case where the quartic coupling is zero. In the absence of some mechanism such as supersymmetry, which can give rise to flat directions in the dilaton potential, spontaneous breaking therefore requires a tuning of the quartic coupling.

From the 5D viewpoint, this tuning can be readily identified in RS+GW type models as the tuning of the IR brane tension [45]; however in soft-wall models the situation is more subtle and related to the various superpotentials which can arise for a given bulk potential. Generically we expect a Δ_--type superpotential that is a non-analytic function of ϕ. In addition there may be particular values of the integration constant in Eq. (5.3) which lead to Δ_+-type solutions or Δ_--type solutions with an analytic superpotential (i.e. $\xi = 0$). Situations where such solutions not only exist but also satisfy the regularity conditions in the IR are clearly non-generic and generally arise from carefully constructed bulk potentials. In addition, by evaluating the on-shell action one can easily demonstrate that such solutions correspond to a dilaton potential where the quartic term is set to zero as we shall see in Section 5.3.3.

We note that while our solution should therefore be considered tuned, it nevertheless provides a useful model for a spontaneously broken conformal sector where the background equations can be solved analytically. In other words our solution corresponds to a soft-wall version of pure RS, but describes the more realistic case of spontaneous breaking by a finite-dimensional operator. In Section 5.4 we shall consider a more general bulk potential to investigate the more generic (un-tuned) case where we have a non-zero quartic term in the dilaton potential.

5.3.2 Mass Spectrum

Next we determine the mass spectrum for the scalar modes of the solution (5.14). In the case of massive modes, the metric and bulk scalar perturbations can be parametrised as in Eqs. (2.44). After performing a Kaluza-Klein (KK) expansion, the dynamical equation for the scalar sector can be written in terms of the gauge

invariant variable $\zeta = \Psi - \delta\phi/\beta$ as [62]

$$\frac{1}{A^4\beta^2}\frac{d}{dy}\left[A^4\beta^2\zeta_n'\right] + \frac{m_n^2}{A^2}\zeta_n = 0\,. \tag{5.23}$$

Recall that for massless modes, the perturbations should instead be decomposed in terms of a light-cone basis. After gauge fixing, this yields the decomposition in Eqs. (2.45) and the coupled equations of motion in Eqs. (2.53).

In both cases we also have the constraint equation

$$\Psi' - \frac{A'}{A}\Phi + \frac{1}{3M^3}\phi'\,\delta\phi = 0\,. \tag{5.24}$$

The UV boundary condition is given by

$$\delta\phi' - \phi'\Phi = \frac{1}{2}U''(\phi)\,\delta\phi\,, \tag{5.25}$$

while at the dynamical IR boundary we have

$$A^4\delta\phi' = 0\,. \tag{5.26}$$

There will also be an additional normalisation condition.

5.3.2.1 Massless Dilaton from Spontaneous Breaking

We begin by investigating under which circumstances it is possible to obtain a massless dilaton from spontaneous breaking of conformal invariance. The solution to Eqs. (2.53) contains two dynamical scalar degrees of freedom $c_{1,2}$ and is given by [60]

$$\zeta_1 = c_1(x), \qquad \zeta_2 = \frac{A'}{A^3}\,c_2(x) - 2\left(\frac{A'}{A^3}\int dy\,A^2\right)(y)\,c_1(x)\,, \tag{5.27}$$

where $\zeta_1 = \Psi - \delta\phi/\beta$ and $\zeta_2 = \delta\phi/\beta$. We can immediately remove the c_2 mode by imposing the IR boundary condition, leaving just a single 4D massless mode, c_1.

In the presence of a finite UV cut-off it is expected that the dilaton will acquire a mass due to the coupling of the CFT to the dynamical source. This indeed turns out to be the case and can be easily checked by imposing the UV boundary condition (5.25) for finite y_0. One then finds that the above solution does not satisfy the boundary conditions, with the usual exception when there is a tuning between the boundary and bulk masses. On the other hand, as the UV cut-off

is removed ($y_0 \to -\infty$) the source decouples and we should expect a massless dilaton if the conformal symmetry is spontaneously broken. Imposing Dirichlet or Neumann boundary conditions for $\delta\phi$ requires that the leading ($A^{\Delta-}$) or subleading ($A^{\Delta+}$) terms vanish respectively. We then find that the remaining mode, c_1, does indeed satisfy the boundary conditions for $\alpha \geq 2$ (Dirichlet) or $\alpha < 2$ (Neumann) as expected.

5.3.2.2 Light Dilaton with UV Explicit Breaking

Moving now to the case of a massive dilaton, the gauge freedom allows us to make the choice $\Psi = 0$ and express Eq. (5.23) solely in terms of $\delta\phi$. Using (5.24) the UV boundary condition can similarly be written in terms of $\delta\phi$ as

$$\delta\phi' = \left(\frac{1}{2}U''(\phi) + \frac{1}{3M^3}\phi'\beta\right)\delta\phi\,. \tag{5.28}$$

While the equation of motion is non-trivial and can in general only be solved numerically, an approximate solution for $m \ll m_{KK}$ can be found by matching solutions in the UV and IR, where $m_{KK} = [\int dy/A]^{-1}k$. Generalising the procedure used in [228] to allow for general boundary conditions we obtain the following expression for the dilaton mass, m_D

$$\frac{1}{m_D^2} \simeq \left(\int_{y_0}^{y_c} dy\, \frac{1}{A^4\beta^2}\int_y^{y_c} dy'\, A^2\beta^2\right) + \kappa\int_{y_0}^{y_c} dy\, A^2\beta^2\,, \tag{5.29}$$

where

$$\kappa = \frac{1}{A^4\beta^2}\left(\frac{1}{2}U''(\phi) + \frac{1}{3M^3}\phi'\beta - \frac{\beta'}{\beta}\right)^{-1}\Bigg|_{y_0}\,, \tag{5.30}$$

and β' in (5.30) is the derivative with respect to y. Unfortunately in our case the first term above can still only be evaluated numerically[†]. Taking the $m_{UV} \to \infty$ limit, which forces $\delta\phi = 0$ on the UV boundary, we have $\kappa \to 0$ and the expression reduces to that given in Ref. [228].

We have also solved Eq. (5.23) numerically for the masses and profiles of the dilaton and the lowest few KK modes using the shooting method. The results are given in Figure 5.3, where the dashed line shows the approximate solution (5.29) and we have taken $m_{UV} \to \infty$. Note that the approximate solution is in good agreement with the full numerical solution in the cases where we have a light dilaton.

[†]A reasonable approximation can be obtained by noticing that the inner integral gives a constant of order m_{KK}^2 for all values of y, except near $y = y_c$. An analytic expression for the dilaton mass can then be obtained by evaluating the outer integral and keeping only the dominant UV boundary term.

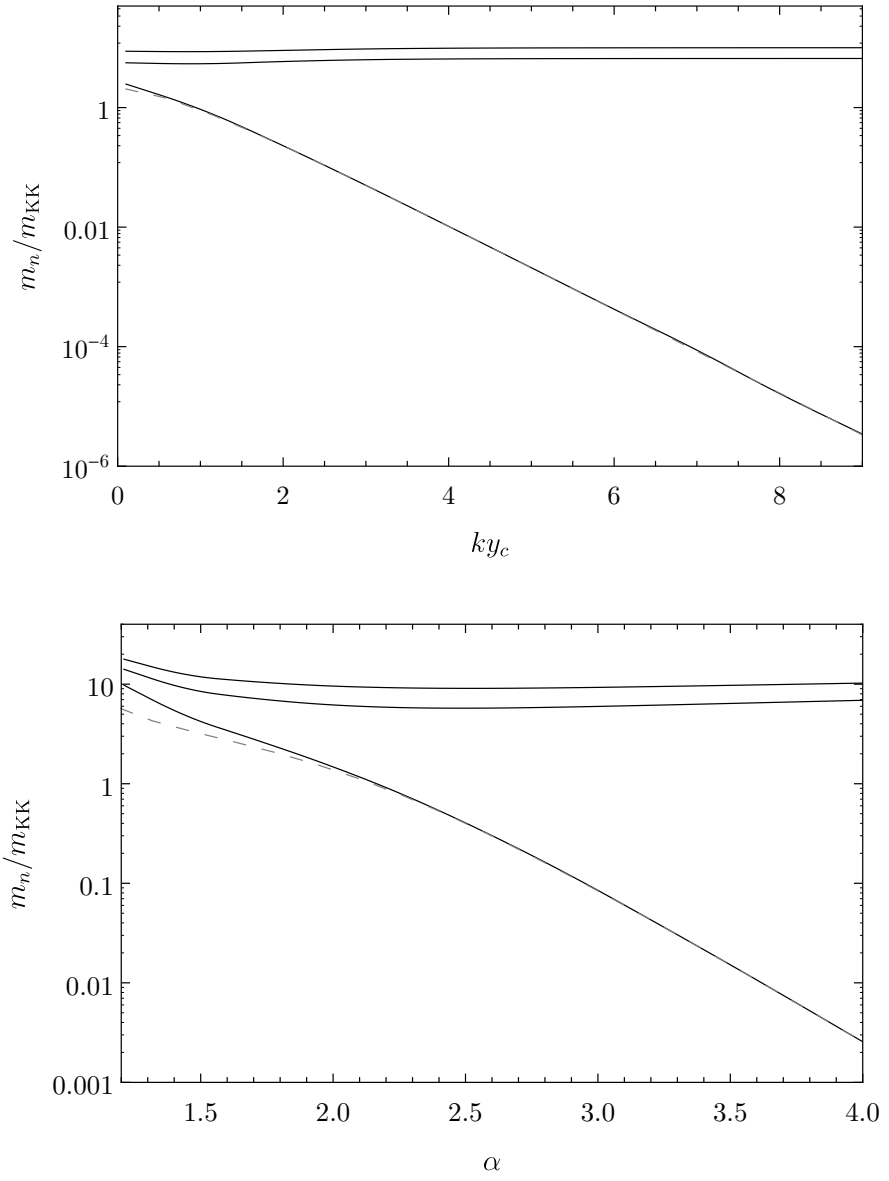

FIGURE 5.3: Masses of the three lightest modes as a function of ky_c for $\alpha = 3.6$ (top panel) and as a function of α for $ky_c = 4$ (bottom panel). The dashed line shows the approximate solution (5.29). We have set $y_0 = 0$.

Focusing initially on the top panel, where $\alpha = 3.6$, we find that there exists a very light mode as the separation between the UV brane and the soft-wall becomes large. This is not surprising, since for $\alpha \geq 2$ we expect to obtain a massless mode from the spontaneous breaking when the explicit breaking effects of the UV cut-off are decoupled. In this scenario the dilaton mass is arising solely due to the coupling of the CFT to the dynamical source and the small dilaton mass is directly related to the fact that $\mu_0 \gg m_{KK}$, where the UV scale $\mu_0 \equiv kA(y_0)$. A similar effect for a soft-wall background was also obtained in Ref. [59]. For large hierarchies it is therefore possible to exponentially suppress the dilaton mass relative to the confinement/symmetry breaking scale. We emphasise however that the presence

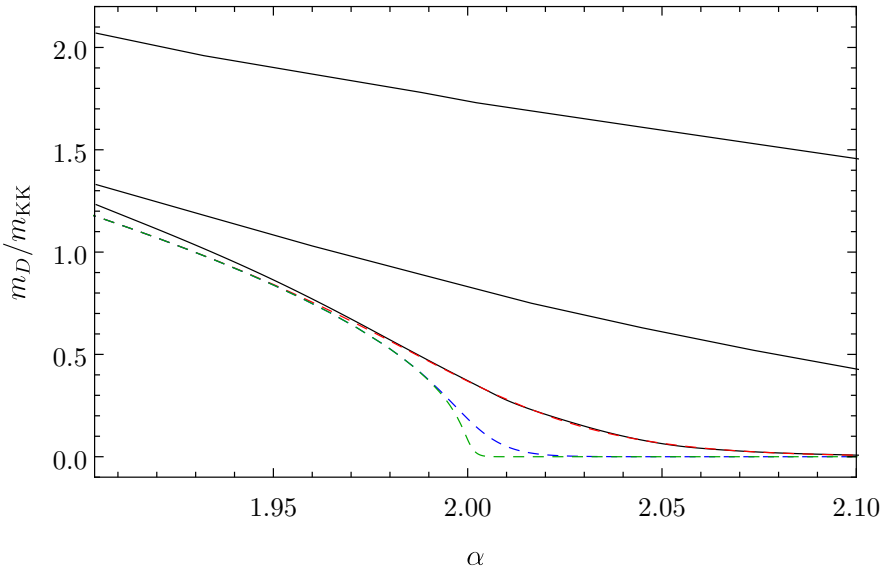

FIGURE 5.4: Dilaton mass near $\alpha = 2$ for $ky_0 = -2, -10, -50, -200, -1000$ (top to bottom). The dashed curves are obtained using Eq. (5.29). We have set $ky_c = 1$.

of such a light mode is dependent on the fact that we have a Δ_+-type solution in this regime, and as discussed in Section 5.2.1 such scenarios should be considered tuned. Finally, it is worth noting that this contribution to the dilaton mass does not appear in hard-wall models of spontaneous breaking, where the dilaton is a purely composite state. In the standard RS case, the dilaton remains massless even in the presence of the UV brane due to the fact that the IR brane corresponds to spontaneous breaking by an infinite dimensional operator and is therefore not sensitive to the UV cut-off.

Considering now the bottom panel in Figure 5.3, we see that for smaller values of α (in particular $\alpha < 2$) there is no longer a light mode in the spectrum. This is again to be expected, since in this regime we have a Δ_--type solution corresponding to a deformed CFT. The dilaton therefore acquires a large mass even in the absence of a UV cut-off. This is shown more clearly in Figure 5.4, where we have plotted the dilaton mass near $\alpha = 2$ for various values of y_0. As discussed previously, for $\alpha > 2$ we obtain a massless mode as $y_0 \to -\infty$, while for $\alpha < 2$ the dilaton quickly becomes massive.

Interestingly it seems possible to obtain a light dilaton from a deformed CFT with a Δ_--type solution when approaching $\alpha = 2$ from below, albeit only for large hierarchies. The existence of this light mode can be understood by looking at the behaviour of Eq. (5.29) in the limit $y_0 \to -\infty$. Firstly, the inner integrand in this expression simply gives a constant of order m_{KK}^2 for all values of y (except near $y = y_c$) and so the behaviour of the mass is largely determined by the outer

integral. Now, in the UV the metric is approximately AdS and we can rewrite this as an integral over the warp factor, A. Then using the fact that the β-function in the UV is well approximated by $\beta(\phi) = -\Delta_- \phi$ and substituting in the leading behaviour $\phi \sim A^{-\Delta_-}$ we obtain

$$\int dA\, A^{2\Delta_- - 5}\,. \tag{5.31}$$

For $\Delta_- = 2$ this integral clearly becomes divergent as $A \to \infty$ ($y_0 \to -\infty$), giving rise to a massless dilaton. Near $\Delta_- \lesssim 2$ the dilaton mass is then described by

$$m_D \sim \sqrt{2 - \Delta_-}\, m_{KK}\,. \tag{5.32}$$

We therefore find a light dilaton with an operator of dimension 2, in contrast to the well-studied scenario where a naturally light dilaton is obtained with a near-marginal operator [226, 227]. However, the presence of this light mode is a consequence of the particular form of our bulk potential and relies upon the fact that our solution transitions to a Δ_+-type solution at $\alpha = 2$. The light mode is therefore a result of the tuning in this model arising from the absence of a non-perturbative term in the superpotential. For a more general bulk potential, where the solution remains of the Δ_--type, the leading order behaviour of ϕ at $\Delta = 2$ is given by $\phi \sim \log(A) A^{-2}$. This logarithmic behaviour ensures that the above integral remains finite and there is no light mode.

5.3.3 Effective Potential

Similar to the approach commonly undertaken in hard-wall models [42, 45], it is useful to construct a 4D effective potential for the dilaton by integrating out the extra dimension. After using the bulk equations of motion, it is straightforward to show that the effective potential in the presence of a soft-wall is given by

$$V_{eff} = A^4(y_0)\,\left[U(\phi(y_0)) - 2W(\phi(y_0))\right] - \frac{2}{3}\lim_{y \to y_c} A^4(y)\, W(\phi(y))\,. \tag{5.33}$$

Provided that the superpotential satisfies certain boundary conditions in the IR, as discussed in Section 5.2.1, the last term in the above expression will be zero and can be ignored. Once again this will be the case for our solution provided $\alpha < 4$.

It is worth pointing out that unlike the hard-wall case the warp-factor depends on the dilaton vacuum expectation value through y_c. Therefore, simply minimising Eq. (5.33) for fixed y_0 may lead to unphysical minima which do not satisfy the boundary equations of motion (2.23). Instead one should minimise the potential

while keeping the physical UV scale μ_0 fixed. Then, parametrising the dilaton by[†] $\chi \equiv e^{-ky_c}$, the effective potential is given by

$$\frac{V_{eff}(\chi)}{\mu_0^4} = \Lambda_{UV} + m_{UV} k \left(\phi_0 + \sqrt{\frac{3M^3}{\alpha}} \log(F(\chi)) \right)^2 - 3kM^3 \left(F(\chi) + \frac{1}{F(\chi)} \right) , \quad (5.34)$$

where

$$F(\chi) = \left(\frac{\chi}{\mu_0} \right)^{\alpha} \left(-2 + \sqrt{4 + \left(\frac{\chi}{\mu_0} \right)^{-2\alpha}} \right) . \quad (5.35)$$

The effective potential is plotted in Figure 5.5. The top panel shows the unstabilised case in the absence of a boundary mass term, while in the bottom panel we can clearly see the generation of a non-zero minimum for the dilaton once the bulk scalar obtains a vacuum expectation value on the boundary.

While the general expression (5.34) is complicated, the situation becomes much simpler as the UV cut-off is removed. Taking the limit $\mu_0 \to \infty$ and adding appropriate counterterms to subtract the divergent terms[‡] leads to

$$V_{eff}(\chi) = \begin{cases} \bar{\Lambda}_{UV} + k\,\bar{m}_{UV}\bar{\phi}_0^2 & \\ \quad -4k\sqrt{\frac{3M^3}{\alpha}}\bar{\phi}_0\bar{m}_{UV}\,\chi^{\alpha} + 12k\frac{M^3}{\alpha}\bar{m}_{UV}\,\chi^{2\alpha} & , \quad \alpha < 2\,, \\ \bar{\Lambda}_{UV} + k\,\bar{m}_{UV}\bar{\phi}_0^2 & , \quad \alpha \geq 2\,, \end{cases} \quad (5.36)$$

where we have simultaneously performed the rescaling $\Lambda_{UV} = \bar{\Lambda}_{UV}\,\mu_0^{-4}$, $\phi_0 = \bar{\phi}_0\,\mu_0^{-\Delta_-}$ and $m_{UV} = \bar{m}_{UV}\,\mu_0^{2(\Delta_- - 2)}$. From the 4D viewpoint this rescaling simply corresponds to running the couplings up to the scale μ_0 and ensures that the IR scale remains fixed when taking the limit $\mu_0 \to \infty$.

If we consider the alternative CFT description, where the operator dimension is given by Δ_-, then the on-shell action is identified with the 1PI effective action in the CFT [104]. We can then straightforwardly interpret Eq. (5.36) as it is directly related to the effective potential in the alternative CFT. This becomes more evident if we compare Eqs. (5.9)[§] and (5.14) to obtain the relation $\langle \mathcal{O} \rangle \sim \chi^{\alpha}$.

Let us initially focus on $\alpha < 2$ where we have a Δ_--type solution. If we then take $\bar{m}_{UV} = 0$ in Eq. (5.36) we obtain a flat potential, consistent with spontaneous

[†]One could also choose to parametrise the dilaton by the inverse conformal volume, $(kz_c)^{-1}$. However it can be easily shown that the two parametrisations are equivalent up to a simple rescaling, which depends only on α.

[‡]The specific counterterms necessary to subtract the divergent terms in Eq. (5.34) are given by $6kM^3 + 3k\frac{M^3}{\alpha}\Delta_- \log(F(\chi))^2$.

[§]In this case the leading term in Eq. (5.9) is identified with the condensate, $\langle \mathcal{O} \rangle$.

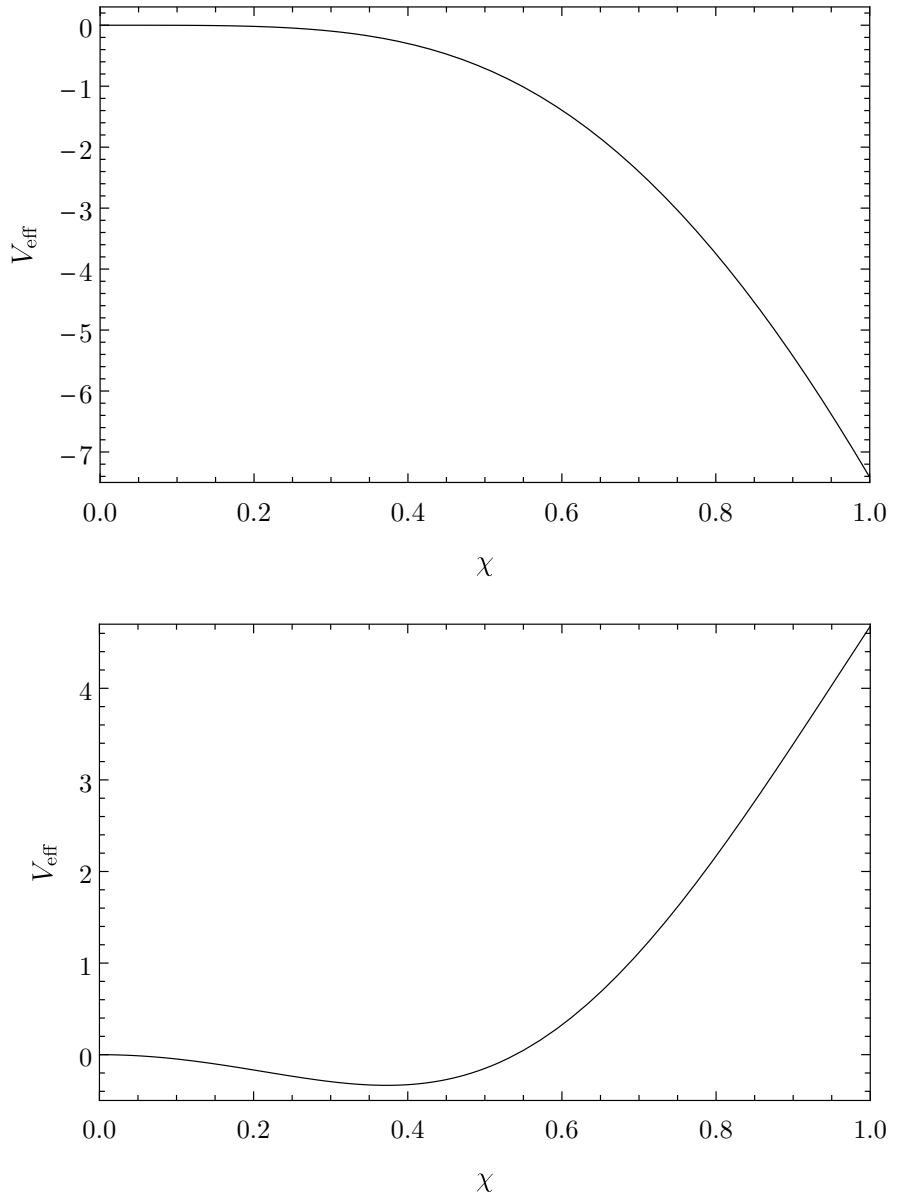

FIGURE 5.5: Effective potential, where the dilaton has been parametrised by $\chi = e^{-ky_c}$. The top panel corresponds to the case $m_{UV} = 0$, while the bottom panel has $m_{UV} = 5$ and $\phi_0 = 0.2$. We have set $M = k = \mu_0 = 1$, $\alpha = 2$ and fixed $\Lambda_{UV} = 6kM^3 - k\, m_{UV}\phi_0^2$.

breaking by an operator of dimension Δ_-. It is worth noting however that in this case the potential becomes unstable for finite μ_0. For non-zero $\bar{m}_{UV}$, the boundary conditions are modified and the two χ-dependent terms in Eq. (5.36) can be identified with turning on a source for a single and double-trace deformation in the CFT [290]. This results in a non-zero condensate and minimising (5.36) for $\alpha < 2$ we obtain

$$\langle \chi \rangle = \left(\frac{1}{2} \sqrt{\frac{\alpha}{3M^3}}\, \bar{\phi}_0 \right)^{\frac{1}{\alpha}} . \tag{5.37}$$

It can also be shown that this is consistent with the result obtained by directly solving the boundary conditions by taking the limit $y_0 \to \infty$ in Eq. (5.16).

We now turn to the case $\alpha \geq 2$ where we have a Δ_+-type solution. When considering the alternative CFT description, Δ_+-type solutions can only describe the situation where $\langle \mathcal{O} \rangle = 0$ (because the leading term is absent in (5.9)) and so a non-trivial potential cannot be generated in Eq. (5.36). Since there is no spontaneous breaking we do not obtain a massless mode with Neumann boundary conditions when $\alpha \geq 2$ as seen in Section 5.3.2. If we move to the standard CFT description instead, Δ_+-type solutions now describe the case of zero source and this means that Eq. (5.36) can still be interpreted as the effective potential in the CFT. We then have a flat potential consistent with spontaneous breaking by an operator of dimension Δ_+.

Importantly, in the case of both Δ_- and Δ_+-type solutions, the only terms which survive the $\mu_0 \to \infty$ limit in Eq. (5.36) are boundary terms and there is generally no quartic term in the potential. As mentioned in Section 5.3.1 this is due to the fact that we have chosen a superpotential which is analytic in ϕ^2. More generally, the superpotential will include a leading non-analytic term of the form ϕ^{4/Δ_-}, which directly gives rise to a non-zero quartic term in the effective potential. This can be easily shown using Eqs. (5.9) and (5.10) and then identifying the dilaton according to $\langle \mathcal{O} \rangle \sim \chi^{4-\Delta_-}$ in the case of standard quantisation or $\langle \mathcal{O} \rangle \sim \chi^{\Delta_-}$ for the alternative quantisation.

Finally, it is worth highlighting that an accurate expression for the dilaton mass cannot generally be obtained by simply expanding the effective potential around the minimum. While this may provide a good approximation to the dilaton mass in certain regions, for example $\alpha > 2$, it fails to capture the correct behaviour in other regions such as near $\alpha \lesssim 2$. In order to obtain the physical dilaton mass one should of course compute the full effective action, in particular the dilaton kinetic term.

5.4 An Analytic Potential Model

So far we have been considering a simple model with an analytic superpotential, which allowed us to straightforwardly solve for the warp factor and bulk scalar profile. While this model provides a useful description of a conformal sector spontaneously broken by a finite dimensional operator, we have seen that it corresponds

to the special case of a vanishing quartic term in the dilaton potential. In the absence of some symmetry (e.g. supersymmetry) to enforce this condition, we must consider such cases tuned and instead look to a more general model.

Simply considering a superpotential which is non-analytic in ϕ will generally not lead to a bulk potential with an AdS extremum and so one should instead begin by choosing a general form for the bulk potential and then solve Eq. (5.3) to obtain the superpotential. Unfortunately the cases where there exists a known solution to (5.3) are limited and for most bulk potentials the superpotential can only be determined numerically. However, such a numerical approach is indeed still useful and will allow us to determine the background solutions and dilaton mass for more general bulk potentials.

The simplest extension of our previous superpotential model leads to the following form for the bulk potential

$$V(\phi) = \frac{3}{2}k^2M^3\left[\tau\cosh^2\left(\sqrt{\frac{\alpha}{3M^3}}\,\phi\right) - (4+\tau)\right], \tag{5.38}$$

which is parametrised by the two constant parameters α and τ and reduces to Eq. (5.13) in the special case $\tau = \alpha - 4$. The above potential will indeed alleviate the tuning found in our simple model and consequently give rise to a non-zero quartic term in the dilaton potential. However we have numerically verified there is no light dilaton in the spectrum except in the regions of parameter space where we approach the tuned solution.

We will therefore focus instead on a different form for the bulk potential, which as we shall see can indeed give rise to a naturally light dilaton. We will be interested in the following potential

$$V(\phi) = V_0\, e^{\tanh\left(\frac{\gamma}{\nu}\right)\sqrt{\frac{\alpha}{3M^3}}\phi}\cosh^\nu\left[\frac{1}{\nu}\left(\gamma - \sqrt{\frac{\alpha}{3M^3}}\phi\right)\right], \tag{5.39}$$

parametrised by the constant parameters α, γ, ν and where

$$V_0 = -6k^2M^3\,\mathrm{sech}^\nu\left(\frac{\gamma}{\nu}\right). \tag{5.40}$$

The coefficient of ϕ in the exponent has been chosen such that the potential once again possesses an AdS extremum at $\phi = 0$. Expanding around this point gives

$$V(\phi) = -6k^2M^3 - \frac{\alpha}{\nu}\,\mathrm{sech}^2\left(\frac{\gamma}{\nu}\right)k^2\,\phi^2 + O(\phi^3), \tag{5.41}$$

and we again identify

$$\Delta_{\pm} = 2 \pm \sqrt{4 - \frac{2\alpha}{\nu} \operatorname{sech}^2\left(\frac{\gamma}{\nu}\right)} \,. \tag{5.42}$$

This potential has a couple of interesting features. Firstly, in certain regions of parameter space (e.g. $|\nu| \ll 1$) it possess an approximate shift symmetry, $\phi \to \phi + c$, in the UV. Furthermore, for large ϕ the potential behaves as a simple exponential and this shift symmetry is then realised as an overall rescaling. It was pointed out in Ref. [228] that such a potential may be considered technically natural provided that the intermediate symmetry breaking region is small. Interestingly they also demonstrated that such a condition should also be satisfied in order for the spectrum to contain a light dilaton. We shall see this explicitly for our potential below.

In order to obtain a solution which satisfies the IR boundary condition, it will be numerically simpler to solve for the β-function rather than directly solving Eq. (5.3) for the superpotential. Combining (5.3) with the definition of the β-function (5.5) yields the following equation

$$\beta'\beta = \left(\beta^2 - 12M^3\right)\left(\frac{\beta}{3M^3} + \frac{V'}{2V}\right) , \tag{5.43}$$

which is an example of Abel's equation of the second kind. It is clear from the above equation that it is the quantity V'/V, rather than the potential itself, which determines the behaviour of the β-function. Let us then consider more carefully the following expression

$$\frac{V'(\phi)}{V(\phi)} = \sqrt{\frac{\alpha}{3M^3}}\left(\tanh\left[\frac{\gamma}{\nu}\right] - \tanh\left[\frac{1}{\nu}\left(\gamma - \sqrt{\frac{\alpha}{3M^3}}\phi\right)\right]\right) . \tag{5.44}$$

We can now clearly identify the role of the various parameters in our potential. For $\nu \ll 1$ the above expression behaves as a step-function, with the location of the inflection point given by $\phi = \sqrt{3M^3/\alpha}\,\gamma$. The steepness of the step is determined by α/ν, while for small ν the asymptotic value in the IR is largely determined by α. There are then three distinct regions for V'/V: two approximately flat regions for small and large ϕ, and an intermediate transition region. We shall find that the β-function also exhibits a very similar behaviour with the three regions corresponding to a β-function which is walking in the UV; has an intermediate region identified with the turning on of a condensate; and then confines in the IR.

Recall that for a β-function which is both confining and satisfies the IR boundary conditions, there is limit on the asymptotic value in the IR of $\sqrt{3M^3} < -\beta_\infty <$

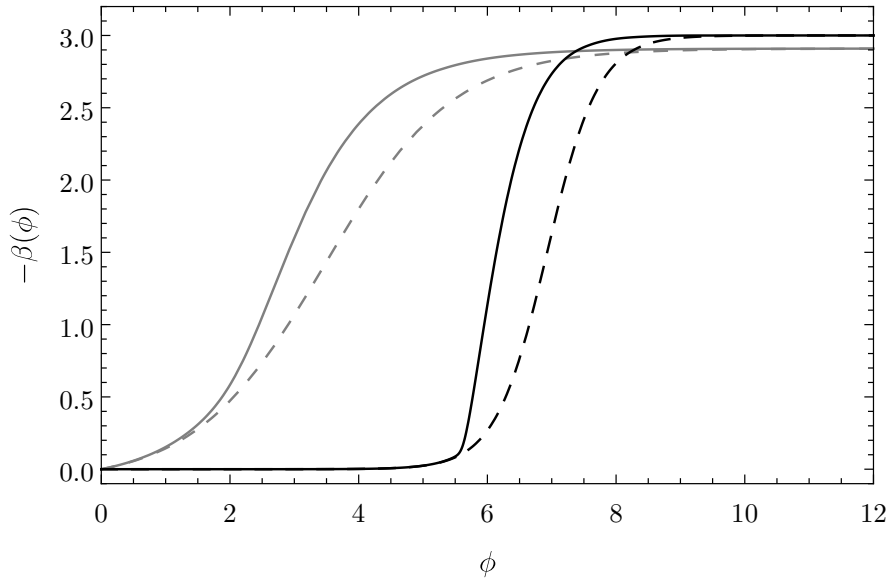

FIGURE 5.6: The β-function as a function of ϕ. The dashed lines show $\frac{3M^3}{2}\frac{V'}{V}$ for comparison. The black lines correspond to values of $\nu = 0.8$ and $\gamma = 4\sqrt{\alpha}$, while the grey lines are for $\nu = 2$ and $\gamma = 2\sqrt{\alpha}$. We have set $\alpha = 3$ and $M = k = 1$.

$2\sqrt{3M^3}$. From Eq. (5.43) it is then clear that for solutions which satisfy this condition the IR value of the β-function is simply given by

$$-\beta_\infty = \lim_{\phi\to\infty} \frac{3}{2}M^3\frac{V'(\phi)}{V(\phi)} = \frac{1}{2}\sqrt{3M^3\alpha}\left(1+\tanh\left(\frac{\gamma}{\nu}\right)\right). \tag{5.45}$$

For $\gamma/\nu \gg 1$ this leads once again to the requirement that $1 \lesssim \alpha \lesssim 4$.

It is now straightforward to numerically solve Eq. (5.43) by shooting from the above value in the IR. The β-function is shown for various parameter choices in Figure 5.6. Notice in particular that for the solid black curve, corresponding to $\nu = 0.8$, the β-function exhibits the behaviour described above. It is walking in the UV, corresponding to a nearly marginal deformation, followed by the turning on of a condensate and a sharp rise to confinement in the IR. This is in contrast to the β-function for our superpotential model in Figure 5.2 where there is no walking region and the condensate turns on at $\phi = 0$.

Note also that when $\gamma = 0$ the potential simplifies, but in this case values of α and ν which lead to a near-marginal operator result in a β-function with no clear transition region and a slow rise to confinement. It will become clear that this case, similarly to the potential in Eq. (5.38), will not lead to a light dilaton.

Now that we have a solution for the β-function, the background metric and scalar profile can easily be obtained by numerically integrating Eqs. (5.5) and (2.21). The solutions are shown in Figure 5.7. Notice that for the case of small ν the scalar

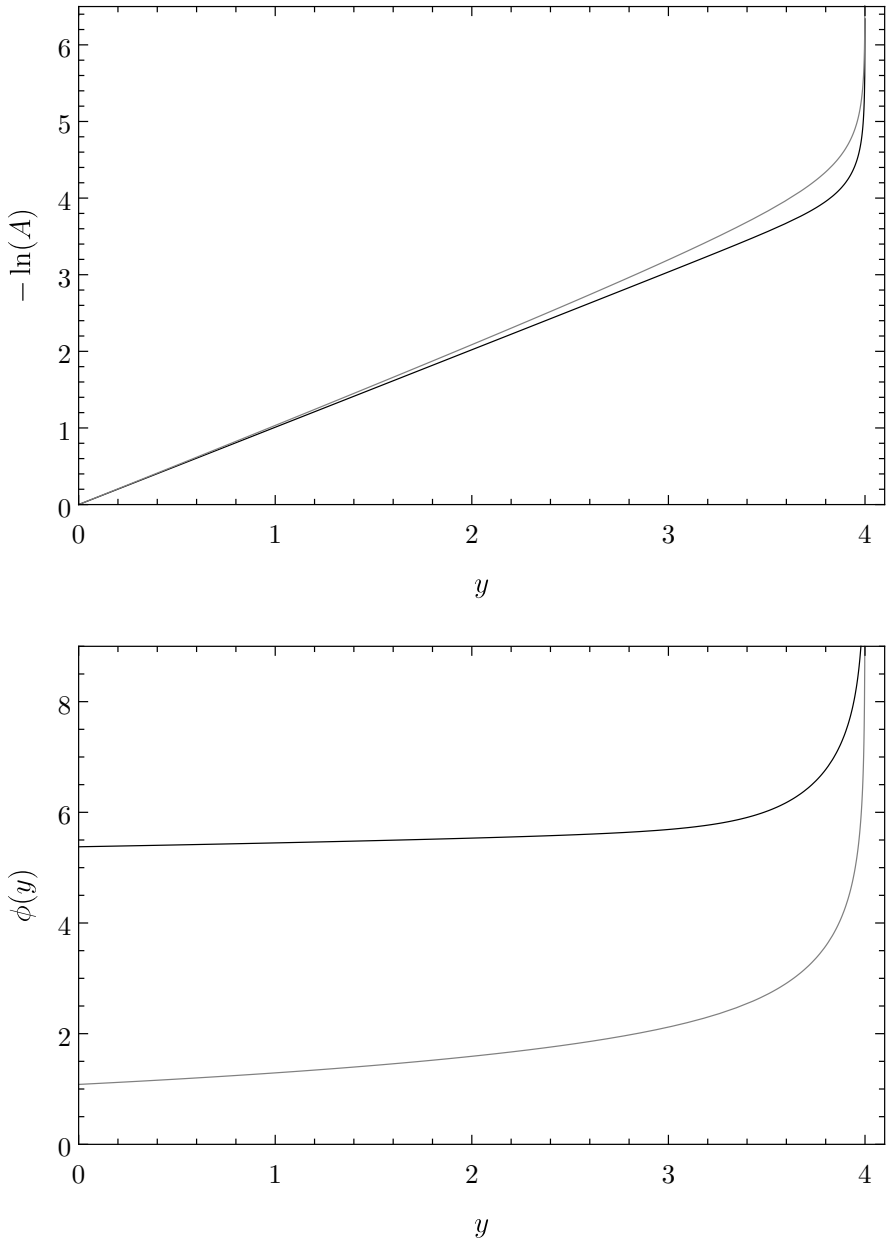

FIGURE 5.7: The top and bottom panels show the solutions for the warp factor and bulk scalar profile respectively. The black lines correspond to values of $\nu = 0.8$ and $\gamma = 4\sqrt{\alpha}$, while the grey lines are for $\nu = 2$ and $\gamma = 2\sqrt{\alpha}$. We have set $\alpha = 3$, $y_c = 4$ and $M = k = 1$.

profile is approximately constant in the UV, consistent with the fact that we have a nearly marginal operator with the dimension explicitly given by

$$[\mathcal{O}] \simeq 4 - \frac{2\alpha}{\nu} e^{-\frac{2\gamma}{\nu}} . \tag{5.46}$$

5.4.1 Dilaton Mass

We are now in a position to investigate the behaviour of the dilaton mass for our potential in Eq. (5.39). It was demonstrated in Ref. [228] that there are two conditions which should be satisfied in order for the dilaton to be light. Firstly, the β-function must remain small into the IR region where the condensate is turning on. This corresponds to the original statement in [282] that a light dilaton occurs for near-marginal operators. The second condition requires that the rise of the β-function to confinement is sufficiently fast. From Figure 5.6 it is clear that using our form for the bulk potential we are able to satisfy both of these conditions and thus expect to find a light dilaton in the spectrum.

Again solving Eq. (5.23) in the $m_{UV} \to \infty$ limit we obtain the masses of the dilaton and two lightest KK modes, which are shown as a function of ν/α^2 in Figure 5.8. Notice that the behaviour of the dilaton mass is almost independent of the choice of values for α and γ. This suggests that the ratio ν/α^2 determines both the value of the β-function where the condensate is turning on as well as the gradient in the transition region. The criterion for obtaining a light dilaton is then simply $\nu/\alpha^2 \lesssim 0.1$. We can see from Eq. (5.44) that the gradient of V'/V in the transition region is determined by the ratio $\alpha/(2\nu)$ and so cases which satisfy our condition for a light dilaton correspond as expected to a fast transition between the walking UV and confining IR.

In Figure 5.9 we have also plotted Δ_- as a function of ν/α^2. This clearly demonstrates that simply having a near-marginal operator is not on its own a sufficient condition to obtain a light dilaton. However it can be seen that, for our potential, cases where the transition to confinement is sufficiently fast will necessarily correspond to cases where we have a near-marginal operator. We also point out that although Δ_- is clearly dependent on γ, by looking again at Eq. (5.44) we see in the limit $\gamma/\nu \gg 1$ that γ simply corresponds to a shift in ϕ and so is not expected to have an effect on the dilaton mass. This highlights the fact that in order to obtain a light dilaton it is the β-function which must remain small at the condensate scale, rather than just $\Delta_- \ll 1$.

Finally, we comment briefly on the naturalness of our model. Since we are only able to solve the equations of motion numerically for the bulk potential in Eq. (5.39), it is difficult to directly construct the dilaton effective potential as in Section 5.3.3 and verify the existence of a non-zero quartic term for the dilaton. However, a closer look at our solution suggests that this construction is indeed natural. Firstly, it is clear from Figure 5.6 that we have a Δ_--type solution in the parameter regions

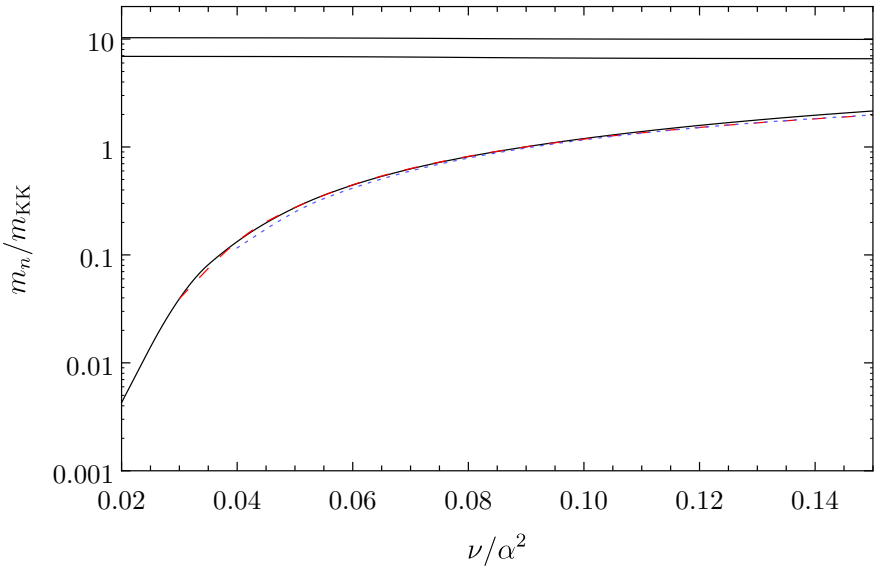

FIGURE 5.8: Masses of the three lightest modes as a function of ν/α^2 for fixed values of α and γ. The solid black and dashed red lines are for $\alpha = 3.8$ with $\gamma = 2\sqrt{\alpha}$ and $4\sqrt{\alpha}$ respectively. The dotted blue lines are for $\alpha = 2$ and $\gamma = 2\sqrt{\alpha}$. We have set $ky_c = 4$.

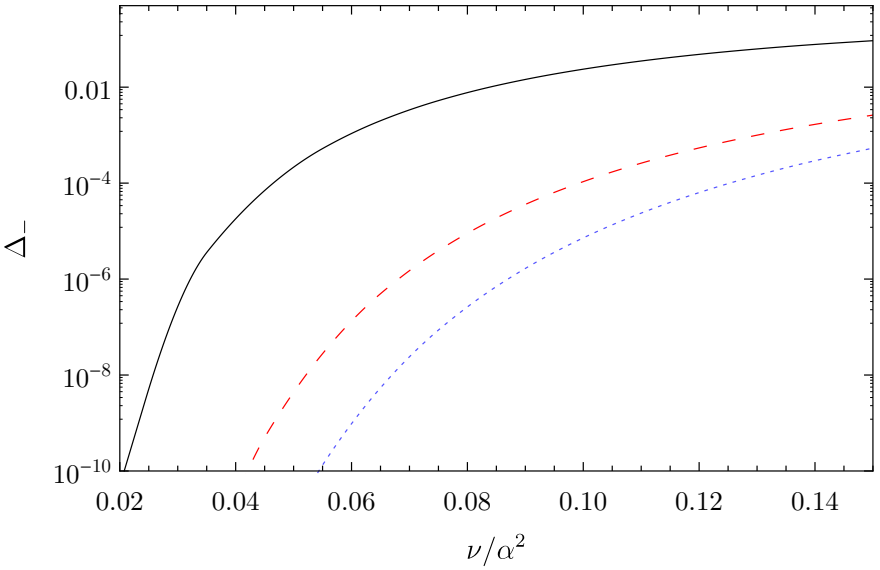

FIGURE 5.9: Δ_- as a function of ν/α^2 for fixed values of α and γ. The different curves are as in Figure 5.8.

of interest. In fact this is guaranteed once we require that the β-function is walking in the UV. Secondly, near-marginal operators do not admit an alternative CFT description and therefore tuned Δ_--type solutions (with $\xi = 0$ and zero quartic potential) describe deformed CFTs. These tuned solutions are not expected to give rise to a light mode except as $\Delta_- \to 2$ or if one directly imposes a tuning between the bulk and boundary masses for a finite UV cut-off; an explicit example of this is seen in Section 5.3. Clearly neither of these situations are relevant for our

scenario. We therefore conclude that our model does indeed correspond to the case described in [282] whereby a large quartic coupling in the UV is driven towards zero at some hierarchically small scale by the running of a near-marginal operator, leading to spontaneous breaking of conformal symmetry and a light dilaton.

5.5 Summary

In this chapter we have presented two solutions of the Einstein equations that exhibit the properties of a dilaton in a soft-wall background. The first solution, obtained using the superpotential method, describes a CFT with conformal symmetry broken by a finite-dimensional operator with dimension $1 < [\mathcal{O}] < 4$. This represents a more realistic scenario compared to hard-wall models that are dual to theories with an infinite-dimensional operator. When the symmetry is spontaneously broken, a light dilaton appears in the spectrum provided there is a hierarchy between the UV and IR scales. In the case of explicit breaking a light dilaton is obtained when the operator dimension is near two. However in both cases the quartic coupling of the effective dilaton potential is tuned and requires an additional symmetry, such as supersymmetry, to be naturally realised. This is not surprising since the solution is based on an analytic superpotential which does not contain a non-perturbative term.

The second solution generalises the bulk scalar potential obtained from the superpotential method to allow for non-analytic terms in the β-function. The bulk scalar potential depends on three parameters that control the form of the β-function from the UV to the IR scale. Interestingly it is possible to obtain a β-function that remains approximately constant from the UV scale until the condensation scale, at which point the β-function rises sharply to an approximately constant order-one value at the IR scale. Our parametrisation relates the slope of this fast rise precisely to the near-marginality of the operator dimension. In this case we explicitly find a naturally light dilaton, which agrees with the results obtained in Ref. [228]. Our solution provides a simple example of how to obtain a naturally light dilaton from nearly-marginal CFT deformations in a soft-wall background. It would be interesting to study the underlying dual theory that is responsible for the particular bulk scalar potential. This could then be useful for applying these ideas to electroweak symmetry and the Higgs sector in the Standard Model.

Unnatural Composite Higgs

6.1 Introduction

In this chapter we move our focus away from the 5D warped framework and instead consider a model defined from the 4D perspective, in which the Higgs arises as a pNGB of a spontaneously broken global symmetry. This general class of models was reviewed in Chapter 2. Here, motivated by recent LHC results, we focus on a particular model known as the *Unnatural Composite Higgs* [148].

The discovery of a light Higgs boson and the conspicuous absence of new states beyond the Standard Model at Run-I of the LHC suggests that the scale of new physics may well be beyond that suggested by naturalness arguments. Composite Higgs models have therefore come under increased scrutiny as lower limits on resonance masses strain the boundaries imposed by naturalness. This tension is further exacerbated by precision electroweak and flavour constraints, both of which prefer a much larger value of the spontaneous global-symmetry breaking scale, f, than can be directly probed at the LHC.

A simple solution that can satisfy all of the relevant constraints is to require that $f \gtrsim 10$ TeV. This leads to an unnatural, or split, composite Higgs model in which the Higgs mass-squared is tuned to the order of 10^{-4} and the particle spectrum splits into light pseudo Nambu-Goldstone bosons and heavy composite-sector resonances. Despite their unnaturalness, these models can provide improved gauge coupling unification if the strong sector possesses an unbroken $SU(5)$ symmetry and $f \lesssim 500$ TeV. An immediate consequence is that the low-energy spectrum always contains a colour-triplet, pseudo Nambu-Goldstone boson; the colour-triplet partner of the composite Higgs doublet. In addition discrete symmetries, which arise from proton stability, furnish these models with a singlet scalar dark matter candidate, S. In the minimal model, the same discrete symmetries imply that the colour-triplet scalar, T, decays to quarks and a pair of singlet scalars

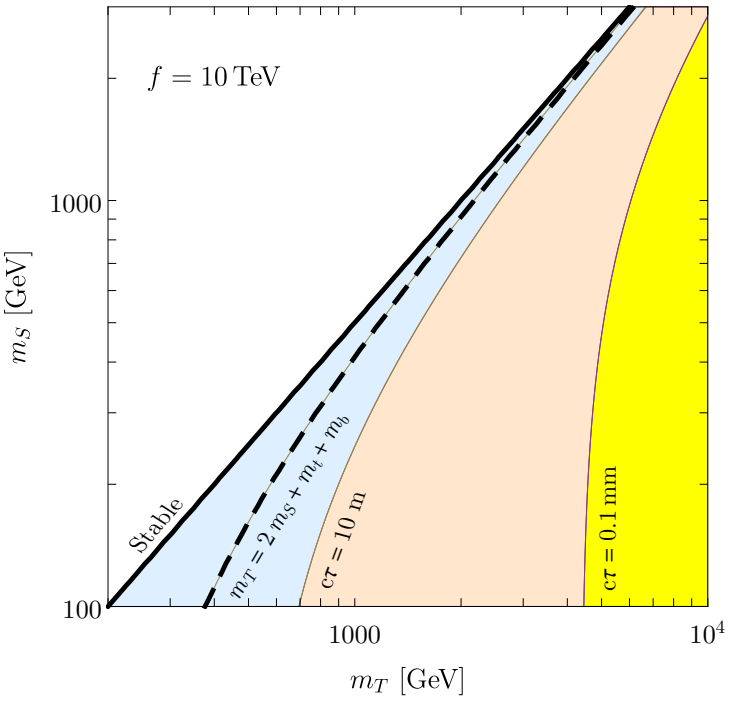

FIGURE 6.1: A schematic diagram of the possible types of decays as a function of the colour-triplet scalar mass m_T and singlet scalar mass m_S. The three shaded regions from left to right correspond to decays that are collider stable, displaced and prompt, respectively. The dashed line represents the kinematic limit for the decay $T \to t^c b^c SS$ and the black solid line represents the limit when $m_T = 2m_S$.

via a dimension-six term in the low-energy, effective Lagrangian. Since this high-dimension term is suppressed by the large symmetry-breaking scale, $f \gtrsim 10$ TeV, the triplet-scalar is often metastable. Long-lived, colour-triplet scalars therefore provide a unique way to test unnaturalness in composite Higgs models.

Motivated by unnatural composite Higgs models we study the collider limits on long-lived, colour-triplet scalars and the prospects for detecting them at future colliders. The colour-triplet will be pair-produced via QCD processes and has the same quantum numbers as a right-handed scalar bottom quark. If long-lived, a colour-triplet will hadronise to form an R-hadron and can be detected in various ways depending on its decay length. The range of decay lengths as a function of the singlet mass m_S and triplet mass m_T is shown in Figure 6.1.

First, if the colour-triplet scalar is collider stable (i.e. decaying outside the detector), charged R-hadrons will leave a track in the inner detector and possibly the muon chamber. R-hadron searches at the LHC can then be used to place mass limits on the colour-triplet. Current limits from LHC Run-I results forbid a collider-stable colour-triplet with a mass below about 845 GeV. At Run-II similar searches will be performed and we show that with 300 fb^{-1} of integrated luminosity

triplet masses up to about 1.4 (1.5) TeV can be discovered (excluded) for lifetimes corresponding to $c\tau \gtrsim 10$ m. The discovery reach is significantly increased at a 100 TeV proton collider where discovery of a colour-triplet scalar with a mass up to 2-6 TeV, depending on its lifetime, will be possible, otherwise exclusion limits ranging from 2-7 TeV can be set. These limits depend only on the mass and width of the colour-triplet, therefore the results we obtain are quite general and can be applied to any other model predicting a similar, long-lived particle.

A second possibility is that the colour-triplet scalar decays within the detector (at radial distances greater than about 4 mm) and produces a displaced vertex (DV) in the inner detector. The colour-triplet in the minimal model decays into a top quark, bottom quark and two singlet scalars, so the collider signature is predominantly jets from the quarks and missing energy from the singlets. This signal has previously been used to search for long-lived superparticles such as gluinos and squarks. While current results from displaced searches do not constrain the colour-triplet mass, these searches will become increasingly important at Run-II and beyond. With 300 fb^{-1} at $\sqrt{s} = 13$ TeV we find that colour-triplet masses up to 1.8 (1.9) TeV can be discovered (excluded) for singlet masses below 450 GeV. In the future a 100 TeV collider would significantly improve the discovery reach, up to colour-triplet masses in the range 3-10 TeV depending on the singlet mass.

The final possibility is that the colour-triplet scalar decays promptly, dominantly producing jets and missing energy. These decays become relevant when the colour-triplet is heavier than about 4 TeV. For such heavy colour-triplets the production cross section at LHC energies is quite small and there will be too few events to detect them, even at the high-luminosity (HL) LHC. Instead, prompt decays could be searched for at a hypothetical 100 TeV proton collider. Using a similar search strategy to that used for gluinos, we show that a future collider is potentially able to exclude colour-triplet masses in the range 4-7 TeV for singlet masses in the range 100-900 GeV.

Indirect limits on the colour-triplet scalar mass can also be obtained by constraining modifications to the Higgs couplings. Using the current LHC results we find that colour-triplet masses are mostly constrained by the Higgs coupling to gluons to be in the range $m_T \gtrsim 100$ GeV. This limit will improve at the HL-LHC and ILC, although the most robust limits are inferior to the bound obtained from requiring that the triplet be heavier than twice the singlet scalar mass. The latter is constrained by direct detection experiments, with the current LUX bound giving $m_S \gtrsim 150$ GeV and hence $m_T \gtrsim 300$ GeV. Details concerning the limits from Higgs couplings can be found in our published work [291].

Previous studies of long-lived particles have primarily focused on supersymmetric models, motivated by the idea of split supersymmetry [292–295] or simplified toy models with R-parity violation [296–301]. This work is the first analysis of models based on the composite Higgs idea. It is a complete framework, incorporating gauge coupling unification, dark matter and an explanation for the fermion mass hierarchies, that represents an alternative to split supersymmetric models. Interestingly, unnatural (or split) composite Higgs models lead to similar decay signals albeit with different properties of the decaying particle and decay products. It will therefore be interesting to experimentally distinguish between these two ideas at future colliders.

The outline for the rest of this chapter is as follows. In Section 6.2 we review the unnatural composite Higgs model and derive the decay width and corresponding decay length for the colour-triplet scalar. The limits from experimental searches are presented in Section 6.3. We first discuss direct limits from R-hadron searches at the LHC and a future 100 TeV collider, followed by limits from displaced-vertex searches and limits from prompt decays. We summarise our results in Section 6.4.

6.2 The Unnatural Composite Higgs Model

6.2.1 Model Review

We begin by briefly reviewing the unnatural composite Higgs model of Ref. [148]. Motivated by the absence of new physics at the LHC and the strong bounds from electroweak and flavour observables, this model considers the case where $f \gg v$ in order to evade current experimental constraints at the expense of fine tuning in the Higgs potential. As we reviewed in Chapter 2, the strongest bounds come from Kaon mixing and lepton flavour violation, which require $f \gtrsim 10\,\text{TeV}$. In principle the scale f could be arbitrarily large, although at some point the hierarchy problem ceases to become a viable motivation. However, imposing the additional and well-motivated requirement of precision gauge coupling unification in fact provides an upper bound on the symmetry breaking scale.

Gauge coupling unification in composite models can be achieved by satisfying two criteria [302]: (i) the right-handed top quark should be a fully composite state; (ii) the entire Standard Model gauge group should be embedded in a simple subgroup of the global symmetry in the strong sector, e.g. $\text{SU}(5) \subset \mathcal{H} \subset \mathcal{G}$. As a result, all composite states will form complete GUT (SU(5)) multiplets. This is potentially problematic, since we would then expect additional light, composite fermions to

fill out the multiplet containing the right-handed top quark. These additional fermions can be decoupled by including additional elementary fermions to provide them with Dirac partners, which also ensures cancellation of gauge anomalies. These elementary states, χ, mix with composite sector operators via terms of the form

$$\mathcal{L} \supset \lambda_\chi \mathcal{O}_t \chi \,. \tag{6.1}$$

The mass eigenstates arising from this mixing are known as top companions[†] and have masses of order $m_\chi \sim \lambda_\chi f$. The fact that the strong sector preserves the GUT symmetry means it contributes universally to the running of the gauge couplings, at least up to one-loop in the elementary fields. The running does however depend significantly on the masses of the top-companions, and requiring precision unification leads to a bound of $f \lesssim 100 - 1000\,\text{TeV}$ (assuming $\lambda_\chi \sim 1$) and a unification scale of order $10^{15}\,\text{GeV}$.

A common concern in any GUT is the existence of baryon and lepton number violating operators, which can lead to proton decay in conflict with experimental bounds. In composite models the commonly taken approach is to simply assume that the composite sector respects both baryon and lepton number [303, 304], the latter also preventing the generation of large neutrino masses. In this framework the SM fermions do not fill out complete GUT multiplets, which have well-defined baryon number. Provided the elementary-composite mixing also preserves baryon and lepton number, the only violation of these symmetries will be due to sphaleron processes [305] and gravitational effects.

This model also accommodates a pNGB dark matter candidate, which can be significantly lighter than the other composite sector resonances. The minimal coset that contains an unbroken SU(5) global symmetry and sufficient NGBs to accommodate the Higgs doublet and a stabilised SM singlet is $\text{SU}(7)/\text{SU}(6)\times\text{U}(1)$. It contains twelve NGBs, including $\tilde{H}$, which transforms as a complex **5** of $\text{SU}(5) \subset \text{SU}(6)$, and the complex singlet, S. The Goldstone matrix can be expressed as a **7** of SU(7)

$$w = e^{i\Pi}\begin{pmatrix}0_{(6)}\\1\end{pmatrix} = \frac{1}{\sqrt{|\tilde{H}|^2+|S|^2}}\begin{pmatrix} i\tilde{H}\sin\left(\frac{\sqrt{|\tilde{H}|^2+|S|^2}}{f}\right)\\ iS\sin\left(\frac{\sqrt{|\tilde{H}|^2+|S|^2}}{f}\right)\\ \sqrt{|\tilde{H}|^2+|S|^2}\cos\left(\frac{\sqrt{|\tilde{H}|^2+|S|^2}}{f}\right)\end{pmatrix}. \tag{6.2}$$

[†]These are distinct from the top partners commonly consider in composite Higgs models, which are purely composite sector resonances.

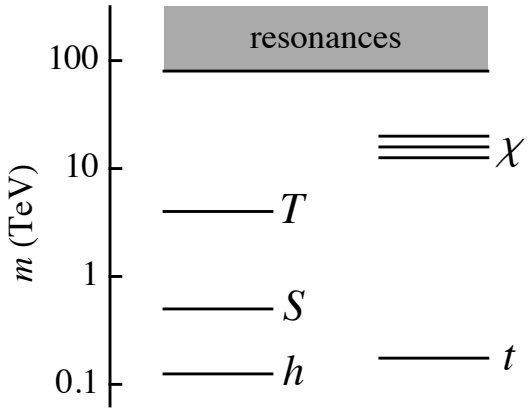

FIGURE 6.2: A schematic diagram of the composite particle spectrum in the "unnatural" composite Higgs model. States on the left are bosons and those on the right are fermions. Reproduced from Ref. [148].

The symmetry breaking is realised by an adjoint or **48** of SU(7) and the low energy effective Lagrangian is consequently expressed in terms of the field $\Sigma = ww^\dagger$. The SU(5) **5**−plet contains the Higgs doublet and an additional colour-triplet partner to the Higgs. This colour-triplet state is a generic prediction of models with an unbroken SU(5) symmetry.

As is usual in composite models, a potential for the NGBs is generated via the elementary-composite mixing and induces EWSB. A tuning of order $v^2/f^2 \lesssim 10^{-4}$ is required in order to obtain the correct Higgs vev, while the physical Higgs mass is proportional to m_W and requires no additional tuning. The large value of $f \gtrsim 10\,\text{TeV}$ means that this model has a split spectrum, with the pNGBs significantly lighter than the generic composite sector resonances and likely the only states accessible at current and future colliders. The colour-triplet scalar therefore determines the phenomenology of this model relevant for collider searches. The generic spectrum is shown schematically in Figure 6.2, which has been reproduced from Ref. [148].

The elementary fermion embeddings under the strong sector symmetry are given in Table 6.1 and include an additional right-handed neutrino, N^c. The elementary-composite couplings explicitly break the SU(7) symmetry, while the additional elementary fermions required to fill out the SU(5) multiplets are assumed to acquire GUT scale masses. This is akin to the doublet-triplet splitting problem of supersymmetric GUTs, although here it instead arises in the fermion sector. The last two lines of Table 6.1 describe the top companions, which transform under the Standard Model gauge group as

$$\chi \equiv \tilde{q}^c \oplus \tilde{e} \oplus \tilde{d}^c \oplus \tilde{l} = (\overline{\mathbf{3}}, \mathbf{2})_{-\frac{1}{6}} \oplus (\mathbf{1}, \mathbf{1})_{-1} \oplus (\overline{\mathbf{3}}, \mathbf{1})_{\frac{1}{3}} \oplus (\mathbf{1}, \mathbf{2})_{-\frac{1}{2}} \tag{6.3}$$

	SU(7)	SU(6)	SU(5)	$U(1)_L$	$U(1)_B$
$q_{(u)}$	$\overline{\mathbf{35}}$	**20**	**10**	0	$\frac{1}{3}$
$q_{(d)}$	**35**	**20**	**10**	0	$\frac{1}{3}$
u^c	**35**	**15**	**10**	0	$-\frac{1}{3}$
d^c	$\overline{\mathbf{35}}$	$\overline{\mathbf{15}}$	$\overline{\mathbf{5}}$	0	$-\frac{1}{3}$
$l_{(\nu)}$	$\overline{\mathbf{21}}$	$\overline{\mathbf{15}}$	$\overline{\mathbf{5}}$	1	0
$l_{(e)}$	$\overline{\mathbf{21}}$	$\overline{\mathbf{6}}$	$\overline{\mathbf{5}}$	1	0
N^c	**21**	**6**	**1**	-1	0
e^c	**21**	**15**	**10**	-1	0
$(\tilde{q}^c, \tilde{e})$	$\overline{\mathbf{35}}$	$\overline{\mathbf{15}}$	$\overline{\mathbf{10}}$	0	$\frac{1}{3}$
$(\tilde{d}^c, \tilde{l})$			$\overline{\mathbf{5}}$	0	0

TABLE 6.1: Elementary fermion embeddings. The subscripts on $q_{(u)}$ and $q_{(d)}$ denote the embeddings responsible for generating the up- and down-type Yukawas respectively, and similarly in the lepton sector for $l_{(\nu)}$ and $l_{(e)}$. Reproduced from Ref. [148].

Dark matter stability in this model arises as a consequence of the fact that the strong sector preserves baryon number. This results in an additional unbroken $\mathbb{Z}_3$ symmetry known as baryon triality

$$\mathbb{Z}_B = 3B - n_C \mod 3\,, \tag{6.4}$$

where n_C is the number of fundamental colour ($SU(3)_C$) indices. All SM fields are neutral under this symmetry, while the colour-triplet has $B(T) = B(H) = 0$ and $n_C = 1$. The singlet on the other hand can be arranged to have $B(S) = \frac{1}{3}$. Provided that $m_T > m_S$ this then ensures that the singlet is stable and a viable dark matter candidate. The baryon triality symmetry also has significant consequences for the colour-triplet phenomenology as we will discuss in the following section. Finally, the dark matter phenomenology is governed by a Higgs portal coupling and we refer the reader to Ref. [148] for the details.

6.2.2 Colour-Triplet Decay

As mentioned previously, the colour-triplet, T, is charged under baryon triality ($\mathbb{Z}_B = +2$) and hence must decay to the singlet, S, which has $\mathbb{Z}_B = +1$. Since the composite sector additionally preserves baryon and lepton number the minimal allowed decay is

$$T \to u^c d^c S S\,, \tag{6.5}$$

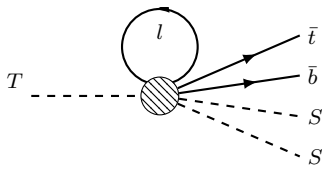

FIGURE 6.3: Leading Feynman diagram for colour-triplet scalar decay.

where u^c, d^c are $SU(2)$ singlet quarks with $\mathbb{Z}_B = 0$. Furthermore, it is clear that t^c, b^c will dominate other final states, as the third generation couples most strongly to the composite sector. We would expect this decay to correspond to a dimension-6 operator in the low-energy effective Lagrangian after integrating out the heavy composite resonances. However, no such operator is generated in the model due to accidental symmetries associated with the necessary fermion representations. Instead, this decay is generated by the dimension-10 operator

$$\mathcal{L} \supset \frac{\Pi_3}{6\Lambda^4 f^2}\, \lambda_{b^c}\lambda_\nu\lambda_\tau^*\, \epsilon_{i_3 j_3 k_3}\, (b^c)^{i_3}(t^c)^{j_3}(T^\dagger)^{k_3}\, S^2\, l^\dagger \not{p} l\,, \tag{6.6}$$

where $\Pi_3 \sim 1 + \mathcal{O}(p^2/\Lambda^2)$ is a form factor, $\Lambda \approx g_\rho f$ is the approximate resonance mass, g_ρ a strong sector coupling, and the λ's are spurions for the partial compositeness couplings of the SM fermions. This operator exploits the fact that the lepton doublet has two couplings to the composite sector. It generates the decay of Eq. (6.5) after closing the leptons into a loop and this turns out to be less suppressed than the six-body final state.

Eq. (6.6) is only the leading contribution to the T decay. Integrating out the composite sector will generate additional operators at higher orders. Further contributions to the decay (6.5) necessarily involve additional loops of elementary particles and are suppressed by $\lambda^2/(16\pi^2 g_\rho^2)$, where λ denotes the appropriate elementary-composite spurion couplings. Other decay modes must involve at least two additional fermions, so are phase-space suppressed by $m_T^2/(8\pi\Lambda^2)$. It is therefore a good approximation to neglect alternative operators.

The relevant Feynman diagram is shown in Figure 6.3. Neglecting the lepton mass the matrix element becomes

$$i\mathcal{M} = -\frac{2i}{3\Lambda^4 f^2}\, \lambda_{b^c}\lambda_\nu\lambda_\tau^*\, \epsilon_{i_3 j_3 k_3}\, \bar{u}(p_t) P_R u(p_b) \int \frac{d^4 p_l}{(2\pi)^4}\, (-1)\mathrm{Tr}\left[\frac{\not{p}_l}{p_l^2}\not{p}_l P_L\right]\Pi_3\,, \tag{6.7}$$

where i_3, j_3, k_3 are colour indices, $u, \bar{u}$ are spinors and $P_{L,R}$ are projection operators. The loop integral is cut off by the presence of composite resonances at the scale Λ. We cannot compute this integral without knowledge of the physics at that

scale, so we define

$$\int \frac{d^4p_l}{(2\pi)^4}\,(-1)\mathrm{Tr}\left[\frac{\not{p}_l}{p_l^2}\not{p}_l P_L\right]\Pi_3 = -2\int \frac{d^4p_l}{(2\pi)^4}\Pi_3 = -2c_3^T\frac{\Lambda^4}{(4\pi)^2}\,, \tag{6.8}$$

where c_3^T is an order-one constant. The matrix element now takes a simple form

$$\frac{1}{3}\sum|\mathcal{M}|^2 = \left(\frac{c_3^T}{6\pi^2 f^2}\right)^2 |\lambda_{b^c}\lambda_\nu\lambda_\tau^*|^2\, p_t\cdot p_b\,. \tag{6.9}$$

The calculation of the decay width is straightforward, though details regarding the four-body phase space integral are given in Appendix D.1. We define a dimensionless function, J, to capture the phase-space suppression from non-zero final state masses

$$J(m_t,m_S) = \frac{72}{m_T^6}\int dQ_1^2\,dQ_2^2\,Q_1^2\sqrt{I\left(\frac{Q_1^2}{m_T^2},\frac{Q_2^2}{m_T^2}\right)}\left(1-\frac{m_t^2}{Q_1^2}\right)^2\sqrt{1-\frac{4m_S^2}{Q_2^2}}\,, \tag{6.10}$$

where the function $I(a,b)$ is defined in Eq. (D.4). The limits on the integrals are given by Eqs. (D.11) and (D.12). By construction, $J(0,0)=1$. The total width is

$$\Gamma = \frac{(c_3^T)^2}{2^{19}3^4\pi^9}\,|\lambda_{b^c}\lambda_\nu\lambda_\tau^*|^2\,\frac{m_T^5}{f^4}\,J(m_t,m_S)\,. \tag{6.11}$$

Finally, making the replacements $\lambda_{b^c}\sim\sqrt{3g_\rho y_b}$ and $\lambda_\nu\sim\lambda_\tau\sim\sqrt{2g_\rho y_\tau}$, where $y_b\,(y_\tau)$ are the bottom (tau) Yukawa couplings, we obtain the approximate expression for the decay length

$$c\tau = 0.6\text{ mm}\left(\frac{1}{c_3^T}\right)^2\left(\frac{8}{g_\rho}\right)^3\left(\frac{3\text{ TeV}}{m_T}\right)^5\left(\frac{f}{10\text{ TeV}}\right)^4\frac{1}{J(m_t,m_S)}\,. \tag{6.12}$$

We see that for typical parameters in the unnatural composite Higgs model the decay length is of order the millimetre scale. The decay length can be substantially larger by either increasing the scale f, reducing the triplet mass, or having kinematic suppression $m_T\approx 2m_S+m_t$ (i.e. $J(m_t,m_S)\approx 0$). This behaviour is depicted in Figure 6.1 as a function of the colour-triplet and singlet scalar masses.

6.2.3 Colour-Triplets in Other Unnatural Composite Higgs Models

Any composite Higgs model that unifies via an $SU(5)$ gauge group will contain (at least) a colour-triplet pseudo Nambu-Goldstone boson like the one discussed here. Although other unification patterns are possible, precision unification in composite Higgs models is only known to occur via an $SU(5)$ gauge group, and only when the

right-handed top quark is fully composite [302]. Unless a qualitatively different solution for precision unification is found light, colour-triplet scalars can therefore be considered a generic feature of unnatural composite Higgs models.

Whether the colour-triplet scalar is long-lived or not depends more on the details of the model. It will necessarily be charged under baryon triality, a symmetry that must hold at least approximately in order to prevent proton decay. This has a stabilising effect on the colour-triplet and means that it will preferentially decay via other exotic states. Furthermore, because the colour-triplet scalar is a pseudo Nambu-Goldstone boson the only available states are other pseudo Nambu-Goldstone bosons. In itself this is not enough to guarantee a long-lived state but, in the minimal model proposed in Ref. [148], including the SM matter content resulted in several additional, accidental symmetries that stabilised the scalar colour-triplet further. Accidental symmetries like these are increasingly likely to occur in more complicated models with larger initial symmetry groups so, while it is by no means certain, long-lived colour-triplet scalars seem likely to be a feature of most unnatural composite Higgs models exhibiting precision gauge coupling unification.

6.3 Experimental Searches

We next discuss experimental searches for colour-triplet scalars. We present limits from various direct searches that look for decays over a range of decay lengths from prompt to collider-stable.

6.3.1 R-hadron Searches

ATLAS and CMS have published comprehensive R-hadron searches, including searches for charged R-hadrons escaping the detector [306, 307] and searches for R-hadrons getting stopped by and then decaying within the detector [308, 309]. The former analyses give rise to the strongest bounds so we shall use them to derive constraints on unnatural composite Higgs models, and also generalise them to estimate the R-hadron discovery and exclusion potentials of future experiments. Since our results depend only on the mass and width of the colour-triplet scalar they can be applied to any model predicting a long-lived particle of a similar nature.

The searches are characterised by low backgrounds, between zero and one event after 20 fb^{-1} of 8 TeV collisions, and signal efficiencies around 10%. In order to derive constraints from these searches, we first simulate the pair production of R-hadrons using the R-hadronisation routines in `PYTHIA 8.1` [310–312] and normalise

the events according to the total production cross sections given in Ref. [313]. We have been able to exploit the fact that the colour-triplet has the same quantum numbers as a right-handed sbottom, allowing us to repurpose various tools originally designed for SUSY. We then discard R-hadrons with kinetic energies below 20 GeV, which according to the ATLAS study in Ref. [308] are likely to be stopped within the detector.

Since this search is virtually insensitive to the final state of the R-hadron decay and because the backgrounds are so low, we weight each event by a survival factor rather than allowing the R-hadrons to decay directly in `PYTHIA`. Prohibitively large numbers of events are otherwise needed to investigate the discovery and exclusion potentials of future experiments. The survival factor, p, for each R-hadron is given by

$$p(r_{\text{decay}} > r_{\text{detector}}) = e^{-\beta_T r_{\text{detector}} \Gamma/\gamma}\,, \tag{6.13}$$

where β_T is the R-hadron's transverse speed and γ its overall Lorentz factor, both derived from the mass, energy, and transverse momentum of the R-hadron. Γ is the colour-triplet width and we assume a value of $r_{\text{detector}} = 10$ m for the detector radius throughout this study. Finally, we apply the signal acceptance-times-efficiency value of 0.084 reported by the ATLAS study in Ref. [306].

For the number of background events we assume that the existing values will simply scale up with luminosity at future experiments. Taking the value from Ref. [306] gives 0.27 events per 19.1 fb^{-1}. Similarly, we assume that the signal acceptance-times-efficiency will remain constant.

The results of this analysis are the discovery and exclusion contours shown in Figures 6.4 & 6.5. These are presented in the plane of the colour-triplet mass, m_T, versus its lifetime, $c\tau$. We find that the final LHC dataset will be able to discover long-lived, colour-triplets with a mass up to around 1.4 TeV, and exclude those with a mass up to around 1.5 TeV. A 100 TeV collider would increase these values considerably, to 6 and 7 TeV respectively.

6.3.2 Displaced-Vertex Searches

Traditional heavy stable charged particle or R-hadron searches provide good sensitivity when the colour-triplet scalar is stable or has a long enough lifetime such that most of the decays occur outside the detector. However for shorter lifetimes

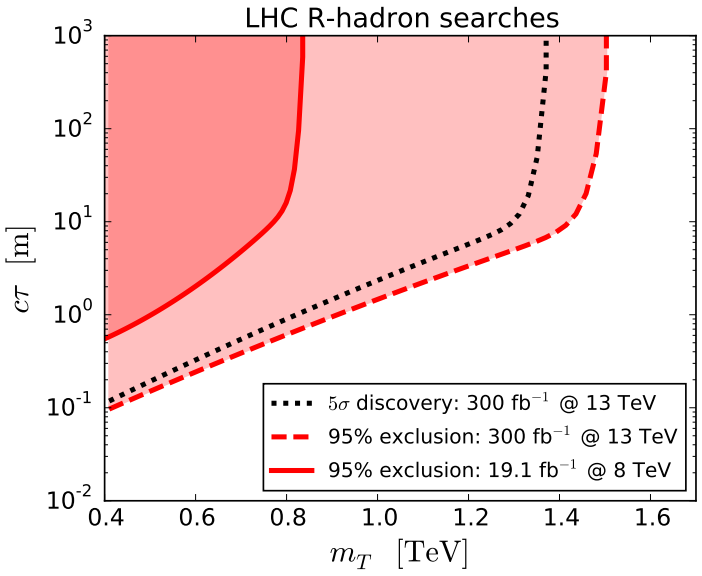

FIGURE 6.4: Current status and future prospects for R-hadron searches at the LHC as functions of colour-triplet scalar mass and lifetime.

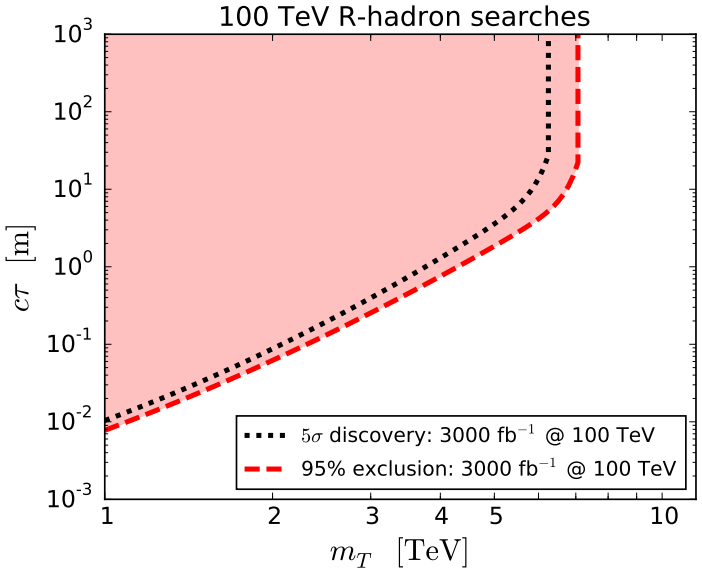

FIGURE 6.5: Current status and future prospects for R-hadron searches at a hypothetical $\sqrt{s} = 100\,\text{TeV}$ collider as functions of colour-triplet scalar mass and lifetime.

these types of searches begin to lose sensitivity[†] as seen in Figures 6.4 & 6.5. Dedicated searches for displaced decays are therefore essential in order to cover the entire parameter space of the model. There are now a variety of ATLAS [315–319] and CMS [320–323] searches specifically targeting displaced signals. However,

[†]ATLAS has now also performed a search for metastable R-hadrons [314] which decay within the detector at radial distances greater than 45 cm. This search is expected to have lower sensitivity than the displaced-vertex search we consider here, except for a narrow range of lifetimes approaching the collider stable case.

	Selection criteria
displaced vertex	≥ 5 tracks satisfying $p_T > 1$ GeV, $\lvert d_0 \rvert > 2$ mm DV position: $r_{DV} < 300$ mm, $\lvert z_{DV} \rvert < 300$ mm and ≥ 4 mm from PV in transverse direction $m_{DV} > 10$ GeV (assuming $m_\pi^\pm$ for individual tracks) material veto
DV+jets	≥ 4 jets ($p_T > 90$ GeV) or ≥ 5 jets ($p_T > 65$ GeV) or ≥ 6 jets ($p_T > 55$ GeV) and $\lvert \eta \rvert < 2.8$
DV+$\not{E}_T$	$\not{E}_T > 180$ GeV

TABLE 6.2: Displaced vertex requirements and final selection criteria for the ATLAS displaced-vertex search in the DV+jets and DV+$\not{E}_T$ channels.

recasting limits from these searches is difficult without access to the complete detector simulations used by the collaborations. Nevertheless, several recent papers [296–299, 301] have demonstrated that, with some reasonable assumptions, good agreement with the full experimental analyses can be achieved. The most relevant search for our model is the ATLAS displaced-vertex search [319] and we shall take a similar approach to that of Ref. [299], which also reinterpreted this search but in the context of supersymmetric models with R-parity violation.

The ATLAS displaced-vertex search targets long-lived particles which decay within the inner detector, up to radial distances ~ 30 cm. The search looks for displaced vertices containing at least five charged particle tracks in addition to the presence of a high-p_T muon or electron, jets, or missing energy ($\not{E}_T$). All channels are essentially background free with less than one event expected. We will focus on the DV+jets and DV+$\not{E}_T$ channels as these are expected to give the highest sensitivity to our colour-triplet decay. The displaced vertex requirements along with the final selection criteria in each of the channels are detailed in Table 6.2.

In replicating the experimental analysis we must also take into account the ATLAS tracking and vertex reconstruction procedures in addition to the above selections. The standard ATLAS tracking algorithms have a low efficiency for reconstructing tracks with large impact parameters (d_0, z_0) arising from displaced vertices. Therefore additional offline retracking is performed with looser requirements on d_0 and z_0. In order to account for this we have included an additional $|d_0|$-dependent efficiency factor multiplying the standard prompt efficiencies in the `DELPHES 3` [324] detector simulation.

In simulating the ATLAS vertex reconstruction algorithm we adopt the same procedure as Ref. [299]. Firstly we consider only tracks with $p_T > 1$ GeV, $|d_0| > 2$ mm and truth-level origins satisfying $4 < r < 300$ mm and $|z| < 300$ mm. Vertices

are then reconstructed by firstly combining all track pairs with origins separated by < 1 mm into a DV. The momentum vectors, $\vec{p}$, of these tracks must also satisfy $\vec{d} \cdot \vec{p}/|\vec{p}| > -20$ mm, where the vertex position, $\vec{d}$, with respect to the primary vertex (PV) is taken as the average position of its constituent track origins. Any vertices separated by < 1 mm are then iteratively combined. Lastly vertices formed at radial distances corresponding to dense regions of the detector according to Ref. [319] are removed.

Finally, we must also make some additional assumptions about how the long-lived R-hadrons and their decay products interact with and are reconstructed by the detector. This is particularly important in the case of the DV+$\not{E}_T$ channel in order to accurately estimate the missing energy. Firstly, we neglect any prompt tracks from R-hadrons that decay within the detector and which are anyway ignored when reconstructing displaced vertices. We also neglect the curvature of these R-hadron trajectories in the magnetic field, which will generally be small due to their large momenta. The decay products (excluding neutrinos) of R-hadrons decaying within the calorimeters are assumed to deposit all of their energy, although clearly this assumption is not expected to be valid for R-hadrons decaying near the outer edge. We neglect any energy deposits from the R-hadrons themselves which are expected to be small. R-hadrons decaying within the muon spectrometers are unlikely to be reconstructed as muons and are therefore assumed to contribute to $\not{E}_T$. Finally, charged R-hadrons which escape the detector are assumed to be reconstructed as muons.

Similarly to the previous analysis, signal events were generated using the R-hadronisation routines in `PYTHIA` although with additional matrix-element re-weighting to correctly capture the kinematics of the 4-body decays of the triplet. The dominant (albeit very small) source of background for this search is due to low-m_{DV} vertices which are crossed by an unrelated high-p_T track. We assume that the current background expectations scale with increased luminosity while the systematic uncertainties remain fixed. We also assume a systematic uncertainty of 20% on the signal efficiency. The 5σ discovery reach and 95% CLs exclusion limits in the (m_T, m_S) plane are then shown in Figures 6.6, 6.7 and 6.8. Limits were computed in the `ROOSTATS` [325] framework using the asymptotic formula for the profile likelihood [326] and Gaussian constraints for the systematic uncertainties.

We find that with the existing 8 TeV dataset this analysis does not have sufficient sensitivity to provide constraints on our colour-triplet scalar. This is due to the fact that for masses where the cross section is sufficiently large, the triplet is in most cases decaying outside the detector and R-hadron searches provide the only

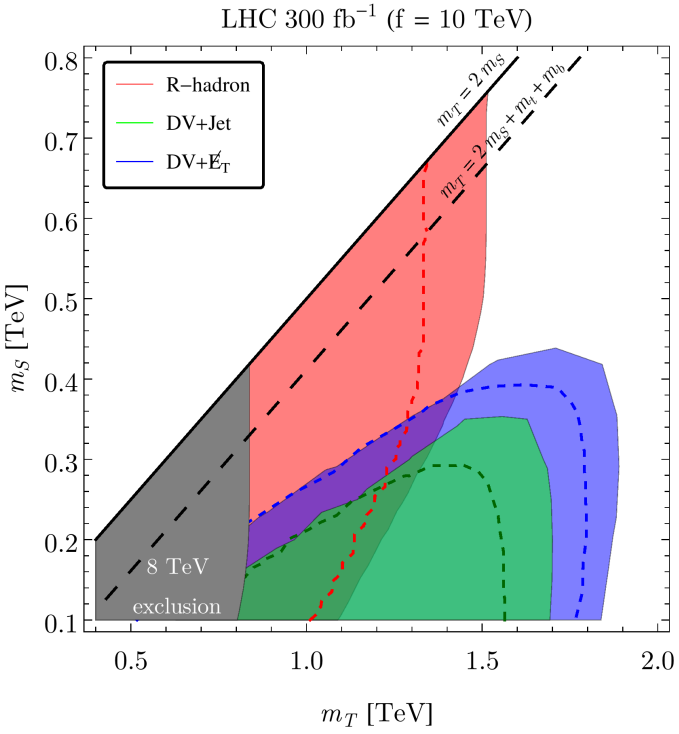

FIGURE 6.6: Projections for the R-hadron and displaced-vertex searches at the LHC with 300 fb^{-1} of integrated luminosity at $\sqrt{s} = 13$ TeV as functions of the scalar mass m_S and triplet mass m_T. The shaded regions can potentially be excluded at 95% CLs and the dashed lines denote the 5σ discovery reach. The grey shaded region is excluded by current R-hadron searches at $\sqrt{s} = 8$ TeV.

constraints. However, displaced searches will become important to probe the full parameter space in Run-II and beyond. In Figure 6.6 we see that with 300 fb^{-1} of integrated luminosity this search can potentially discover our colour-triplet up to masses of 1.8 TeV and exclude it up to 1.9 TeV. Furthermore this search is clearly complementary to the R-hadron searches considered in the previous section and the combination of both searches provides good coverage of the (m_T, m_S) plane. For both searches the upper bound on the colour-triplet mass is cross section limited and the reach is expected to improve with the increased dataset of the HL-LHC. Finally, we can also consider larger values of $f \gtrsim 100$ TeV, which increases the lifetime of the colour-triplet. In this case R-hadron searches will provide the only constraints at the LHC.

In Figures 6.7 & 6.8 we also consider the prospects for this search at a hypothetical $\sqrt{s} = 100$ TeV collider. We have assumed the same experimental cuts as the current ATLAS analysis, which leads to signal efficiencies of up to $\sim 70\%$ for the highest colour-triplet masses considered. Of course in practice the cuts are likely to be more stringent, driven either by trigger considerations or background expectations derived from data. Although note that the signal efficiency can reach 60% for some of the benchmark models considered in the existing analysis, suggesting

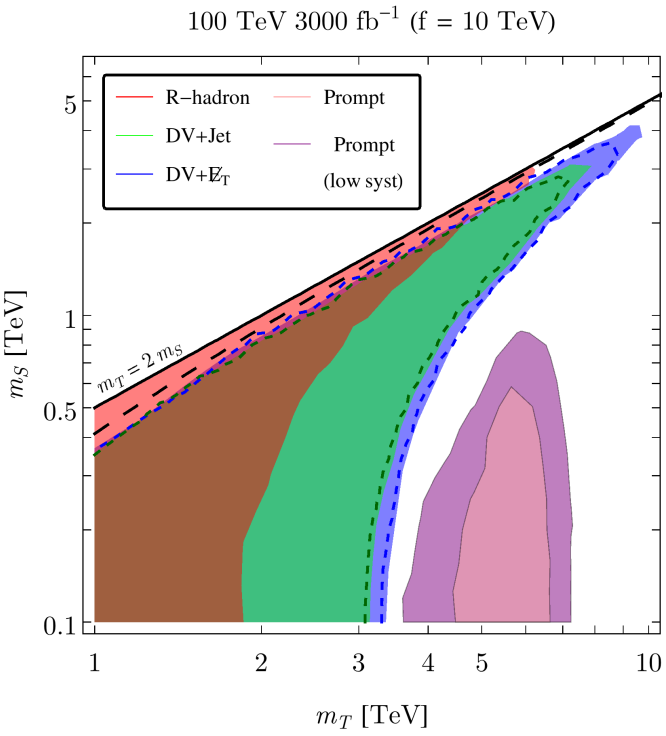

FIGURE 6.7: Projections for a hypothetical $\sqrt{s} = 100$ TeV collider with 3000 fb^{-1} of integrated luminosity as functions of the scalar mass m_S and triplet mass m_T. The shaded regions show the 5σ discovery reach (95% CLs exclusion limit) for the R-hadron/displaced (prompt) searches. The dashed lines include an additional factor of two reduction in the signal efficiency for DV searches to account for the impact of more stringent experimental cuts.

that our estimate is not unreasonable. Nevertheless we also show results with the signal efficiency reduced by a factor of two in order to provide a more conservative estimate of the discovery reach. Regardless, we find that the reach would be significantly greater than at the LHC with potential discovery of the scalar triplet up to masses around 10 TeV.

6.3.3 Prompt Decay Searches

Standard searches for prompt decays of the colour-triplet are not expected to provide useful constraints at the LHC. This is simply due to the fact that for masses below about 4 TeV (assuming[†] $f = 10$ TeV) most of the colour-triplet decays will be displaced, while for higher masses the LHC will not produce enough events even by the end of the planned HL-LHC upgrade. However, future colliders may be able to probe this region of parameter space where the colour-triplet lifetime is small enough to lead to prompt decays, displaced by less than about 2 mm.

[†]For larger values $f \gtrsim 100$ TeV, prompt-decay searches will not be constraining even at a future $\sqrt{s} = 100$ TeV collider and all limits will be from displaced-vertex and R-hadron searches.

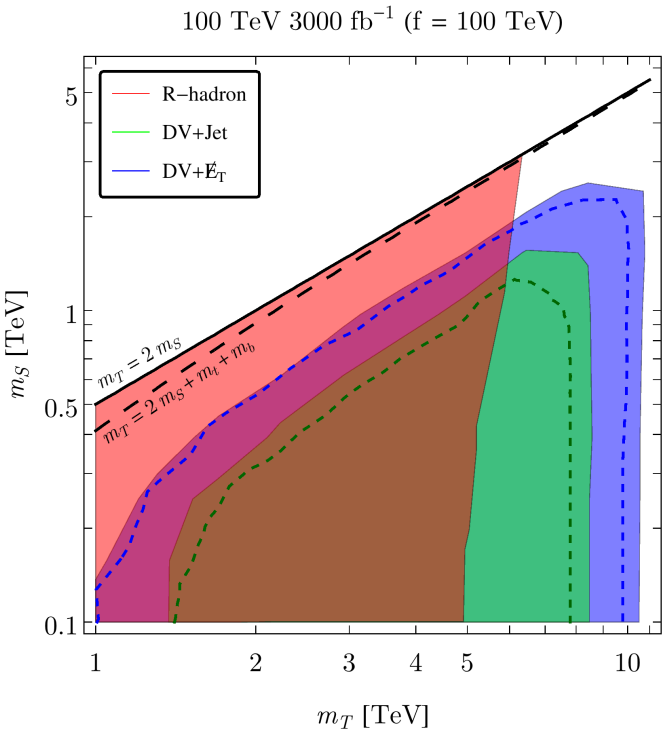

FIGURE 6.8: Projections for a hypothetical $\sqrt{s} = 100$ TeV collider as described in Figure 6.7. Here we have taken a larger value of $f = 100\,\text{TeV}$.

We therefore investigate the potential limits from a hypothetical 100 TeV proton collider. Of course many assumptions have to be made about the future performance of such a machine and we will use the Snowmass detector [327] implemented in `DELPHES` to model the detector performance. We also make use of the Snowmass background Monte-Carlo event samples [328]. Signal events were again generated using `PYTHIA` and we use the same weighted event generation procedure as used for the background events in order to obtain a sample suitable for studies with high integrated-luminosity. In our case the events are separated in bins of p_T to allow for straightforward implementation using `PYTHIA` and 50 000 events are generated in each bin.

The ATLAS experiment has recently performed a search for gluinos [329] which considers a similar final state to that which arises from the pair production of our colour-triplet. We will employ a similar search strategy for our 100 TeV analysis, however extracting the signal for the colour-triplet case is significantly more challenging due to the reduced cross section and, as we shall see, this leads to a relatively limited reach even at $\sqrt{s} = 100$ TeV. We will focus on a search using the purely hadronic final state. Searches in the leptonic channel were also considered but are expected to be less sensitive for higher triplet masses due to the small cross sections combined with a lower branching fraction. To begin we make the following preselection cuts:

- ≥ 4 jets with $p_T > 50$ GeV, $|\eta| < 2.5$,
- ≥ 3 b-tagged,
- leading jet $p_T > 150$ GeV,
- $\delta\phi^{4j}_{min} > 0.5$,
- $\not{E}_T > 400$ GeV,
- $m_{\text{eff}} > 2000$ GeV,
- No isolated leptons ($p_T > 20$ GeV, $|\eta| < 2.5$).

Jets are reconstructed using the anti-k_T algorithm [330, 331] with $R = 0.5$ and we use the Snowmass loose b-tagging working point with a b-tag efficiency of 70-75% and a light quark (c-quark) mis-tag rate of 3% (30%). $\delta\phi^{4j}_{min}$ is defined as the minimum azimuthal separation between $\not{E}_T$ and each of the four leading jets with $p_T > 20$ GeV and $|\eta| < 4.5$. The cut on this variable is designed to reduce the contribution to $\not{E}_T$ from poorly reconstructed jets or neutrinos emitted in the direction of a jet. Combined with the cut on $\not{E}_T$ this is expected to reduce the QCD background to a negligible amount, although the QCD background has not been simulated as part of the background sample. Finally, m_{eff} is defined as the scalar sum of $\not{E}_T$ and all jets with $p_T > 50$ GeV and $|\eta| < 4.5$. We also neglect events where the triplet decay vertex is displaced by more than 2 mm in the radial direction since they would likely fail b-tagging track requirements [332, 333].

After these preselection cuts the background still dominates over the signal in the selected sample by several orders of magnitude. The dominant background for this search is $t\bar{t}+$ jets. While we expect our signal to exhibit a higher b-jet multiplicity and increased $\not{E}_T$ compared to the background, the large $t\bar{t}$ cross section means that the number of background events can still easily exceed the signal expectation even in the tails of the background distributions. This can be clearly seen in Figure 6.9 where we have plotted the signal and background distributions of $\not{E}_T$ and m_{eff} after applying the preselection cuts for three benchmark signal points.

Next we optimise the cuts[†] on the number of b-jets (N_b), $\not{E}_T$ and m_{eff} in order to obtain the optimal background rejection as a function of signal efficiency using the `TMVA` package [334] in `ROOT v5.34`. This was performed separately for each signal point in a scan over the (m_T, m_S) plane. However we find that the cuts yielding the maximum signal significance do not vary significantly over the parameter ranges of

[†]Additional cuts on the number of jets and leading jet p_T were also considered but found not to provide significant improvement in the background rejection.

	Preselection	Final selection ($N_b \geq 4$, $\not{E}_T > 2.5$ TeV, $m_{\text{eff}} > 10$ TeV)
$t\bar{t}^{(*)}$ + jets	7.2×10^5	27
W/Z + jets	9.1×10^4	10
$t\bar{t}$ + W/Z	3.9×10^4	3.8
Other	1.1×10^4	1.7
Total background	8.6×10^5	39
$m_T = 4000$ GeV $m_S = 200$ GeV	1720	13
$m_T = 5975$ GeV $m_S = 835$ GeV	378	19
$m_T = 7020$ GeV $m_S = 160$ GeV	147	22

TABLE 6.3: Background and signal event yields before and after the final selection for three benchmark signal points.

interest. We therefore impose the following final cuts when deriving the exclusion limits: $N_b \geq 4$, $\not{E}_T > 2.5$ TeV, $m_{\text{eff}} > 10$ TeV. The background and signal yields for three benchmark points after imposing the preselection and final cuts are shown in Table 6.3.

We can now compute 95% CLs exclusion curves in the (m_T, m_S) plane. The following systematic uncertainties are assumed in computing the limits: background normalisation (20%), signal efficiency (15%), PDF (5%) and luminosity (2.8%). We also consider the more optimistic assumption of 10% and 5% systematics for the background normalisation and signal efficiency respectively[†]. The final exclusion curves are shown in Figure 6.7. We see that for the lowest singlet masses we are able to potentially exclude triplet masses in the range 4-7 TeV. This upper reach is consistent with previous studies of colour-triplets at $\sqrt{s} = 100$ TeV colliders in the context of supersymmetric simplified models [335]. However note that in our scenario there is no region in the (m_T, m_S) parameter space where we are able to achieve a 5σ discovery potential. One might expect this to be attainable for lower masses, where the cross section is larger, however the colour-triplet then becomes long-lived and we must turn instead to displaced searches for the strongest limits. Once again this search is clearly complementary to the R-hadron and displaced-vertex searches and all three search strategies will be essential in

[†]With reduced systematic uncertainties the analysis does benefit from additional signal regions (e.g. $\not{E}_T > 1.8$ TeV, $m_{\text{eff}} > 6$ TeV) targeting the low mass region. In this case we derive our exclusion limits using the optimal cuts for each (m_T, m_S) point.

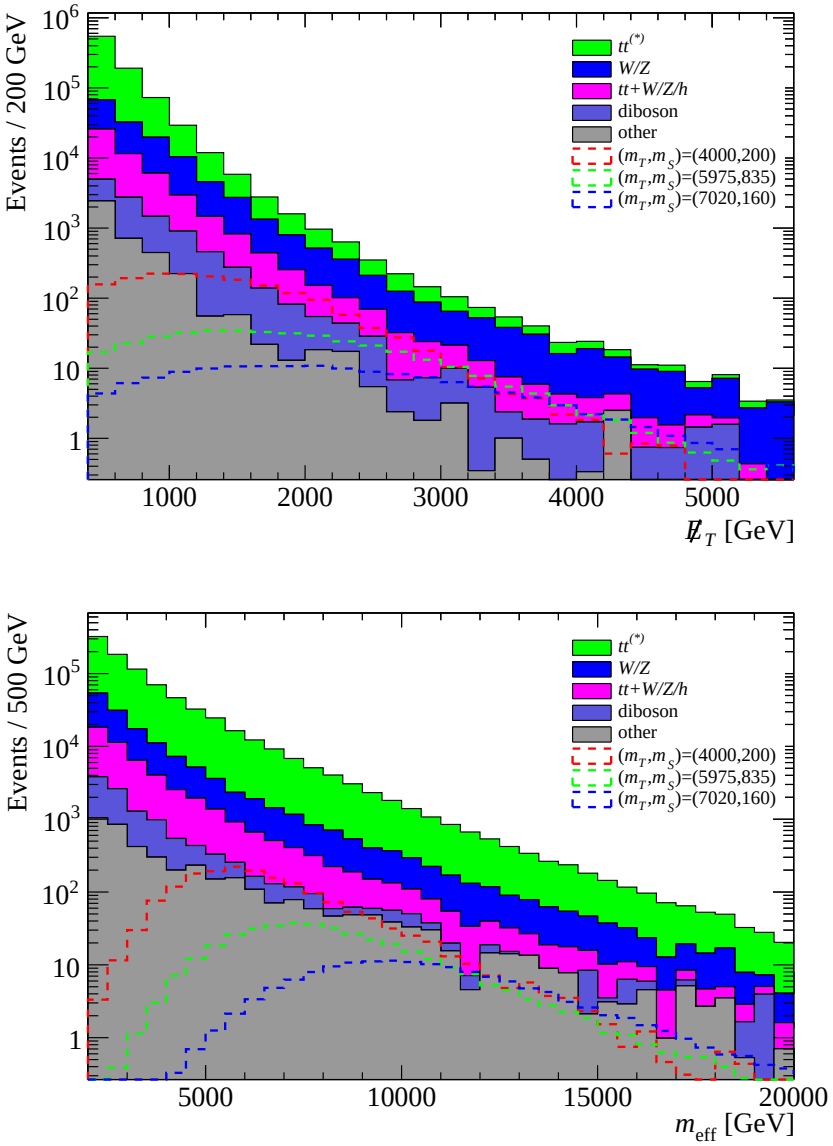

FIGURE 6.9: The $\not{E}_T$ (upper) and m_{eff} (lower) distributions for the backgrounds and three benchmark signal points after imposing the preselection cuts.

order to probe the entire (m_T, m_S) plane. Although we see from Figure 6.7 that there remains a narrow region between the prompt and displaced regimes which may be challenging to explore.

Finally, there are inevitably many assumptions which must be made in estimating the reach of future colliders. The analysis considered here relies heavily on b-tagging and this is likely to provide the largest source of uncertainty. We have chosen to use the loose b-tagging point defined for the Snowmass detector in our analysis as this assumes a reasonably conservative estimate on the mis-tag rate of 3%. Improvements in b-tagging at the LHC have demonstrated that this kind

of performance is reasonable for both highly boosted jets [336] and in high pile-up environments [333, 337]. We have also neglected the effects of pile-up in our analysis, however we do not expect this to have a significant effect beyond the impact on b-tagging. The assumptions made about the systematic uncertainties also have a significant effect on the final exclusion limit.

6.4 Summary

In the unnatural, or split, composite Higgs model electroweak precision and flavour constraints are simply eliminated by requiring that $f \gtrsim 10$ TeV. This causes a splitting of the particle spectrum as the pseudo Nambu-Goldstone bosons are much lighter than the composite-sector resonances. In order to preserve gauge-coupling unification the model has a composite right-handed top quark and the strong sector must remain invariant under an $SU(5)$ global symmetry. This means that the low-energy spectrum generically contains the $SU(5)$ colour-triplet partner of the Higgs doublet, as well as a singlet scalar that plays the role of dark matter. In the minimal model, residual symmetries related to proton and dark matter stability cause the colour-triplet scalar to decay via a dimension-six term in the Lagrangian and, since $f \gtrsim 10$ TeV, it can be metastable. Thus a long-lived colour-triplet scalar provides a distinctive experimental signal to test for unnaturalness.

R-hadron searches can be used to place limits on the colour-triplet mass and the current lower limit on a collider-stable ($c\tau \gtrsim 10$ m) colour-triplet from LHC Run-I results is around 845 GeV. We have shown that with 300 fb^{-1} of integrated luminosity at $\sqrt{s} = 13$ TeV there is potential for a discovery up to a colour-triplet mass of 1.4 TeV. These limits significantly increase at a 100 TeV collider where, depending on the lifetime, triplets with masses ranging from 2 to 6 TeV can be discovered. Note that our limits from R-hadron searches are actually quite general, depending only on the mass and lifetime of the colour-triplet, and can be applied to any other model. If the triplet decays in the inner detector (4 mm $< r_{DV} <$ 30 cm) then displaced-vertex searches can be used to obtain limits. We find that the LHC can discover colour-triplet masses up to 1.8 TeV for singlet masses below 450 GeV. At a 100 TeV collider the discovery reach is extended up to colour-triplet masses in the range 3-10 TeV depending on the singlet mass. There is also the possibility that the colour-triplet decays promptly when the mass $m_T \gtrsim 4$ TeV. In this case the colour-triplet can only be searched for at a future 100 TeV collider, giving a potential exclusion for triplet masses ranging from 4 to 7 TeV, provided the singlet mass is less than around 900 GeV.

Finally, it should be noted that long-lived colour-triplet scalars are a sign of unnaturalness in composite Higgs models in much the same way that long-lived gluinos signal unnaturalness in split supersymmetric models. In both cases the experimental signals are quite similar because the decays produce jets and missing energy. Nevertheless there are differences related to the spin of the decaying particle and the particle(s) carrying the missing energy, as well as the large difference in the production cross section. Given that current LHC results suggest that the Higgs potential may be tuned, it would therefore be worthwhile to study how these two unnatural possibilities could be distinguished at future colliders.

Conclusion

Despite its many successes, it is clear that the Standard Model cannot provide the complete description of our universe. In this thesis we have considered several models of physics beyond the Standard Model which are primarily motivated by the hierarchy problem. These models share the common hypothesis that the Higgs boson arises as a composite bound state of some new strong dynamics. The compositeness scale then provides a cut-off, beyond which the Higgs mass is insensitive to physics at higher scales, avoiding the potential for a naturalness problem. It has been known for some time that many of these models have a dual description in terms of a warped extra dimension via the AdS/CFT correspondence. The limit of strong coupling and large N in the 4D conformal gauge theory corresponds to weak coupling in the 5D gravity description, where the theory is under perturbative control. 5D warped models then provide a simple framework within which to construct concrete, calculable models, which is often far more difficult from the 4D viewpoint where the physics is non-perturbative. We have taken advantage of both viewpoints throughout this thesis.

Models with a composite Higgs boson can be further split into two categories. In the first case the Higgs is a generic bound state of the new strong dynamics; this is the situation most commonly considered in Randall-Sundrum models. The second possibility is that the Higgs arises as a pseudo-Nambu Goldstone Boson of a spontaneously broken global symmetry in the strong sector. This is the viewpoint adopted in 4D composite Higgs models and their corresponding 5D gauge-Higgs unification constructions. These models have the additional benefit of potentially being able to explain why the Higgs should be lighter than the other composite sector resonances. We have investigated models which consider both of these possibilities. In both cases we have focused much of our attention on the pNGBs, since these are expected to be the lightest composite states and could be the first new physics to show up in collider searches. In the case where the Higgs itself is a pNGB, there may be additional pNGBs associated with the spontaneous breaking of the global symmetries. However, even in models where the Higgs is a generic

bound state of the strong dynamics and neglecting the possibility of spontaneously broken global symmetries, an additional pNGB can arise if the dynamics is conformal. While there are additional complexities due to the spacetime nature of the symmetry, there may be a light dilaton associated with spontaneous breaking of scale/conformal invariance.

In Chapter 3 we considered the 5D linear dilaton model which incorporates aspects of both ADD and RS models through a large ∼nm scale extra dimension and a warped metric. This model contains a bulk scalar field, which we showed can be used to stabilise a large extra dimension via the Goldberger-Wise mechanism. We then solved the coupled scalar-gravity equations of motion in order to determine the scalar mass spectrum. We found that the spectrum is characterised by a mass gap of order the curvature scale followed by a series of closely spaced ($\sim 30\,\text{GeV}$) KK modes, similar to the graviton spectrum. However, depending on the boundary mass parameters, the radion and lowest KK mode can be parametrically lighter than the other modes. This model includes a coupling between the bulk scalar and the Standard Model fields confined to the IR brane. This introduces couplings of the radion to the SM Lagrangian in addition to the usual coupling to the trace of the energy-momentum tensor. This additional coupling can significantly modify the radion phenomenology and in particular leads to an enhanced branching ratio to photons. The couplings of the KK modes are suppressed relative to the radion such that we would initially expect to observe a single mode at colliders, despite the closely spaced mass spectrum. Finally, we determined the bounds on the radion from recent LHC searches and found that the diphoton channel already provides strong constraints on this model, leading to a bound on the 5D Planck mass of $M \gtrsim 3.5{-}6.5\,\text{TeV}$ for values of the curvature scale in the range $0.5 \lesssim |\alpha| \lesssim 2.6\,\text{TeV}$.

In models with a light radion/dilaton, mixing is generically expected between the radion and the Higgs. We explored the consequences of this mixing in the context of the Randall-Sundrum model with the Higgs localised in the bulk of the extra dimension in Chapter 4. In addition to kinetic mixing which arises via a coupling of the Higgs to the 5D Ricci scalar, we showed that mass mixing between the radion and the Higgs is generically expected once the back-reaction of the scalar field is included. Allowing the Higgs to propagate in the bulk also significantly modifies the radion phenomenology relative to the more commonly considered brane-localised case. Importantly, we found that the radion coupling to the gauge boson mass terms vanishes due to the conformal symmetry. This allows it to evade the stringent constraints from resonance searches in the WW/ZZ final states. Motivated by the 5D model, we then constructed the most general 4D effective Lagrangian between the radion and the Higgs, which are the lightest states in

the model. We performed a scan over the relevant parameter space, identifying the lighter eigenstate with the observed 125 GeV state and imposing the bounds from Higgs measurements and resonance searches. We found that a light radion could have remained hidden from existing searches and that significant mixing between the radion and the Higgs is allowed for values of the radion coupling scale $\Lambda_r \gtrsim 3\,\text{TeV}$. For masses below 250 GeV, the heavier state must be strongly radion-like with suppressed couplings to the massive gauge bosons; future searches in the $\gamma\gamma$ channel will be most sensitive to this region. For higher masses the $\bar{t}t$ and diboson channels will play an important role in probing these models in the cases of small and large mixing respectively. These complementary search channels will all play an important role in probing this class of models at Run-II of the LHC. We also demonstrated that the radion in a bulk Higgs model could be responsible for the observed diphoton excess at an invariant mass of 750 GeV in early Run-II data. If the radion-Higgs mixing lies near the alignment limit, an extra dimension of size $kL \lesssim 20$ and compositeness scale $\Lambda_r \gtrsim 2\,\text{TeV}$ can explain the observed excess while also satisfying all existing Run-I constraints. Searches in the $t\bar{t}$ channel will provide the best prospects for probing this scenario in the immediate future.

As a spacetime symmetry, conformal invariance differs from the case of spontaneously broken internal symmetries in that it admits a non-derivative quartic coupling for the dilaton. This coupling is incompatible with spontaneous breaking and a massless dilaton unless it is made to vanish either by fine-tuning or supersymmetry. However, a light dilaton can still be obtained via explicit breaking of the conformal symmetry by a marginally relevant operator. In Chapter 5 we considered such a scenario in the context of a 5D soft-wall model, where a single scalar operator/bulk field is responsible for the explicit breaking and also develops a non-zero condensate. We firstly considered a model with an analytic superpotential and demonstrated that this corresponds to the fine-tuned case of zero quartic coupling for the dilaton. The bulk scalar potential was then generalised to allow for non-analytic terms in the $\beta-$function, corresponding to a deformed CFT with non-zero dilaton quartic coupling. We then found that a naturally light dilaton only occurs for the case of nearly-marginal operators, where the $\beta-$function is approximately constant in the UV and rapidly transitions to an order-one constant in the IR. Our solution therefore provides a simple example for obtaining a naturally light dilaton in a soft wall background, without the need for introducing a second source of spontaneous breaking associated with an IR brane.

Models in which the Higgs arises as a pNGB of a spontaneously broken global symmetry have been extensively considered in the literature. However, electroweak precision and flavour constraints, together with the absence of new resonances

at the LHC, generally prefer large values of the spontaneous symmetry breaking scale that are in tension with naturalness bounds. This motivates the Unnatural (or split) composite Higgs model, which assumes a large symmetry breaking scale $f \gtrsim 10\,\text{TeV}$ at the expense of fine-tuning in the Higgs potential. This results in a split spectrum with the pNGBs the only states potentially accessible at the LHC or future colliders. The unbroken SU(5) global symmetry means that these models contain a colour-triplet pNGB partner of the Higgs, which is often metastable. In Chapter 6 we explored the colour-triplet phenomenology both at the LHC and a hypothetical $\sqrt{s} = 100\,\text{TeV}$ collider. The dominant colour-triplet decay mode is to a top and bottom quark and the scalar singlet dark matter candidate. If long-lived, the colour triplet will hadronise to form an R-hadron, which can be detected in various ways depending on its decay length. In the collider stable case, charged R-hadrons can be identified via tracks in the inner detector and possibly muon chambers, with Run-I LHC results leading to a bound on the triplet mass of 845 GeV. At $\sqrt{s} = 13\,\text{TeV}$ with 300fb^{-1} of integrated luminosity the discovery reach is extended to 1.4 TeV and up to 6 TeV at a future 100 TeV collider. Another possibility is that the colour-triplet can decay in the inner detector, leading to a displaced vertex in conjunction with jets or missing transverse energy. With 300fb^{-1}, triplet masses up to 1.8 TeV could be discovered at the LHC for singlet masses below 450 GeV. Finally, the triplet can decay promptly when it is heavier than about 4 TeV. While beyond the reach of the LHC, searches for b-jets plus missing energy at a 100 TeV collider could potentially exclude colour-triplet masses in the range 4–7 TeV for singlet masses in the range 100–900 GeV.

In this thesis we have explored several scenarios from both the 5D warped extra dimensional and 4D strongly-coupled viewpoints in which the Higgs arises as a bound state of some new strong dynamics. Motivated by the hierarchy problem, these models lead to many interesting phenomenological signatures that can be explored in a complementary way both at the LHC and through precision electroweak and flavour measurements. In particular, we have shown that the LHC is already exploring the parameter space of these models and beginning to impose significant constraints. Finally, we know the Standard Model cannot provide the complete picture, and although new physics has so far remained well hidden, there are still many reasons to expect that it could be waiting just around the corner.

Publications

[1] P. Cox and T. Gherghetta, *Radion Dynamics and Phenomenology in the Linear Dilaton Model*, *JHEP* **05** (2012) 149, [arXiv:1203.5870].

[2] P. Cox, A. D. Medina, T. S. Ray, and A. Spray, *Radion/Dilaton-Higgs Mixing Phenomenology in Light of the LHC*, *JHEP* **02** (2014) 032, [arXiv:1311.3663].

[3] P. Cox and T. Gherghetta, *A Soft-Wall Dilaton*, *JHEP* **02** (2015) 006, [arXiv:1411.1732].

[4] J. Barnard, P. Cox, T. Gherghetta, and A. Spray, *Long-Lived, Colour-Triplet Scalars from Unnaturalness*, *JHEP* **03** (2016) 003, [arXiv:1510.06405].

[5] P. Cox, A. D. Medina, T. S. Ray, and A. Spray, *Novel collider and dark matter phenomenology of a top-philic Z'*, *JHEP* **06** (2016) 110, [arXiv:1512.00471].

[6] P. Cox, A. D. Medina, T. S. Ray, and A. Spray, *Diphoton Excess at 750 GeV from a Radion in the Bulk-Higgs Scenario*, arXiv:1512.05618.

References

[1] **ATLAS** Collaboration, G. Aad et al., *Observation of a new particle in the search for the Standard Model Higgs boson with the ATLAS detector at the LHC*, *Phys. Lett.* **B716** (2012) 1–29, [arXiv:1207.7214].

[2] **CMS** Collaboration, S. Chatrchyan et al., *Observation of a new boson at a mass of 125 GeV with the CMS experiment at the LHC*, *Phys. Lett.* **B716** (2012) 30–61, [arXiv:1207.7235].

[3] **Planck** Collaboration, P. A. R. Ade et al., *Planck 2015 results. XIII. Cosmological parameters*, arXiv:1502.01589.

[4] A. D. Sakharov, *Violation of CP Invariance, c Asymmetry, and Baryon Asymmetry of the Universe*, *Pisma Zh. Eksp. Teor. Fiz.* **5** (1967) 32–35. [Usp. Fiz. Nauk161,61(1991)].

[5] A. A. Belavin, A. M. Polyakov, A. S. Schwartz, and Yu. S. Tyupkin, *Pseudoparticle Solutions of the Yang-Mills Equations*, *Phys. Lett.* **B59** (1975) 85–87.

[6] C. A. Baker et al., *An Improved experimental limit on the electric dipole moment of the neutron*, *Phys. Rev. Lett.* **97** (2006) 131801, [hep-ex/0602020].

[7] R. D. Peccei and H. R. Quinn, *CP Conservation in the Presence of Instantons*, *Phys. Rev. Lett.* **38** (1977) 1440–1443.

[8] R. D. Peccei and H. R. Quinn, *Constraints Imposed by CP Conservation in the Presence of Instantons*, *Phys. Rev.* **D16** (1977) 1791–1797.

[9] S. Weinberg, *A New Light Boson?*, *Phys. Rev. Lett.* **40** (1978) 223–226.

[10] J. E. Kim, *Weak Interaction Singlet and Strong CP Invariance*, *Phys. Rev. Lett.* **43** (1979) 103.

[11] M. A. Shifman, A. I. Vainshtein, and V. I. Zakharov, *Can Confinement Ensure Natural CP Invariance of Strong Interactions?*, *Nucl. Phys.* **B166** (1980) 493–506.

[12] A. R. Zhitnitsky, *On Possible Suppression of the Axion Hadron Interactions. (In Russian)*, *Sov. J. Nucl. Phys.* **31** (1980) 260. [Yad. Fiz.31,497(1980)].

[13] M. Dine, W. Fischler, and M. Srednicki, *A Simple Solution to the Strong CP Problem with a Harmless Axion*, *Phys. Lett.* **B104** (1981) 199–202.

[14] H. Georgi and S. L. Glashow, *Unity of All Elementary Particle Forces*, *Phys. Rev. Lett.* **32** (1974) 438–441.

[15] H. Georgi, *The State of the Art—Gauge Theories*, *AIP Conf. Proc.* **23** (1975) 575–582.

[16] H. Fritzsch and P. Minkowski, *Unified Interactions of Leptons and Hadrons*, *Annals Phys.* **93** (1975) 193–266.

[17] E. Gildener, *Gauge Symmetry Hierarchies*, *Phys. Rev.* **D14** (1976) 1667.

[18] L. Susskind, *Dynamics of Spontaneous Symmetry Breaking in the Weinberg-Salam Theory*, *Phys. Rev.* **D20** (1979) 2619–2625.

[19] H. Georgi, H. R. Quinn, and S. Weinberg, *Hierarchy of Interactions in Unified Gauge Theories*, *Phys. Rev. Lett.* **33** (1974) 451–454.

[20] G. 't Hooft, *Naturalness, chiral symmetry, and spontaneous chiral symmetry breaking*, *NATO Sci. Ser. B* **59** (1980) 135.

[21] S. P. Martin, *A Supersymmetry primer*, *Adv. Ser. Direct. High Energy Phys.* **18** (1997) 1–98, [hep-ph/9709356].

[22] S. R. Coleman and J. Mandula, *All Possible Symmetries of the S Matrix*, *Phys. Rev.* **159** (1967) 1251–1256.

[23] R. Barbieri, L. J. Hall, Y. Nomura, and V. S. Rychkov, *Supersymmetry without a Light Higgs Boson*, *Phys. Rev.* **D75** (2007) 035007, [hep-ph/0607332].

[24] S. Weinberg, *Implications of Dynamical Symmetry Breaking*, *Phys. Rev.* **D13** (1976) 974–996.

[25] S. Weinberg, *Implications of Dynamical Symmetry Breaking: An Addendum*, *Phys. Rev.* **D19** (1979) 1277–1280.

[26] P. W. Graham, D. E. Kaplan, and S. Rajendran, *Cosmological Relaxation of the Electroweak Scale*, *Phys. Rev. Lett.* **115** (2015), no. 22 221801, [arXiv:1504.07551].

[27] **UTfit** Collaboration, M. Bona et al., *Model-independent constraints on $\Delta F = 2$ operators and the scale of new physics*, *JHEP* **03** (2008) 049, [arXiv:0707.0636].

[28] N. Arkani-Hamed, S. Dimopoulos, and G. R. Dvali, *The Hierarchy problem and new dimensions at a millimeter*, *Phys. Lett.* **B429** (1998) 263–272, [hep-ph/9803315].

[29] I. Antoniadis, N. Arkani-Hamed, S. Dimopoulos, and G. R. Dvali, *New dimensions at a millimeter to a Fermi and superstrings at a TeV*, *Phys. Lett.* **B436** (1998) 257–263, [hep-ph/9804398].

[30] S. Dimopoulos and R. Emparan, *String balls at the LHC and beyond*, *Phys. Lett.* **B526** (2002) 393–398, [hep-ph/0108060].

[31] S. Dimopoulos and G. L. Landsberg, *Black holes at the LHC*, *Phys. Rev. Lett.* **87** (2001) 161602, [hep-ph/0106295].

[32] S. B. Giddings and S. D. Thomas, *High-energy colliders as black hole factories: The End of short distance physics*, *Phys. Rev.* **D65** (2002) 056010, [hep-ph/0106219].

[33] **ATLAS** Collaboration, G. Aad et al., *Search for strong gravity in multijet final states produced in pp collisions at $\sqrt{s} = 13$ TeV using the ATLAS detector at the LHC*, *JHEP* **03** (2016) 026, [arXiv:1512.02586].

[34] **ATLAS** Collaboration, *Search for TeV-scale gravity signatures in high-mass final states with leptons and jets with the ATLAS detector at $\sqrt{s} = 13$ TeV*, ATLAS-CONF-2016-006.

[35] **CMS** Collaboration, *Search for Black Holes with Early Run 2 Data*, CMS-PAS-EXO-15-007.

[36] L. Randall and R. Sundrum, *A Large mass hierarchy from a small extra dimension*, *Phys. Rev. Lett.* **83** (1999) 3370–3373, [hep-ph/9905221].

[37] J. W. York, Jr., *Role of conformal three geometry in the dynamics of gravitation*, *Phys. Rev. Lett.* **28** (1972) 1082–1085.

[38] G. W. Gibbons and S. W. Hawking, *Action Integrals and Partition Functions in Quantum Gravity*, *Phys. Rev.* **D15** (1977) 2752–2756.

[39] K. Agashe, H. Davoudiasl, G. Perez, and A. Soni, *Warped Gravitons at the LHC and Beyond*, *Phys. Rev.* **D76** (2007) 036006, [hep-ph/0701186].

[40] L. Randall and M. D. Schwartz, *Quantum field theory and unification in AdS5*, *JHEP* **11** (2001) 003, [hep-th/0108114].

[41] N. Arkani-Hamed, S. Dimopoulos, and J. March-Russell, *Stabilization of submillimeter dimensions: The New guise of the hierarchy problem*, *Phys. Rev.* **D63** (2001) 064020, [hep-th/9809124].

[42] W. D. Goldberger and M. B. Wise, *Modulus stabilization with bulk fields*, *Phys. Rev. Lett.* **83** (1999) 4922–4925, [hep-ph/9907447].

[43] W. D. Goldberger and M. B. Wise, *Phenomenology of a stabilized modulus*, *Phys. Lett.* **B475** (2000) 275–279, [hep-ph/9911457].

[44] W. D. Goldberger and I. Z. Rothstein, *Quantum stabilization of compactified AdS(5)*, *Phys. Lett.* **B491** (2000) 339–344, [hep-th/0007065].

[45] B. Bellazzini, C. Csaki, J. Hubisz, J. Serra, and J. Terning, *A Higgslike Dilaton*, *Eur. Phys. J.* **C73** (2013), no. 2 2333, [arXiv:1209.3299].

[46] O. DeWolfe, D. Z. Freedman, S. S. Gubser, and A. Karch, *Modeling the fifth-dimension with scalars and gravity*, *Phys. Rev.* **D62** (2000) 046008, [hep-th/9909134].

[47] K. R. Dienes, E. Dudas, and T. Gherghetta, *Anomaly induced gauge unification and brane / bulk couplings in gravity localized theories*, *Nucl. Phys.* **B567** (2000) 111–132, [hep-ph/9908530].

[48] S. Chang, J. Hisano, H. Nakano, N. Okada, and M. Yamaguchi, *Bulk standard model in the Randall-Sundrum background*, *Phys. Rev.* **D62** (2000) 084025, [hep-ph/9912498].

[49] T. Gherghetta and A. Pomarol, *Bulk fields and supersymmetry in a slice of AdS*, *Nucl. Phys.* **B586** (2000) 141–162, [hep-ph/0003129].

[50] H. Davoudiasl, B. Lillie, and T. G. Rizzo, *Off-the-wall Higgs in the universal Randall-Sundrum model*, *JHEP* **08** (2006) 042, [hep-ph/0508279].

[51] W. D. Goldberger and M. B. Wise, *Bulk fields in the Randall-Sundrum compactification scenario*, *Phys. Rev.* **D60** (1999) 107505, [hep-ph/9907218].

[52] Y. Grossman and M. Neubert, *Neutrino masses and mixings in nonfactorizable geometry*, *Phys. Lett.* **B474** (2000) 361–371, [hep-ph/9912408].

[53] H. Davoudiasl, J. L. Hewett, and T. G. Rizzo, *Bulk gauge fields in the Randall-Sundrum model*, *Phys. Lett.* **B473** (2000) 43–49, [hep-ph/9911262].

[54] A. Pomarol, *Gauge bosons in a five-dimensional theory with localized gravity*, *Phys. Lett.* **B486** (2000) 153–157, [hep-ph/9911294].

[55] T. Gherghetta, *A Holographic View of Beyond the Standard Model Physics*, in *Physics of the large and the small, TASI 09, proceedings of the Theoretical Advanced Study Institute in Elementary Particle Physics, Boulder, Colorado, USA, 1-26 June 2009*, pp. 165–232, 2011, [arXiv:1008.2570].

[56] P. Breitenlohner and D. Z. Freedman, *Positive Energy in anti-De Sitter Backgrounds and Gauged Extended Supergravity*, *Phys. Lett.* **B115** (1982) 197–201.

[57] S. J. Huber and Q. Shafi, *Fermion masses, mixings and proton decay in a Randall-Sundrum model*, *Phys. Lett.* **B498** (2001) 256–262, [hep-ph/0010195].

[58] A. Delgado, A. Pomarol, and M. Quiros, *Electroweak and flavor physics in extensions of the standard model with large extra dimensions*, *JHEP* **01** (2000) 030, [hep-ph/9911252].

[59] T. Gherghetta and M. Peloso, *Stability analysis of 5D gravitational solutions with N bulk scalar fields*, *Phys. Rev.* **D84** (2011) 104004, [arXiv:1109.5776].

[60] E. Kiritsis and F. Nitti, *On massless 4D gravitons from asymptotically AdS(5) space-times*, *Nucl. Phys.* **B772** (2007) 67–102, [hep-th/0611344].

[61] L. Randall and R. Sundrum, *An Alternative to compactification*, *Phys. Rev. Lett.* **83** (1999) 4690–4693, [hep-th/9906064].

[62] L. Kofman, J. Martin, and M. Peloso, *Exact identification of the radion and its coupling to the observable sector*, *Phys. Rev.* **D70** (2004) 085015, [hep-ph/0401189].

[63] M. E. Peskin and T. Takeuchi, *Estimation of oblique electroweak corrections*, *Phys. Rev.* **D46** (1992) 381–409.

[64] R. Barbieri, A. Pomarol, R. Rattazzi, and A. Strumia, *Electroweak symmetry breaking after LEP-1 and LEP-2*, *Nucl. Phys.* **B703** (2004) 127–146, [hep-ph/0405040].

[65] **Particle Data Group** Collaboration, K. A. Olive et al., *Review of Particle Physics*, *Chin. Phys.* **C38** (2014) 090001.

[66] M. Quiros, *Higgs Bosons in Extra Dimensions*, *Mod. Phys. Lett.* **A30** (2015), no. 15 1540012, [arXiv:1311.2824].

[67] K. Agashe, A. Delgado, M. J. May, and R. Sundrum, *RS1, custodial isospin and precision tests*, *JHEP* **08** (2003) 050, [hep-ph/0308036].

[68] K. Agashe, R. Contino, L. Da Rold, and A. Pomarol, *A Custodial symmetry for $Zb\bar{b}$*, *Phys. Lett.* **B641** (2006) 62–66, [hep-ph/0605341].

[69] B. Batell, T. Gherghetta, and D. Sword, *The Soft-Wall Standard Model*, *Phys. Rev.* **D78** (2008) 116011, [arXiv:0808.3977].

[70] J. A. Cabrer, G. von Gersdorff, and M. Quiros, *Warped Electroweak Breaking Without Custodial Symmetry*, *Phys. Lett.* **B697** (2011) 208–214, [arXiv:1011.2205].

[71] J. A. Cabrer, G. von Gersdorff, and M. Quiros, *Suppressing Electroweak Precision Observables in 5D Warped Models*, *JHEP* **05** (2011) 083, [arXiv:1103.1388].

[72] H. Davoudiasl, J. L. Hewett, and T. G. Rizzo, *Brane localized kinetic terms in the Randall-Sundrum model*, *Phys. Rev.* **D68** (2003) 045002, [hep-ph/0212279].

[73] M. Carena, E. Ponton, T. M. P. Tait, and C. E. M. Wagner, *Opaque branes in warped backgrounds*, *Phys. Rev.* **D67** (2003) 096006, [hep-ph/0212307].

[74] H. Georgi, A. K. Grant, and G. Hailu, *Brane couplings from bulk loops*, *Phys. Lett.* **B506** (2001) 207–214, [hep-ph/0012379].

[75] G. von Gersdorff, *Flavor Physics in Warped Space*, *Mod. Phys. Lett.* **A30** (2015), no. 15 1540013, [arXiv:1311.2078].

[76] M. Bauer, S. Casagrande, U. Haisch, and M. Neubert, *Flavor Physics in the Randall-Sundrum Model: II. Tree-Level Weak-Interaction Processes*, *JHEP* **09** (2010) 017, [arXiv:0912.1625].

[77] J. A. Cabrer, G. von Gersdorff, and M. Quiros, *Flavor Phenomenology in General 5D Warped Spaces*, *JHEP* **01** (2012) 033, [arXiv:1110.3324].

[78] G. Cacciapaglia, C. Csaki, J. Galloway, G. Marandella, J. Terning, and A. Weiler, *A GIM Mechanism from Extra Dimensions*, *JHEP* **04** (2008) 006, [arXiv:0709.1714].

[79] A. L. Fitzpatrick, G. Perez, and L. Randall, *Flavor anarchy in a Randall-Sundrum model with 5D minimal flavor violation and a low Kaluza-Klein scale*, *Phys. Rev. Lett.* **100** (2008) 171604, [arXiv:0710.1869].

[80] J. Santiago, *Minimal Flavor Protection: A New Flavor Paradigm in Warped Models*, *JHEP* **12** (2008) 046, [arXiv:0806.1230].

[81] C. Csaki, A. Falkowski, and A. Weiler, *A Simple Flavor Protection for RS*, *Phys. Rev.* **D80** (2009) 016001, [arXiv:0806.3757].

[82] P. R. Archer, S. J. Huber, and S. Jager, *Flavour Physics in the Soft Wall Model*, *JHEP* **12** (2011) 101, [arXiv:1108.1433].

[83] M. Bauer, R. Malm, and M. Neubert, *A Solution to the Flavor Problem of Warped Extra-Dimension Models*, *Phys. Rev. Lett.* **108** (2012) 081603, [arXiv:1110.0471].

[84] O. Gedalia, Y. Grossman, Y. Nir, and G. Perez, *Lessons from Recent Measurements of D0 - anti-D0 Mixing*, *Phys. Rev.* **D80** (2009) 055024, [arXiv:0906.1879].

[85] K. Agashe, G. Perez, and A. Soni, *Flavor structure of warped extra dimension models*, *Phys. Rev.* **D71** (2005) 016002, [hep-ph/0408134].

[86] C. Cheung, A. L. Fitzpatrick, and L. Randall, *Sequestering CP Violation and GIM-Violation with Warped Extra Dimensions*, *JHEP* **01** (2008) 069, [arXiv:0711.4421].

[87] K. Agashe, A. E. Blechman, and F. Petriello, *Probing the Randall-Sundrum geometric origin of flavor with lepton flavor violation*, *Phys. Rev.* **D74** (2006) 053011, [hep-ph/0606021].

[88] C. Csaki, Y. Grossman, P. Tanedo, and Y. Tsai, *Warped penguin diagrams*, *Phys. Rev.* **D83** (2011) 073002, [arXiv:1004.2037].

[89] M.-C. Chen and H.-B. Yu, *Minimal Flavor Violation in the Lepton Sector of the Randall-Sundrum Model*, *Phys. Lett.* **B672** (2009) 253–256, [arXiv:0804.2503].

[90] G. Perez and L. Randall, *Natural Neutrino Masses and Mixings from Warped Geometry*, *JHEP* **01** (2009) 077, [arXiv:0805.4652].

[91] C. Csaki, C. Delaunay, C. Grojean, and Y. Grossman, *A Model of Lepton Masses from a Warped Extra Dimension*, *JHEP* **10** (2008) 055, [arXiv:0806.0356].

[92] K. Agashe, *Relaxing Constraints from Lepton Flavor Violation in 5D Flavorful Theories*, *Phys. Rev.* **D80** (2009) 115020, [arXiv:0902.2400].

[93] M. Atkins and S. J. Huber, *Suppressing Lepton Flavour Violation in a Soft-Wall Extra Dimension*, *Phys. Rev.* **D82** (2010) 056007, [arXiv:1002.5044].

[94] **ATLAS** Collaboration, G. Aad et al., *A search for $t\bar{t}$ resonances using lepton-plus-jets events in proton-proton collisions at $\sqrt{s} = 8$ TeV with the ATLAS detector*, *JHEP* **08** (2015) 148, [arXiv:1505.07018].

[95] **CMS** Collaboration, S. Chatrchyan et al., *Searches for new physics using the $t\bar{t}$ invariant mass distribution in pp collisions at $\sqrt{s}$=8 TeV*, *Phys. Rev. Lett.* **111** (2013), no. 21 211804, [arXiv:1309.2030]. [Erratum: Phys. Rev. Lett. 112 (2014), no. 11 119903].

[96] **ATLAS** Collaboration, G. Aad et al., *Search for high-mass dilepton resonances in pp collisions at $\sqrt{s} = 8$ TeV with the ATLAS detector*, *Phys. Rev.* **D90** (2014), no. 5 052005, [arXiv:1405.4123].

[97] **ATLAS** Collaboration, *Search for resonances in diphoton events with the ATLAS detector at $\sqrt{s}$ = 13 TeV*, .

[98] **CMS** Collaboration, V. Khachatryan et al., *Search for physics beyond the standard model in dilepton mass spectra in proton-proton collisions at $\sqrt{s} = 8$ TeV*, *JHEP* **04** (2015) 025, [arXiv:1412.6302].

[99] **CMS** Collaboration, *Search for new physics in high mass diphoton events in proton-proton collisions at 13 TeV*, CMS-PAS-EXO-15-004.

[100] J. M. Maldacena, *The Large N limit of superconformal field theories and supergravity*, *Int. J. Theor. Phys.* **38** (1999) 1113–1133, [hep-th/9711200]. [Adv. Theor. Math. Phys.2,231(1998)].

[101] O. Aharony, S. S. Gubser, J. M. Maldacena, H. Ooguri, and Y. Oz, *Large N field theories, string theory and gravity*, *Phys. Rept.* **323** (2000) 183–386, [hep-th/9905111].

[102] S. S. Gubser, I. R. Klebanov, and A. M. Polyakov, *Gauge theory correlators from noncritical string theory*, *Phys. Lett.* **B428** (1998) 105–114, [hep-th/9802109].

[103] E. Witten, *Anti-de Sitter space and holography*, *Adv. Theor. Math. Phys.* **2** (1998) 253–291, [hep-th/9802150].

[104] I. R. Klebanov and E. Witten, *AdS / CFT correspondence and symmetry breaking*, *Nucl. Phys.* **B556** (1999) 89–114, [hep-th/9905104].

[105] N. Arkani-Hamed, M. Porrati, and L. Randall, *Holography and phenomenology*, *JHEP* **08** (2001) 017, [hep-th/0012148].

[106] R. Rattazzi and A. Zaffaroni, *Comments on the holographic picture of the Randall-Sundrum model*, *JHEP* **04** (2001) 021, [hep-th/0012248].

[107] M. Perez-Victoria, *Randall-Sundrum models and the regularized AdS / CFT correspondence*, *JHEP* **05** (2001) 064, [hep-th/0105048].

[108] G. 't Hooft, *A Planar Diagram Theory for Strong Interactions*, *Nucl. Phys.* **B72** (1974) 461.

[109] G. 't Hooft, *A Two-Dimensional Model for Mesons*, *Nucl. Phys.* **B75** (1974) 461.

[110] E. Witten, *Baryons in the 1/n Expansion*, *Nucl. Phys.* **B160** (1979) 57–115.

[111] D. B. Kaplan, *Flavor at SSC energies: A New mechanism for dynamically generated fermion masses*, *Nucl. Phys.* **B365** (1991) 259–278.

[112] R. Contino and A. Pomarol, *Holography for fermions*, *JHEP* **11** (2004) 058, [hep-th/0406257].

[113] B. Batell and T. Gherghetta, *Holographic mixing quantified*, *Phys. Rev.* **D76** (2007) 045017, [arXiv:0706.0890].

[114] B. Batell and T. Gherghetta, *Warped phenomenology in the holographic basis*, *Phys. Rev.* **D77** (2008) 045002, [arXiv:0710.1838].

[115] D. B. Kaplan and H. Georgi, *SU(2) x U(1) Breaking by Vacuum Misalignment*, *Phys. Lett.* **B136** (1984) 183–186.

[116] D. B. Kaplan, H. Georgi, and S. Dimopoulos, *Composite Higgs Scalars*, *Phys. Lett.* **B136** (1984) 187–190.

[117] T. Banks, *Constraints on SU(2) x U(1) Breaking by Vacuum Misalignment*, *Nucl. Phys.* **B243** (1984) 125–130.

[118] H. Georgi, D. B. Kaplan, and P. Galison, *Calculation of the Composite Higgs Mass*, *Phys. Lett.* **B143** (1984) 152–154.

[119] H. Georgi and D. B. Kaplan, *Composite Higgs and Custodial SU(2)*, *Phys. Lett.* **B145** (1984) 216–220.

[120] M. J. Dugan, H. Georgi, and D. B. Kaplan, *Anatomy of a Composite Higgs Model*, *Nucl. Phys.* **B254** (1985) 299–326.

[121] R. Contino, *The Higgs as a Composite Nambu-Goldstone Boson*, in *Physics of the large and the small, TASI 09, proceedings of the Theoretical Advanced Study Institute in Elementary Particle Physics, Boulder, Colorado, USA, 1-26 June 2009*, pp. 235–306, 2011, [arXiv:1005.4269].

[122] G. Panico and A. Wulzer, *The Composite Nambu-Goldstone Higgs*, *Lect. Notes Phys.* **913** (2016) pp.1–316, [arXiv:1506.01961].

[123] S. Dimopoulos and J. Preskill, *Massless Composites With Massive Constituents*, *Nucl. Phys.* **B199** (1982) 206–222.

[124] S. R. Coleman, J. Wess, and B. Zumino, *Structure of phenomenological Lagrangians. 1.*, *Phys. Rev.* **177** (1969) 2239–2247.

[125] C. G. Callan, Jr., S. R. Coleman, J. Wess, and B. Zumino, *Structure of phenomenological Lagrangians. 2.*, *Phys. Rev.* **177** (1969) 2247–2250.

[126] C. Csáki and P. Tanedo, *Beyond the Standard Model*, in *Proceedings, 2013 European School of High-Energy Physics (ESHEP 2013): Paradfurdo, Hungary, June 5-18, 2013*, pp. 169–268, 2015, [arXiv:1602.04228].

[127] J. Wess and B. Zumino, *Consequences of anomalous Ward identities*, *Phys. Lett.* **B37** (1971) 95–97.

[128] E. Witten, *Global Aspects of Current Algebra*, *Nucl. Phys.* **B223** (1983) 422–432.

[129] C.-S. Chu, P.-M. Ho, and B. Zumino, *Non-Abelian Anomalies and Effective Actions for a Homogeneous Space G/H*, *Nucl. Phys.* **B475** (1996) 484–504, [hep-th/9602093].

[130] N. Arkani-Hamed, A. G. Cohen, E. Katz, A. E. Nelson, T. Gregoire, and J. G. Wacker, *The Minimal moose for a little Higgs*, *JHEP* **08** (2002) 021, [hep-ph/0206020].

[131] N. Arkani-Hamed, A. G. Cohen, E. Katz, and A. E. Nelson, *The Littlest Higgs*, *JHEP* **07** (2002) 034, [hep-ph/0206021].

[132] I. Low, W. Skiba, and D. Tucker-Smith, *Little Higgses from an antisymmetric condensate*, *Phys. Rev.* **D66** (2002) 072001, [hep-ph/0207243].

[133] S. Chang and J. G. Wacker, *Little Higgs and custodial SU(2)*, *Phys. Rev.* **D69** (2004) 035002, [hep-ph/0303001].

[134] S. Chang, *A 'Littlest Higgs' model with custodial SU(2) symmetry*, *JHEP* **12** (2003) 057, [hep-ph/0306034].

[135] R. Contino, Y. Nomura, and A. Pomarol, *Higgs as a holographic pseudoGoldstone boson*, *Nucl. Phys.* **B671** (2003) 148–174, [hep-ph/0306259].

[136] M. Schmaltz, *The Simplest little Higgs*, *JHEP* **08** (2004) 056, [hep-ph/0407143].

[137] K. Agashe, R. Contino, and A. Pomarol, *The Minimal composite Higgs model*, *Nucl. Phys.* **B719** (2005) 165–187, [hep-ph/0412089].

[138] Z. Chacko, H.-S. Goh, and R. Harnik, *The Twin Higgs: Natural electroweak breaking from mirror symmetry*, *Phys. Rev. Lett.* **96** (2006) 231802, [hep-ph/0506256].

[139] E. Katz, A. E. Nelson, and D. G. E. Walker, *The Intermediate Higgs*, *JHEP* **08** (2005) 074, [hep-ph/0504252].

[140] Z. Chacko, Y. Nomura, M. Papucci, and G. Perez, *Natural little hierarchy from a partially goldstone twin Higgs*, *JHEP* **01** (2006) 126, [hep-ph/0510273].

[141] B. Gripaios, A. Pomarol, F. Riva, and J. Serra, *Beyond the Minimal Composite Higgs Model*, *JHEP* **04** (2009) 070, [arXiv:0902.1483].

[142] M. Schmaltz, D. Stolarski, and J. Thaler, *The Bestest Little Higgs*, *JHEP* **09** (2010) 018, [arXiv:1006.1356].

[143] J. Galloway, J. A. Evans, M. A. Luty, and R. A. Tacchi, *Minimal Conformal Technicolor and Precision Electroweak Tests*, *JHEP* **10** (2010) 086, [arXiv:1001.1361].

[144] J. Mrazek, A. Pomarol, R. Rattazzi, M. Redi, J. Serra, and A. Wulzer, *The Other Natural Two Higgs Doublet Model*, *Nucl. Phys.* **B853** (2011) 1–48, [arXiv:1105.5403].

[145] E. Bertuzzo, T. S. Ray, H. de Sandes, and C. A. Savoy, *On Composite Two Higgs Doublet Models*, *JHEP* **05** (2013) 153, [arXiv:1206.2623].

[146] M. Chala, *$h \to \gamma\gamma$ excess and Dark Matter from Composite Higgs Models*, *JHEP* **01** (2013) 122, [arXiv:1210.6208].

[147] L. Vecchi, *The Natural Composite Higgs*, arXiv:1304.4579.

[148] J. Barnard, T. Gherghetta, T. S. Ray, and A. Spray, *The Unnatural Composite Higgs*, *JHEP* **01** (2015) 067, [arXiv:1409.7391].

[149] R. Contino, L. Da Rold, and A. Pomarol, *Light custodians in natural composite Higgs models*, *Phys. Rev.* **D75** (2007) 055014, [hep-ph/0612048].

[150] B. Bellazzini, C. Csáki, and J. Serra, *Composite Higgses*, *Eur. Phys. J.* **C74** (2014), no. 5 2766, [arXiv:1401.2457].

[151] J. Barnard, T. Gherghetta, and T. S. Ray, *UV descriptions of composite Higgs models without elementary scalars*, *JHEP* **02** (2014) 002, [arXiv:1311.6562].

[152] G. Ferretti and D. Karateev, *Fermionic UV completions of Composite Higgs models*, *JHEP* **03** (2014) 077, [arXiv:1312.5330].

[153] G. Ferretti, *UV Completions of Partial Compositeness: The Case for a SU(4) Gauge Group*, *JHEP* **06** (2014) 142, [arXiv:1404.7137].

[154] S. R. Coleman and E. J. Weinberg, *Radiative Corrections as the Origin of Spontaneous Symmetry Breaking*, *Phys. Rev.* **D7** (1973) 1888–1910.

[155] S. Weinberg, *Precise relations between the spectra of vector and axial vector mesons*, *Phys. Rev. Lett.* **18** (1967) 507–509.

[156] E. Witten, *Some Inequalities Among Hadron Masses*, *Phys. Rev. Lett.* **51** (1983) 2351.

[157] H. Georgi, *Vector Realization of Chiral Symmetry*, *Nucl. Phys.* **B331** (1990) 311–330.

[158] G. F. Giudice, C. Grojean, A. Pomarol, and R. Rattazzi, *The Strongly-Interacting Light Higgs*, *JHEP* **06** (2007) 045, [hep-ph/0703164].

[159] A. Manohar and H. Georgi, *Chiral Quarks and the Nonrelativistic Quark Model*, *Nucl. Phys.* **B234** (1984) 189–212.

[160] H. Georgi, *Generalized dimensional analysis*, *Phys. Lett.* **B298** (1993) 187–189, [hep-ph/9207278].

[161] N. Arkani-Hamed, A. G. Cohen, and H. Georgi, *Electroweak symmetry breaking from dimensional deconstruction*, *Phys. Lett.* **B513** (2001) 232–240, [hep-ph/0105239].

[162] G. Panico, M. Redi, A. Tesi, and A. Wulzer, *On the Tuning and the Mass of the Composite Higgs*, *JHEP* **03** (2013) 051, [arXiv:1210.7114].

[163] O. Matsedonskyi, G. Panico, and A. Wulzer, *Light Top Partners for a Light Composite Higgs*, *JHEP* **01** (2013) 164, [arXiv:1204.6333].

[164] M. Geller and O. Telem, *Holographic Twin Higgs Model*, *Phys. Rev. Lett.* **114** (2015) 191801, [arXiv:1411.2974].

[165] R. Barbieri, D. Greco, R. Rattazzi, and A. Wulzer, *The Composite Twin Higgs scenario*, *JHEP* **08** (2015) 161, [arXiv:1501.07803].

[166] M. Low, A. Tesi, and L.-T. Wang, *Twin Higgs mechanism and a composite Higgs boson*, *Phys. Rev.* **D91** (2015) 095012, [arXiv:1501.07890].

[167] D. B. Fairlie, *Higgs' Fields and the Determination of the Weinberg Angle*, *Phys. Lett.* **B82** (1979) 97–100.

[168] N. S. Manton, *A New Six-Dimensional Approach to the Weinberg-Salam Model*, *Nucl. Phys.* **B158** (1979) 141–153.

[169] Y. Hosotani, *Dynamical Mass Generation by Compact Extra Dimensions*, *Phys. Lett.* **B126** (1983) 309–313.

[170] Y. Hosotani, *Dynamical Gauge Symmetry Breaking as the Casimir Effect*, *Phys. Lett.* **B129** (1983) 193–197.

[171] A. Falkowski, *About the holographic pseudo-Goldstone boson*, *Phys. Rev.* **D75** (2007) 025017, [hep-ph/0610336].

[172] N. Arkani-Hamed, A. G. Cohen, and H. Georgi, *(De)constructing dimensions*, *Phys. Rev. Lett.* **86** (2001) 4757–4761, [hep-th/0104005].

[173] C. T. Hill, S. Pokorski, and J. Wang, *Gauge invariant effective Lagrangian for Kaluza-Klein modes*, *Phys. Rev.* **D64** (2001) 105005, [hep-th/0104035].

[174] G. Panico and A. Wulzer, *The Discrete Composite Higgs Model*, *JHEP* **09** (2011) 135, [arXiv:1106.2719].

[175] S. De Curtis, M. Redi, and A. Tesi, *The 4D Composite Higgs*, *JHEP* **04** (2012) 042, [arXiv:1110.1613].

[176] R. Barbieri, B. Bellazzini, V. S. Rychkov, and A. Varagnolo, *The Higgs boson from an extended symmetry*, *Phys. Rev.* **D76** (2007) 115008, [arXiv:0706.0432].

[177] K. Agashe and R. Contino, *The Minimal composite Higgs model and electroweak precision tests*, *Nucl. Phys.* **B742** (2006) 59–85, [hep-ph/0510164].

[178] C. Grojean, O. Matsedonskyi, and G. Panico, *Light top partners and precision physics*, *JHEP* **10** (2013) 160, [arXiv:1306.4655].

[179] C. Csaki, A. Falkowski, and A. Weiler, *The Flavor of the Composite Pseudo-Goldstone Higgs*, *JHEP* **09** (2008) 008, [arXiv:0804.1954].

[180] R. Barbieri, G. Isidori, and D. Pappadopulo, *Composite fermions in Electroweak Symmetry Breaking*, *JHEP* **02** (2009) 029, [arXiv:0811.2888].

[181] M. Redi and A. Weiler, *Flavor and CP Invariant Composite Higgs Models*, *JHEP* **11** (2011) 108, [arXiv:1106.6357].

[182] R. Barbieri, D. Buttazzo, F. Sala, and D. M. Straub, *Flavour physics from an approximate $U(2)^3$ symmetry*, *JHEP* **07** (2012) 181, [arXiv:1203.4218].

[183] M. Redi, *Composite MFV and Beyond*, *Eur. Phys. J.* **C72** (2012) 2030, [arXiv:1203.4220].

[184] B. Keren-Zur, P. Lodone, M. Nardecchia, D. Pappadopulo, R. Rattazzi, and L. Vecchi, *On Partial Compositeness and the CP asymmetry in charm decays*, *Nucl. Phys.* **B867** (2013) 394–428, [arXiv:1205.5803].

[185] F. del Aguila, A. Carmona, and J. Santiago, *Neutrino Masses from an A4 Symmetry in Holographic Composite Higgs Models*, *JHEP* **08** (2010) 127, [arXiv:1001.5151].

[186] C. Hagedorn and M. Serone, *Leptons in Holographic Composite Higgs Models with Non-Abelian Discrete Symmetries*, *JHEP* **10** (2011) 083, [arXiv:1106.4021].

[187] C. Hagedorn and M. Serone, *General Lepton Mixing in Holographic Composite Higgs Models*, *JHEP* **02** (2012) 077, [arXiv:1110.4612].

[188] M. Redi, *Leptons in Composite MFV*, *JHEP* **09** (2013) 060, [arXiv:1306.1525].

[189] **ATLAS** Collaboration, G. Aad et al., *Search for pair and single production of new heavy quarks that decay to a Z boson and a third-generation quark in pp collisions at $\sqrt{s} = 8$ TeV with the ATLAS detector*, *JHEP* **11** (2014) 104, [arXiv:1409.5500].

[190] **ATLAS** Collaboration, G. Aad et al., *Search for vector-like B quarks in events with one isolated lepton, missing transverse momentum and jets at $\sqrt{s} = 8$ TeV with the ATLAS detector*, *Phys. Rev.* **D91** (2015), no. 11 112011, [arXiv:1503.05425].

[191] I. Schmidt and M. Siddikov, *Nuclear effects in neutrino production of pions*, *Phys. Rev.* **D91** (2015), no. 7 073002, [arXiv:1501.04306].

[192] **ATLAS** Collaboration, G. Aad et al., *Search for the production of single vector-like and excited quarks in the Wt final state in pp collisions at $\sqrt{s} = 8$ TeV with the ATLAS detector*, *JHEP* **02** (2016) 110, [arXiv:1510.02664].

[193] **ATLAS** Collaboration, G. Aad et al., *Search for single production of vector-like quarks decaying into Wb in pp collisions at $\sqrt{s} = 8$ TeV with the ATLAS detector*, arXiv:1602.05606.

[194] **ATLAS** Collaboration, *Search for production of vector-like top quark pairs and of four top quarks in the lepton-plus-jets final state in pp collisions at $\sqrt{s} = 13$ TeV with the ATLAS detector*, ATLAS-CONF-2016-013.

[195] **CMS** Collaboration, S. Chatrchyan et al., *Search for top-quark partners with charge 5/3 in the same-sign dilepton final state*, *Phys. Rev. Lett.* **112** (2014), no. 17 171801, [arXiv:1312.2391].

[196] **CMS** Collaboration, V. Khachatryan et al., *Search for pair-produced vector-like B quarks in proton-proton collisions at $\sqrt{s} = 8$ TeV*, arXiv:1507.07129.

[197] **CMS** Collaboration, V. Khachatryan et al., *Search for vector-like charge 2/3 T quarks in proton-proton collisions at sqrt(s) = 8 TeV*, *Phys. Rev.* **D93** (2016), no. 1 012003, [arXiv:1509.04177].

[198] **CMS** Collaboration, *Search for pair production of vector-like T quarks in the lepton plus jets final state*, CMS-PAS-B2G-16-002.

[199] **CMS** Collaboration, *Search for top quark partners with charge 5/3 at $\sqrt{s} = 13$ TeV*, CMS-PAS-B2G-15-006.

[200] D. Pappadopulo, A. Thamm, R. Torre, and A. Wulzer, *Heavy Vector Triplets: Bridging Theory and Data*, *JHEP* **09** (2014) 060, [arXiv:1402.4431].

[201] D. Greco and D. Liu, *Hunting composite vector resonances at the LHC: naturalness facing data*, *JHEP* **12** (2014) 126, [arXiv:1410.2883].

[202] C. Bini, R. Contino, and N. Vignaroli, *Heavy-light decay topologies as a new strategy to discover a heavy gluon*, *JHEP* **01** (2012) 157, [arXiv:1110.6058].

[203] M. Chala, J. Juknevich, G. Perez, and J. Santiago, *The Elusive Gluon*, *JHEP* **01** (2015) 092, [arXiv:1411.1771].

[204] M. Berkooz, M. Rozali, and N. Seiberg, *Matrix description of M theory on T**4 and T**5*, *Phys. Lett.* **B408** (1997) 105–110, [hep-th/9704089].

[205] N. Seiberg, *New theories in six-dimensions and matrix description of M theory on T**5 and T**5 / Z(2)*, *Phys. Lett.* **B408** (1997) 98–104, [hep-th/9705221].

[206] N. Itzhaki, J. M. Maldacena, J. Sonnenschein, and S. Yankielowicz, *Supergravity and the large N limit of theories with sixteen supercharges*, *Phys. Rev.* **D58** (1998) 046004, [hep-th/9802042].

[207] I. Antoniadis, S. Dimopoulos, and A. Giveon, *Little string theory at a TeV*, *JHEP* **05** (2001) 055, [hep-th/0103033].

[208] I. Antoniadis, A. Arvanitaki, S. Dimopoulos, and A. Giveon, *Phenomenology of TeV Little String Theory from Holography*, *Phys. Rev. Lett.* **108** (2012) 081602, [arXiv:1102.4043].

[209] M. Baryakhtar, *Graviton Phenomenology of Linear Dilaton Geometries*, *Phys. Rev.* **D85** (2012) 125019, [arXiv:1202.6674].

[210] G. F. Giudice, R. Rattazzi, and J. D. Wells, *Graviscalars from higher dimensional metrics and curvature Higgs mixing*, *Nucl. Phys.* **B595** (2001) 250–276, [hep-ph/0002178].

[211] C. Csaki, M. L. Graesser, and G. D. Kribs, *Radion dynamics and electroweak physics*, *Phys. Rev.* **D63** (2001) 065002, [hep-th/0008151].

[212] E. Boos, S. Keizerov, E. Rahmetov, and K. Svirina, *Higgs boson-radion similarity in production processes involving off-shell fermions*, *Phys. Rev.* **D90** (2014), no. 9 095026, [arXiv:1409.2796].

[213] S. Bae, P. Ko, H. S. Lee, and J. Lee, *Radion phenomenology in the Randall-Sundrum scenario*, in *COSMO-2000. Particle physics and the early universe. Proceedings, 4th International Workshop, COSMO 2000, Cheju, Korea, September 4-8, 2000*, pp. 243–255, 2001, [hep-ph/0103187].

[214] S. Bae, P. Ko, H. S. Lee, and J. Lee, *Phenomenology of the radion in Randall-Sundrum scenario at colliders*, *Phys. Lett.* **B487** (2000) 299–305, [hep-ph/0002224].

[215] K.-m. Cheung, *Phenomenology of radion in Randall-Sundrum scenario*, *Phys. Rev.* **D63** (2001) 056007, [hep-ph/0009232].

[216] **CTEQ** Collaboration, H. L. Lai, J. Huston, S. Kuhlmann, J. Morfin, F. I. Olness, J. F. Owens, J. Pumplin, and W. K. Tung, *Global QCD analysis of parton structure of the nucleon: CTEQ5 parton distributions*, *Eur. Phys. J.* **C12** (2000) 375–392, [hep-ph/9903282].

[217] **CMS** Collaboration, V. Khachatryan et al., *Search for diphoton resonances in the mass range from 150 to 850 GeV in pp collisions at $\sqrt{s} = 8$ TeV*, *Phys. Lett.* **B750** (2015) 494–519, [arXiv:1506.02301].

[218] **CMS** Collaboration, V. Khachatryan et al., *Search for a Higgs Boson in the Mass Range from 145 to 1000 GeV Decaying to a Pair of W or Z Bosons*, *JHEP* **10** (2015) 144, [arXiv:1504.00936].

[219] **ATLAS** Collaboration, G. Aad et al., *Search for a high-mass Higgs boson decaying to a W boson pair in pp collisions at $\sqrt{s} = 8$ TeV with the ATLAS detector*, *JHEP* **01** (2016) 032, [arXiv:1509.00389].

[220] **ATLAS** Collaboration, G. Aad et al., *Search for an additional, heavy Higgs boson in the $H \to ZZ$ decay channel at $\sqrt{s} = 8$ TeV in pp collision data with the ATLAS detector*, *Eur. Phys. J.* **C76** (2016), no. 1 45, [arXiv:1507.05930].

[221] **ATLAS** Collaboration, G. Aad et al., *Searches for Higgs boson pair production in the $hh \to bb\tau\tau, \gamma\gamma WW^*, \gamma\gamma bb, bbbb$ channels with the ATLAS detector*, *Phys. Rev.* **D92** (2015) 092004, [arXiv:1509.04670].

[222] C. Csaki, M. L. Graesser, and G. D. Kribs, *Radion dynamics and electroweak physics*, *Phys. Rev.* **D63** (2001) 065002, [hep-th/0008151].

[223] D. Dominici, B. Grzadkowski, J. F. Gunion, and M. Toharia, *The Scalar sector of the Randall-Sundrum model*, *Nucl. Phys.* **B671** (2003) 243–292, [hep-ph/0206192].

[224] T. G. Rizzo, *Radion couplings to bulk fields in the Randall-Sundrum model*, *JHEP* **06** (2002) 056, [hep-ph/0205242].

[225] **ATLAS, CMS** Collaborations, G. Aad et al., *Combined Measurement of the Higgs Boson Mass in pp Collisions at $\sqrt{s} = 7$ and 8 TeV with the ATLAS and CMS Experiments*, *Phys. Rev. Lett.* **114** (2015) 191803, [arXiv:1503.07589].

[226] B. Bellazzini, C. Csaki, J. Hubisz, J. Serra, and J. Terning, *A Naturally Light Dilaton and a Small Cosmological Constant*, *Eur. Phys. J.* **C74** (2014) 2790, [arXiv:1305.3919].

[227] F. Coradeschi, P. Lodone, D. Pappadopulo, R. Rattazzi, and L. Vitale, *A naturally light dilaton*, *JHEP* **11** (2013) 057, [arXiv:1306.4601].

[228] E. Megias and O. Pujolas, *Naturally light dilatons from nearly marginal deformations*, *JHEP* **08** (2014) 081, [arXiv:1401.4998].

[229] P. Cox and T. Gherghetta, *A Soft-Wall Dilaton*, *JHEP* **02** (2015) 006, [arXiv:1411.1732].

[230] **ATLAS** Collaboration, *Search for resonances decaying to photon pairs in 3.2 fb^{-1} of pp collisions at $\sqrt{s}$ = 13 TeV with the ATLAS detector*, ATLAS-CONF-2015-081.

[231] **CMS** Collaboration, *Search for new physics in high mass diphoton events in* 3.3 fb^{-1} *of proton-proton collisions at* $\sqrt{s} = 13$ TeV *and combined interpretation of searches at* 8 TeV *and* 13 TeV, CMS-PAS-EXO-16-018.

[232] D. Dominici, B. Grzadkowski, J. F. Gunion, and M. Toharia, *The Scalar sector of the Randall-Sundrum model*, *Nucl. Phys.* **B671** (2003) 243–292, [hep-ph/0206192].

[233] Z. Chacko and R. K. Mishra, *Effective Theory of a Light Dilaton*, *Phys. Rev.* **D87** (2013), no. 11 115006, [arXiv:1209.3022].

[234] Z. Chacko, R. K. Mishra, and D. Stolarski, *Dynamics of a Stabilized Radion and Duality*, *JHEP* **09** (2013) 121, [arXiv:1304.1795].

[235] H. de Sandes and R. Rosenfeld, *Radion-Higgs mixing effects on bounds from LHC Higgs Searches*, *Phys. Rev.* **D85** (2012) 053003, [arXiv:1111.2006].

[236] H. Kubota and M. Nojiri, *Radion-higgs mixing state at the LHCwith the KK contributions to the production and decay*, *Phys. Rev.* **D87** (2013) 076011, [arXiv:1207.0621].

[237] N. Desai, U. Maitra, and B. Mukhopadhyaya, *An updated analysis of radion-higgs mixing in the light of LHC data*, *JHEP* **10** (2013) 093, [arXiv:1307.3765].

[238] G. Cacciapaglia, C. Csaki, G. Marandella, and J. Terning, *The Gaugephobic Higgs*, *JHEP* **02** (2007) 036, [hep-ph/0611358].

[239] A. Salam and J. A. Strathdee, *Nonlinear realizations. 2. Conformal symmetry*, *Phys. Rev.* **184** (1969) 1760–1768.

[240] L. Vecchi, *Phenomenology of a light scalar: the dilaton*, *Phys. Rev.* **D82** (2010) 076009, [arXiv:1002.1721].

[241] M. Montull, F. Riva, E. Salvioni, and R. Torre, *Higgs Couplings in Composite Models*, *Phys. Rev.* **D88** (2013) 095006, [arXiv:1308.0559].

[242] R. Malm, M. Neubert, K. Novotny, and C. Schmell, *5D Perspective on Higgs Production at the Boundary of a Warped Extra Dimension*, *JHEP* **01** (2014) 173, [arXiv:1303.5702].

[243] C. Csaki, J. Hubisz, and S. J. Lee, *Radion phenomenology in realistic warped space models*, *Phys. Rev.* **D76** (2007) 125015, [arXiv:0705.3844].

[244] A. Djouadi, *The Anatomy of electro-weak symmetry breaking. I: The Higgs boson in the standard model*, *Phys. Rept.* **457** (2008) 1–216, [hep-ph/0503172].

[245] G. Belanger, B. Dumont, U. Ellwanger, J. F. Gunion, and S. Kraml, *Global fit to Higgs signal strengths and couplings and implications for extended Higgs sectors*, *Phys. Rev.* **D88** (2013) 075008, [arXiv:1306.2941].

[246] **CMS** Collaboration, *Update on the search for the standard model Higgs boson in pp collisions at the LHC decaying to W + W in the fully leptonic final state*, CMS-PAS-HIG-13-003.

[247] **CMS** Collaboration, *Properties of the Higgs-like boson in the decay H to ZZ to 4l in pp collisions at $\sqrt{s}$=7 and 8 TeV*, CMS-PAS-HIG-13-002.

[248] **ATLAS** Collaboration, *Search for a high-mass Higgs boson in the $H \to WW \to l\nu l\nu$ decay channel with the ATLAS detector using 21 fb^{-1} of proton-proton collision data*, in *Proceedings, 2013 European Physical Society Conference on High Energy Physics (EPS-HEP 2013)*, 2013.

[249] **CMS** Collaboration, *Search for a narrow spin-2 resonance decaying to Z bosons in the semileptonic final state*, CMS-PAS-EXO-12-022.

[250] **CMS** Collaboration, *Search for new resonances decaying to WW to l nu q qbar' in the final state with a lepton, missing transverse energy, and single reconstructed jet*, CMS-PAS-EXO-12-021.

[251] **ATLAS** Collaboration, G. Aad et al., *Search for Extra Dimensions in diphoton events using proton-proton collisions recorded at $\sqrt{s} = 7$ TeV with the ATLAS detector at the LHC*, *New J. Phys.* **15** (2013) 043007, [arXiv:1210.8389].

[252] **CMS** Collaboration, *Search for Narrow Resonances using the Dijet Mass Spectrum with 19.6fb-1 of pp Collisions at $\sqrt{s}$=8 TeV*, CMS-PAS-EXO-12-059.

[253] **ATLAS** Collaboration, G. Aad et al., *Search for high-mass diphoton resonances in pp collisions at $\sqrt{s} = 8$ TeV with the ATLAS detector*, *Phys. Rev.* **D92** (2015), no. 3 032004, [arXiv:1504.05511].

[254] A. Ahmed, B. M. Dillon, B. Grzadkowski, J. F. Gunion, and Y. Jiang, *Higgs-radion interpretation of 750 GeV di-photon excess at the LHC*, arXiv:1512.05771.

[255] M. T. Arun and P. Saha, *Gravitons in multiply warped scenarios - at 750 GeV and beyond*, arXiv:1512.06335.

[256] C. Han, H. M. Lee, M. Park, and V. Sanz, *The diphoton resonance as a gravity mediator of dark matter*, *Phys. Lett.* **B755** (2016) 371–379, [arXiv:1512.06376].

[257] D. Bardhan, D. Bhatia, A. Chakraborty, U. Maitra, S. Raychaudhuri, and T. Samui, *Radion Candidate for the LHC Diphoton Resonance*, arXiv:1512.06674.

[258] H. Davoudiasl and C. Zhang, *750 GeV messenger of dark conformal symmetry breaking*, *Phys. Rev.* **D93** (2016), no. 5 055006, [arXiv:1512.07672].

[259] M. T. Arun and D. Choudhury, *Bulk gauge and matter fields in nested warping: II. Symmetry Breaking and phenomenological consequences*, *JHEP* **04** (2016) 133, [arXiv:1601.02321].

[260] S. B. Giddings and H. Zhang, *Kaluza-Klein graviton phenomenology for warped compactifications, and the 750 GeV diphoton excess*, arXiv:1602.02793.

[261] V. Sanz, *Theoretical interpretation of a spin-two diphoton excess*, arXiv:1603.05574.

[262] M. Bauer, C. Hoerner, and M. Neubert, *Diphoton Resonance from a Warped Extra Dimension*, arXiv:1603.05978.

[263] A. Falkowski and J. F. Kamenik, *Di-photon portal to warped gravity*, arXiv:1603.06980.

[264] C. Csaki and L. Randall, *A Diphoton Resonance from Bulk RS*, arXiv:1603.07303.

[265] J. L. Hewett and T. G. Rizzo, *750 GeV Diphoton Resonance in Warped Geometries*, arXiv:1603.08250.

[266] A. Carmona, *A 750 GeV graviton from holographic composite dark sectors*, arXiv:1603.08913.

[267] B. M. Dillon and V. Sanz, *A Little KK Graviton at 750 GeV*, arXiv:1603.09550.

[268] N. Chakrabarty, B. Mukhopadhyaya, and S. SenGupta, *Diphoton excess via Chern-Simons interaction in a warped geometry scenario*, arXiv:1604.00885.

[269] D. Buttazzo, A. Greljo, and D. Marzocca, *Knocking on new physics' door with a scalar resonance*, *Eur. Phys. J.* **C76** (2016), no. 3 116, [arXiv:1512.04929].

[270] **ATLAS** Collaboration, G. Aad et al., *Search for new resonances in $W\gamma$ and $Z\gamma$ final states in pp collisions at $\sqrt{s} = 8$ TeV with the ATLAS detector*, *Phys. Lett.* **B738** (2014) 428–447, [arXiv:1407.8150].

[271] **CMS** Collaboration, *Search for scalar resonances in the 200–1200 GeV mass range decaying into a Z and a photon in pp collisions at $\sqrt{s} = 8$ TeV*, CMS-PAS-HIG-16-014.

[272] **ATLAS** Collaboration, G. Aad et al., *Search for new phenomena in the dijet mass distribution using $p - p$ collision data at $\sqrt{s} = 8$ TeV with the ATLAS detector*, *Phys. Rev.* **D91** (2015), no. 5 052007, [arXiv:1407.1376].

[273] **CMS** Collaboration, *Search for Resonances Decaying to Dijet Final States at $\sqrt{s} = 8$ TeV with Scouting Data*, CMS-PAS-EXO-14-005.

[274] **ATLAS, CMS** Collaborations, *Measurements of the Higgs boson production and decay rates and constraints on its couplings from a combined ATLAS and CMS analysis of the LHC pp collision data at $\sqrt{s} = 7$ and 8 TeV*, ATLAS-CONF-2015-044.

[275] **ATLAS, CMS** Collaborations, *Measurements of the Higgs boson production and decay rates and constraints on its couplings from a combined ATLAS and CMS analysis of the LHC pp collision data at sqrt s = 7 and 8 TeV*, CMS-PAS-HIG-15-002.

[276] **LHC Higgs Cross Section Working Group** Collaboration, J. R. Andersen et al., *Handbook of LHC Higgs Cross Sections: 3. Higgs Properties*, arXiv:1307.1347.

[277] H. Davoudiasl, G. Perez, and A. Soni, *The Little Randall-Sundrum Model at the Large Hadron Collider*, *Phys. Lett.* **B665** (2008) 67–71, [arXiv:0802.0203].

[278] H. Davoudiasl, T. McElmurry, and A. Soni, *Precocious Diphoton Signals of the Little Radion at Hadron Colliders*, *Phys. Rev.* **D82** (2010) 115028, [arXiv:1009.0764]. [Erratum: Phys. Rev.D86,039907(2012)].

[279] D. P. George and K. L. McDonald, *Gravity on a Little Warped Space*, *Phys. Rev.* **D84** (2011) 064007, [arXiv:1107.0755].

[280] C. J. Isham, A. Salam, and J. A. Strathdee, *Spontaneous breakdown of conformal symmetry*, *Phys. Lett.* **B31** (1970) 300–302.

[281] I. Low and A. V. Manohar, *Spontaneously broken space-time symmetries and Goldstone's theorem*, *Phys. Rev. Lett.* **88** (2002) 101602, [hep-th/0110285].

[282] R. Contino, A. Pomarol, and R. Rattazzi, *see talks by R. Rattazzi at Planck 2010 [indico/contribId=163 & confId=75810], and by A. Pomarol at the XVI IFT Xmas Workshop 2010 [http://www.ift.uam-csic.es/workshops/Xmas10/doc/pomarol.pdf], (unpublished work).*

[283] F. Coradeschi, P. Lodone, D. Pappadopulo, R. Rattazzi, and L. Vitale, *A naturally light dilaton*, *JHEP* **11** (2013) 057, [arXiv:1306.4601].

[284] K. Behrndt, *Domain walls of D = 5 supergravity and fixpoints of N=1 superYang Mills*, *Nucl. Phys.* **B573** (2000) 127–148, [hep-th/9907070].

[285] J. de Boer, E. P. Verlinde, and H. L. Verlinde, *On the holographic renormalization group*, *JHEP* **08** (2000) 003, [hep-th/9912012].

[286] D. Anselmi, L. Girardello, M. Porrati, and A. Zaffaroni, *A Note on the holographic beta and C functions*, *Phys. Lett.* **B481** (2000) 346–352, [hep-th/0002066].

[287] J. A. Cabrer, G. von Gersdorff, and M. Quiros, *Soft-Wall Stabilization*, *New J. Phys.* **12** (2010) 075012, [arXiv:0907.5361].

[288] S. S. Gubser, *Curvature singularities: The Good, the bad, and the naked*, *Adv. Theor. Math. Phys.* **4** (2000) 679–745, [hep-th/0002160].

[289] I. Papadimitriou, *Multi-Trace Deformations in AdS/CFT: Exploring the Vacuum Structure of the Deformed CFT*, *JHEP* **05** (2007) 075, [hep-th/0703152].

[290] E. Witten, *Multitrace operators, boundary conditions, and AdS / CFT correspondence*, hep-th/0112258.

[291] J. Barnard, P. Cox, T. Gherghetta, and A. Spray, *Long-Lived, Colour-Triplet Scalars from Unnaturalness*, *JHEP* **03** (2016) 003, [arXiv:1510.06405].

[292] J. D. Wells, *Implications of supersymmetry breaking with a little hierarchy between gauginos and scalars*, in *11th International Conference on Supersymmetry and the Unification of Fundamental Interactions (SUSY 2003) Tucson, Arizona, June 5-10, 2003*, 2003, [hep-ph/0306127].

[293] N. Arkani-Hamed and S. Dimopoulos, *Supersymmetric unification without low energy supersymmetry and signatures for fine-tuning at the LHC*, *JHEP* **06** (2005) 073, [hep-th/0405159].

[294] A. Arvanitaki, N. Craig, S. Dimopoulos, and G. Villadoro, *Mini-Split*, *JHEP* **02** (2013) 126, [arXiv:1210.0555].

[295] N. Arkani-Hamed, A. Gupta, D. E. Kaplan, N. Weiner, and T. Zorawski, *Simply Unnatural Supersymmetry*, arXiv:1212.6971.

[296] Y. Cui and B. Shuve, *Probing Baryogenesis with Displaced Vertices at the LHC*, *JHEP* **02** (2015) 049, [arXiv:1409.6729].

[297] Z. Liu and B. Tweedie, *The Fate of Long-Lived Superparticles with Hadronic Decays after LHC Run 1*, *JHEP* **06** (2015) 042, [arXiv:1503.05923].

[298] A. de la Puente and A. Szynkman, *Long-lived Colored Scalars at the LHC*, *Eur. Phys. J.* **C76** (2016), no. 3 124, [arXiv:1504.07293].

[299] C. Csaki, E. Kuflik, S. Lombardo, O. Slone, and T. Volansky, *Phenomenology of a Long-Lived LSP with R-Parity Violation*, *JHEP* **08** (2015) 016, [arXiv:1505.00784].

[300] N. Zwane, *Long-Lived Particle Searches in R-Parity Violating MSSM*, arXiv:1505.03479.

[301] N. Nagata, H. Otono, and S. Shirai, *Probing Bino-Wino Coannihilation at the LHC*, *JHEP* **10** (2015) 086, [arXiv:1506.08206].

[302] K. Agashe, R. Contino, and R. Sundrum, *Top compositeness and precision unification*, *Phys. Rev. Lett.* **95** (2005) 171804, [hep-ph/0502222].

[303] K. Agashe and G. Servant, *Warped unification, proton stability and dark matter*, *Phys. Rev. Lett.* **93** (2004) 231805, [hep-ph/0403143].

[304] K. Agashe and G. Servant, *Baryon number in warped GUTs: Model building and (dark matter related) phenomenology*, *JCAP* **0502** (2005) 002, [hep-ph/0411254].

[305] V. A. Kuzmin, V. A. Rubakov, and M. E. Shaposhnikov, *On the Anomalous Electroweak Baryon Number Nonconservation in the Early Universe*, *Phys. Lett.* **B155** (1985) 36.

[306] **CMS** Collaboration, S. Chatrchyan et al., *Searches for long-lived charged particles in pp collisions at $\sqrt{s}$=7 and 8 TeV*, *JHEP* **07** (2013) 122, [arXiv:1305.0491].

[307] **ATLAS** Collaboration, G. Aad et al., *Searches for heavy long-lived charged particles with the ATLAS detector in proton-proton collisions at $\sqrt{s} = 8$ TeV*, *JHEP* **01** (2015) 068, [arXiv:1411.6795].

[308] **ATLAS** Collaboration, G. Aad et al., *Search for long-lived stopped R-hadrons decaying out-of-time with pp collisions using the ATLAS detector*, *Phys. Rev.* **D88** (2013), no. 11 112003, [arXiv:1310.6584].

[309] **CMS** Collaboration, V. Khachatryan et al., *Search for Decays of Stopped Long-Lived Particles Produced in Proton–Proton Collisions at $\sqrt{s} = 8$ TeV*, *Eur. Phys. J.* **C75** (2015), no. 4 151, [arXiv:1501.05603].

[310] T. Sjostrand, S. Mrenna, and P. Z. Skands, *PYTHIA 6.4 Physics and Manual*, *JHEP* **05** (2006) 026, [hep-ph/0603175].

[311] M. Fairbairn, A. C. Kraan, D. A. Milstead, T. Sjostrand, P. Z. Skands, and T. Sloan, *Stable massive particles at colliders*, *Phys. Rept.* **438** (2007) 1–63, [hep-ph/0611040].

[312] T. Sjostrand, S. Mrenna, and P. Z. Skands, *A Brief Introduction to PYTHIA 8.1*, *Comput. Phys. Commun.* **178** (2008) 852–867, [arXiv:0710.3820].

[313] C. Borschensky, M. Krämer, A. Kulesza, M. Mangano, S. Padhi, T. Plehn, and X. Portell, *Squark and gluino production cross sections in pp collisions at $\sqrt{s}$ = 13, 14, 33 and 100 TeV*, *Eur. Phys. J.* **C74** (2014), no. 12 3174, [arXiv:1407.5066].

[314] **ATLAS** Collaboration, G. Aad et al., *Search for metastable heavy charged particles with large ionisation energy loss in pp collisions at $\sqrt{s} = 8$ TeV using the ATLAS experiment*, *Eur. Phys. J.* **C75** (2015), no. 9 407, [arXiv:1506.05332].

[315] **ATLAS** Collaboration, G. Aad et al., *Search for charginos nearly mass degenerate with the lightest neutralino based on a disappearing-track signature in pp collisions at $\sqrt{(s)}$=8 TeV with the ATLAS detector*, *Phys. Rev.* **D88** (2013), no. 11 112006, [arXiv:1310.3675].

[316] **ATLAS** Collaboration, G. Aad et al., *Search for long-lived neutral particles decaying into lepton jets in proton-proton collisions at $\sqrt{s} = 8$ TeV with the ATLAS detector*, *JHEP* **11** (2014) 088, [arXiv:1409.0746].

[317] **ATLAS** Collaboration, G. Aad et al., *Search for pair-produced long-lived neutral particles decaying in the ATLAS hadronic calorimeter in pp collisions at $\sqrt{s} = 8$ TeV*, *Phys. Lett.* **B743** (2015) 15–34, [arXiv:1501.04020].

[318] **ATLAS** Collaboration, G. Aad et al., *Search for long-lived, weakly interacting particles that decay to displaced hadronic jets in proton-proton collisions at $\sqrt{s} = 8$ TeV with the ATLAS detector*, *Phys. Rev.* **D92** (2015), no. 1 012010, [arXiv:1504.03634].

[319] **ATLAS** Collaboration, G. Aad et al., *Search for massive, long-lived particles using multitrack displaced vertices or displaced lepton pairs in pp collisions at $\sqrt{s} = 8$ TeV with the ATLAS detector*, *Phys. Rev.* **D92** (2015), no. 7 072004, [arXiv:1504.05162].

[320] **CMS** Collaboration, V. Khachatryan et al., *Search for Displaced Supersymmetry in events with an electron and a muon with large impact parameters*, *Phys. Rev. Lett.* **114** (2015), no. 6 061801, [arXiv:1409.4789].

[321] **CMS** Collaboration, V. Khachatryan et al., *Search for Long-Lived Neutral Particles Decaying to Quark-Antiquark Pairs in Proton-Proton Collisions at $\sqrt{s} = 8$ TeV*, *Phys. Rev.* **D91** (2015), no. 1 012007, [arXiv:1411.6530].

[322] **CMS** Collaboration, V. Khachatryan et al., *Search for long-lived particles that decay into final states containing two electrons or two muons in proton-proton collisions at $\sqrt{s} = 8$ TeV*, *Phys. Rev.* **D91** (2015), no. 5 052012, [arXiv:1411.6977].

[323] **CMS** Collaboration, *Search for displaced photons using conversions at 8 TeV*, CMS-PAS-EXO-14-017.

[324] **DELPHES 3** Collaboration, J. de Favereau, C. Delaere, P. Demin, A. Giammanco, V. Lemaître, A. Mertens, and M. Selvaggi, *DELPHES 3, A modular framework for fast simulation of a generic collider experiment*, *JHEP* **02** (2014) 057, [arXiv:1307.6346].

[325] L. Moneta, K. Belasco, K. S. Cranmer, S. Kreiss, A. Lazzaro, D. Piparo, G. Schott, W. Verkerke, and M. Wolf, *The RooStats Project*, *PoS* **ACAT2010** (2010) 057, [arXiv:1009.1003].

[326] G. Cowan, K. Cranmer, E. Gross, and O. Vitells, *Asymptotic formulae for likelihood-based tests of new physics*, *Eur. Phys. J.* **C71** (2011) 1554, [arXiv:1007.1727]. [Erratum: Eur. Phys. J.C73,2501(2013)].

[327] J. Anderson et al., *Snowmass Energy Frontier Simulations*, in *Community Summer Study 2013: Snowmass on the Mississippi (CSS2013) Minneapolis, MN, USA, July 29-August 6, 2013*, 2013, [arXiv:1309.1057].

[328] A. Avetisyan et al., *Methods and Results for Standard Model Event Generation at $\sqrt{s}$ = 14 TeV, 33 TeV and 100 TeV Proton Colliders (A Snowmass Whitepaper)*, in *Community Summer Study 2013: Snowmass on the Mississippi (CSS2013) Minneapolis, MN, USA, July 29-August 6, 2013*, 2013, [arXiv:1308.1636].

[329] **ATLAS** Collaboration, G. Aad et al., *Search for strong production of supersymmetric particles in final states with missing transverse momentum and at least three b-jets at $\sqrt{s}$= 8 TeV proton-proton collisions with the ATLAS detector*, *JHEP* **10** (2014) 024, [arXiv:1407.0600].

[330] M. Cacciari, G. P. Salam, and G. Soyez, *The Anti-k(t) jet clustering algorithm*, *JHEP* **04** (2008) 063, [arXiv:0802.1189].

[331] M. Cacciari, G. P. Salam, and G. Soyez, *FastJet User Manual*, *Eur. Phys. J.* **C72** (2012) 1896, [arXiv:1111.6097].

[332] **ATLAS** Collaboration, *Expected performance of the ATLAS b-tagging algorithms in Run-2*, Tech. Rep. ATL-PHYS-PUB-2015-022, CERN, Geneva, Jul 2015.

[333] **CMS** Collaboration, P. Jindal, *Tracking and b-Tagging Performance with an Upgraded CMS Pixel Detector*, *Phys. Procedia* **37** (2012) 1032–1038.

[334] A. Hocker et al., *TMVA - Toolkit for Multivariate Data Analysis*, *PoS* **ACAT** (2007) 040, [physics/0703039].

[335] T. Cohen, T. Golling, M. Hance, A. Henrichs, K. Howe, J. Loyal, S. Padhi, and J. G. Wacker, *SUSY Simplified Models at 14, 33, and 100 TeV Proton Colliders*, *JHEP* **04** (2014) 117, [arXiv:1311.6480].

[336] **ATLAS** Collaboration, *b-tagging in dense environments*, Tech. Rep. ATL-PHYS-PUB-2014-014, CERN, Geneva, Aug 2014.

[337] A. Azatov, R. Contino, A. Di Iura, and J. Galloway, *New Prospects for Higgs Compositeness in $h \to Z\gamma$*, *Phys. Rev.* **D88** (2013), no. 7 075019, [arXiv:1308.2676].

Appendix A

A.1 Conformal Group

The conformal group consists of transformations of the coordinates x_μ, which leave the metric invariant up to a rescaling of the form

$$g'_{\mu\nu}(x'_\mu) = \Omega(x_\mu) g_{\mu\nu}(x_\mu)\,. \tag{A.1}$$

It is isomorphic to $\mathrm{SO}(d,2)$ and for $d \geq 3$ includes: the Poincaré transformations

$$x_\mu \to \Lambda^\nu_\mu x_\nu + a_\mu\,, \tag{A.2}$$

the special conformal transformations

$$x_\mu \to \frac{x_\mu + x^2 b_\mu}{1 + 2b^\mu x_\mu + b^2 x^2}\,, \tag{A.3}$$

and the dilatations

$$x_\mu \to e^{-\omega} x_\mu\,, \tag{A.4}$$

where $\Lambda \in \mathrm{O}(d-1,1)$ and a_μ, b_μ, and ω are real parameters. It is therefore a 15 parameter group in four dimensions.

The generators of the conformal group have the representation

$$M_{\mu\nu} \equiv i\left(x_\mu \partial_\nu - x_\nu \partial_\mu\right)\,, \tag{A.5a}$$

$$P_\mu \equiv -i\partial_\mu\,, \tag{A.5b}$$

$$D \equiv -i x_\mu \partial^\mu\,, \tag{A.5c}$$

$$K_\mu \equiv i\left(x^2 \partial_\mu - 2x_\mu x_\nu \partial^\nu\right)\,, \tag{A.5d}$$

where $M_{\mu\nu}$ are the Lorentz generators, P_μ is the generator of translations, and K_μ and D generate the special conformal transformations and dilatations respectively.

The conformal algebra is defined by the commutation relations

$$[D, K_\mu] = -iK_\mu \,, \tag{A.6a}$$

$$[D, P_\mu] = iP_\mu \,, \tag{A.6b}$$

$$[K_\mu, P_\nu] = 2i\left(\eta_{\mu\nu} D - M_{\mu\nu}\right) \,, \tag{A.6c}$$

$$[K_\rho, M_{\mu\nu}] = i\left(\eta_{\rho\mu} K_\nu - \eta_{\rho\nu} K_\mu\right) \,, \tag{A.6d}$$

$$[P_\rho, M_{\mu\nu}] = i\left(\eta_{\rho\mu} P_\nu - \eta_{\rho\nu} P_\mu\right) \,, \tag{A.6e}$$

$$[M_{\mu\nu}, M_{\rho\sigma}] = i\left(\eta_{\nu\rho} M_{\mu\sigma} + \eta_{\mu\sigma} M_{\nu\rho} - \eta_{\nu\sigma} M_{\mu\rho} - \eta_{\mu\rho} M_{\nu\sigma}\right) \,. \tag{A.6f}$$

Appendix B

B.1 Wavefunction Normalisation

In order to calculate the couplings to the Standard Model fields we need to ensure that the Q_n modes are canonically normalised by fixing the normalisation constant N_n. Since the equations of motion are only linear in the perturbations they do not contain sufficient information to correctly normalise the modes. It therefore becomes necessary to diagonalise the action (3.1) to second order in the perturbations. This analysis has been done for the general case in Ref. [62]. Using their result, we obtain the following free action for the 4D physical modes of the system,

$$S_n^{free} = C_n \int d^4x\, Q_n \left[\Box - m_n^2\right] Q_n, \tag{B.1}$$

$$C_n = \frac{27M^3}{2\alpha^2}\int_0^{r_c} dz\, e^{-\alpha z}\left[\Phi_n'^2 - \frac{4\alpha}{3}\Phi_n'\Phi_n + \frac{2\alpha^2}{3}\Phi_n^2\right] \equiv \frac{1}{2}. \tag{B.2}$$

Here we provide the complete normalised wavefunctions for the radion and KK modes. The wavefunctions take the form of (3.24), where the normalisation constant N_n is given by

$$\begin{aligned} N_n = \frac{4\sqrt{\beta_n}}{3M^{3/2}}&\left[4\beta_n^2\alpha\epsilon + \alpha^3(1+\epsilon)\right]\times \\ &\Big[6\beta_n r_c(4\beta_n^2+\alpha^2)(16\beta_n^4\epsilon^2 + 4\beta_n^2\alpha^2(9+2\epsilon+2\epsilon^2) + \alpha^4(1+\epsilon)^2) \\ &- 8\beta_n\alpha\Big(16\beta_n^4\epsilon(9+\epsilon) + 8\beta_n^2\alpha^2\epsilon(1+\epsilon) + \alpha^4(-8-7\epsilon+\epsilon^2)\Big)\sin(\beta_n r_c)^2 \\ &+ 3\Big(64\beta_n^6\epsilon^2 + 16\beta_n^4\alpha^2(-9-2\epsilon+\epsilon^2) - 4\beta_n^2\alpha^4(-6+4\epsilon+\epsilon^2) \\ &- \alpha^6(1+\epsilon)^2\Big)\sin(2\beta_n r_c)\Big]^{-1/2}. \end{aligned} \tag{B.3}$$

Here we have defined $\epsilon \equiv \epsilon_{vis}$ for simplicity, while β_n is defined near (3.24) and can depend on both ϵ_{vis} and ϵ_{hid}.

B.2 Higgs-radion KK mixing

We consider the effect of the Higgs mixing with the closely spaced radion KK modes. The Lagrangian that needs to be diagonalised is now given by

$$\mathcal{L} = -\frac{1}{2}h\Box h - \frac{1}{2}m_h^2 h^2 + \sum_n \left(-\frac{1}{2}Q_n\Box Q_n - \frac{1}{2}m_n^2 Q_n^2 + \frac{6\xi\kappa_{\Phi,n}v}{M}h\Box Q_n\right) - \frac{3\xi v^2}{M^2}\sum_m\sum_n \kappa_{\Phi,m}\left(\kappa_{\Phi,n} - \kappa_{\phi,n}\right)Q_m\Box Q_n. \quad \text{(B.4)}$$

We see that in addition to the Higgs-KK mixing, the last term also introduces a kinetic mixing between the KK modes. However, this term is suppressed by an additional factor of $1/M$. We shall therefore work to leading order in $1/M$, which allows us to neglect the mixing between the KK modes and focus instead on the mixing with the Higgs. The analysis can now proceed as for the single radion case and we diagonalise the kinetic terms via the transformation

$$h = h' + \frac{6\xi v}{M}\sum_n \kappa_{\Phi,n}Q_n. \quad \text{(B.5)}$$

The Lagrangian now takes the form

$$\mathcal{L} = -\frac{1}{2}h'\Box h' - \frac{1}{2}\sum_n Q_n\Box Q_n - \frac{1}{2}f^i m^{ij} f^j, \quad \text{(B.6)}$$

where we have defined the vector

$$f^i = \begin{pmatrix} h' \\ r \\ Q_1 \\ \vdots \end{pmatrix}, \quad \text{(B.7)}$$

and the mass matrix is given by

$$m^{ij} = m_h^2 \begin{pmatrix} 1 & \frac{6\xi\kappa_{\Phi,r}v}{M} & \frac{6\xi\kappa_{\Phi,1}v}{M} & \cdots \\ \frac{6\xi\kappa_{\Phi,r}v}{M} & \frac{m_r^2}{m_h^2} & & 0 \\ \frac{6\xi\kappa_{\Phi,1}v}{M} & & \frac{m_1^2}{m_h^2} & \\ \vdots & 0 & & \ddots \end{pmatrix}. \quad \text{(B.8)}$$

It is now straightforward to diagonalise the mass matrix numerically. We find that the mixing with the Higgs remains small and there is one mass eigenstate which

is largely composed of the Higgs gauge eigenstate. So despite their relatively close mass spacing, the cumulative effect of the KK modes is still too small to have a significant effect on the Higgs phenomenology. There is however an exception when one of the KK modes has a mass very close to the mass of the Higgs, in which case the mixing between those two states becomes significant. However the mixing with the other KK modes reduces this effect compared to the radion only case discussed previously.

B.3 Feynman Rules

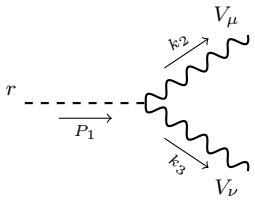

$$\frac{ib_1\kappa_\phi}{M}\left(P_2{\cdot}P_3\eta^{\mu\nu} - P_2^\nu P_3^\mu\right) + 2im_V^2\left(\frac{b_1}{M}\left(\frac{\kappa_\phi}{2} - \kappa_\Phi\right) + \frac{a_1}{v}\right)\eta^{\mu\nu} \quad \text{(B.9)}$$

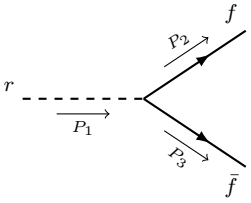

$$im_\Psi\left(\frac{b_1\kappa_\Phi}{M} - \frac{a_1}{v}\right) \quad \text{(B.10)}$$

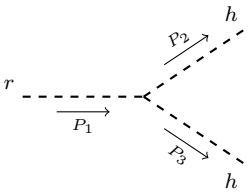

$$-\frac{2ia_0^2b_1}{M}\left(\frac{\kappa_\phi}{2} + \kappa_\Phi(6\xi - 1)\right)P_2{\cdot}P_3 - \frac{6i\xi a_0^2 b_1}{M}\kappa_\Phi\left(P_2{\cdot}P_2 + P_3{\cdot}P_3\right) + 2ia_0^2m_h^2\left(\frac{b_1}{M}\left(2\kappa_\Phi - \frac{\kappa_\phi}{2}\right) - \frac{3a_1}{2v}\right) \quad \text{(B.11)}$$

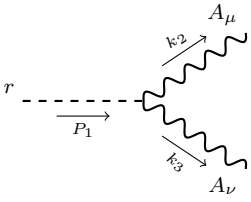

$$\frac{ib_1}{M}\left(\kappa_\phi + \frac{\alpha_{EM}}{2\pi}\kappa_\Phi(b_2 + b_Y)\right)\left(k_2{\cdot}k_3\eta^{\mu\nu} - k_2^\nu k_3^\mu\right) \quad \text{(B.12)}$$

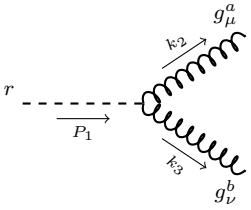

$$\frac{ib_1}{M}\left(\kappa_\phi + \frac{\alpha_s b_{QCD}}{2\pi}\kappa_\Phi\right)\left(k_2{\cdot}k_3\eta^{\mu\nu} - k_2^\nu k_3^\mu\right)\delta_b^a \quad \text{(B.13)}$$

Appendix C

C.1 Higgs VEV and Profiles

We provide details from the derivation of Section 4.3.2. Given the action Eq. (4.6), with brane potentials in Eqs. (4.7) and (4.8), we wish to find the profiles of the Higgs vev $v(y)$ and lightest mode $h(x,y)$. We begin by expanding the Higgs field in the unitary gauge as a bulk vev plus a fluctuation

$$H(x,y) = \frac{1}{\sqrt{2}} \begin{pmatrix} 0 \\ v(y) + h(x,y) \end{pmatrix}, \tag{C.1}$$

and concentrate for the moment on the background solution. Variation of the action Eq. (4.6) gives the following bulk equations of motion

$$v'' - 4\tilde{A}'v' + 4\xi(2\tilde{A}'' - 5\tilde{A}'^2)v - \sqrt{2}\frac{\partial V}{\partial H^\dagger}\bigg|_{H=\frac{v}{\sqrt{2}}} = 0, \tag{C.2}$$

$$\tilde{A}'' - \frac{v'^2 + 2\xi(v'^2 + v\,v'' + \tilde{A}'v\,v')}{3(M^3 + \xi v^2)} = 0, \tag{C.3}$$

$$6(M^3 + \xi v^2)\tilde{A}'^2 - \frac{v'^2}{2} + V - 8\xi\tilde{A}'v\,v' = 0, \tag{C.4}$$

where primes denote differentiation with respect to y. We also have the boundary conditions

$$\tilde{A}' = \pm\frac{\lambda_\alpha}{3(M^3 + \xi v^2)}, \qquad v' = \pm\left(\sqrt{2}\frac{\partial\lambda_\alpha}{\partial H^\dagger}\bigg|_{H=\frac{v}{\sqrt{2}}} - 8\xi\tilde{A}'v\right), \tag{C.5}$$

where the upper and lower signs correspond to the UV and IR branes respectively.

We assume that we can neglect the back-reaction of the Higgs. Then we have $\tilde{A}(y) = ky$ and the vev, $v(y)$, is given by

$$v''(y) - 4kv'(y) - (c^2 + 20\xi)k^2 v(y) = 0, \tag{C.6}$$

$$\left(v'(y) + \frac{\tilde{\lambda}}{2k^2} v(y) \left(v^2(y) - \left(\tilde{v}_{IR}^2 + \frac{16\xi}{\tilde{\lambda}} \right) k^3 \right) \right) \Big|_{IR} = 0, \tag{C.7}$$

$$\left(v'(y) - (m_{UV} - 8\xi k) v(y) \right) |_{UV} = 0. \tag{C.8}$$

From these expressions we infer the redefinitions noted in Eq. (4.16). The general solution for the equation of motion in the bulk then takes the usual form

$$v(y) = A_1 \, e^{(2-\beta)ky} + A_2 \, e^{(2+\beta)ky}, \tag{C.9}$$

where $\beta = \sqrt{4 + c^2}$ and A_1 and A_2 are constants to be determined by the boundary conditions. We use the UV boundary condition to select the solution growing towards the IR brane; choosing $m_{UV} = (2 + \beta)k$ enforces $A_1 = 0$. The other constant A_2 is fixed by the IR boundary condition leading to the solution

$$v(y) = k^{3/2} e^{(2+\beta)k(y-L)} \sqrt{\frac{\tilde{\lambda}\tilde{v}_{IR}^2 - 2(2+\beta)}{\tilde{\lambda}}}. \tag{C.10}$$

We can relate the constants $\tilde{v}_{IR}$ and $\tilde{\lambda}$ to the electroweak vev v_{ew} by considering the SM gauge boson masses. We must satisfy

$$\int_0^L dy \, e^{-2ky} \, v^2(y) = v_{ew}^2. \tag{C.11}$$

This directly leads to Eqs. (4.10) and (4.11) that we quoted earlier.

We must now check whether this solution does indeed correspond to a small back-reaction for the Higgs vev. Evaluating the conditions at $y = L$, where $v(y)$ takes its maximum value, we obtain

$$\begin{aligned} \frac{|\xi| v^2}{M^3} &= |\xi| \left(\frac{k}{M} \right)^3 \frac{2(1+\beta) v_{ew}^2}{\tilde{k}^2} \ll 1, \\ \frac{|v'^2 - c^2 k^2 v^2 + 16\xi \tilde{A}' v \, v'|}{12 k^2 M^3} &= \\ \frac{1}{12} \left(\frac{k}{M} \right)^3 &\left((2+\beta)^2 \; - c^2 + 16\xi(2+\beta) \right) \frac{2(1+\beta) v_{ew}^2}{\tilde{k}^2} \ll 1. \end{aligned} \tag{C.12}$$

These conditions are easily satisfied for $O(1)$ values of ξ, β, c, provided that $k/M < 1$ and $v_{ew} < \tilde{k}$.

Moving now to the Higgs fluctuation, it satisfies the equations

$$\mathcal{H}''(y) - 4k\mathcal{H}'(y) - c^2k^2\mathcal{H}(y) + m_h^2 e^{2ky}\mathcal{H}(y) = 0, \tag{C.13}$$

$$\left(\mathcal{H}'(y) + \left[\frac{\tilde{\lambda}v^2(L)}{k^2} - (2+\beta)k\right]\mathcal{H}(y)\right)\Big|_{IR} = 0, \tag{C.14}$$

$$\left(\mathcal{H}'(y) - m_{UV}\mathcal{H}(y)\right)|_{UV} = 0, \tag{C.15}$$

where in the IR boundary condition we have kept only linear terms in $\mathcal{H}(y)$. Note that Eq. (C.13) differs from Eq. (C.6) only through the last term proportional to the Higgs mass, which is a small correction when $m_h \ll \tilde{k}$. So we expect that the Higgs and vev profiles are similar. The general solution to the bulk equation of motion takes the form

$$\mathcal{H}(y) = e^{2ky}\left(J_{-\beta}\left(\frac{e^{ky}m_h}{k}\right)\Gamma(1-\beta)B_1 + J_\beta\left(\frac{e^{ky}m_h}{k}\right)\Gamma(1+\beta)B_2\right), \tag{C.16}$$

where B_1 and B_2 are constants whose ratio is fixed by the UV boundary condition and are completely determined once we normalise the 4D kinetic term of the Higgs fluctuation. Using the UV boundary condition and that $\epsilon_h = m_h/k \ll 1$, we can expand the arguments of the Bessel functions

$$J_{-\beta}(\epsilon_h) = \epsilon_h^{-\beta}\left(\frac{2^\beta}{\Gamma(1-\beta)} + \mathcal{O}(\epsilon_h)\right), \qquad J_\beta(\epsilon_h) = \epsilon_h^{\beta}\left(\frac{2^{-\beta}}{\Gamma(1+\beta)} + \mathcal{O}(\epsilon_h)\right), \tag{C.17}$$

and find that

$$\frac{B_1}{B_2} \approx \epsilon_h^{2+2\beta} g(\beta), \tag{C.18}$$

where $g(\beta)$ is a regular function of β, $g(\beta) \sim \mathcal{O}(1)$ and we have replaced $m_{UV} = (2+\beta)k$. Now at large values of y, the two Bessel functions will behave in an analogous way (neither will be more important than the other in terms of magnitude). Thus at large values of y, given the ratio (C.18), we see that the solution with B_2 dominates. At small values of y this is still the case since the first term in the general solution for $\mathcal{H}(y)$ goes as $\epsilon_h^{2+\beta}B_2$ while the second term goes as $\epsilon_h^{\beta}B_2$. Therefore, in the $\epsilon_h \ll 1$ limit we can neglect the first term in the general solution for $\mathcal{H}(y)$ and write

$$\mathcal{H}(y) \approx 2^{-\beta}e^{(2+\beta)ky}\left(\frac{m_h}{k}\right)^\beta B_2, \tag{C.19}$$

where we have used that $m_h \ll k$ and also that $m_h \ll \tilde{k}$. Normalising the 4D kinetic term for the fluctuation according to

$$\int_0^L dy\, e^{-2ky}\,\mathcal{H}(y)^2 = 1, \tag{C.20}$$

determines the final constant B_2 and thus we have Eq. (4.12),

$$\mathcal{H}(y) = \sqrt{2(1+\beta)k}\, e^{ky} e^{(1+\beta)k(y-L)}. \tag{C.21}$$

Appendix D

D.1 Four-Body Phase Space Integral

We present the calculation of the four-body phase space integral that is needed to obtain the decay width of the colour-triplet scalar. We follow the common approach for many-body phase space integrals, and rewrite them as several two-body integrals. Given that the colour-triplet T decays to $t^c b^c SS$, where $t\,(b)$ is the top (bottom) quark and S is a singlet scalar, let $Q_1 = p_t + p_b$ and $Q_2 = p_{S_1} + p_{S_2}$. Note that the squared matrix element (6.9) depends only on Q_1^2, and is independent of all other kinematic variables. The four-body phase space integral can be written

$$\int d\Pi_4(p_T; p_t, p_b, p_{S_1}, p_{S_2}) = \int d\widetilde{\Pi}_2(p_T; Q_1, Q_2)\, d\Pi_2(Q_1; p_t, p_b)\, d\Pi_2(Q_2; p_{S_1}, p_{S_2})\,, \quad \text{(D.1)}$$

where

$$d\Pi_2(p_a; p_1, p_2) = \frac{d^4p_1}{(2\pi)^4}\,\frac{d^4p_2}{(2\pi)^4}\,2\pi\theta(p_1^0)\delta(p_1^2 - m_1^2)\,2\pi\theta(p_2^0)\delta(p_2^2 - m_2^2) \times (2\pi)^4\delta^{(4)}(p_a - p_1 - p_2)\,, \quad \text{(D.2)}$$

$$d\widetilde{\Pi}_2(p_a; p_1, p_2) = \frac{d^4p_1}{(2\pi)^4}\,\frac{d^4p_2}{(2\pi)^4}(2\pi)^4\delta^{(4)}(p_a - p_1 - p_2)\,. \quad \text{(D.3)}$$

We can then trivially perform the integrals over all momenta other than $Q_{1,2}$. Let us introduce the triangle function

$$I(a, b) = 1 + a^2 + b^2 - 2a - 2b - 2ab\,. \quad \text{(D.4)}$$

The two-body phase space integral may then be written as

$$\int d\Pi_2(p_a; p_1, p_2) = \frac{1}{8\pi}\left(\frac{2|\vec{p}_1|}{p_a^0}\right)_{COM} = \frac{1}{8\pi}\sqrt{I\left(\frac{m_1^2}{m_a^2}, \frac{m_2^2}{m_a^2}\right)}\,. \quad \text{(D.5)}$$

The first result is the well-known expression for the two-body phase space in the centre of mass frame; the second result expresses this in Lorentz-invariant form. Since the integral is manifestly Lorentz-invariant this result holds in all frames. In the two specific cases we require this simplifies further. Neglecting the bottom quark mass we have

$$\int d\Pi_2(Q_1; p_t, p_b) = \frac{1}{8\pi}\left(1 - \frac{m_t^2}{Q_1^2}\right), \tag{D.6}$$

$$\int d\Pi_2(Q_2; p_{S_1}, p_{S_2}) = \frac{1}{16\pi}\sqrt{1 - \frac{4m_S^2}{Q_2^2}}\,. \tag{D.7}$$

The additional factor of one-half in the latter equation is due to the presence of identical final states.

Next, we rewrite the integral over Q_1 and Q_2. It is easy to see that, if $p_{1,2}^0$ are constrained positive,

$$d\widetilde{\Pi}_2(p_a; p_1, p_2) = \frac{dm_1^2}{2\pi}\,\frac{dm_2^2}{2\pi}\,d\Pi_2(p_a; p_1, p_2)\,. \tag{D.8}$$

This condition applies to $Q_{1,2}$. Therefore we may write

$$\int d\widetilde{\Pi}_2(p_t; Q_1, Q_1) = \int \frac{dQ_1^2}{2\pi}\,\frac{dQ_2^2}{2\pi}\,\frac{1}{8\pi}\sqrt{I\left(\frac{Q_1^2}{m_T^2}, \frac{Q_2^2}{m_T^2}\right)}\,. \tag{D.9}$$

Putting all of this together, we have the final result

$$\int d\Pi_4(p_T; p_t, p_b, p_{S_1}, p_{S_2}) = \frac{1}{2^{12}\pi^5}\int dQ_1^2\, dQ_2^2 \sqrt{I\left(\frac{Q_1^2}{m_T^2}, \frac{Q_2^2}{m_T^2}\right)}\left(1 - \frac{m_t^2}{Q_1^2}\right)\sqrt{1 - \frac{4m_S^2}{Q_2^2}}\,. \tag{D.10}$$

Finally we need the bounds of integration. It is straightforward to see that the absolute bounds on Q_1^2 are

$$m_t^2 < Q_1^2 < (m_T - 2m_S)^2\,. \tag{D.11}$$

The lower bound occurs when the b quark is produced at rest, and the upper bound when the two S are at rest. For any given Q_1^2 there is an upper bound on Q_2^2 and so

$$4m_S^2 < Q_2^2 < \left(m_T - \sqrt{Q_1^2}\right)^2\,. \tag{D.12}$$

The lower bound arises from when the two S are at rest, while the upper bound is obtained when they are back-to-back.

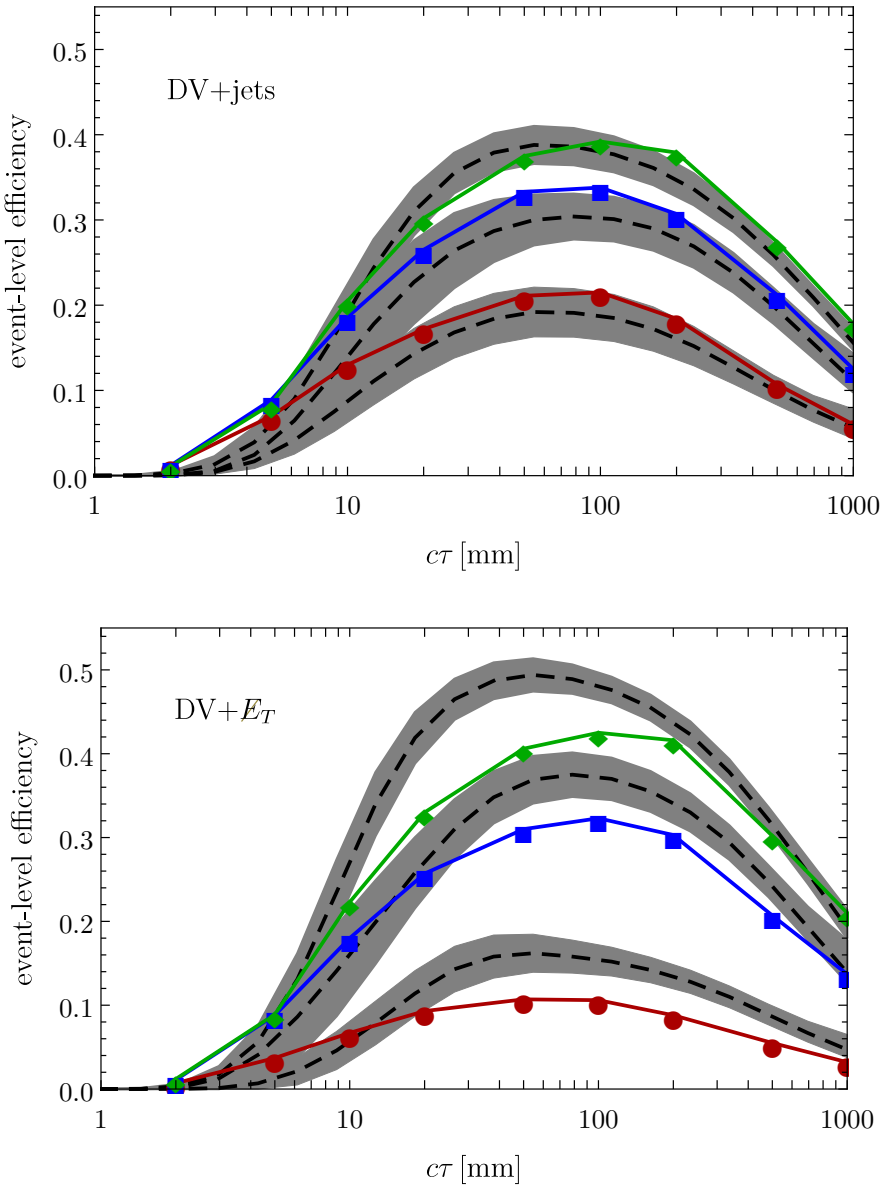

FIGURE D.1: Comparison of the event-level efficiencies from our analysis (data points) and the ATLAS analysis (shaded regions) for the case of a long-lived gluino decaying to $tt\tilde{\chi}_0$. From top to bottom the curves correspond to gluino masses of 1400, 1000 and 600 GeV. The top and bottom panels are for the DV+jets and DV+$\not{E}_T$ channels respectively.

D.2 Displaced-Vertex Search Validation

Given the challenges involved in recasting displaced searches and the various assumptions that must be made, it is important to check the validity of our implementation against the full experimental analysis. We have therefore also simulated events for one of the signal processes considered in the ATLAS paper [319]. We have chosen the case of a long-lived gluino decaying to two top quarks and a 100

GeV neutralino since this most closely resembles the final-state that is produced by the decay of our colour-triplet.

In Figure D.1 we compare the event-level efficiencies obtained from our analysis (data points) with the results reported by ATLAS (shaded regions) for both the DV+jets and DV+$\not{E}_T$ channels. Overall we find that our analysis gives reasonably good agreement with the full experimental analysis, especially in the DV+jets channel. The discrepancies in the DV+$\not{E}_T$ channel suggest that our assumptions regarding the reconstruction of the decay products from displaced R-hadron decays leads to an underestimate of the missing energy. The difference in signal efficiency is not expected to have a significant effect on the exclusion limits we derive, especially at higher center-of-mass energies where the expected missing energy from our signal can be significantly greater than the experimental cuts.